UNIVERSITÀ DELLA CALABRIA

UNIVERSITA' DELLA CALABRIA

Dipartimento di Biologia, Ecologia e Scienze della Terra

Scuola di Dottorato

"Archimede" in Scienze, Comunicazione e Tecnologie

Indirizzo

Scienze della Terra

Con il contributo di

PON AMICUS 01_02818

CICLO

XXVII

Geological, stratigraphic and hydrostratigraphic setting of the lower Crati valley reconstructed by geophysical and well data and relationship with the land subsidence detected by InSAR data

Settore Scientifico Disciplinare GEO/02

Direttore: Ch.mo Prof. Pietro Salvatore Pantano

Supervisore: Dott. Rocco Dominici

Co-Tutor: Dott. Maurizio Polemio

Dott. Cristiano Tolomei

Dott. Carlo Alberto Brunori

Dottorando: Dott.Giuseppe Cianflone

Preface

The main aim of this work is the improvement of the geological knowledge about the lower Crati valley (northeastern Calabria, Italy) useful to better understand the risks (subsidence and groundwater salinization) which affect this area.

This work is sponsored by *PON01_02818 "AMICUS"* project and its results have been supported the activities of *"Cuneo Salino"* subproject.

The lower Crati valley represents a large and very flat coastal plain (called Sibari Plain) with significant agricultural development and cultural appeal related to the presence of ancient *Sybaris*, a powerful Greek colony of *Magna Grecia* founded in 720 B.C..

The geological investigations performed in this study are mainly based on subsoil (wells and geophysical) data due to the absence of outcrops. Several kinds (geophysical technique, scale) of data are used and have been allowed to analyze different (scale, time, topics) geological themes.

Deep well and seismic data realized for hydrocarbon exploration (available in ViDEPI project) are used to investigate the buried late Miocene-early Pliocene sedimentary succession and to reconstruct the basin evolution.

Surface well-logs (by literature and inedited) and inedited shallow geophysical data (resistivity electrical tomographies and seismic ambient noise) have been consented to examine the Holocene evolution which are strictly related to tectonics, sea-level changes and autogenic sedimentary mechanisms.

The hydrogeological characterization realized in this work consists of the reconstruction of the hydrostratigraphic framework, the estimation of water table variation and aquifers recharge and a general hydrogeochemical investigation based on the major ions analysis.

Finally, the land subsidence has been investigated by the application of the Small Baseline Subset multi-temporal InSAR technique (SBAS) to two SAR datasets acquired from 2003 up to 2013 by Envisat (ESA, European Space Agency) and COSMO-SkyMed (ASI, Italian Space Agency) satellites.

The main and innovative outcomes resulting from this work are: 1) the identification and characterization of the northernmost sector of the late Miocene-early Pliocene foreland basin system of the northern Calabrian Arc; 2) the reconstruction of the fault-controlled Holocene evolution of the lower Crati valley that represents an important aspect for future neotectonics studies; 3) the better (at this day) hydrostratigraphic characterization of the coastal plain aquifers; 4) the exclusion of the seawater intrusion as the main/only cause of groundwater salinization and the suggestion of the presence of probably deep plumes of mineralized waters; 5) the first analysis of ground

subsidence referring to the whole plain; 6) the identification of geological processes as the main subsidence triggers.

This work is sponsored by *PON Ricerca & Competitività 2007/2013 – Regioni Convergenza - Asse I "Sostegno ai mutamenti strutturali" - Obiettivo Operativo 4.1.1.1 "Aree scientifico-tecnologiche generatrici di processi di trasformazione del sistema produttivo e creatrici di nuovi settori" - Azione II "Interventi di sostegno della ricerca industriale", nell'ambito del Progetto* ***PON01_02818 "AMICUS****", finanziato dal MIUR con Decreto Direttoriale Prot.n. 678/Ric del 14 ottobre 2011, CUP B71H11000880005.*

Table of contents

CHAPTER 4 - Natural and anthropogenic ground subsidence detected by InSAR time series analysis

CHAPTER 1

Stratigraphic architecture and evolution of the Mio-Pliocene foreland basin system of the northeastern Calabrian Arc reconstructed by seismic and well data

1.1 Introduction

The progressive northeastern drift of the Calabrian Arc (CA) during the late Miocene generated, since the Tortonian, an uplifted thrust belt, made up by northern Calabrian terranes, with a well developed foreland basin system along its frontal edge characterized by a km-thick late Miocene-Quaternarny succession. During late Tortonian-Messinian time the sedimentation is controlled by eastern shift of foreland depocentres and the CA uplift with the overlapping of the Messinian Salinity Crisis (MSC). Since early to middle Pliocene a wrench tectonic style, with the development of regional subvertical shear zones in the northern CA (*Knott and Turco* 1990; *Van Dijk et al.* 2000; *Tansi et al.,* 2007) produces the lateral displacement and partitioning of wedge top depozones.

The mio-pliocenic fill of this foreland basin system is well studied in Crotone and Rossano Basin, where it crops out, but poorly investigated along North CA edge because it is overlay by a 1000m-thick Quaternary deposits. The aim of this work is the reconstruction of the late Miocene-early Pliocene stratigraphic architecture of this sector, defined Sibari-Corigliano Basin according to *Turco et al.* (1990).

Our work is based on the well and seismic data analysis and their interpretation depending on the current models of the Messinian Salinity Crisis facies associations and the correlation with the outcropping successions of the Crotone and Rossano Basins.

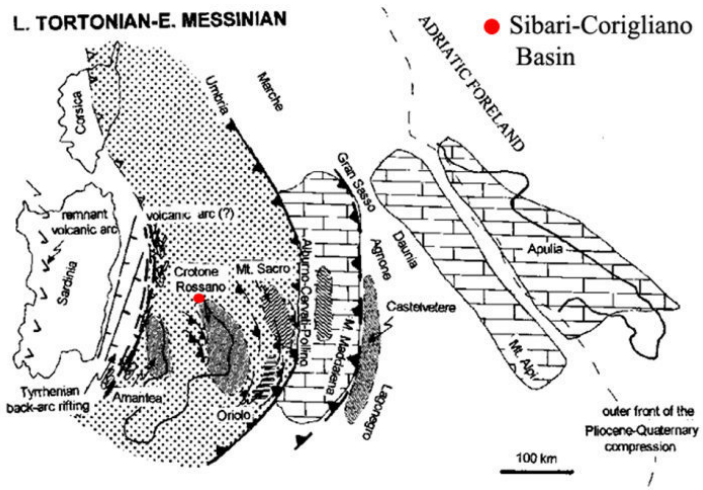

Fig.1.1. Late Tortonian-early Messinian palinspastic restoration of the Apenninic domains (*Critelli*, 1999) with supposed location of the Sibari-Corigliano Basin

1.2 Geological setting

The CA represents a fault-bounded continental fragment within the western Mediterranean orogen, located at the intersection of the E–W-trending Sicilian Maghrebides on the South and NW–SE-trending Southern Apennines (SA) on the North (*Bonardi et al.*, 2004).

The SA, CA and related accretionary prism is closely connected to the retreatment of the subduction of Ionian oceanic lithosphere and the consequent slab roll-back.

Progressive slab roll-back produced a series of back-arc basins which allowed the eastward migration of CA of about 775 km during the late Oligocene along a section crossing northern Calabria, the Tyrrhenian Sea, Sardinia and the Provencal Basin (*Malinverno and Ryan*, 1986; *Faccenna et al.*, 1997; *Gueguen et al.*, 1998; *Wortel and Spakman*, 2000; *Rosenbaum and Lister*, 2004; *Mattei et al.*, 2007).

The CA migration has been influenced by a series of events: during the late Burdigalian the Tyrrhenian Basin opening allowed the separation between Sardinian block and Calabrian-Peloritan massif (*Gueguen et al.*, 1998); during late Messinian the slab roll-back rate increased and decreased respectively in Southern and Northern Tyrrhenian Basin (*Rosenbaum and Lister,* 2004).

At the boundary late Miocene-early Pliocene a migration rate increase happened due to the oceanization of the Vavilov Basin (*Gueguen et al.*, 1998; *Faccenna et al.*, 2004). The thick evaporite sequence of the Messinian Salinty Crisis acts as preferential detachment level after late Messinian time (*Minelli and Faccenna*, 2010). Later, the rapid oceanization of the Marsili Basin happened between 3Myr (*Kastens et al.*, 1988; *Gueguen et al.*, 1998; *Rosenbaum and Lister*, 2004) and 2 Myr (*Sartori*, 1990; *Marani and Trua*, 2002; *Nicolosi et al.*, 2006) favoured by slab rupture at 2.1 Myr (*Chiarabba et al.*, 2008). Actually the slab roll-back is not active and the subduction has a rate of few mm/yr (*Hollenstein et al.*, 2003; *D'Agostino and Selvaggi*, 2004; *Mattei et al.*, 2007).

The CA is characterized by a duplex structure composed by a meso-Cenozoic fragment of Alpine chain overthrusted upon the Triassic-Miocene Apennine-Maghrebian chain during Miocene (*Amodio Morelli et al.*, 1976; *Finetti et al.*, 1996). The first one includes the metamorphic terranes of Sila Unit (*Messina et al.*, 1994) intruded by upper Paleozoic plutonic rocks of Sila batolith, with their Meso-Cenozoic sedimentary covers, and ophiolite-bearing units of the Neotethys domain. The second one is characterized by carbonate units which in the North sector of CA are correlated to Verbicaro Unit (*Amodio-Morelli et al.*, 1976) or to SanDonato-Campotenese Unit (*Bousquet and Grandjacquets*, 1969; *Van Dijk et al.*, 2000).

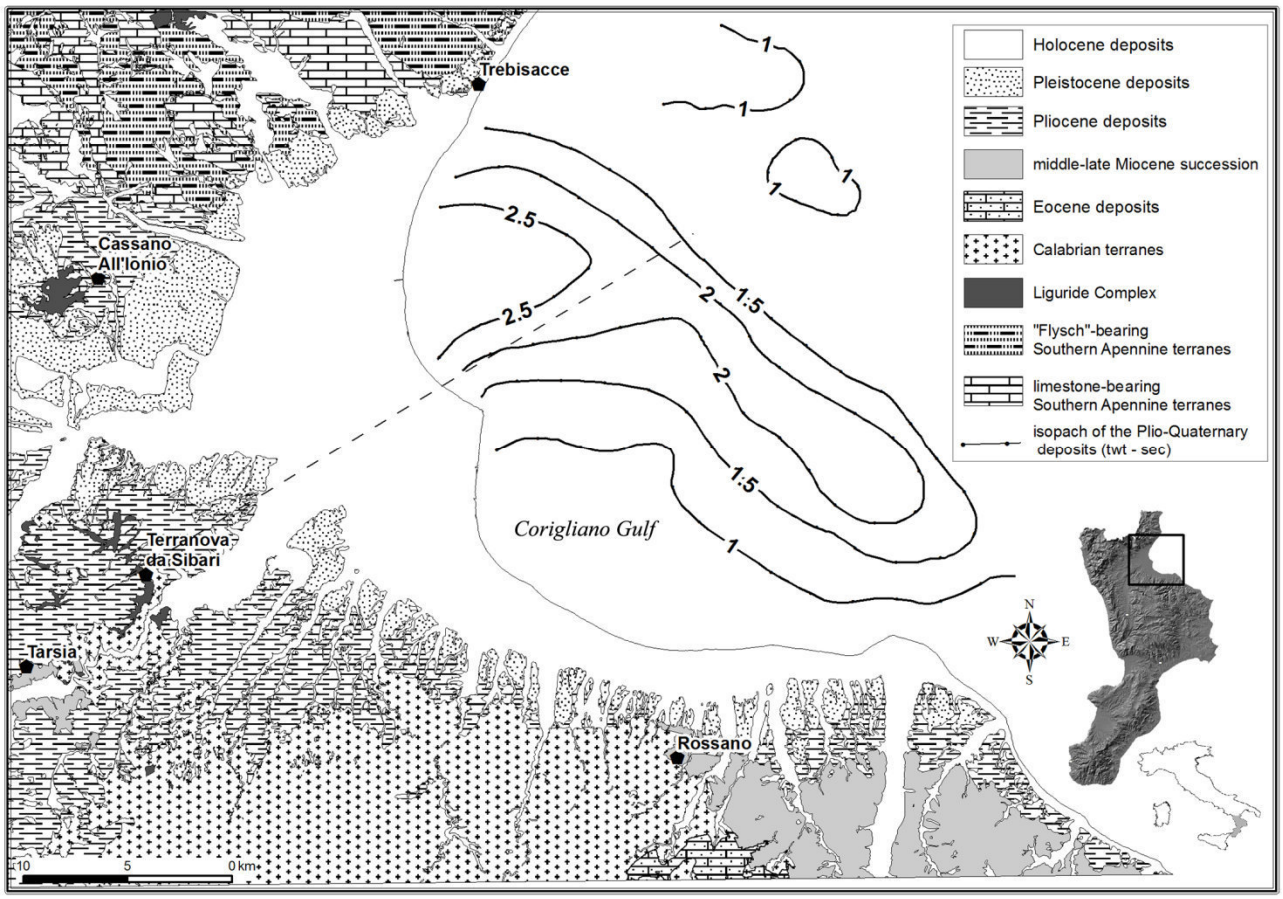

Fig.1.2. Simplified lithological map of the northeastern sector of the Calabria Region. In the Corigliano Gulf is shown the isopach map of Plio-Quaternary deposits (from *Bigi et al*., 1991). Dashed black line represents the trace of the profile showed in fig.1.3.

During the continental collision and following fragmentation and migration of the CA towards SE are formed several NW-trending shear-zones which influenced the development of basin located along the Eastern and Western Arc boundaries (*Knott and Turco*, 1991; *Van Dijk et al.* 2000; *Tansi et al.*, 2007).

The study area is located along the Northern margin of the CA, near the boundary with Southern Apennines. *Cello et al.* (1981), through a deep seismic profile (fig.1.3), recognize that in this sector the Alpine nappes form only the thin superficial portion of the chain which is prevalently composed by Apenninic terranes. The same Authors subdivide the Calabrian terranes in a basal complex formed by Frido Unit (ophiolitic terrain and relative covers) and a top complex which includes Bagni and Polia-Copanello Units.

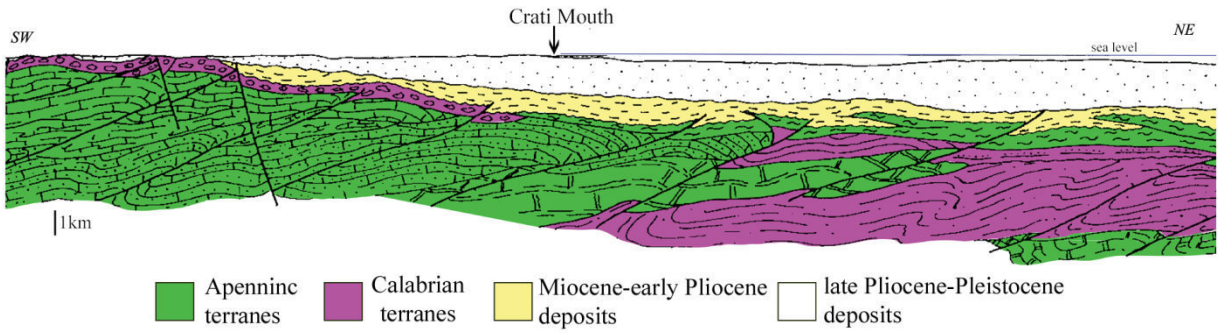

Fig.1.3. Deep seismic profile, modified from *Cello et al.* (1981), showing the thin Calabrid units overlapping the Southern Apennine units. Profile trace in fig.1.2.

The Apenninic Chain sector in the study area is built by carbonatic succession of the Pollino tectonic Unit (ISPRA, 2009)**,** ascribed to a Mesozoic-Tertiary paleogeographic domain of the Afro-Adriatic margin (*D'Argenio et al.,* 1973; *Mostardini and Merlini*, 1986) and represented the basal chain of duplex Apenninic structure. The Pollino tectonic Unit is made up, from bottom, by the Calcari and Calcari Dolomitici (ISPRA, 2009), the oligo-miocenic Trentinara Fm. (*Selli*, 1962), the Cerchiara Fm (*Selli*, 1962) with Burdigalian age (*Ogniben*, 1969) and the Bifurto Fm. (*Selli*, 1957). Above the Pollino tectonic Unit is present the North-Calabrian tectonic Unit (ISPRA, 2009), consists of Late Jurassic ophiliotes and their sedimentary covers, the Crete Nere Fm. (*Selli*, 1962) with Aptian-Albian age (*Vezzani*, 1968a) dated at Middle Eocene in the top portion (*Bonardi et al.*, 1988), the Saraceno Fm. (*Selli*, 1962) with late Jurassic (*Vezzani*, 1968b, *Torricelli and Amore*, 2003) or late Eocene-Aquitanian age (*Bonardi et al.,* 1988; *Di Staso and Giardino*, 2002), and the Albidona Fm. (*Selli*, 1962) with Oligocene-Miocene (*Zuppetta et al.*, 1984) or Eocene (*Baruffini et al.*, 2000) age. The external sector of chain is built up by the Sicilide tectonic Unit (ISPRA, 2009) consists of Argille Variegate Group (ISPRA, 2009). The latter is made up by the Argille Vari Colori Inferiori (*Lentini*, 1979) (containing Pollino Unit, Flysch Rosso and Flysch Numidico olistolites) and Monte Sant'Arcangelo Fm. (*Selli*, 1972); both are covered by Corleto-Perticara Fm. (*Selli*, 1972).

Along South margin of the study area *Finetti et al.* (1996) describe the presence of the Palinuro Fault with left-lateral movements and Pleistocenic activity. The surface expression of this structure is probably represented by the Rossano-Corigliano fault system (*Moretti*, 1999). In the North-western sector, the NE-SW oriented Sangineto Line represents the boundary between CA and SA (*Amodio Morellli et al.*, 1976; *Ghisetti*, 1979; *Lanzafame and Tortorici*, 1981; *Van Dijk et al.*, 2000). *Lanzafame and Tortorici* (1981) suppose the presence of two NE-SW normal faults in the area of Crati Delta. Recently *Cinti et al.* (2015 in press) observe inside archeological site of Sybaris the evidence of NE-SW oriented fault zone.

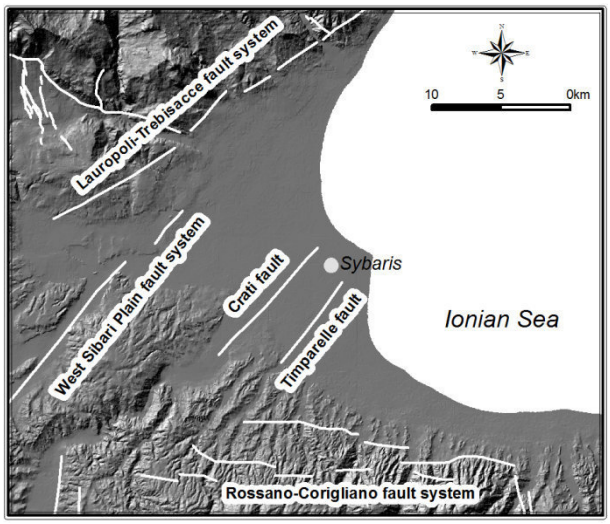

Fig.1.4. Main fault systems of the Sibari Plain (from ITHACA). Crati and Timparelle faults represent the NE-SW normal faults supposed by *Lanzafame and Tortorici* (1981). Lauropoli-Trebisacce and West Sibari Plain fault systems are located along the trace of Sangineto Line.

Spina et al. (2011) through interpretation of onshore seismic and well data observe a decrease of miocenic succession toward North, probably due to the faults activity, and the presence of a morphological or structural high almost coincident with seismic line CS304-81.

Ferranti et al. (2009) suppose the existence of WNW– ESE shallow-crustal folds, involve late middle Pleistocene sediments, grown within a recent and still active transpressional field by the analysis of marine terraces deformation, fluvial geomorphic anomalies and two offshore seismic lines. *Del Ben et al.* (2008) reconstruct the structural map of the Plio-Quaternary base in the offshore sector recognized the presence of WNW– ESE oriented axial depocenter, the parallel alignment of structural highs along strike-slip Sibari Fault and of evaporite domes.

1.2.1 The Sibari-Corigliano Basin

The Miocene kinematic model and sedimentary infill of the Sibari-Corigliano Basin are not studied and only its Plio-Pleistocene tectonic evolution has been investigated (*Ghisetti*, 1979; *Turco et al*., 1990).

Ghisetti (1979), that called this basin Low Crati and Sibari Trough, traces its boundaries represented to the North by a NE-SW fault system (Belvedere Marittimo-Castrovillari-Francavilla Marittima-Trebisacce) and another one WNW-ESE (Rotonda-Castelluccio-Frascineto) while to the South by a ENE-WSW fault system (Rossano-Spezzano Albanese).

Turco et al. (1990) interpret the Sibari-Corigliano Basin as a pull-apart basin developed along the Pollino Line and which origin is due to the anticlockwise and clockwise rotation of the blocks respectively northward and southward referring to the Sangineto Line.

The sedimentary fill is represented by mio-pleistocenic succession, thick above 2,5 km, which *Spina et al.*(2011) only describe and correlate to the Gessoso Solfifera Fm.

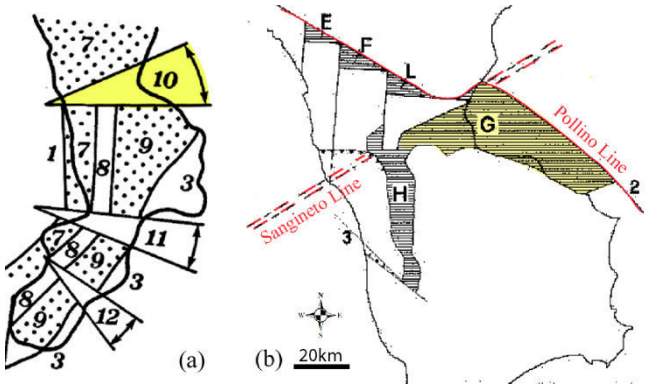

Fig.1.5. Sibari-Corigliano Basin (yellow polygon) a) in the CA block-segmentation model of *Ghisetti* (1979) and b) in the rigid blocks model of *Turco et al.* (1990)

1.2.2 The late Miocene foreland basin systems of the northern Calabrian Arc

The Ionian side of northern CA is characterized by a Neogene basinal domain which includes the Rossano (RB) and Crotone (CB) Basins (*Ogniben* 1962; *Roda* 1964, 1967; *Critelli*, 1999; *Barone et al.*, 2008; *Zecchin et al*., 2013a, b) and the Cirò Basin (*Roda* 1964, 1967; *Van Dijk et al.* 2000). The latter is located between RB and CB and is differentiated from them by the lack of evaporites sedimentation. The pre-Tortonian CR and CB basement consists of the metamorphic lythotipes of Sila Unit (*Messina et al.*, 1994), plutonic rocks of Sila batolith and their Mesozoic-Cenozoic sedimentary covers. In the two basins the basement rocks are unconformably overlapping by a basal transgressive sedimentary fill of Serravallian?–Tortonian age. This one starts with alluvial and fan-delta conglomerate covered by a nearshore sandstones and fossiliferous sandstones represented by Conglomerati Irregolari unit (*Roda*, 1964) and Arenaceo-conglomeratica unit in the RB and by the basal conglomerate unit (*Van Dijk*, 1990) and the San Nicola unit in the CB. The succession passes upward to deep-water deposits (clay and marl) of the Argilloso marnosa unit in the RB and the Ponda unit in the CB, both covered by olistostrome bodies of varicolored clays correlated to Sicilide Complex (*Critelli* 1999; *Barone et al.*, 2008). The Tortonian–Messinian boundary is marked by Tripoli Fm. which represents the prelude of Messinian Salinity Crisis (MSC). In the RB, the first MSC deposits are made by Calcare di Base unit, interpreted as microbial limestone by *Guido et al.* (2007), and coverd above an erosional angular unconformity by the Molassa di Castiglione unit which consists of conglomerate, breccias and sandstones. In the eastern sector of RB the lateral equivalent of Molassa di Castiglione unit is represented by Argille marnose salifere unit, consisting of an alternation of halite and clay marls with gypsum and anhydrite nodules and

covered by large olistostrome bodies. The Gessi unit lies on a transgressive surface above the Argille marnose salifere, Molassa di Castiglione and Calcare di Base units and it consists of gypsarenites, with interbeds of gypsum-bearing sandstones. The MSC succession is closed on top by the grayish fossiliferous marls and clays alternating with thin turbidite sandstone beds of the Garicchi Unit and deltaic sandstones of the Molassa di Palopoli Unit.

In the CB the Tripoli Fm. pass-upward to the Evaporitica inferiore unit made by limestone breccias, gypsrudites–arenites and gypsum-bearing sandstones. This one is covered by the Detritico-salina unit which consists of meter-scale blocks of limestone, gypsarenite breccias, and gypsarenite slumps and characterized by halite diapiric extrusion. The Evaporitica superiore unit, made up of shale, sandstone, and gypsarenite levels and characterized by a Lago-Mare fauna at the top, onlaps the Detritico-salina unit and it is closed by an erosive surface. Above the latter lies the Carvane Conglomerate unit consisting of fluvial conglomerates and deltaic sand lobes.

The Tortonian-Messinian succession of RB and CB is covered by outer-shelf deposits of the Pliocene Cavalieri marly unit (*Zecchin et al.*, 2013a, b).

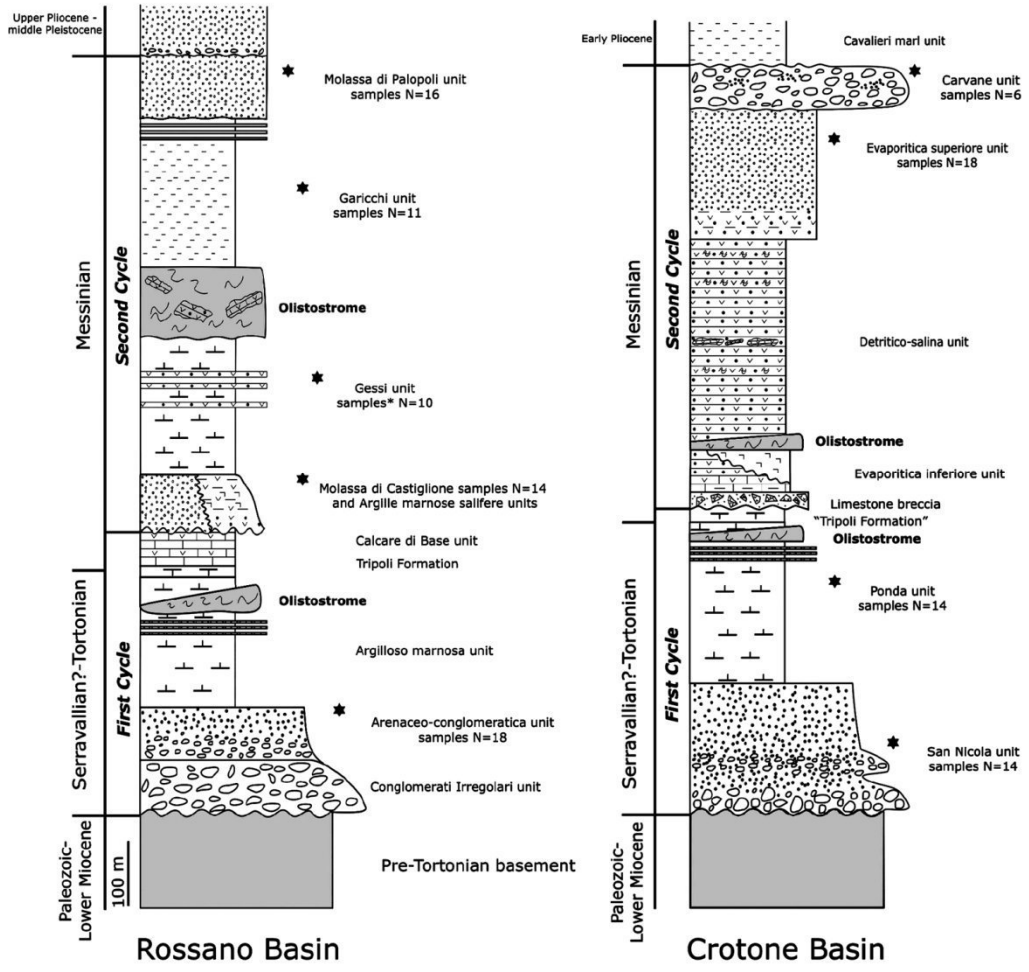

Fig.1.6. Schematic stratigraphic type section of Rossano and Crotone Basins (from *Barone et al.*, 2008)

1.3 Methods

This study is based on the interpretation of multichannel seismic profiles and wells available in the framework of the project ViDEPI (Visibilità Dati Esplorazione Petrolifera in Italia, http://www.videpi.com).

In detail we analyzed 7 onshore wells (Crati 1, Crati 2, Crati 3, Thurio, Ogliastrello, Sibari, Torrente Caldana), 8 offshore wells (Luana, Laura, Lorena, Flora, Francesca, Lina, Licia, Franca), 4 onshore seismic profiles (CS 304-81, CS 306-81, CS 307-81, CS 323-83) and 7 offshore seismic profiles (DR 3021-77, DR 3024-77, DR 3025-77, DF 80-31, DF 80-11,DR 527, DR 77-009).

The identification and the interpretation of the single facies and of facies associations with Tortonian-Messinian age is based on modern studies about MSC (*Manzi et al.*, 2005; *Roveri and Manzi*, 2006; *Lugli et al.,* 2007a; *Manzi et al..*, 2007; *Roveri et al.*, 2007; *Schreiber et al.*, 2007; CIESM, 2008; *Roveri et al.*, 2008; *Lugli et al.,* 2010). For the interpretation of different deposits recognized in the regional context, we correlate them with the successions outcropping in the Rossano and Crotone Basins (*Roda* 1964, 1967; *Lugli et al.,* 2007b; *Barone et al.*, 2008).

The identification of MSC markers and units in the seismic lines interpretation is based on the atlas edited by *Lofi et al.* (2011).

We analyzed in detail the depth of Miocene succession top (TMS) and created a points dataset including information of wells and seismic profiles (each profile was subdivided in points series 500m far). The TMS depth recorded by wells are converted in twt using an average velocity of 2000 m/s for Plesistocene and Pliocene deposits and of 2700 m/s for Miocene ones. These velocities was established trough the analysis of the sonic logs available for the Ogliastrello and Thurio wells performed by *Spina et al.* (2011). The dataset was utilized to create a Digital Surface Model (DSM) useful to investigate the morphology of TMS.

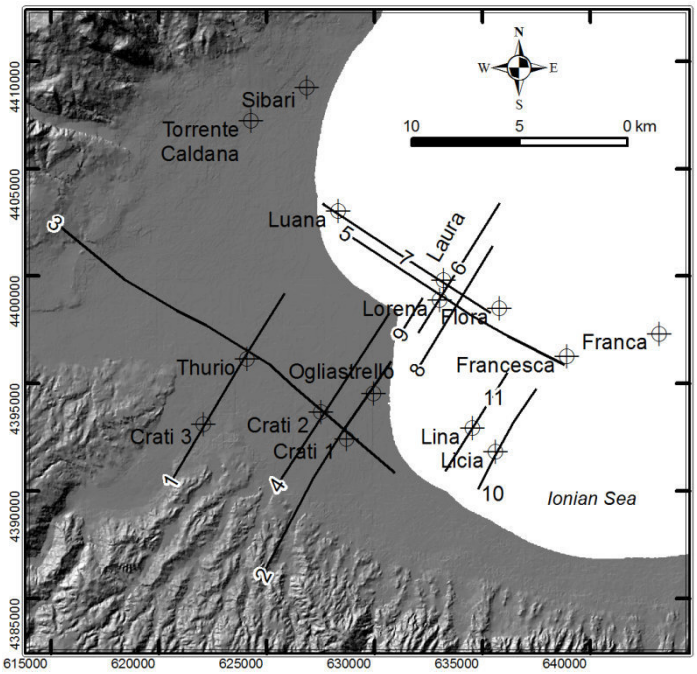

Fig.1.7. Location of ViDEPI wells and seismic profiles (1=CS304-81; 2=CS306-811; 3=CS307-81; 4=CS323-83; 5=DF80-11; 6=DF80-31; 7=DR3021-77; 8=DR3024-77; 9=DR3025-77; 10=DR527; 11=DR77-009).

1.4 Well-logs description

Onhore and offshore wells analyzed were useful to reconstruct the mio-pleistocenic sedimentary infilling of the Sibari-Corigliano Basin. The stratigraphic succession starts with Middle-Late Miocene (Serravallian?-Tortonian) deposits. The oldest succession deposits are logged by Flora and Laura wells and lie along unconformity surface on igneous-metamorphic bedrock.

The bedrock is logged for 12m of thickness by offshore Licia well and it is formed by garnet gneiss. In the onshore Crati 3 well the bedrock is logged for 1889m of thickness and it , from top to bottom, consists of garnet gneiss, ophiolitic rocks associated to quartz-siltites and clay-schists, calcareous and marly calcareous lithotypes. In the North sector pre-Tortonian bedrock consists of arenaceous-pelitic alternance logged by Torrente Caldana.

The Tortonian-early Messinian succession is made by conglomeratic-sandy unit passing upward to clayey deposits overlain by gypsum layers with intercalations of clays and sometimes of limestone (Laura and Flora wells). The succession is characterized by halite deposit which covered gypsum layers and clayey deposits in the central area. The halite deposits are logged with different thickness by Thurio well (421m), Licia well (118m), Crati1, Crati2, Laura and Flora wells (m to dam-thick).

The following deposits are characterized by gypsum and clayey layers and occasionally limestone layers (Crati 1 and Licia wells).

The top of Messinian succession is mainly made by sandy-conglomeratic deposits and clayey and clayey-marly deposits, except in Thurio, Crati 1 and Crati 2 wells in which prevail the second ones.

In onshore (Crati, Crati 2, Torrente Caldana and Sibari wells) and offshore (Larissa well) the late Miocene succession is covered by late Pliocene clayey and clayey-marly deposits, with intercalations of sandy and silty layers. In other wells, the top of Miocene succession passes upward to a Pleistocene-Holocene succession (maximum thickness of 1500m)

The lower part of the Quaternary succession consists of clay and clay-marl with some ash layers (Ogliastrello, Lorena, Flora, Franca and Francesca wells). Toward the top the succession evolves to sand and conglomerate. In the Crati 3 well the pleistocenic succession is characterized by intercalations of gypsum and halite layers.

1.5 Well-logs interpretation

In the sothern sector of Sibari-Corigliano Basin the bedrock, logged by Crati 3 and Licia wells, consists of CA igneous-metamorphic terranes overlapping Apenninic terranes.

In details, the CA terranes are made by gneiss, which represents the Sila Unit (*Messina et al.*, 1994), and ophiolites with their metasedimentary covers assigned to Diamante-Terranova Unit (*Dietrich et al.*, 1977) which crop out near Terranova da Sibari and on the Cassano structural high (*Spadea et aii., 1976;* ISPRA, 2010*)*.

Along the NW margin of Sibari-Corigliano Basin, in the Caldana well the substratum is made by Eocene-Miocene units related to the Albidona Fm. and Saraceno Fm. covered by plio-pleistocenic succession. In the valley of the Marzuca Stream (eastward from Trebisacce village), the Saraceno Fm. is covered, along an angular unconformity surface, by the Torrente Straface Marly Clays (Pliocene-Lower Pleistocene) which passing upward to continental-marine lithofacies related to nearshore and alluvial fan environments (*Caruso et al.,* 2013).

The Calabrian terranes are covered by a transgressive succession with Tortonian-early Messinian age. The bottom of the succession is made by basal continental conglomerate and nearshore sandstone, passing upward to marine sandy clay and marl. This sedimentary succession crops out near Tarsia village (*Romeo and Tortorici*, 1980; ISPRA, 2010) and can be correlated with transgressive Serravallian?–Tortonian sedimentary fill of the Rossano and Crotone Basin.

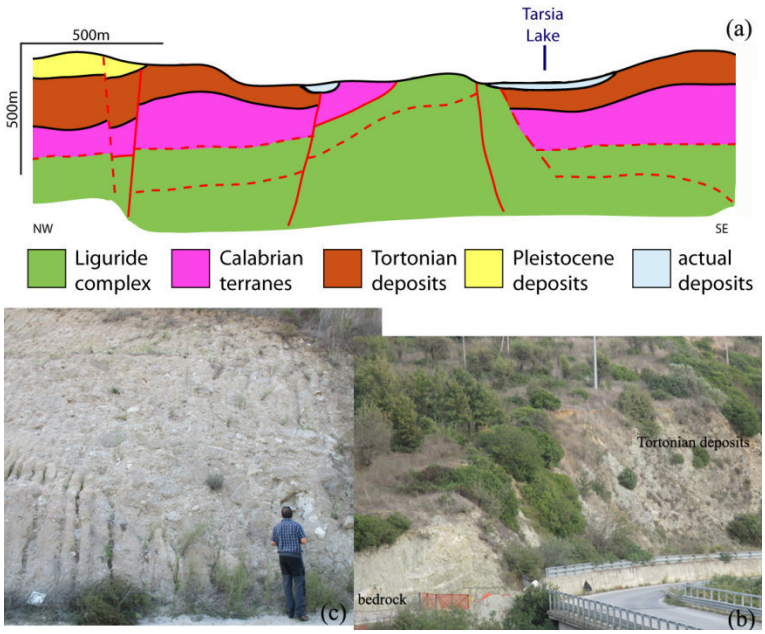

Fig.1.8. a) Geological section (modified from ISPRA, 2010) close to the Tarsia Village showing the basal unconformity between Calabrian terranes and Tortonian succession (b). c) Close-up view of the gravelly-sandy deposits mainly made by clasts of granitoid rocks.

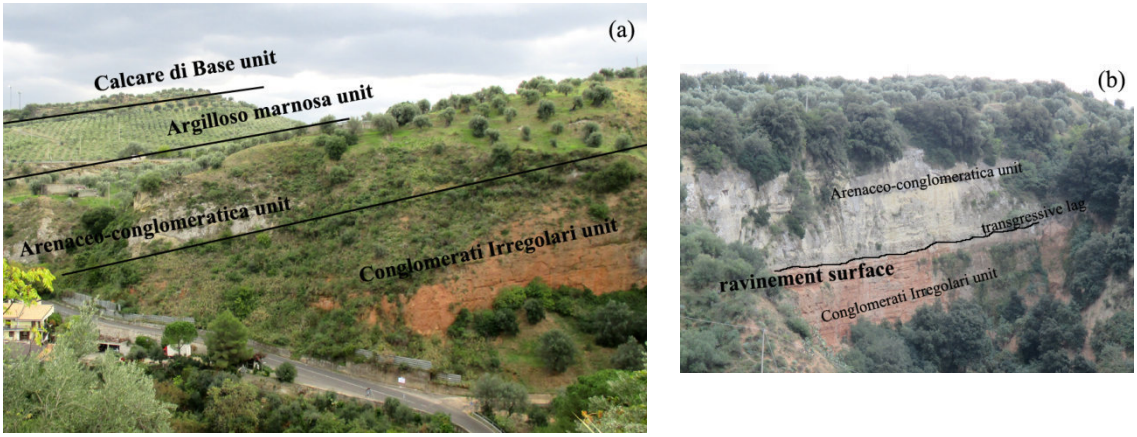

Fig.1.9. Rossano Basin: a) View of the transgressive Serravallian?-early Messinian succession characterized by the transgression of the Arenaceo-conglomeratica unit on the Conglomerati Irregolari unit. Upward, the basin deepening is recorded by the clayey and marly deposits of the Argilloso marnosa unit passing to Calcare di Base unit. b) Close-up view of the ravinement surface on the top of the Conglomerati Irregolari unit

The Messinian succession starts in Sibari-Corigliano Basin with an alternation of gypsum and clayey-marly layers which, on the strength of its stratigraphic position below halite deposits and the facies model proposed by *Roveri et al.* (2008) for Caltanissetta Basin, can be correlated with *Resedimented Lower Gypsum* (*Manzi et al.*, 2005); this alternation represents the equivalent of the Gessi Unit (RB) and the Evaporitica Inferiore Unit (CB).

The halite body, correlated with the Argille Salifere Unit (RB) and the Detritico Salina Unit (CB), represents the MSC acme (CIESM, 2008). The interpretation of the alternation of gypsum and clayey deposits overlapping the halite body is ambiguous due to the insufficient description. In

effect, it can be interpreted as Upper Evaporites (CIESM, 2008; *Roveri et al.*, 2008; *Manzi et al.*, 2009) but also, at least the lower portion, as *Resedimented Lower Gypsum* (*Manzi et al.*, 2005; *Roveri et al.*, 2008).

Messinian succession is closed by conglomeratic-sandy and clayey deposits correlated to the Garicchi Unit and the Molassa di Palopoli (RB) and the Carvane Conglomerate (CB).

Late Pliocene clayey and clayey-marly lithotypes can be correlated to the Torrente Straface Marly Clay (ISPRA, 2009) cropping out northward from the Villapiana village.

The Quaternary succession is characterized by a large lateral variability, with a lower portion made mainly by clayey-marly deposits and higher portion by sandy-conglomeratic portion. We think that these deposits are probably related with deposits that actually crop out along the Sibari Plain outer limit. These consists of fan delta deposits of San Lorenzo del Vallo system (*Colella* , 1984, 1988; *Colella et al.*, 1987), the Lauropoli Conglomerates (*Ghisetti and Vezzani*, 1983) and terraced marine deposits (*Carobene*, 1996; *Carobene et al.*, 1997; ISPRA, 2009; *Caruso et al.*, 2013).

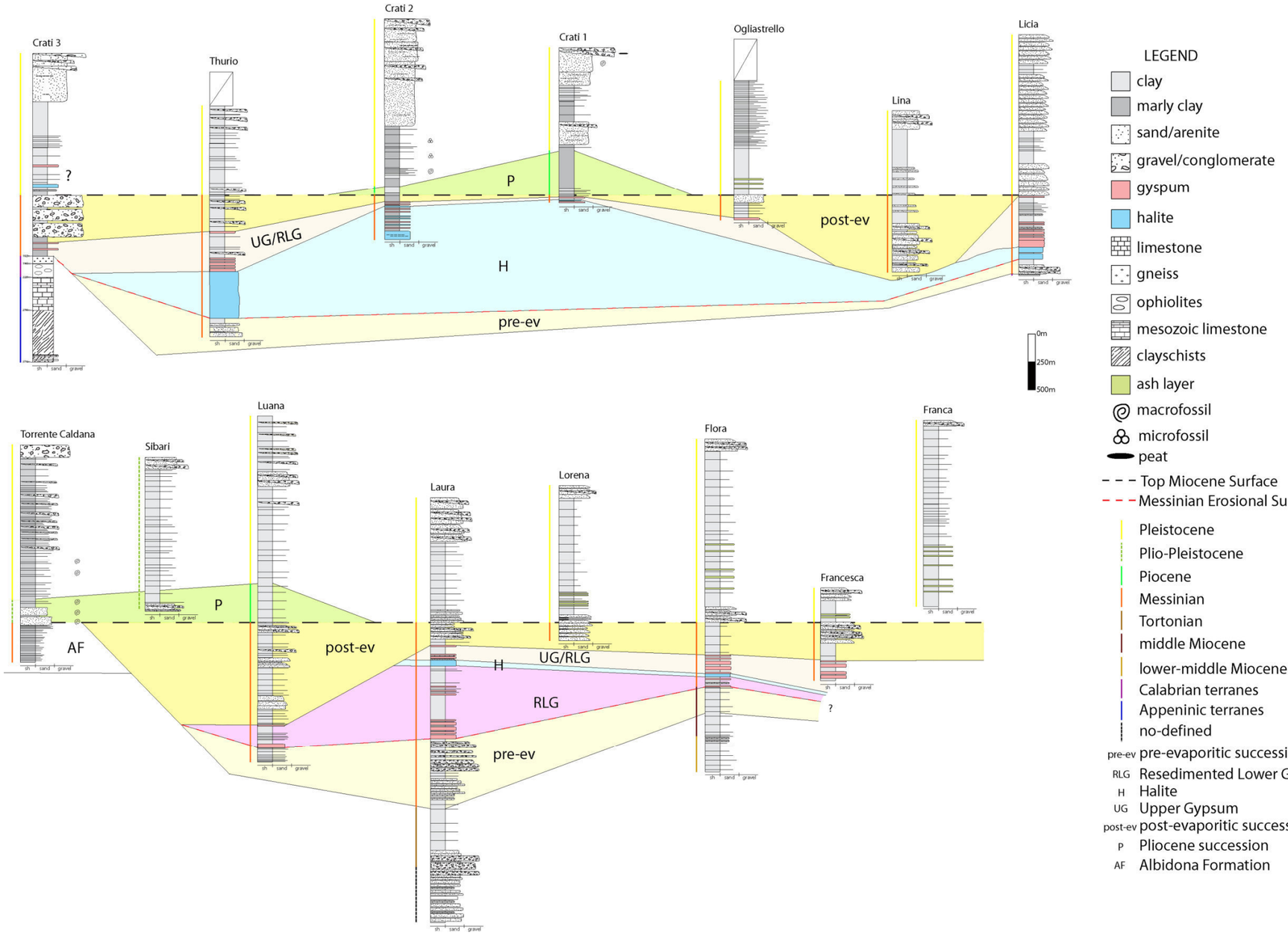
Crati 3
Thurio
Crati 2
Crati 1
Ogliastrello
Lina
Licia
Torrente Caldana
Sibari
Luana
Laura
Lorena
Flora
Francesca
Franca
?
P
UG/RLG
H
post-ev
pre-ev
AF
RLG
sh
sand
gravel
0m
250m
500m
LEGEND
clay
marly clay
sand/arenite
gravel/conglomerate
gyspum
halite
limestone
gneiss
ophiolites
mesozoic limestone
clayschists
ash layer
macrofossil
microfossil
peat
Top Miocene Surface
Messinian Erosional Surface
Pleistocene
Plio-Pleistocene
Piocene
Messinian
Tortonian
middle Miocene
lower-middle Miocene
Calabrian terranes
Appeninic terranes
no-defined
pre-ev pre-evaporitic succession
RLG Resedimented Lower Gypsum
H Halite
UG Upper Gypsum
post-ev post-evaporitic succession
P Pliocene succession
AF Albidona Formation

Fig.1.10. Correlation panel documenting the Mio-Quaternary sedimentary fill of the Sibari-Corigliano Basin. Inside the Miocene succession are identified the Serravallian?-Tortonian terrigenous deposits overlaid the basement, the main MSC facies and the post-evaporitic sediments.

1.6 Seismic profiles description and interpretation

In the onshore NE-SW profiles , CS304-81, CS306-81 and CS323-83 (described also by *Spina et al.*, 2011) we recognized the Bottom Miocene Surface (BMS) and Top Miocene Surface (TMS) with depth decreasing from NE toward SW.

In the profile CS304-81, CS306-81 and CS323-83 we identified the typical units of the MSC trilogy (Lower, Mobile e Upper Units in *Lofi et al.*, 2011); the Lower and Upper Units are recognizable thank to the sharp reflectors produced by gypsum layers, while the Mobile Unit is characterized by a transparent acoustic facies due to the halite deposits . In the profiles CS306-81 and CS323-83 Late Pliocene deposits, logged by Crati 1 and Crati 2 well, are visible and lie over TMS which are characterized by deformation due to compressive tectonic; on top of Pliocene succession we observed the onlap of Pleistocene succession which in CS304-81 lies directly over TMS.

In the *onshore* NW-SE CS 307-81 profile BMS, TMS and pre-Tortonian bedrock are recognized. In the NW profile tract we observed the pinch-out of MSC succession on bedrock and the presence of a surface, overlapping by sloping reflectors, correlated to the Bottom Messinian Surface and for which we suppose a possible correlation with Messinian Erosional Surface (MES). In the SE tract of the profile on TMS are present the Late Pliocene succession confined between two morphological highs. In the central portion of the profile, inside the Messinian succession Mobile and Upper Unit (*Lofi et al.*, 2011), logged by Thurio well, are recognizable. In correspondence of the Thurio well we observe an anticline structure involving the bedrock and the Miocene succession.

In the offshore sector we analyzed the seismic profiles in front of the actual Crati Delta. In the NW-SE DR3021-77 profile, in correspondence of Laura well, a morphological high, involving the Miocene succession and probably the bedrock, are recognized. Along its NW flank we observed the onlap of Late Pliocene succession on TMS. This morphological high is also visible in the profiles DF80-31, DR3024-77 and DR3025-77, wherein it appears bordered by NE and SW-dipping inverse faults. Furthermore in these profiles the three MSC units and the onlap of Pliocene deposits on TMS are observed. In the NW-SE DF80-11 profile we observed a decrease of TMS depth between western and eastern sectors. In the profiles DR527 and DR77-009 we recognized the inland pinch-out of Tortonian-Messinian succession over the igneous-metamorphic bedrock.

The MES are traced in many profile and includes both the margin erosion surface and its conformable surface in the basin.

The TMS Digital Surface Model, created starting by points dataset from wells and seismic data, allows to observe NW-SE alignment of structural highs and a parallel depocenters. Furthermore it is possible to recognize a NE-SW structural lineament which shifted the evaporitic succession. In the southeastern sector a morphological high is shown by the DSM.

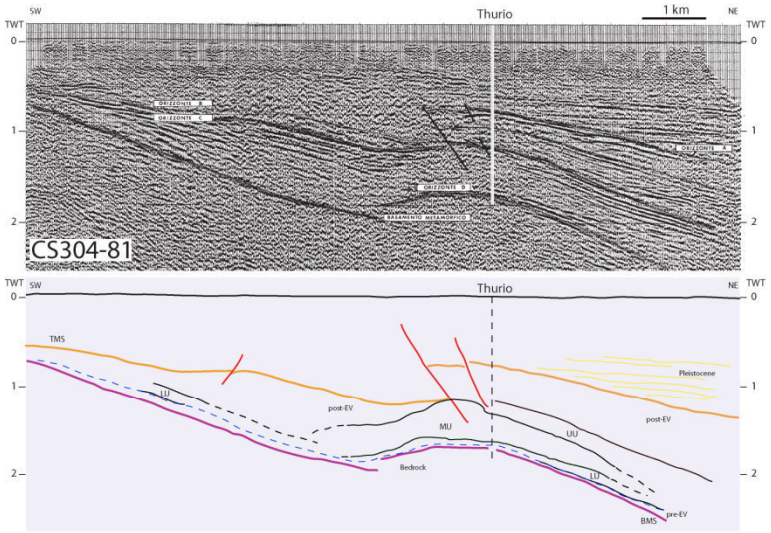

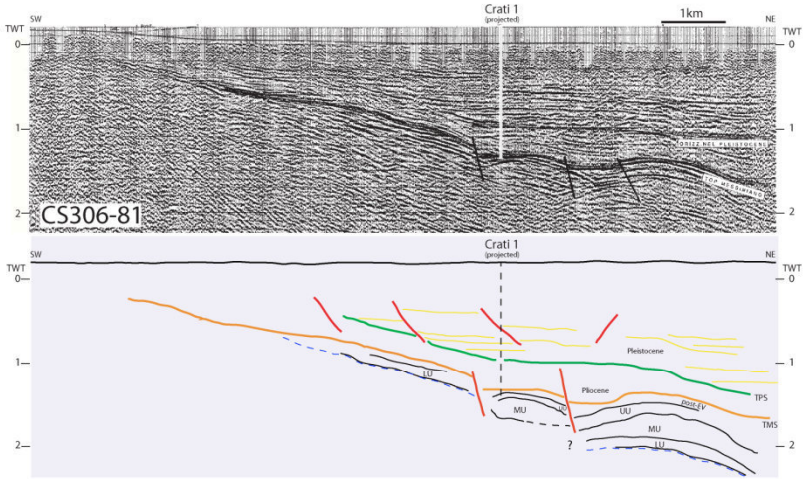

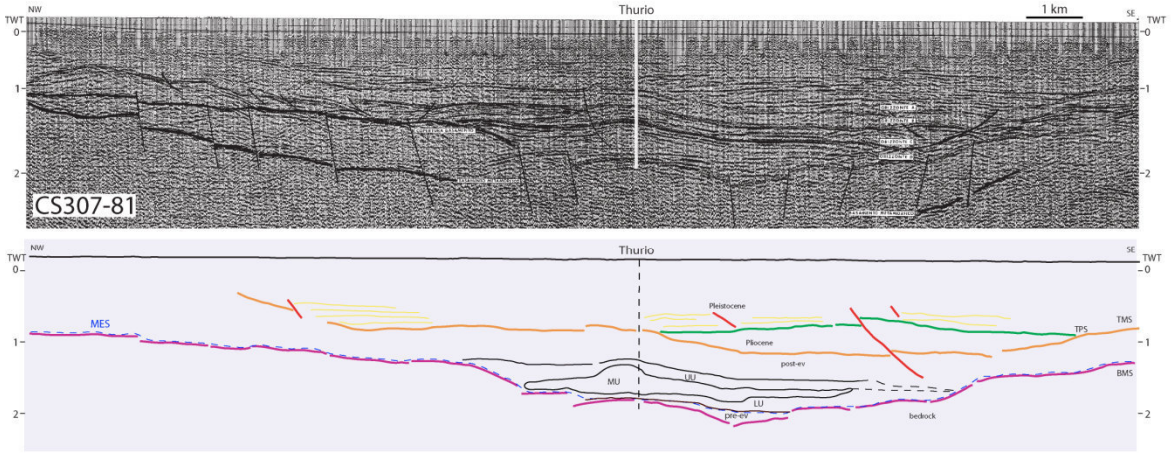

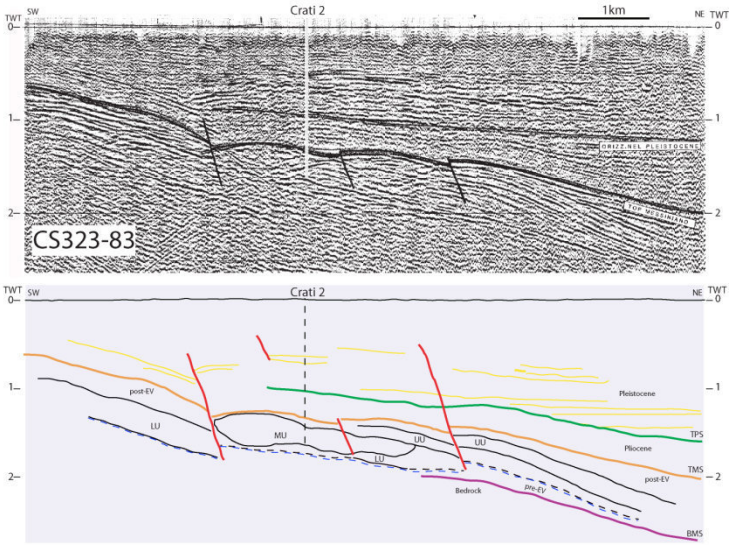

LEGEND

- TPS (Top Pliocene Surface)
- TMS (Top Miocene Surface)
- BMS (Bottom Miocene Surface)
- Statigraphic boundary
- Supposed statigraphic boundary
- Fault
- Messinian Erosional Surface

seismic facies

post-eV	post-evaporitic succession	
UU	Upper Unit	*Lofi et al. (2011)*
MU	Mobile Unit	
LU	Lower Unit	
pre-eV	pre-evaporitic succession	

corresponding lithostratigraphic facies

late Messinian terrigenous deposits
Messinian gypsum-bearing deposits (UG)
Messinian halite deposits
Messinian gypsum-bearing residemented deposits (RLG)
Serravallian-Tortonian deposits

continued …

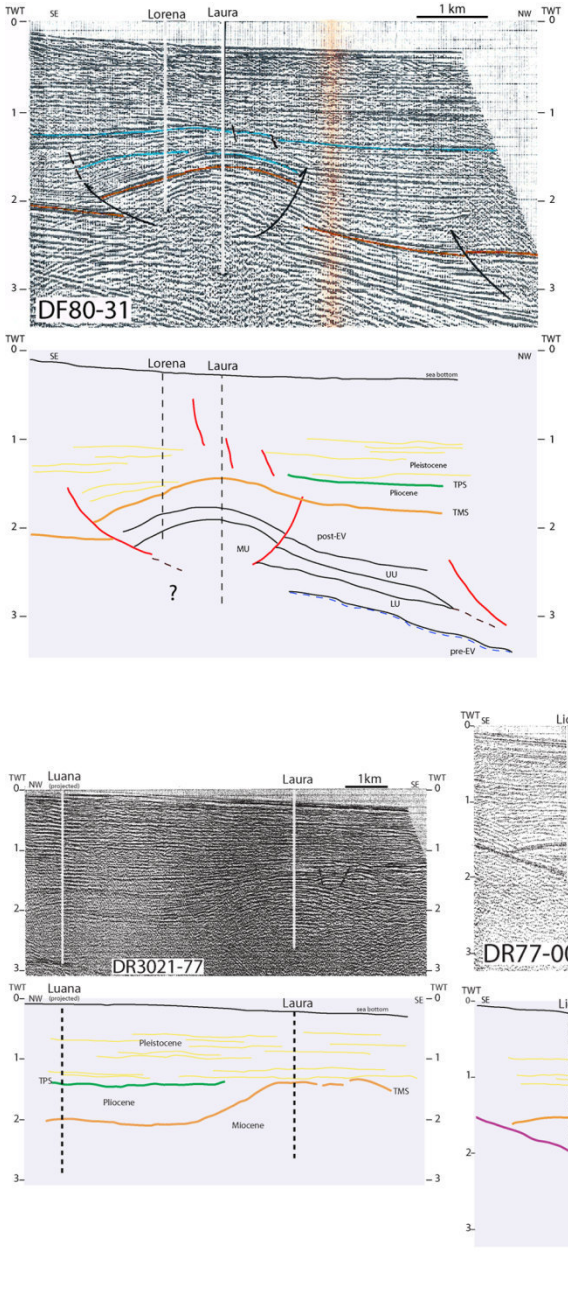
DF80-31
Lorena
Laura
1 km
SE
NW
TWT
Pleistocene
Pliocene
TPS
TMS
post-EV
MU
UU
LU
pre-EV
?
sea bottom
DR3024-77
Laura
(projected)
1km
Bedrock
BMS
DF80-11
DR3021-77
Luana
DR77-009
Licia
DR527
Lina
DR3025-77
SW
NE
Miocene
Bedrock

Fig.1.11. Interpretation of the ViDEPI multichannel seismic profiles. The main boundary surfaces (Miocene Bottom and Top, Pliocene Top) are recognized in seismic profiles. The MSC units identification is based on the description of the seismic MSC markers observed in the Mediterranean Sea by *Lofi et alii* (2011). The MES includes Margin Erosion Surface, Bottom Surface and Bottom Erosion Surface of *Lofi et alii* (2011). Vertical scale is expressed in twt (sec).

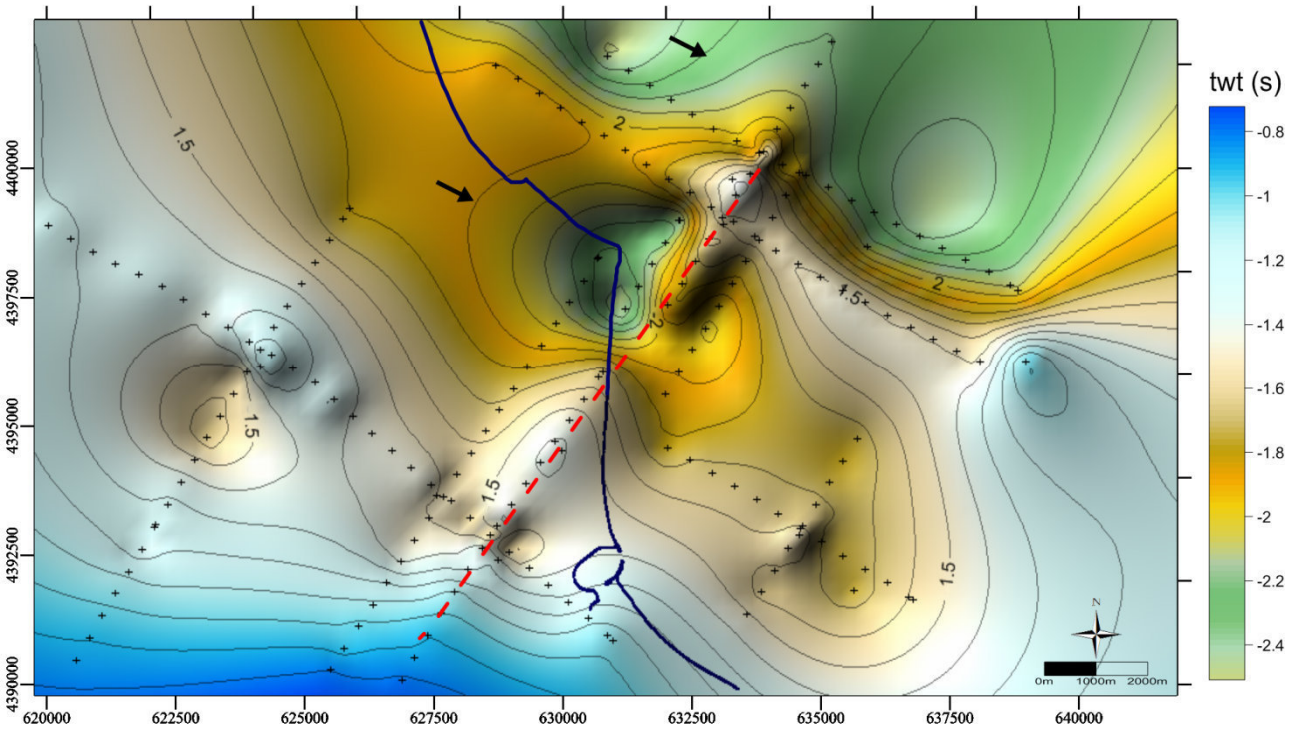

Fig.1.12. DSM of the Top Miocene Surface obtained by points (black crosses) interpolation. Dashed red line represents the supposes NE-SW strike-slip fault. Black arrows indicate the Pliocene depocenters.

1.8 Discussion

The analysis of well and seismic data allowed to identify the boundaries of the Tortonian-Messinian Sibari-Corigliano Basin. Along NW area the pinch-out of MSC succession (CS 307-81 profile) on Appennine margin (Saraceno Fm. and Albidona Fm.) defines the NW boundary in correspondence the Sangineto Line (*Ghisetti*, 1979; *Turco et al.,* 1990), which represents the junction between CA and SA domains (*Amodio Morellli et al.*, 1976; *Ghisetti*, 1979; *Van Dijk et al.*, 2000).

Along southern margin we observe the progressive thinning of the Tortonian-Messinian succession toward SW (CS304-81, CS306-81 and CS323-83 profiles) and its pinch-out over Calabrian terranes (Licia well and offshore DR527 and DR77-009 profiles).

The litostratigraphic descripition of the Tortonian-Messinian units and their stratigraphic relationship suggest that the Sibari-Corigliano Basin represents the northward extension of Rossano Basin and so of the foreland basins system of the northern CA during Tortonian-Messinian time. The MSC lithofacies association and their lateral thickness variations allow to identify the basin geometry. The thickeness of the Halite body decreases toward SE where a morphological

high (showed by CS307-81 profile and TMS DSM) is present. The shallower depth of the pre-Tortonian basement is recorded in this area by Licia well which shows also the absence of the Resedimented Lower Gypsum. This high can be considered as an intrabasinal high which marks the boundary between Sibari-Corigliano and Rossano Basins.

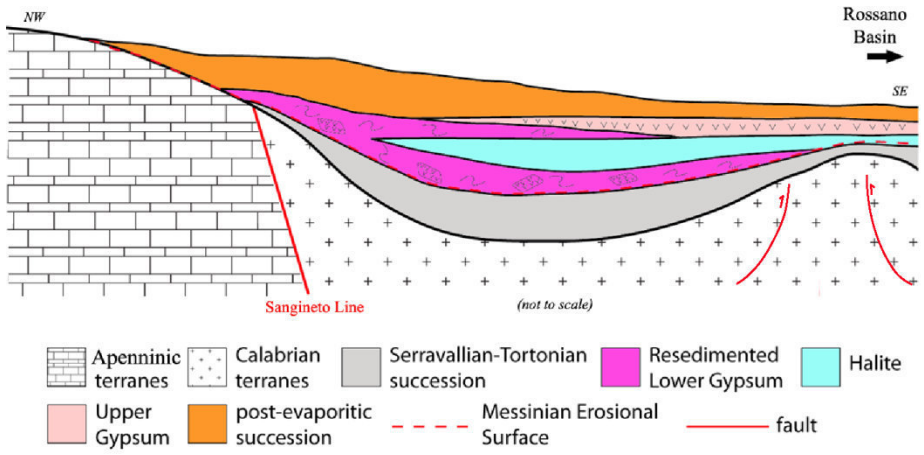

Fig.1.13. Stratigraphic scheme of the Serravallian?-Messinian succession of the Sibari-Corigliano Basin

Furthermore, the geometry of halite deposits does not show the presence of salt domes but reflects the deformation of BM and TMS.

The distribution of late Pliocene deposits logged by wells, their lateral pinch-out over morphological-structural highs observed in seismic profiles and the analysis of 3D reconstruction of TMS suggest the existence of two Pliocene depozones with WNW-ESE oriented axis. The external one corresponds to Plio-Quaternary main depozone described by *Bigi et al.* (1991) (fig.2) and *Del Ben et al.* (2008). The smaller internal depozone is confined between two WNW-ESE structural highs alignments. The latter, according to wells location, can be correlated with the WNW– ESE shallow-crustal folds involving Middle–Upper Quaternary sediments described by *Ferranti et al.* (2009), but unlike these the structures that we observe involve also Miocene succession and bedrocks.

The 3D reconstruction of TMS shows a NE-SW structural lineament with probably left-lateral movement which can explain the greater inland extension of Tortonian-Messinian succession in the area of the Crati Delta. The existence of NE-SW fault zone in this area was supposed by *Lanzafame and Tortorici* (1981), recently observed by *Cinti et al.* (2015 in press) inside archeological areas of Parco del Cavallo and Casa Bianca and in this work (Chapter 2). The post-Messinian activity of this lineament as a left-lateral strike-slip fault agrees to the development of regional high-angle tear faults and the dominant wrench tectonics in the northern Calabrian since the early Pliocene (*Knott and Turco* 1990; *Van Dijk et al.*, 2000; *Tansi et al.*, 2007).

We suppose the activity of the NE-SW structural lineament as a tear fault during Messinian time with generation of the structural high (previously described) which divides two main depozones (Sibari-Corigliano and Rossano Basins) and influences the MSC facies arrangement.

Tectonic activity, characterized by further development of thrust faults and related folds, during late Messinian are also observed as growing synsedimentary folds and similar structures in the offshore and in the upper Messinian succession of the Crotone Basin (*Roveri et al.*, 1992; *Barone et al.*, 2008) and in the Neogene Ionian foredeep (*Doglioni et al.*, 1999).

The migration toward NE of the depozones between Messinian and Pliocene time suggests that the evolution of the Sibari-Corigliano Basin is connected to the post-Messinian progressive CA thrusts front propagation (*Finetti et al.*, 1996; *Van Dijk et al.*, 2000; *Mattei et al.*, 2007; *Minelli and Faccenna*, 2010; *Vignaroli et al.*, 2012). During Tortonian-Messinian time thrusts front was 50-100km southward in respect to the present position inside the Taranto Gulf; in the foredeep depozone happened the deposition the MSC lithofacies characterized by an association which can be correlated with the sedimentary fill of the Caltanisetta and other circum-Mediterranean Basins foredeep (*Roveri et al.* , 2008; CIESM, 2008; *Lofi et al.*, 2011). Within Miocene end and early-Pleistocene carried on the propagation of the accretionary wedge toward the foreland, supported by opening and oceanization of the back-arc Vavilov Basin (*Gueguen et al.*, 1998; *Faccenna et al.*, 2004; *Minelli and Faccenna*, 2010). The thrusts-front moved northward and caused the deformation of Tortonian-Messinian succession; the main Basin depozone is now located northeastward with a internal smaller depocenter, confined between structural highs. During the following time the propagation of the accretionary wedge went on, supported by rapid oceanization of the Marsili Basin between 3Myr and 2Myr (*Kastens et al.*, 1988; *Sartori*, 1990; *Gueguen et al.*, 1998; *Marani and Trua*, 2002; *Rosenbaum and Lister*, 2004; *Nicolosi et al.*, 2006) and with fast rate connected to the presence of the evaporitic sequence which works like a preferential detachment level (*Minelli and Faccenna*, 2010), arriving at the actual position inside Taranto Gulf and involving also Pliocene succession (*Critelli*, 1999; *Van Dijk et al.*, 2000).

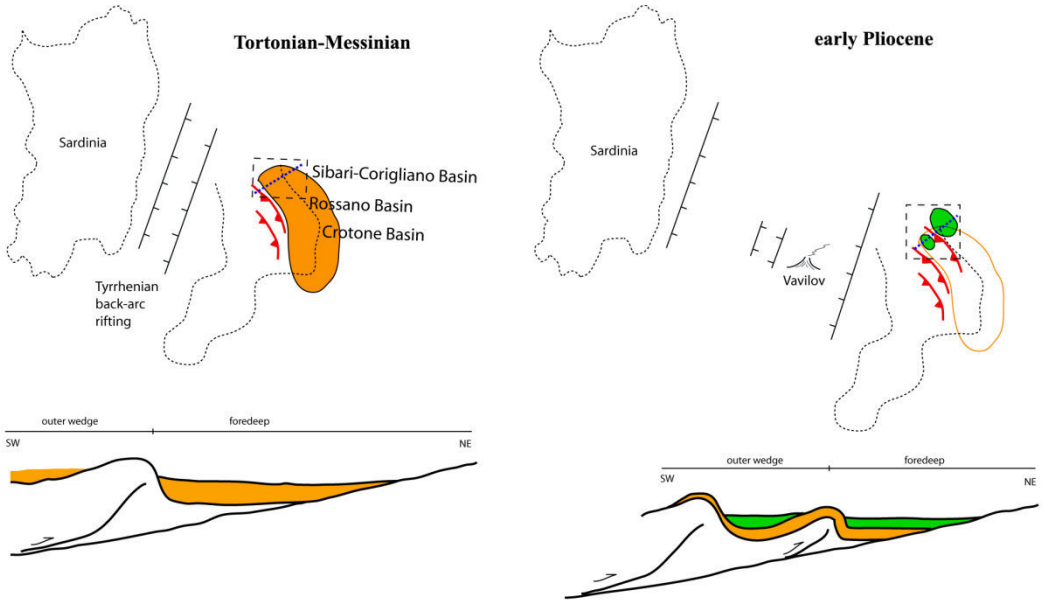

Fig.1.14. Schematic paleotectonic sketch showing the evolution of the Sibari-Corigliano Basin during Tortonian-Messinian (left) and early Pliocene (right).

1.8 Conclusions

The interpretation of seismic and well data, based on the modern knowledge about MSC facies association, allowed the reconstruction of Mio-Pliocene stratigraphic architecture of Sibari-Corigliano Basin and its tectono-sedimentary evolution.

During Tortonian-Messinian time this Basin represents the northernmost extension of CA foreland basin systems with a sedimentary fill made by evaporitic and clastic facies association very similar to the Crotone and Rossano Basins.

The sedimentation in the Sibari-Corigliano Basin is strictly related to the Messinian Salinity Crisis and to the progressive eastward migration of the foreland depocentres, locally controlled also by the activity of a NW-SE tear fault. The latter acts as a left-lateral strike slip fault also in post-Messinian time, according to the wrench tectonic, beginning in the early to middle Pliocene, which prevails in northern CA partitioning previous wedge-top depozones (*Knott and Turc,o* 1990; *Van Dijk et al.*, 2000; *Tansi et al.,* 2007; *Barone et al.*, 2008).

CHAPTER 2

Holocene evolution of the Sibari Plain

2.1 Introduction

The Sibari Plain (SP) is located in the northeastern Calabrian Arc (CA) where the geodynamic setting is characterized by the junction between CA and the Southern Apennine and between the Ionian Basin crust (southward) and the crust of the Apulian platform (northward).

The CA tectonic evolution is related to subduction and rollback of Ionian oceanic lithosphere and the slow convergence between the Eurasian and African–Adriatic continental plates (*Malinverno and Ryan*, 1986; *Faccenna et al.*, 1997; *Gueguen et al.*, 1998; *Wortel and Spakman*, 2000; *Jolivet and Faccenna*, 2000; *Rosenbaum and Lister*, 2004*; Mattei et al.*, 2007; *Chiarabba et al.*, 2008).

The SP is characterized by a low to moderate seismicity while, moving westward, high seismic activity is recorded in the near Pollino mountain chain.

Recently, new information concerning the active tectonics of the SP is shown by *Cinti et al.* (2013, 2015 in press) and an active oblique-contractional belt has been recognized in the Corigliano Gulf (*Ferranti et al.*, 2014).

The shallow stratigraphic framework of the SP records a complex Holocene evolution and arrangement of the depositional elements which can be ascribed to the control on the morphological pattern due to a NE-SW fault system, with dip-slip component, which can be traced thanks to the constraints provided by new shallow geophysical data acquired in the SP.

The progradation of the Crati Delta took place in the tectonics-controlled coastal plain and was driven by the interaction between sea-level variations and local factors (tectonics, climate, anthropic activities). The delta presents a stratigraphic framework and a timing which can be related to other Italian (*Bellotti et al*., 1995; *Amorosi and Milli*, 2001; *Stefani and Vincenzi*, 2005) and Mediterranean (*Coutellier and Stanley*, 1987; *Stanley and Warne*, 1994; *Somoza et al.*, 1998) deltas.

2.2 Geological setting

The SP stays between Sila Massif to the South and Pollino Massif to the North. The SP represents a tectonic depression bounded by dislocations related to plio-holocenic high angle faults. In the NW boundary the SP is delimited by the NW-SE normal fault system of the Sangineto Line (*Lanzafame and Tortorici*, 1981; *Bigi et al.*, 1992) non-active in recent time (*Cucci*, 2004). *Ferranti et al.*(2009) define this system Avena-Lauropoli Fault and interpret it as a listric normal fault system with relatively shallow roots. The boundary with Sila Massif consists of the WNW-ESE Rossano-Corigliano fault interpreted as a normal-oblique system (*Ciaranfi et al.*, 1983; *Knott and Turco*, 1991) and which probably represents the surface expression of the Palinuro Line (*Moretti*, 2000). About its activity, the Rossano-Corigliano fault is considered an active fault (*Galli et al.,* 2000; *Molin et al.,* 2004), a seismogenetic source (*Valensise and Pantosti*, 2001) and a non-active fault (*Cucci*, 2004).

Torward the west side, a series of structural highs and small basins (Castrovillari, Mormanno) break the continuity of the SP. The fault system is related to NNW-SSE Castrovillari fault, which is considered the potential seismogenetic source in the area of Pollino seismic gap (*Cinti et al*., 1997) and to NW-SE Pollino fault interpreted as: a right-lateral strike-slip fault active until late Pleistocene (*Ghisetti and Vezzani*, 1982); a left- lateral strike-slip fault active until early Pleistocene or between late Pleistocene and Holocene (*Moussat et al.*, 1986; *Colella and Cappadona*, 1988; *Turco et al.* ,1990; *Russo and Schiattarella*, 1992; *Van Dijk et al.*, 2000); an active normal fault (*Vittori et al.,* 1995; *Ferrelli et al.*, 1996). The latter hypothesis contrasts with *Cucci and Cinti* (1998) who do not observe marine terrace dislocations between foot wall and hanging wall of this fault.

Lanzafame and Tortorici (1981) suppose the existence of NE-SW normal fault in the area of the Crati Delta; recently evidences of a NE-SW structural lineament (fractures with relative displacements, paleoliquefaction phenomena, rotation of walls, complete walls tearing down) active up to the period between the II and the VII-IX century A.D. are observed in Parco del Cavallo and Casabianca archeological sites (*Cinti et al.,* 2013, 2015 in press).

Ferranti et al. (2009) suppose the existence of WNW– ESE shallow-crustal folds, involve late Middle Pleistocene sediments, grown within a recent and still active transpressional field. Recently, *Ferranti et al.* (2014) describe the presence of an active oblique-contractional belt in the Corigliano Gulf which testify the major compressive active horizontal stress present in this Calabrian Arc sector inferred by the focal mechanism of recent earthquakes in this area (*Pondrelli et al*., 2006).

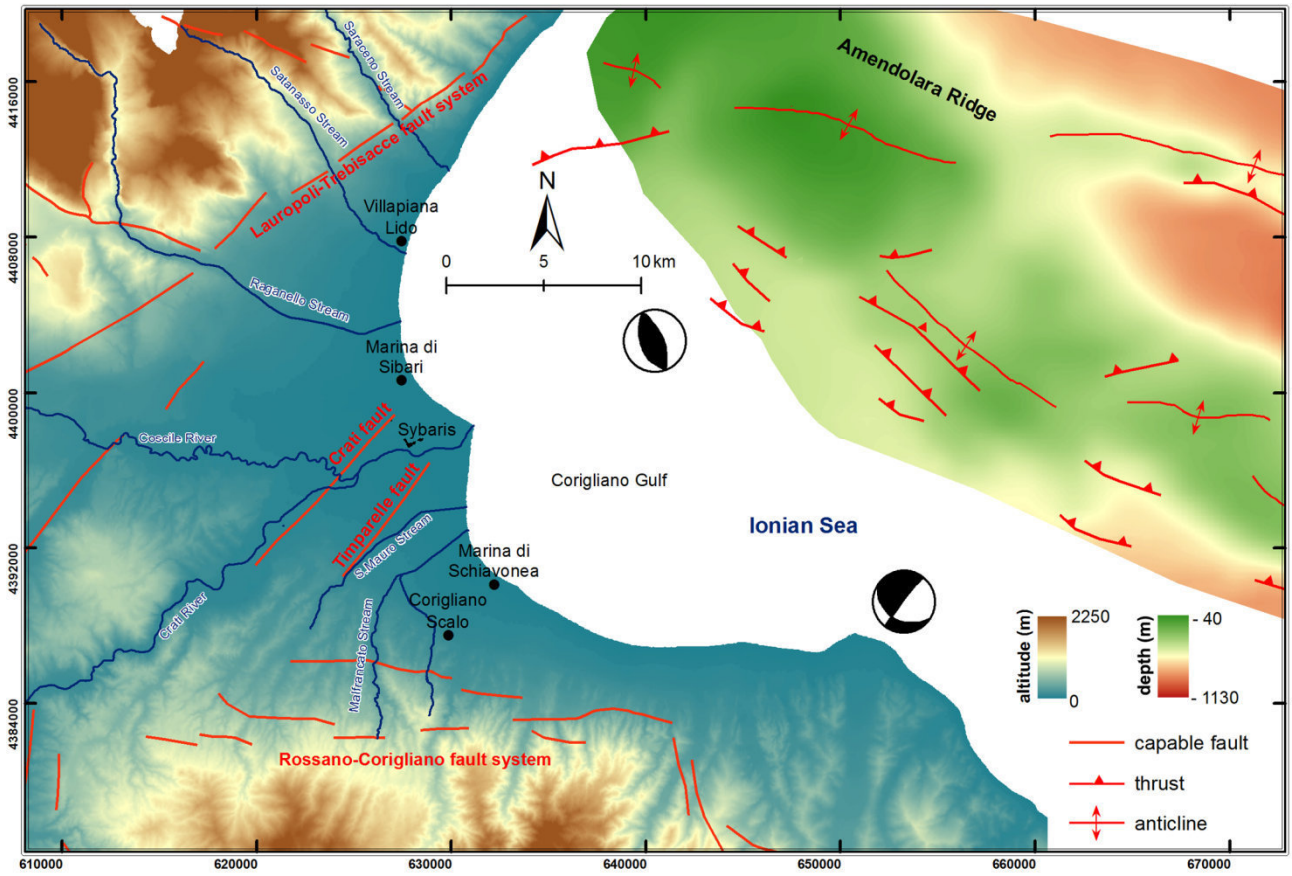

Fig. 2.1. Map of the main tectonic element of the Sibari Plain and Corigliano Gulf: trace of capable fault systems (*ITHACA*), thrusts and anticlines of the Amendolara Ridge (*Ferranti et al.*, 2012). Focal mechanisms (*Pondrelli et al.*, 2009) show a major compressive active horizontal stress.

Marine terraces are recognized along Sibari Plain outer limit. 7 terraces orders are identified by *Cucci and Cinti* (1998) which estimate a average uplift rate, active also during Holocene, of 0,85mm/yr, *Cucci* (2004) maps 5 orders of marine terraces and calculates an average uplift rate of ~1 mm/yr. The marine terraces are 11 in *Santoro et al.* (2009) which evaluate uplift rates, since middle Pleistocene, variable from >3.5mm/yr to 0.5mm/yr.

Holocenic morphological evolution of the plain is strictly related to the Crati Delta progradation (started about 6kyr B.P.) in the middle sector while toward NW the main morphological elements are represented by Raganello and Satanasso Streams alluvial fans active since the middle Pleistocene (*Guerricchio and Melidoro*, 1975).

The Crati River plain represents a cuspate double-winged delta, build by the filling up of coastal lagoons bordered by ridges (*Bellotti et al.*, 2003). The migration of the Crati Delta toward the present position starts at the end of the post-glacial sea level rise (5-6 kyr B.P.) when its mouth was located 2 km eastward from the archeological site of *Favella della Corte* (*Bellotti et al.*, 2003, 2009). The Holocene evolution is controlled by the post-glacial sea level rise, sediment supply of the Crati River and other streams (e.g., Coscile and Garda Rivers, Raganello and Satanasso

Streams) which flowed into the plain, tectonic activity and human-made factors (*Guerricchio and Melidoro*, 1975; *Bellotti et al.*, 2003, 2009; *Pagliarulo*, 2006). During the late Pleistocene, after the Last Glacial Maximum (about 22 kyr B.P.), the level of the Ionian sea was -140m lower than the present one (*Pagliarulo*, 2006 and references therein) and in the study area the shoreline was 0.7-2.2 km more seaward as today (*Bellotti et al.*, 2003). At this time, the development of a alluvial plain was made by the many rivers wandering through the coastal plain. Later, the fast post-glacial sea level rise caused the plain drowning with the development of a large lagoon wherein Coscile River debouched while the Crati River flowed into the sea southward from the present mouth (*Bellotti et al.*, 2003). During this stage, the cold period of the Younger Dryas (about 11kyr B.P.) is recorded in the study area by coarse-grained deposits (*Pagliarulo*, 2006). At the end of the fast post-glacial sea level rise (about 6 kyr B.P.), the coastal system was characterized by a gulf with several river mouths was present and the shoreline was located close to the present 15m-contour line (*Guerricchio and Ronconi*, 1997; *Bellotti et al.*, 2003, 2009). The gulf has been gradually filled by the development of the Crati Delta and alluvial fans of the streams draining the Pollino Massif. During the delta evolution, the SP was characterized by a instable hydrography with repeated captures between Crati and Coscile Rivers (*Guerricchio and Melidoro*, 1975; *Bellotti et al.*, 2003, 2009).

The late Holocene evolution of the Crati Delta was analyzed by various authors (*Bellotti et al.*, 2009; *Stanley and Bernasconi*, 2009, 2012; *Bernasconi et al.*, 2010) taking advantage of the historical information relating to the three ancient Greek (Archaic and Classical periods) and Roman sites built on the delta area.

Guerricchio and Melidoro (1975) detect, using infra-red aerial photographs, present and fossil river beds, fossil dunes and moist areas. *Guerricchio and Ronconi* (1997) trace the paleoshorelines starting from the 1500 A.D. and highlight traces of archeological structures southward from the present Crati Riverbed.

Fig.2.2. Fossil riverbeds traced by *Guerricchio and Melidoro* (1975). The main paleo-channels are related to Crati, Coscile and Garda Rivers. In the offshore area, morphometric map of the Crati Submarine Fan (*Ricci Lucchi et al.*, 1984).

Bellotti et al. (2003), through the analysis of well data, recognize six depositional elements which characterized the surface stratigraphy of the delta area. The deepest element, defined *Braided Fluvial Channel*s, is present at least 70m of depth below the field surface and is made by sands and gravels with late Pleistocene age. It passes upward to mud deposits characterized by brackish fauna, peat and sand beds (*Coastal Barrier Lagoon* element), with an age between 10 and 6 kyr B.P. and a depth variable from -60 and -20m below the field surface. Locally, marine mud with infra- and circalittoral fauna (*Shoreface and Transitional Shelf* elements) are present on top or heteropical with the previous depositional element. The *Coastal Barrier Lagoon* element passes upward to muddy sand with gravel beds and lenses and occasionally vegetal remains (*Inner Delta Plain* element) deposited during the last 6kyr B.P.. Close to the sea, the succession is closed by gravelly sands with littoral fauna (*Outer Delta Plain* element) related to beach and dune ridges mainly developed since 3kyr B.P.

The emerged delta shows different morphological features between right and left delta wings (*Bellotti et al.*, 2003, 2003-2004). The right wing is about 3m higher than the left one and is characterized by the Crati fossil riverbeds traces. On the left wing the ridges (ancient and present) have a better longitudinal development and a greater space one from the other compared to the right wing.

Bellotti et al. (2009) recognize and describe four evolution stages from Neolithic period to present days. In the period 7-4.8 kyr B.P. The Neolithic landscape was characterized by a sea level 20m lower than the present one; the Crati River flowed into the Ionian Sea 2 km eastward from *Favella della Corte* village (about 4.5 km westward from the present coastline) while the Coscile River flowed into the more inland sector of the gulf. Later, during the Sybaris time (2.7-2.5 kyr B.P.) the sea level rise, the Crati Delta moved 3 km northward and 2 km eastward and the Coscile River

continued to flow into the lagoon. From 2.4 to 1.4 kyr B.P. (Greek and Roman period) the Crati advanced more slowly, probably due to the dry climate and the lagoon was gradually filled. During the Middle Ages, the climate deterioration mainly due to the Little Ice Age, caused the flooding and the burial of the Copiae city. At the end of 1980s, the reclamation of the area started and has been gradually produced the present morphological setting. Furthermore, *Bellotti et al.* (2009) add a more detailed paleo-beach ridges location and the location of two Greek-Roman paleobeds of the Crati River in the Lattughelle area to the morphological features proposed by *Guerricchio and Melidoro* (1975).

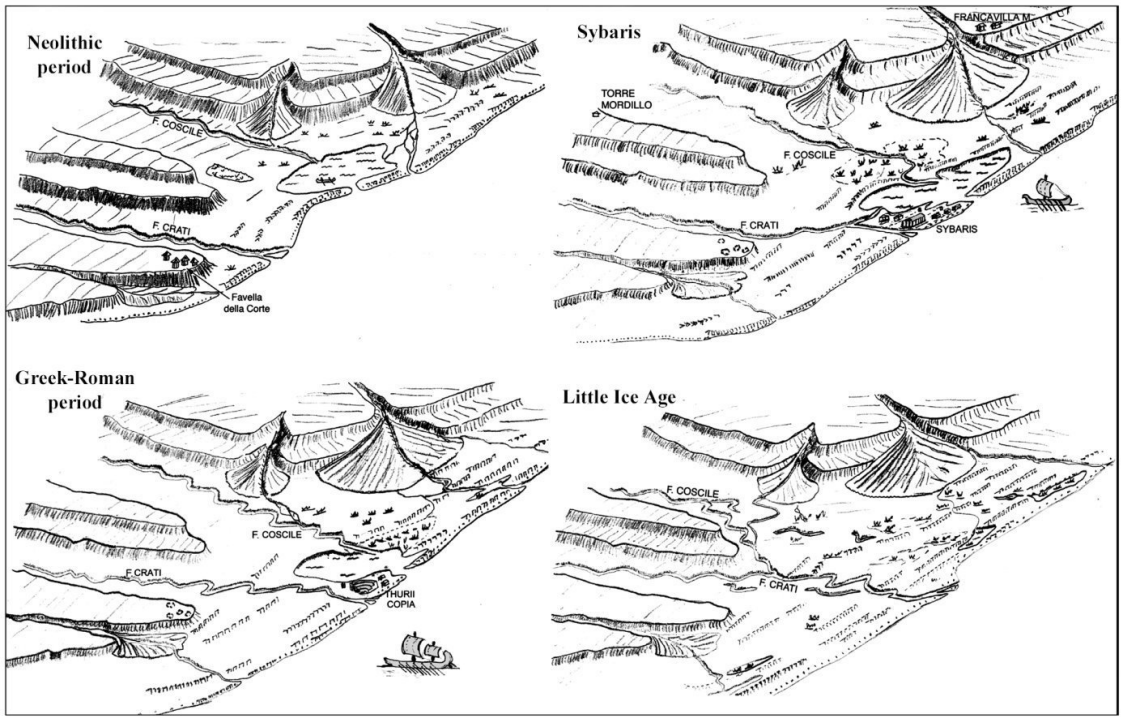

Fig.2.3. Reconstruction of the landscapes from the Neolithic period by *Bellotti et al.* (2009)

Stanley and Bernasconi (2009) and *Bernasconi et al.* (2010) by means of the ecobiostratigraphic analysis of two cores, realized in the Casa Bianca archeological site, observe the evolution from marine to coastal, wetland, and then terrestrial environments, associated with the seaward progradation of the Crati Delta. In detail, the Authors recognized a lower biofacies (Neolithic) with faunas typical of an open marine inner shelf environment, a middle biofacies (late Neolithic) with a poor faunas, mixed with plant matter, indicates a very high energy conditions close to shore and an upper biofacies (early Bronze age to present) with a very meager and mainly terrestrial faunas due to the growing fluviodeltaic influence.

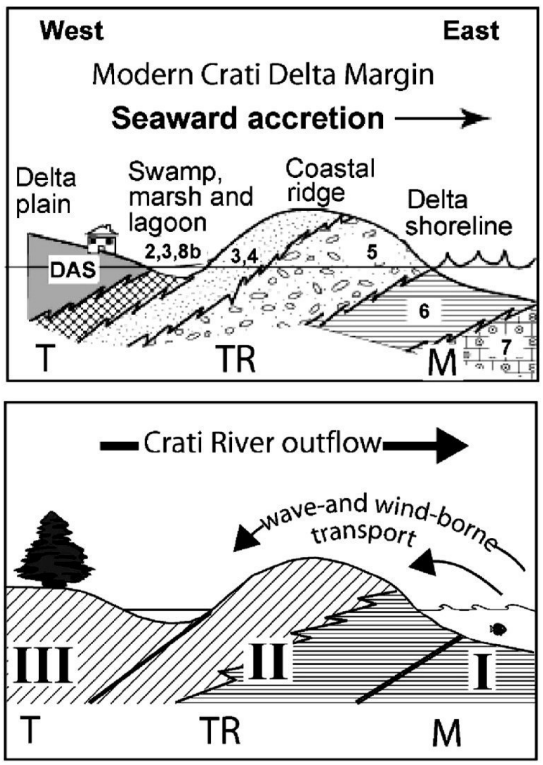

Fig.2.4. Reconstruction of sedimentary facies and depositional environments in the Casa Bianca archeological site (from *Bernasconi et al.*, 2010). M=marine, TR=transitional, T=terrestrial

In front of the Crati mouth, a small (70km^2) submarine fan is present (*Ricci Lucchi et al.*, 1984). The Crati submarine fan has a distorted and east-west elongated shape ad it is characterized by a mud cover due to a mud-rich system fed by the river. The channel system of the fan consists of a main northern trunk and a subordinate southern one, related in the outer fan to two depositional lobes. *Ricci Lucchi et al.* (1984) date the start of the fan growth at 5-6kyr B.P. and recognize in the seismic reflection profiles the presence, on the acoustic basement, of a Pleistocene and Holocene layer underlying the fan deposits. The mud that made the surface fan cover represents the product both of the sediment load discharged by the Crati River and of the littoral processes and reaches the submarine basin via turbidity currents and superficial turbid plumes (*Colella and Di Geronimo*, 1987).

Romagnoli and Gabbianielli (1990) recognize, in the Corigliano Basin, a regional unconformity surface overlaid by a sedimentary body related to the post-glacial high stand and widespread processes of mass-wasting and liquefaction.

2.3 Historical data

Historical maps allow to observe the space and temporal variations of the hydrographic pattern during the last 400 yr. The Crati and Coscile Rivers had a single mouth up to the beginning of 1500 A.D., during the second half of the 1500 A.D. the two rivers were divided while about in the 1800 A.D. the mouth was again single. Furthermore, the transition from double to single mouth around the 1800 A.D..

Historical map	Date (A.D.)	mouths
Tabula nova Italie (M. Beneventanus)	1508	unique
Calabriae Descript. (P. Parisio)	1589	double
Calabria Citra (G.A. Magini)	1620	double
Calabria Citra (H. Hondius)	1627	double
Calabre Citra (W.J. Blaeu)	1640	double
Calabria Citra (A. Bulifon)	1650-1700	double
Calabria Citeriore (G.A. Rizzi Zannoni)	1783	double
Der Napoletanischen Landschaft Calabria Citra (F.J.J. Reilly)	1791	double
Atlas of Regno di Napoli (G.A. Rizzi Zannoni)	1808	unique
Carta delle provincie continentali dell'ex Regno di Napoli. Section10 ColonnaVIII	1822	unique
Provincia di Calabria Citeriore (A. Zuccagni Orlandini)	1840	unique
Provincia di Calabria Citeriore (B. Marzolla)	1851	unique

Table 2.1. Information on Crati and Coscile mouths inferred by historical maps

Fig. 2.5. Historical maps of the Sibari Plain: on the left *Calabria Citra* by C.A.Magini (1602 A.D.) showing two separated mouth for Crati and Coscile Rivers, on the right *Regno di Napoli, Section10 ColonnaVIII* (1825 A.D.) in which the two rivers had a single mouth.

Northward from the Crati River, the historical maps show an instable drainage network characterized by streams (e.g., Garda Stream) flowed into the Ionian Sea while currently they are tributaries of the Coscile River. Moreover, the existence of marshes/lagoons northward of Coscile River between Crati and Coriglianeto Rivers is shown.

Crati and Coscile Rivers captures and avulsions can be deducted also by historical reports. In the 710 B.C., the city of *Sybaris* was founded by the *Achaeans* between *Sybaris* and *Crathis* Rivers (*Strabo*, VI, 1, 13); in the 510 B.C. after the *Traes* River battle, *Sybaris* was destroyed by Crotonians which diverted the *Crathis* River on the enemy city (*Strabo*, VI, 1, 13; *Diodorus Siculus*, XII, 9, 2; *Herodotus*, V, 45). A single river mouth existed also in the 413 B.C. (*Thucydides.*, VII, 35, 1) while in the I century A.D. the two rivers were divided (*Plinio il Vecchio*, III, 97). Probably, the historical *Crathis* riverbed migration can be ascribed to natural causes and not to anthropic activity (*Guerricchio and Melidoro*, 1975; *Taliano Grasso*, 2004).

Taliano Grasso (2004) highlights, through a discriminating rereading of the historical sources, that probably the *Sybaris* and *Crathis* Rivers mentioned by the historical authors correspond respectively to the present Crati and Coscile Rivers and not conversely.

2.4 Well data description and interpretation

The shallow stratigraphic framework of the study area is investigated by well-logs data from bibliographic sources (*Guerricchio and Melidoro*, 1975; *Bellotti et al.*, 2003; *Bernasconi et al.*, 2010; *Cherubini et al.*, 2000; Demanio Idrico della Provincia di Cosenza; Archivio nazionale delle indagini nel sottosuolo L.464/84; ViDEPI) and inedited (B1 and B2).

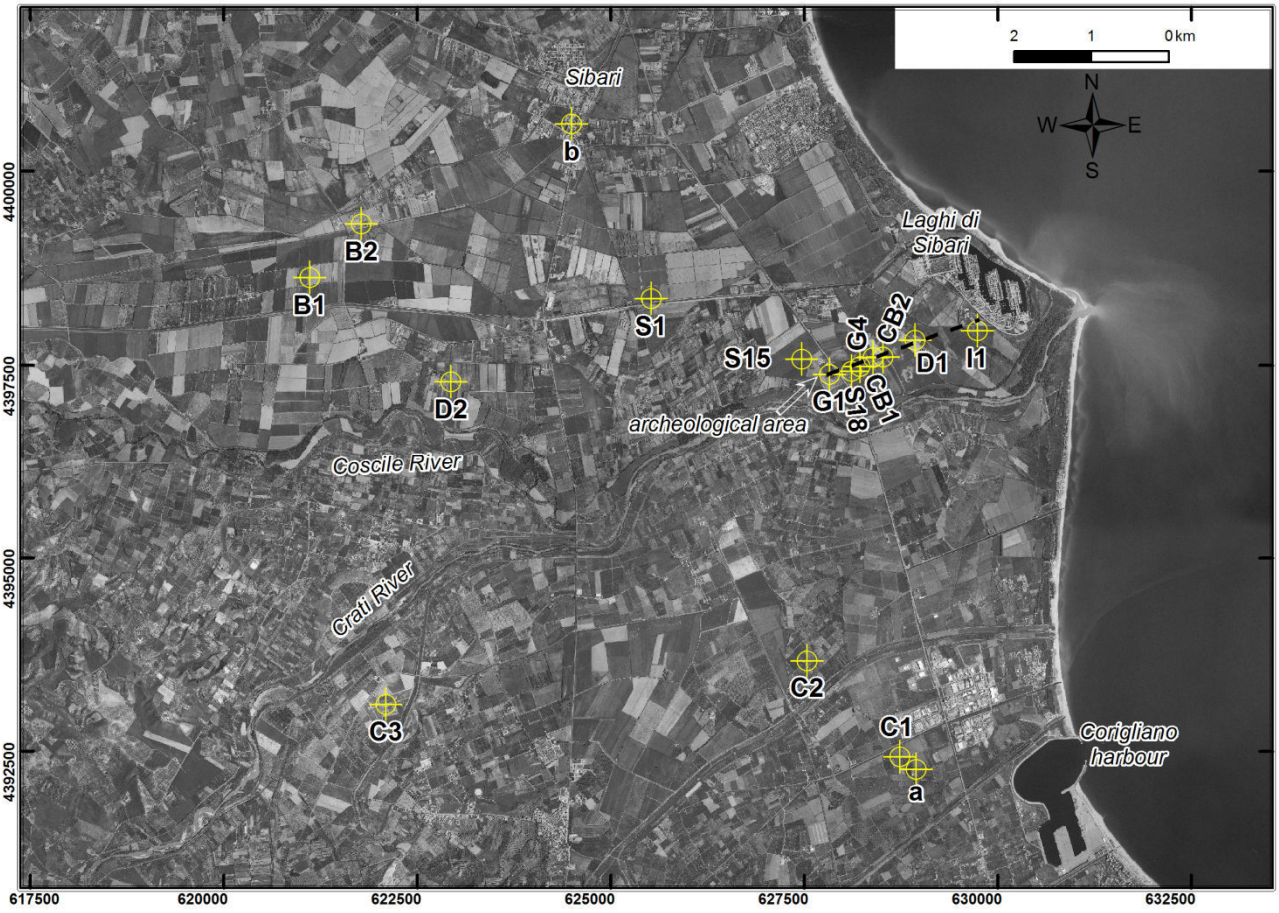

Fig. 2.6. Location of the analyzed well-logs. Dashed black line represent the trace of cross-section in fig. 2.7.

During the well-logs analysis, the study area has been divided in three sectors: two sectors respectively northward and southward referring to the present Crati Riverbed and another one between the archeological settlement and the current coastline.

In the sector close to the *Sybaris* archeological area, the well-logs acquired by scientific papers allow to create a stratigraphic cross section and to recognized four stratigraphic units (fig. 2.7).

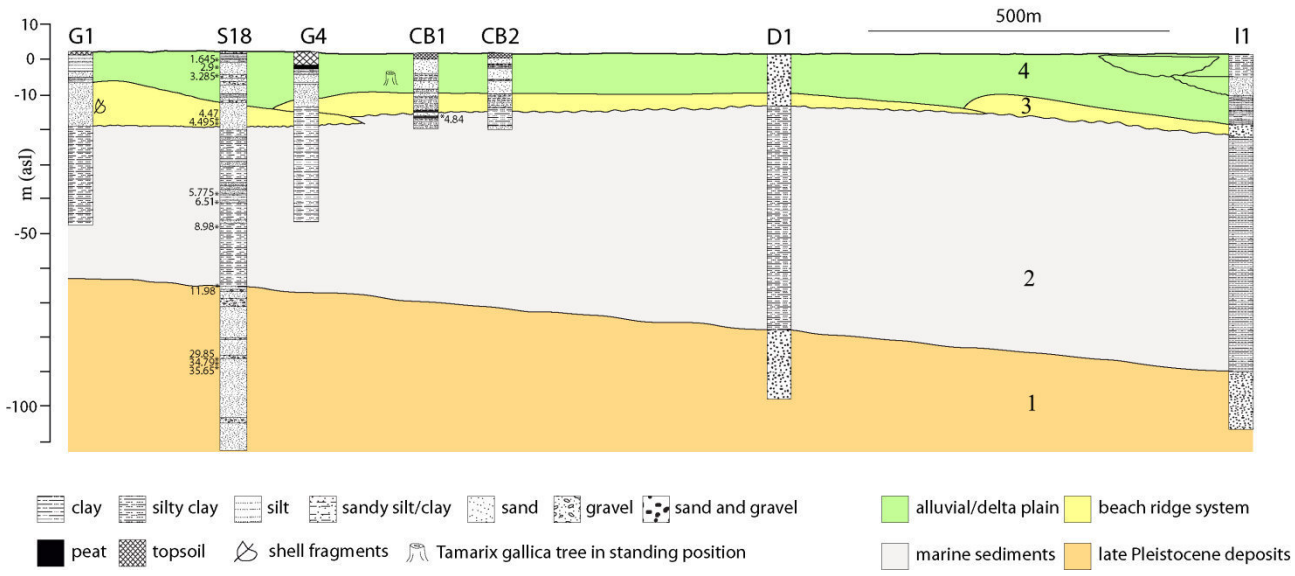

Fig. 2.7. Stratigraphic cross section of the area between archeological site and present coastline.

The lower unit (1) made by sandy-gravelly deposits with a top surface, dated about 12 kyr B.P. based on S18 well-log carbon dating (*Cherubini et al*., 2000), characterized by a depth increasing seaward (from 60 to -90m asl). Upward, a thick clayey-silty wedge-shaped body (unit 2) with sandy intercalations is observed. The microfauna analysis available for G1 and G4 well-logs (*Guerricchio and Melidoro*, 1975) show the presence of a mainly benthic and planktonic foraminifera association at about -50m asl and between -20 and -40m asl. The ecobiostratigraphic analysis of CB1 and CB2 (*Bernasconi et al*., 2010) highlights from -15 to -20m asl molluscan species characteristic of a shallow marine (inner shelf) setting. The top surface of this unit can be dated at about 5 ky B.P. based on carbon dating available for S18 (*Cherubini et al*., 2000) and CB1 (*Bernasconi et al*., 2010) well-logs.

Upward, sandy deposits (unit 3) lie on top of clayey-silty body. In G4 well-log (*Guerricchio and Melidoro*, 1975) a layer made by coarse grained sand with shallow water molluscan association (*Corbula Gibba* and *Acteon Tornatilis*) is recorded at -20m asl. In CB1 well-logs *Bernasconi et al*. (2010) recognize from -16.5 to -9 asl a lower molluscan diversity and abundance including *Chamelea gallina*, *Smaragdia viridis*, and *Lentidium mediterraneum*. In CB2 well-log, the authors describe, between -16 to -10m asl, a biofacies including *Tellina pulchella*, *C. gallina*, *L. mediterraneum*, and *Donax semistriatus* indicating a shallow sandy infralittoral zone.

The sandy layer is overlain by a mainly silty-clayey lithofacies with intercalation peat layers and coarse-grained deposits (unit 4). Toward its top, CB1 and CB2 well-logs (*Bernasconi et al*., 2010) are characterized, respectively from -9m and -10m asl, by few benthic forams, vegetal components, terrestrial gastropods (*Cernuella lineata* and *Helix ligata*), human artefacts and terrestrial vertebrates. In the logs of archeological excavation of Casa Bianca site, *Guerricchio and Melidoro*

(1975) observe a *Tamarix gallica* tree (dated at 2.33 kyr B.P.) in standing position at -4.5m asl and *Cerastoderma lamarcki* shells (0.86 kyr B.P.) at -2.15m asl. Moreover, in Parco del Cavallo area *Helix* shells (1.595 kyr B.P.) are recorded at 0m asl. Fossil channels are observed in the easternmost sector where are also clearly visible in air photo (fig. 2.8).

Fig. 2.8. 1954 I.G.M. air photo showing a paleomeander (indicated by the arrow) of Crati River close to the present coastline.

We assign a late Pleistocene age, based on the carbon dating of S18 (*Cherubini et al.,* 2000), to the lower stratigraphic unit. It is interpreted as a mainly coarse-grained coastal plain developed during the late Pleistocene when in the area the sea level was about 140m lower than the present one (*Lambeck et al.*, 2004). Toward the top, this unit probably records both erosion surface and deposits due to the last post-glacial marine ingression. The presence of an erosion surface can partially explain the average sedimentation rate of about 1mm/yr between 29.85 and 11.98 kyr B.P. calculated referring to S18 well-log (*Cherubini et al.,* 2000).

Upward, the faunal and microfaunal assemblages reveal a bluntly marine environment for the over clayey-silty sediments.

The wedge-shaped sandy bodies on the top of marine deposits is interpreted a transitional zone, as suggested by faunal assemblage, which can be referred to a beach ridge system according to *Stanley and Bernasconi* and *Bernasconi et al.* (2010).

The uppermost stratigraphic unit is clearly constituted by continental deposits recognizable by fossiliferous content, plant matter, tree in growing position and human artefacts. We suggest a delta/alluvial plain environment for these deposits.

We analyzed also well-logs located in northern and southern sectors referring to the Crati River, from Sibari village to the Corigliano harbour.

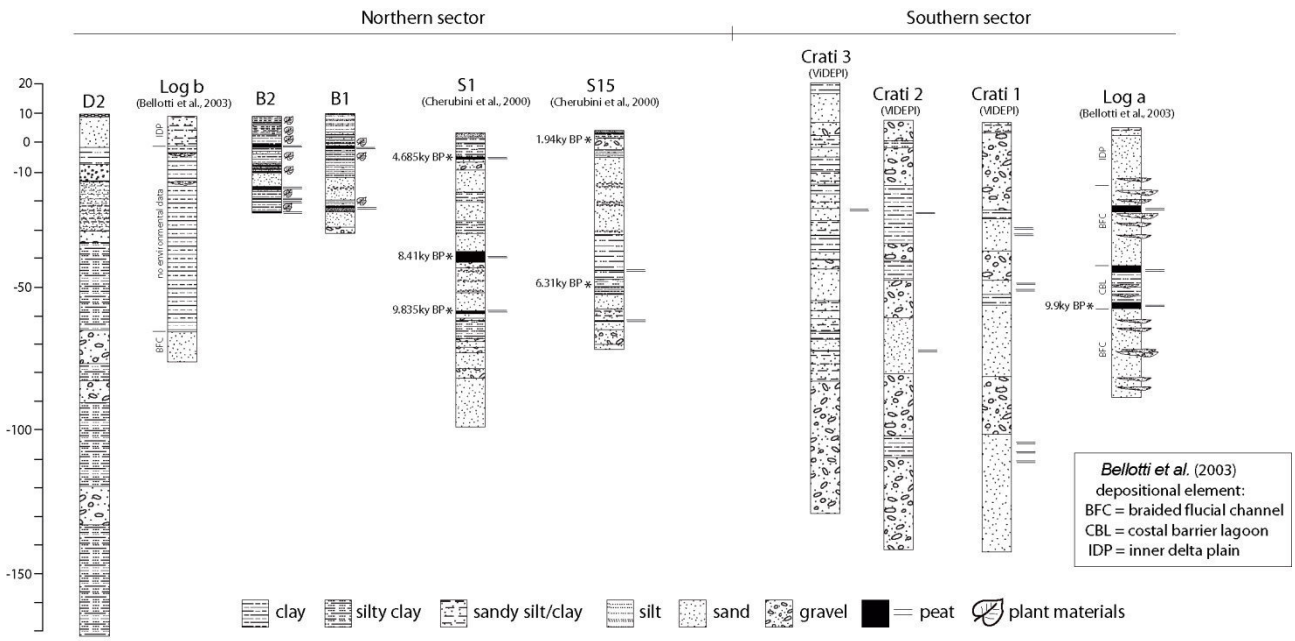

Fig. 2.9. Well-logs analyzed in the northern and southern sectors (referring to present Crati riverbed).

The northernmost well-log b (*Bellotti et al*., 2003) shows a lower stratigraphic unit (from -65 to -75m asl) made by sandy deposits with lens-shaped gravelly bodies passing upward to a 63m-thick clayey deposits with gravelly intercalation toward the top. The succession is closed by 10m-thick sandy-clayey layer. *Bellotti et al.* (2003) interpreted the lower unit as braided fluvial channel deposits and the top one to a inner delta plain environment while no environmental data are available for the middle clayey layer.

Toward SW, B1 and B2 well-logs (this work) crosses fine-grained (clay, silty-clay and silt) deposits rich of plant materials and peat intercalations (up to -25m asl) with sandy and gravelly layers (thick up to 7.5m).

The S1 well-log (*Cherubini et al.,* 2000), records a lower unit (from -68.5 to -100m asl) consists of sandy and gravelly deposits which pass upward to an alternation of coarse-grained (sand and gravel) and silty-clayey layers. Three peat layers (thick up to 3.5m) are present between -5 and -59m asl and are dated respectively at 9.835, 8.41 and 4.685 kyr B.P..

The D2 well-log (*Demanio Idrico office*) is characterized, from -30 to -170m asl, by an alternation of dm-thick silty clayey deposits and m-thick gravelly layers. Upward, the succession is made by sandy-silty clay and clay alternated to sandy-gravelly sediments.

Eastward, the S15 (*Cherubini et al.,* 2000) records a lower gravelly-sandy unit between -61.5 and -71.5m asl passing upward an about 4m-thick sandy-silty layer with peat intercalation. On the top the succession evolves toward sandy sediments (5m thick) following by 20m-thick clayey and silty-clayey deposits with a peat layer at -45m asl. The organic matter dating (*Cherubini et al.,* 2000) at -

50m of depth reveals an age of 6310 ky B.P. Upward, 26m-thick sandy layer with gravelly intercalation is overlaid by clay deposits. The latter evolves toward gravelly sediments which pass upward to silty clay and sandy silt.

In the southern sector from the present Crati riverbed, the C3 well-log (Crati 3, ViDEPI) records a gravelly layer from -83 to -1130 m asl, passing upward to an alternation of sand and sandy clay with sporadic clayey and gravelly intercalations.

The C2 well-logs (Crati 2, ViDEPI) shows gravelly and sandy deposits with sporadic clay intercalations from -35 to -140 m asl. Upward, a 20m-thick clayey body with peat intercalation is followed by gravelly sediments.

Southward, the C1 well-log (Crati1, ViDEPI) is characterized by an alternation of sandy and gravelly deposits with intercalation of peat and rare clayey layers.

The southernmost well-log a (*Bellotti et al*., 2003) records a lower stratigraphic unit (from -58 to -88.5m asl) made by sand with lens-shaped gravelly intercalations. On top, 2m-thick peat layer (dated at 9.9 kyr B.P.) is present and passes upward to a 10m-thick clayey body with lens-shaped gravelly intercalations. Upward, another 2m-thick peat layer is followed by 44m-thick sands with lenticular gravelly bodies and a peat intercalation at -21.5m asl. The logs is closed by a thin (2.5m) sandy-silty layer. *Bellotti et al.* (2003) interpret the lower coarse-grained unit as a braided fluvial channel depositional element evolving to a coastal barrier lagoon environment. Upward, they suggest another fluvial channel depositional element passes to an inner delta plain.

The well-logs analysis shows clear dissimilarities in the stratigraphic framework between the northern and southern sectors.

In the northern sector, the lower sandy-gravelly unit, related to the late Pleistocene coastal plain depositional element, is overlain (at about -65m asl) by clayey and silty deposits. The latter are characterized by the peat intercalations, from about -60m asl (S15 well-log) with maximum age of 9.835 kyr B.P. (S1 well-log), and widespread plant materials. We suggest that the clayey and silty deposits is related to a wetland area with locally coarse-grained channel-fill and crevasse sediments.

In the southern sector, the stratigraphic pattern is dominated by sands and gravels with widespread peat intercalations. These deposits are related to a coarse-grained coastal-alluvial plain persisting from late Pleistocene to Holocene. The available data do not allow to recognized the deposits related to the post-glacial transgression.

2.5 Geoelectrical survey

The good efficiency of the electrical resistivity ground imaging (ERGI) to obtain sedimentological information about the shallow subsurface has been shown by *Baines et al.* (2002). These authors used successfully ERGI to map the geometry of sand and gravel deposits buried by silt or clay in different field sites; one of these is very similar to the geological context of the Crati Delta and consists of a buried delta distributary channel in the Holocene Rhine–Meuse delta overlapping a Pleistocene sandy-gravelly braid-plain. *Froese et al.* (2005) investigate the floodplain stratigraphy of middle Yukon River by means of ERGI and GPR, which are employed also by *Pellicer and Gibson* (2011) to characterize the internal architecture of Quaternary sediments in the midlands of Ireland. *Kilner et al.* (2005) combine resistivity imaging and the electromagnetic induction technique for the characterization of glacial and alluvial Quaternary deposits in Eastern England. ERGI, combining with sedimentological data is also used by *Bersezio et al.* (2007) to map the fluvial architectural elements in the Quaternary Po Plain. Resistivity imaging has been also used in gravel and sand prospecting, resulting a useful tool (*Beresnev et al.*, 2002; *Chambers et al.*, 2013).
In the last decades the electrical resistivity tomography, often associated with other shallow geophysical techniques, have been commonly used for imaging and mapping subsurface active faults (*Suzuki et al.*, 2000; *Caputo et al.*, 2003, 2007; *Nguyen et al.*, 2005, 2007; *Improta et al.*, 2010; *Giacoli et al.*, 2011; *Štěpančíková et al.*, 2011) and also for large scale geological structural studies (*Colella et al.*, 2004).
In this paper the relatively high resistivity contrast between fine- and coarse-grained sediments are used to investigate the boundaries among the different lithofacies deposited during the Holocene evolution of the Crati Delta. Furthermore the electrical resistivity tomographies allow to identify the pre-Holocene bedrock, made up by gravel and sand alluvial plain, and to detect the presence of faults.

2.5.1 Methodology

Electrical Resistivity Tomography (ERT) data were collected using a Syscal Pro Resistivity meter with 96, 72 and 48 electrodes using the Schlumberger reciprocal array. Data collected included 9 profile at 5m and 11 profiles at 10m spacing, with 475m of length for each profile except two profile 710m long. ERTs were collected during 5 surveys. The datasets were inverted using RES2DINV software which generates a calculated model of the pseudosection from the inverted model, the Root Mean Square (RMS) error between the calculated and the measured pseudosection is computed.

profile	electrodes	elec. distance(m)	length (m)	array	configuration	survey date
1a	96	5	475	Schlumberger reciprocal	Rho & IP	January 2014
1b	96	5	475	Schlumberger reciprocal	Rho & IP	January 2014
2	72	10	710	Schlumberger reciprocal	Rho & IP	November 2012
3	96	5	475	Schlumberger reciprocal	Rho & IP	January 2014
4	96	5	475	Schlumberger reciprocal	Rho & IP	January 2014
5	48	10	470	Schlumberger reciprocal	Rho & IP	November 2012
6	72	10	710	Schlumberger reciprocal	Rho & IP	November 2012
7	48	10	475	Schlumberger reciprocal	Rho & IP	April 2014
8	48	10	475	Schlumberger reciprocal	Rho & IP	April 2014
9	48	10	475	Schlumberger reciprocal	Rho & IP	April 2014
10	96	5	475	Schlumberger reciprocal	Rho & IP	February 2014
11	48	10	475	Schlumberger reciprocal	Rho & IP	April 2014
12	96	5	475	Schlumberger reciprocal	Rho & IP	February 2014
13	96	5	475	Schlumberger reciprocal	Rho & IP	February 2014
14	96	5	475	Schlumberger reciprocal	Rho & IP	February 2014
15	96	5	475	Schlumberger reciprocal	Rho & IP	February 2014
16	48	10	475	Schlumberger reciprocal	Rho & IP	April 2014
17	48	10	475	Schlumberger reciprocal	Rho & IP	April 2014
18	48	10	475	Schlumberger reciprocal	Rho & IP	April 2014
20	48	10	475	Schlumberger reciprocal	Rho & IP	April 2014
21	48	10	475	Schlumberger reciprocal	Rho & IP	April 2014

Table 2.2. General information concerning the realized ERT profiles

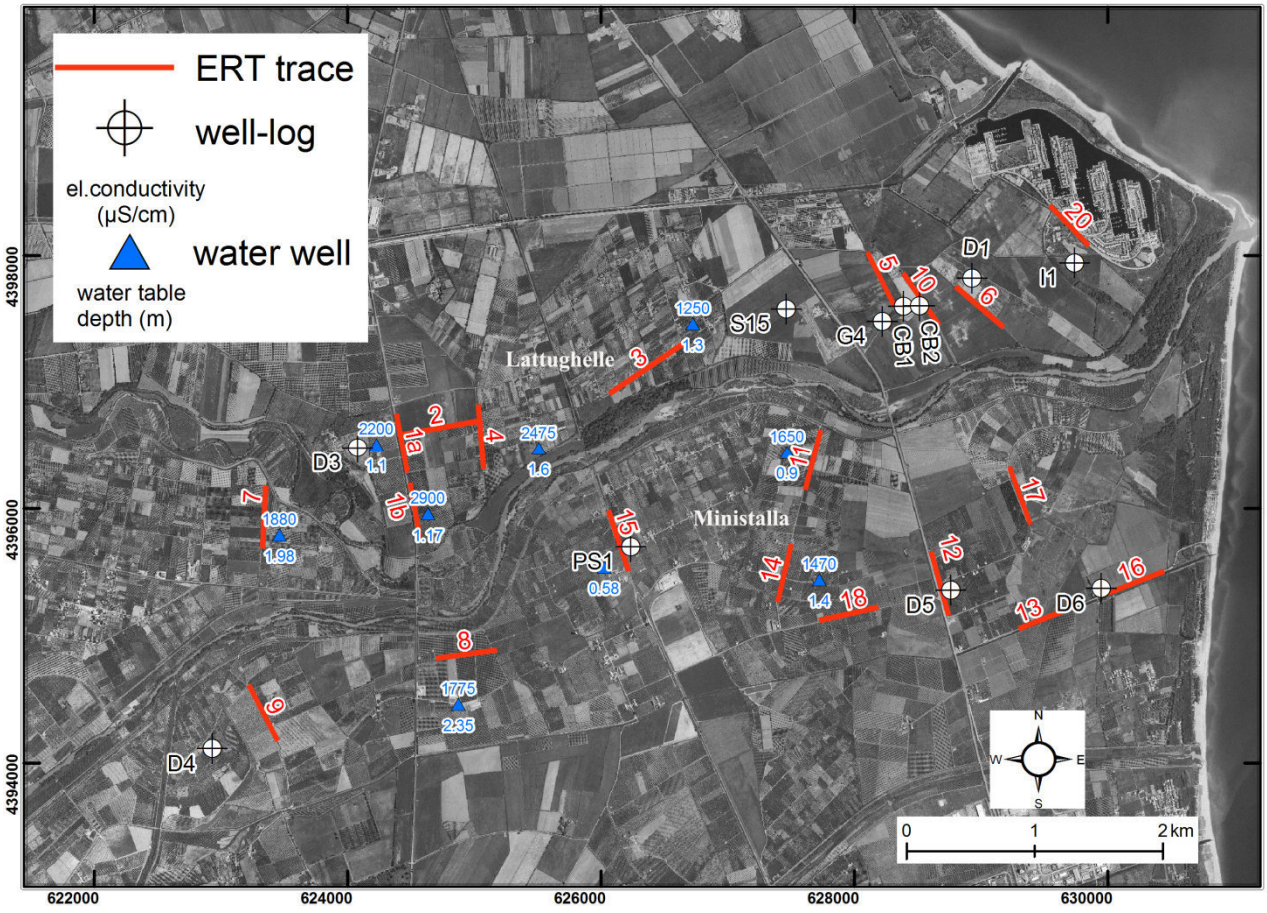

Fig. 2.10. Location of the Electrical Resistivity Tomographies realized in the Sibari Plain. In the map are also present the well-logs used to validate ERT interpretation and water wells which allow to detect.

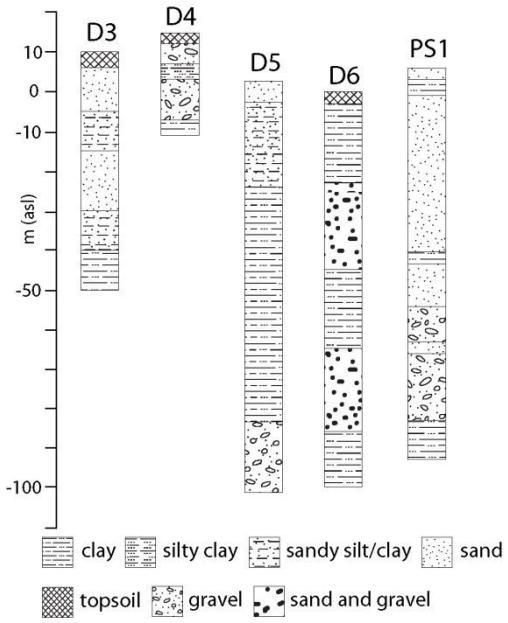

Fig. 2.11. Well-logs used to validate the ERTs interpretation (D=Demanio Idrico office; PS=*Casmez,* 1987). The remaining well-logs in fig. 2.7.

2.5.2 ERT profiles description

ERT 1a, located in the northwestern sector of the study area, is characterized by low resistivity value (<20Ωm). In the central ERT area (from 160m to 320m) lens-shaped bodies with resistivity between 50 and 400 Ωm are present from surface to depth of 25m. Also in the ERT 1b, represented the southward extension of 1a, the low resistivity values prevail but the high resistivity (>30 Ωm) lens-shaped bodies are bigger and more widespread starting from 30m of depth. The low resistivity values observed in the two ERT represent silty-clay deposits logged by D3 well while the lens-shaped bodies can be related to sandy-gravelly ones.

ERT 2, perpendicular to 1a, is entirely characterized by low resistivity values < 30 Ωm, except two isolated bodies with higher resistivity between 25m and 90m of depth. ERT 4, parallel to 1a and 1b and located about 650m seaward from them, shows in the central area (from 220m to 300m) a body with resistivity between 60 and 300Ωm extended from 90m to 20m of depth. The remaining part of the ERT is characterized by low resistivity values (<30-35Ωm) and lens-shaped bodies with resistivity between 60 and 300Ωm from surface to 20m of depth.

The ERT 3, the easternmost one collected in the Lattughelle locality, runs subparallel to the Crati River. Low resistivity values (<30Ωm) with high resistivity (up to 200 Ωm) lens-shaped bodies are typical of the surface area (reaching 34m of depth). High resistivity layer (>70 Ωm) characterizes the lower area (34-98m) except in the sector between 335m and 380m where low resistivity values prevails. The well CherS15, located 500m eastward, logs gravelly and sandy deposits (high resistivity values in the ERT) separated by 20m-thick clayey layer (low resistivity values). The

S15well (*Cherubini et al.*, 2000) , located 750m eastward, logs gravelly and sandy deposits (high resistivity values in the ERT) separated by 20m-thick clayey layer (low resistivity values).

Westward from the Crati-Coscile confluence, the ERT 23 is almost entirely characterized by low resistivity values (<25Ωm) with two lens-shaped high resistivity (>60Ωm) bodies. The bigger one is located from 230 to 290m and between 30 and 60m of depth, the other one from 265 and 285m with depth between 7 and 18m. The low resistivity values can be correlated with clayey and sandy-silty deposits logged 750m northeastward by D3 well.

ERT25-10m is the westernmost ERT in the South side of Crati river. Numerous high resistivity (>60Ωm) bodies divided by low resistivity area occur. The vertical passages between high and low resistivity values are logged by the D4 well (800m westward) as an alternation of gravelly-sandy and clayey deposits. Moving eastward, ERT 24 runs subparallel to the Crati River and is characterized by low resistivity values (<20Ωm); lens-shaped high resistivity bodies are present from middle to east boundary of the ERT and reach 60m of depth.

In the Thurio area, ERT 15, parallel to the railway, are dominated by low resistivity values (<30Ωm). Lens-shaped high resistivity bodies, reaching 60m of depth, are widespread in the central and northern sector of the ERT. This bodies are made up by sandy-gravelly deposits recorded in PS1 well, located 85m eastward from the ERT.

ERT 14 and 22 are collected in Ministalla locality. The first one is characterized by a high resistivity body (>70Ωm) in the central sector (from 150m to 295m) between 30m and 98m of depth. It is overlaid by an irregular low resistivity (<20Ωm) layer with lens-shaped high resistivity bodies. The second one, representing the northward continuation of the ERT 14, shows a high resistivity body in its lower part, up to 50m of depth, passing upward to a low resistivity layer (<20Ωm) with lens-shaped high resistivity bodies. Southward, in the ERT 18 low resistivity (<20Ωm) occur between 30m and 100m of depth; at 67m of depth a lateral clear transition to resistivity values >30Ωm are present. From 30m of depth to surface prevails elongate high resistivity (>30Ωm) bodies.

In the northeastern sector of the study area, between the Sybaris archaeological site and Laghi di Sibari, 4 ERTs are collected. The westernmost ERT 5 shows a low resistivity (<10Ωm) layer passing upward, in correspondence of 15-20m of depth, to a layer with higher resistivity. This vertical transition can be correlated to the passage from sandy to clayey deposits recorded by the G4 well at 16m of depth. The ERT 10, parallel to the previous one, is characterized by a surface high resistivity (>20Ωm) layer 15-20m thick lying on a low resistivity (<10Ωm) layer. In the ERT 6 low resistivity values (<10Ωm) are present in the area between 136m and 20m of depth, while high resistivity values (>20Ωm) dominate from 20m to the surface; these resistivity values are related

respectively to the silty clay passing upward (15m from the surface) to the gravelly-sandy deposits recorded in the D1well.

In the ERT 20 low resistivity value (<10Ωm), with near surface lenticular high resistivity bodies, prevail. In the middle of ERT are present a clear vertical passage from low (<10Ωm) to high (>40Ωm) resistivity values .The prevalence of silty and clayey deposits with m and dam sandy-gravelly intercalations logged by I1well, located 230m southward from the ERT, validates the widespread low resistivity values present in the ERT.

In the southeastern sector of the study area, between the SS106 and the coastline, 4 ERT are collected. In the ERT 12, the surface layer is characterized by high resistivity values (>30Ωm) reaching 40m of depth and sometimes modeling lens-shaped bodies. Below, up to 77m of depth, low resistivity values (<20Ωm) are present and lie on layer with resistivity values >20Ωm. In the southeastern sector of the ERT the intermediate low resistivity layer passes laterally to high resistivity values. The vertical alternation high-low-high resistivity value can be related with the stratigraphy recorded by D5 well characterized from the top by 25m of sandy-gravelly and silty deposits, 65m of clay and 15 of sand and gravel. The ERT 17, runs 800 m north-east of and subparallel to ERT 12, is characterized by a high resistivity (>20Ωm) surface layer, with a maximum thick of 30m in the middle sector, lying on low resistivity irregular body. The latter is well recognizable in the lateral ERT sectors and it disappears in the central sector, where it is replaced by a lower high resistivity (>30Ωm) body along a vertical surface. This body is present also in the northwestern sector. The ERT 13 shows a surface high resistivity layer characterized by lens-shaped geometries ad passing downward to a low resistivity layer reaching a maximum depth of 60m. In the lower ERT area resistivity values >10Ωm are present. ERT 16, representing the eastward prosecution of the ERT 13, is dominated by low resistivity values (>10Ωm). Thin surface high resistivity layer, with maximum thickness in southwestern sector, exist. High resistivity (>20Ωm) values are present from 80m of depth in the middle sector of the ERT (260-290m) and as lens-shaped high body in the northeastern sector between 20m and 48m of depth. The latter body can be related to the sandy and gravelly deposits interbedded with the clays logged by D6 well between 25 and 45m of depth.

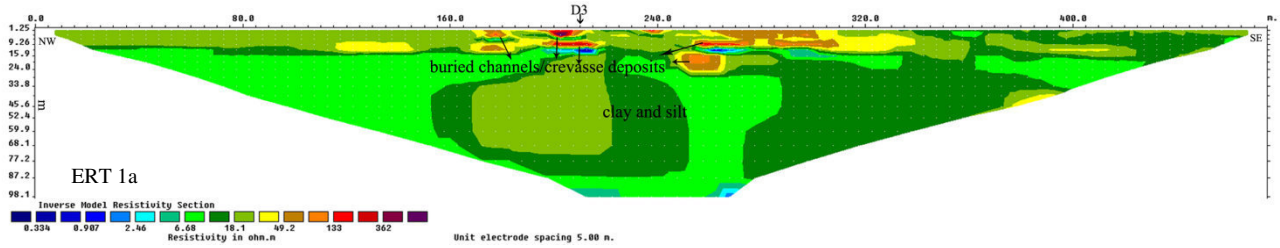

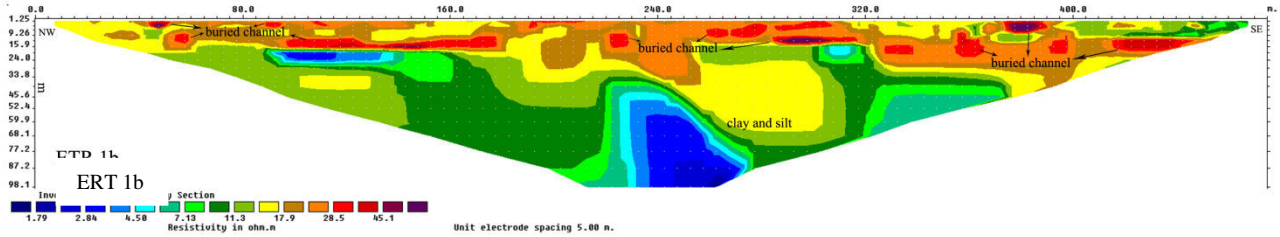
buried channel
buried channel
buried channel
clay and silt
ERT 1b
Resistivity in ohm.m
Unit electrode spacing 5.00 m.

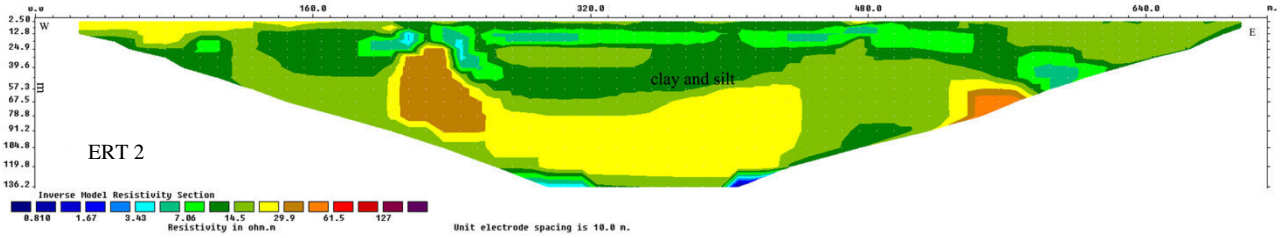
clay and silt
ERT 2
Inverse Model Resistivity Section
Resistivity in ohm.m
Unit electrode spacing is 10.0 m.

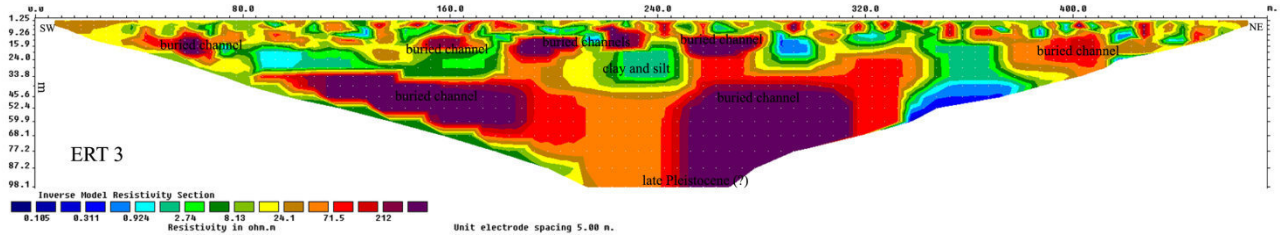
buried channel
buried channel
buried channel
buried channel
buried channel
clay and silt
buried channel
buried channel
late Pleistocene (?)
ERT 3
Inverse Model Resistivity Section
Resistivity in ohm.m
Unit electrode spacing 5.00 m.

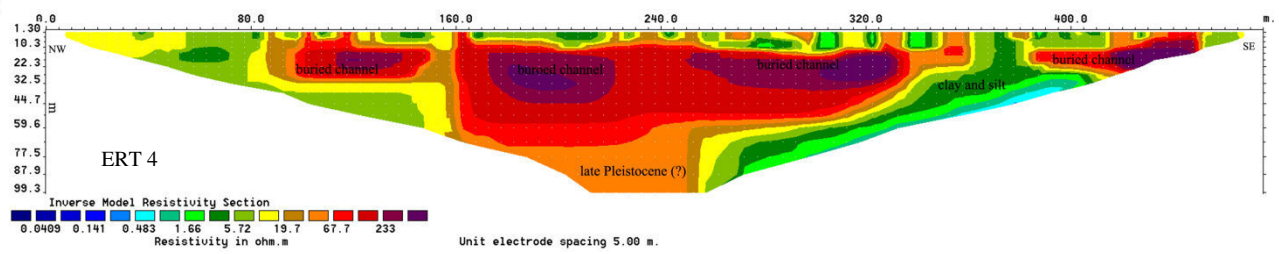
buried channel
buried channel
buried channel
buried channel
clay and silt
late Pleistocene (?)
ERT 4
Inverse Model Resistivity Section
Resistivity in ohm.m
Unit electrode spacing 5.00 m.

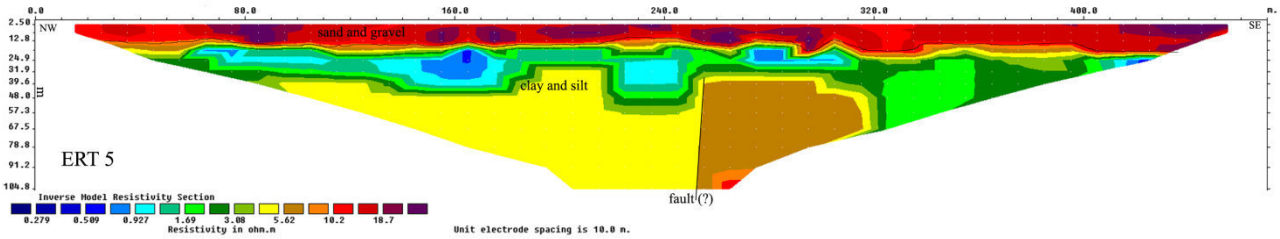
sand and gravel
clay and silt
fault (?)
ERT 5
Inverse Model Resistivity Section
Resistivity in ohm.m
Unit electrode spacing is 10.0 m.

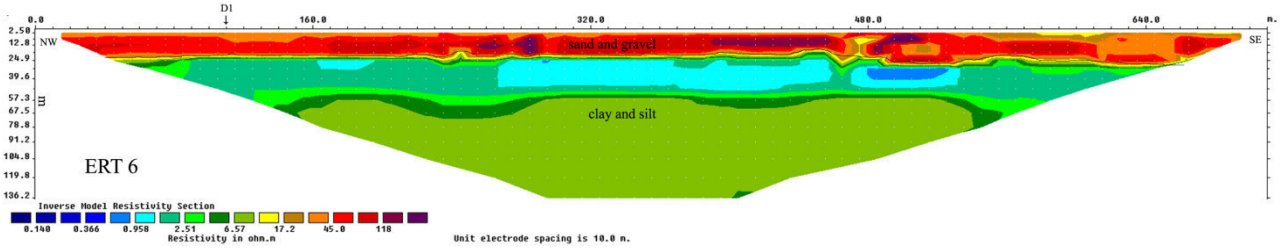
sand and gravel
clay and silt
ERT 6
Inverse Model Resistivity Section
Resistivity in ohm.m
Unit electrode spacing is 10.0 m.

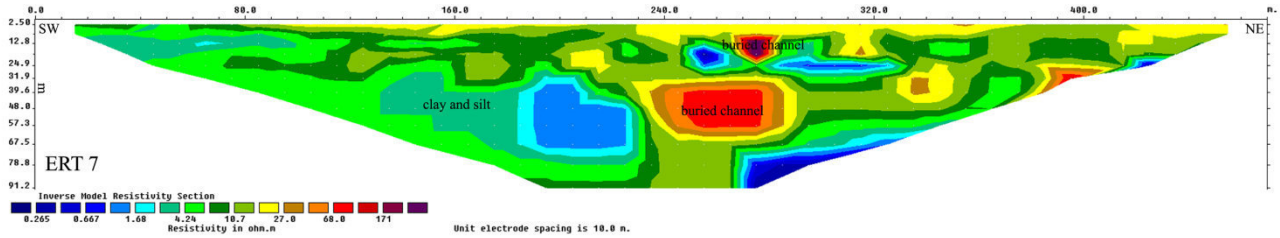
SW
NE
buried channel
clay and silt
buried channel
ERT 7
Inverse Model Resistivity Section
Resistivity in ohm.m
Unit electrode spacing is 10.0 m.

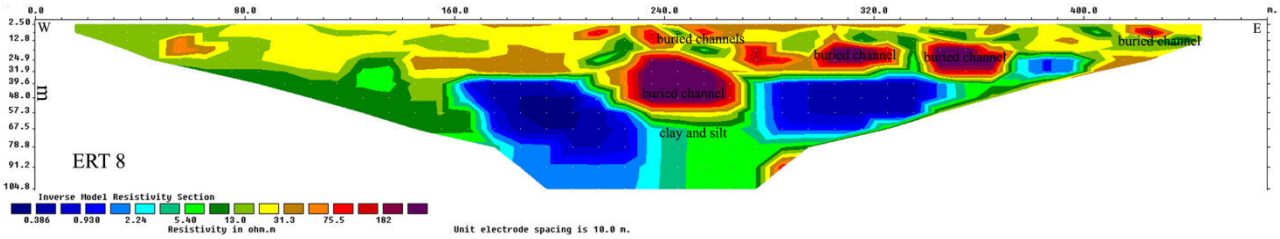
W
E
buried channels
buried channel
buried channel
buried channel
buried channel
clay and silt
ERT 8
Inverse Model Resistivity Section
Resistivity in ohm.m
Unit electrode spacing is 10.0 m.

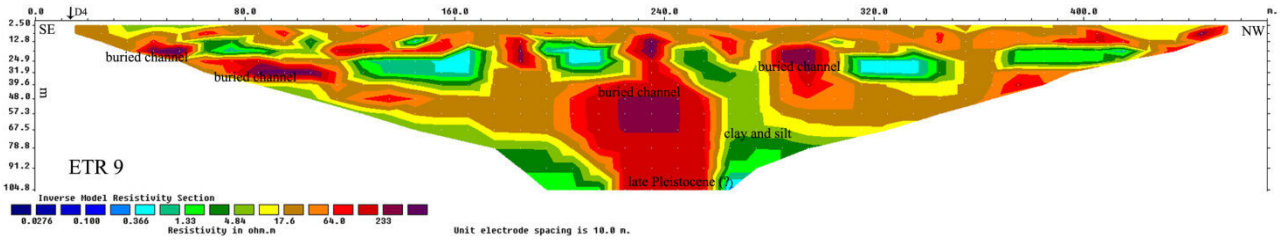
D4
SE
NW
buried channel
buried channel
buried channel
buried channel
clay and silt
late Pleistocene (?)
ETR 9
Inverse Model Resistivity Section
Resistivity in ohm.m
Unit electrode spacing is 10.0 m.

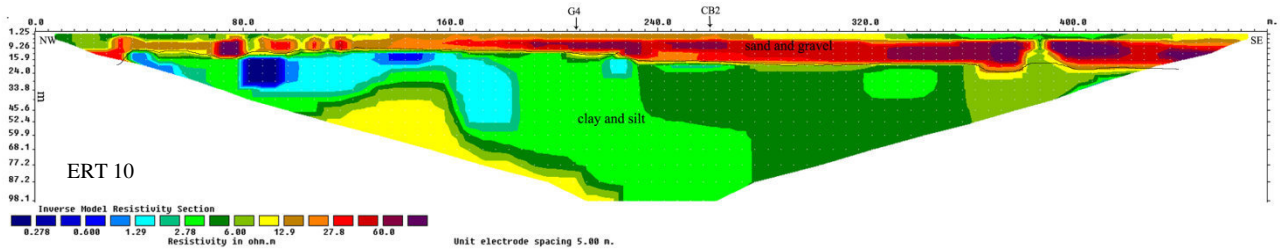
G4
CB2
NW
SE
sand and gravel
clay and silt
ERT 10
Inverse Model Resistivity Section
Resistivity in ohm.m
Unit electrode spacing 5.00 m.

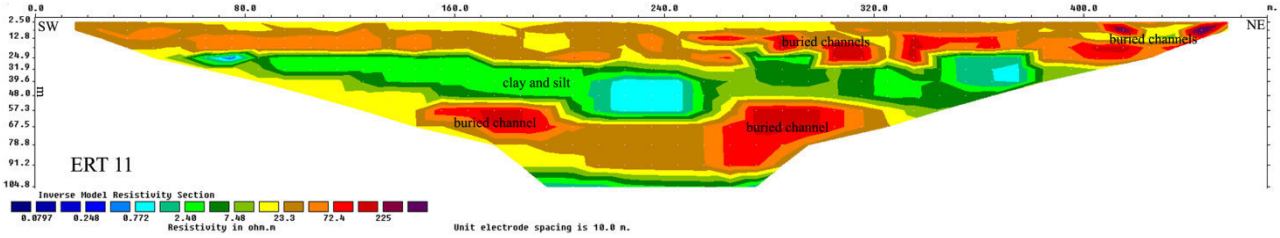
SW
NE
buried channels
buried channels
clay and silt
buried channel
buried channel
ERT 11
Inverse Model Resistivity Section
Resistivity in ohm.m
Unit electrode spacing is 10.0 m.

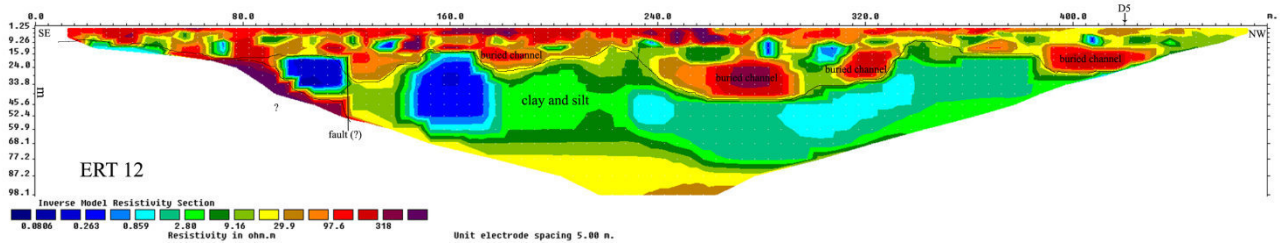
D5
SE
NW
buried channel
buried channel
buried channel
buried channel
clay and silt
?
fault (?)
ERT 12
Inverse Model Resistivity Section
Resistivity in ohm.m
Unit electrode spacing 5.00 m.

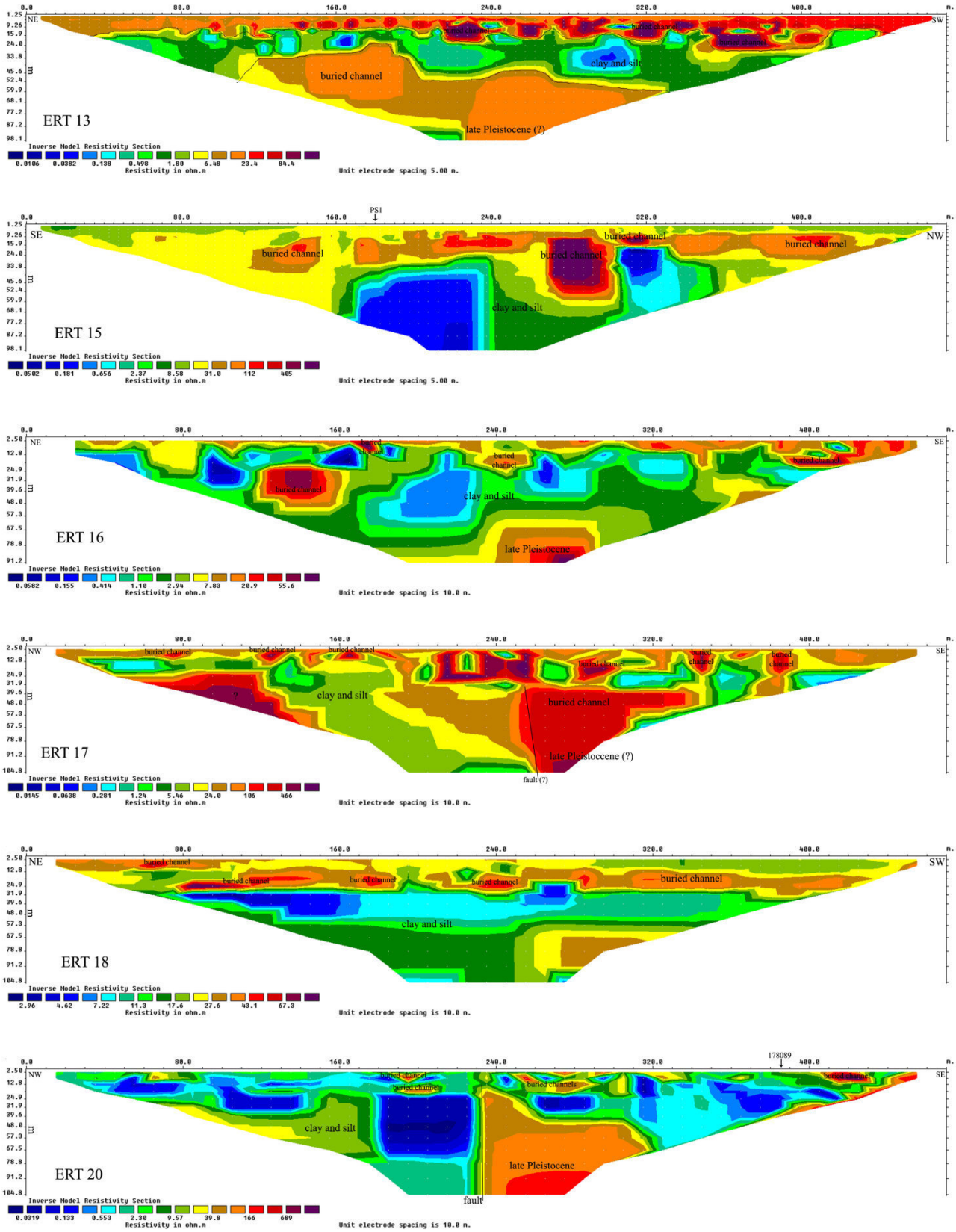

Fig. 2.12. Electrical Resistivity Tomographies realized in the Sibari plain and their interpretation

2.5.3 ERT profiles interpretation

The ETRs show different features in the stratigraphic framework of the investigate area.

In the sector close to the archeological settlement, ETRs (5, 6 and 10) show a 20m-thick high resistivity layer overlapping 80m-thick low resistivity layer. The upper layer can be related to the transitional and continental deposits recognized in the stratigraphic cross section (fig.2.7) while the lower layer to the underlying bluntly marine fine-grained sediments. The easternmost ETR20 shows a clear vertical discontinuity which probably represents a fault plain.

Northward from the Crati River, the landward ETRs (23, 1a, 1b and 2) are mainly characterized by low resistivity values which can be correlated with the fine-grained (silt and clay) deposits recognized in the same area by well-logs analysis. The lens-shaped high resistivity bodies observed in these ETRs can instead related to fossil riverbed of Coscile and/or Crati River. Moving eastward, the ETRs 3 and 4 show thick high resistivity bodies interbedded with low resistivity values and interpreted as channel-fill deposits related to Coscile and/or Crati Rivers. E.g., the ETR 3 is located in correspondence of Greek-Roman Crati fossil riverbed traced by *Bellotti et al.* (2009).

Southward from the Crati River, the landward ETRs 25, 24 and 15 are characterized by widespread lens-shaped high resistivity bodies representing fossil channels of Crati River. Also ETRs 14, 22 and 18 show channelized bodies interbedded with fine-grained deposits. In ETRs 12 ,13 and 16, we observe the same geometries of previous ETR but toward the bottom a transition from low to high resistivity are present and probably is due the stratigraphic transition of the late Pleistocene deposits. In the middle of the ETR 17, the vertical transition from low to high resistivity values can be correlated to a fault plain.

The electrical data reflect the stratigraphic framework observed through the well-logs analysis. In detail, in the archeological area the ETRs record the evolution from marine to continental deposits observed in the stratigraphic cross section (fig.2.7). In the sector northward from the Crati River, the prevalence of fine-grained deposits, with intercalation of channelized deposits. is confirmed and their great thickness is shown n correspondence on the confluence between Crati and Coscile Rivers. In the southern sector, widespread coarse-grained sediments arranged in lens-shaped bodies are observed.

We try to correlate the inverted absolute resistivity values of the main and well-recognizable lithofacies (buried channel and fine-grained delta/alluvial plain deposits with the factors which can influence the field data acquisition. In detail we consider the position of investigated lithofacies referring to water table, groundwater electrical conductivity, the month of data acquisition and the electrodes distance used (*Beresnev et al., 2002; Bersezio et al., 2007)*. For the analysis, we select

only the ERTs realized close to water wells which allows the groundwater level and groundwater electrical conductivity estimation.

					Buried channel	Fine-grained deposits
ERT	**Position referring to water table**	**mean groundwater electrical conductivity(μS/cm)**	**Month of data acquisition**	**Electrodes distance (m)**	**electrical resistivity (Ωm)**	
1a	submerged	2900	January	5	130-350	18-80
1b	submerged	2200	January	5	30-60	15-30
23	submerged	1880	April	10	70-170	10-50
24	submerged	1775	April	10	70-200	7-50
4	submerged	2475	January	10	70-200	5-30
3	submerged	1250	January	5	70-200	5-50
15	submerged	1550	February	5	50-400	10-30
14	submerged	1470	February	5	50-250	5-20
22	submerged	1650	April	10	50-200	15-50

Table 2.3. details of the ERT profiles used in the analysis of the electrical resistivity values of buried channels and fine-grained deposits.

The range of values of the electrical resistivity observed for buried channel and fine-grained delta/alluvial plain deposits are comparable with the values recorded by *Baines et al.* (2002) in the area of the Rhine-Meuse delta (The Netherlands).

The analyzed lithofacies result submerged by the water table which is very shallow in the delta area. No correlation among lithofacies electrical resistivity, the period of data acquisition and electrodes distance is observed. The buried channels electrical resistivity recorded in January shows a direct correlation with groundwater electrical resistivity.

Beresnev et al. (2002) observe a seasonal variability of the coarse-grained deposits absolute resistivity which instead remains stable for fine-grained sediments. Our analysis disagrees with *Beresnev et al.* (2002) about gravelly and sandy deposits resistivity variability. This can be related to the permanent saturated conditions of coarse-grained deposits due to the very little seasonal water table variations in the Crati Delta area.

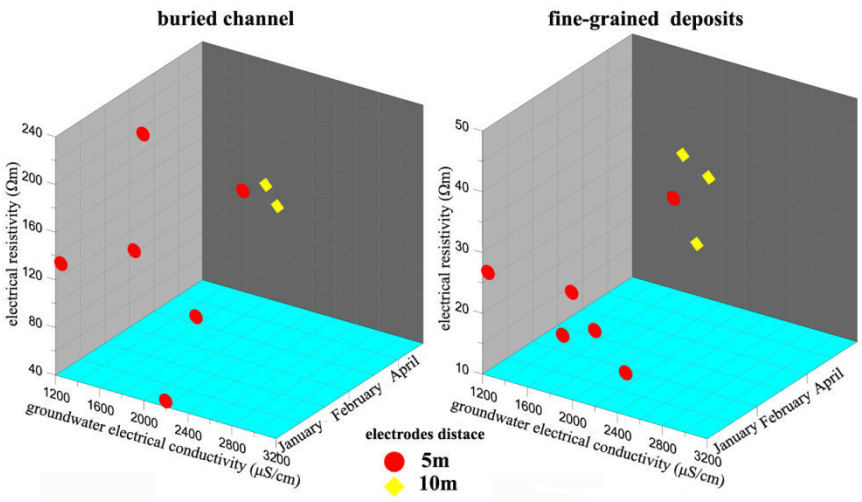

Fig. 2.13. 3D scattered plots for the correlation among the average electrical resistivity of the selected lithofacies, groundwater electrical resistivity, period of data acquisition and electrodes distance.

Fig. 2.14. Water table variation monitored by remote probe installed in Crati Delta area by PON_Amicus project. The diagram shows a seasonal variation (from April 2014 to October 2014) restricted in 1m of range.

2.6 Ambient noise analysis

In the area of Crati and Coscile Rivers confluence, we use passive seismic technique for the stratigraphic investigation of the subsoil. The technique consists of recording and analyzing the seismic ambient noise to retrieve information about subsoil stratigraphy from seismic tremor. In particular, we use the H/V (Horizontal to Vertical Spectral Ratio) technique, which consists of studying the ratio between the Vertical and Horizontal spectral components of the tremor recorded at a single station. The method, originally proposed by *Nogoshi and Igarashi (1970)* and later diffused by *Nakamura (1989)*, provides a direct estimate of the resonance frequencies of subsoil. This well known capability allows to translate the H/V curves into stratigraphy (*Castellaro et al., 2005*). The theoretical bases of this technique are simple only in a 2 layer 1-D model in which parameters are constant within each layer. In the latter case, the depth *h* of the seismic discontinuity is immediately derived from the free-surface resonance equation $h=V/(4f)$, where V is the seismic

wave velocity of the upper layer and f is the resonance frequency which appears as a peak in the H/V curve.

The tremor recordings were acquired with a three-component short period sensors (Lennartz 3D-5s) specifically designed to record seismic noise. Seismic noise was recorded for 60 min. at each site with a sampling frequency of 50 Hz. Data were analyzed with the Geopsy software package.

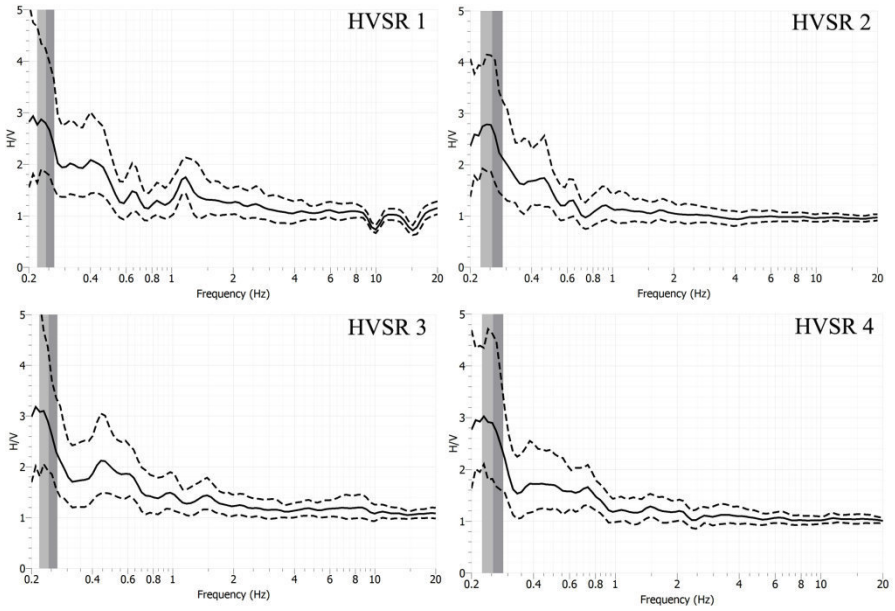

Fig. 2.15. HVSR measurements with Lennartz sismometer

Our target consists of the top the late Pleistocene alluvial plain deposits. We identify it in correspondence to a secondary peak oscillating between 0.9 and 1.8Hz. The conversion from the fundamental frequency (f_0) to depth (m) is realized using an average shear wave velocity of 250m/s for the recent sediment and 350m/s for the underlying Holocene deposits referring to MASW tests realized in the area.

Station	**f_0 of late Pleistocene top (Hz)**	**depth of late Pleistocene top (m)**
1	1.19	73.5
2	1.02	85
3	1.55	56.5
4	1.51	58

Table 2.4. F_0 and relative depth (m) of the late Pleistocene depth recorded in the 4 HVSR stations.

The stations 1 and 2, located northward from Crati River, record a greater depth of late Pleistocene depth than stations 3 and 4 (southward from the river) (fig. 2.16). We suggest the existence of a normal fault system with northward dip to explain the late Pleistocene top deepening.

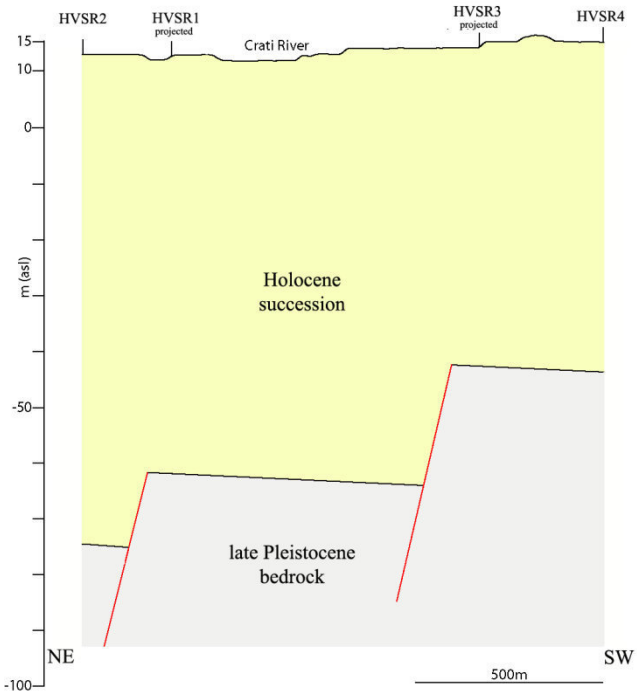

Fig. 2.16. Location of the HVSR stations and reconstruction of the late Pleistocene top (on the right)

2.7 Discussion

The multidisciplinary approach carried out in this work shows a very complex stratigraphic framework for the Sibari Plain.

Well-logs analysis and ETRs interpretation allow to distinguish three sectors with peculiar stratigraphic features. In detail, we identify: a sector, northward from the Crati River, characterized by dam-thick clayey and silty deposits related to a wetland area overlapping a sandy-gravelly unit; a southern sector mainly characterized by sands and gravels deposited in a coastal plain environment; a sector located close to the *Sybaris* archeological site where the stratigraphic pattern consists of a lower coastal plain coarse-grained deposits passing upward to bluntly marine clayey-silty deposits which evolve toward a beach ridge system overlaid by alluvial/deltaic plain sediments.

The northern and southern sectors are divided by a normal fault zone, 55°N-60°N striking, inferred by the ERT20 and the cross-section of the late Pleistocene top obtained by the HVSR measurements. This fault system crosses the archeological settlement where *Cinti et al.* (2013) recognized significant elements of tectonic deformation as NW-SE oriented fractures, paleliquefaction phenomena and rotation of walls.


N
W
E
S
0m
25m
50m

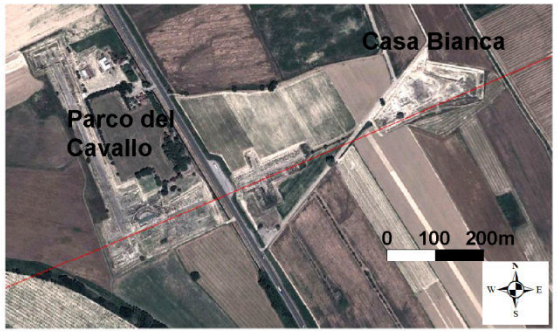
Casa Bianca
Parco del Cavallo
0 100 200m

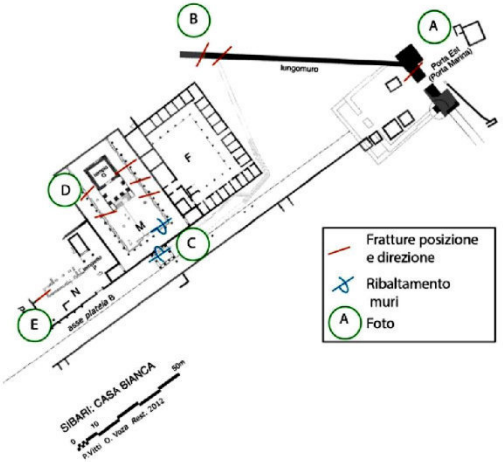
B
A
Ingomuro
Porta Est (Porta Bannia)
D
F
M
C
E
N
Fratture posizione e direzione
Ribaltamento muri
A
Foto
SIBARI: CASA BIANCA

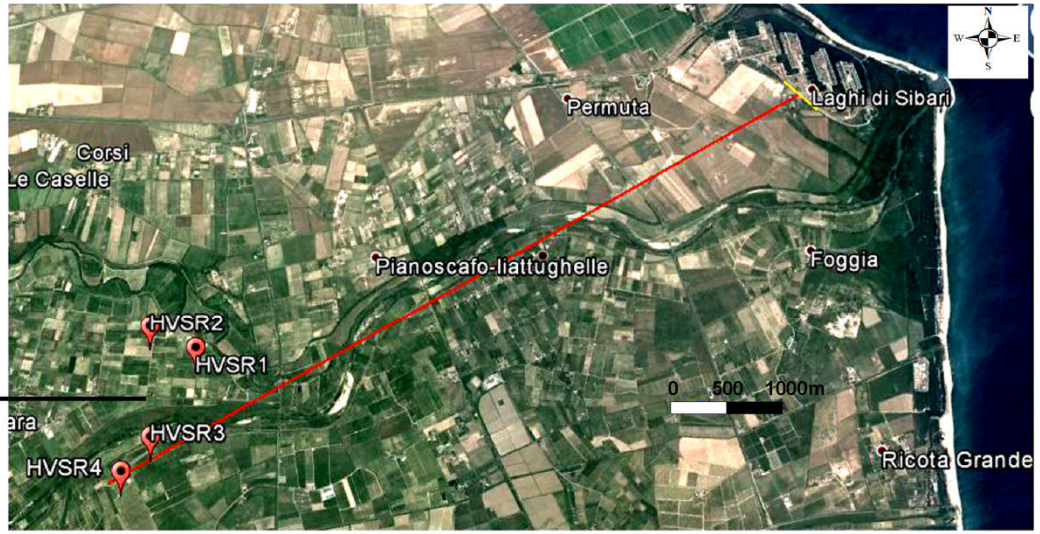
Permuta
Laghi di Sibari
Corsi
Le Caselle
Pianoscafo-liattughelle
Foggia
HVSR2
HVSR1
HVSR3
HVSR4
0 500 1000m
Ricota Grande

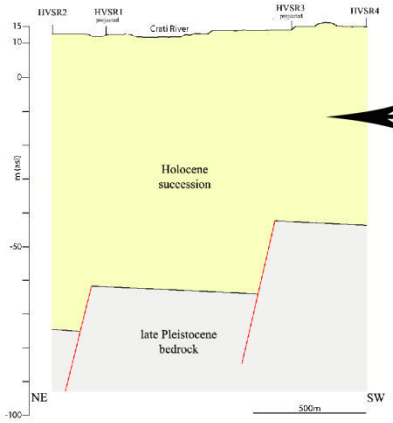
HVSR2
HVSR1
HVSR3
HVSR4
Holocene succession
late Pleistocene bedrock
NE
SW
500m

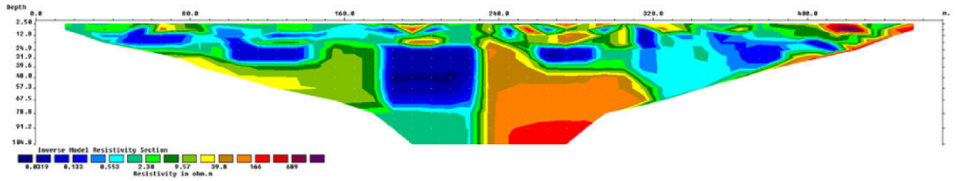

Fig. 2.17. Fault zone inferred by ERT20 and HVSR measurements. Inside the Sybaris archeological site the fault zone trace is compared to the elements of tectonic deformation recognized by *Cinti et al.* (2013)

The tectonic lineament recognized corresponds to the Sybaris fault zone (*Cinti et al.,* 2015 in press) interpreted an oblique normal-dextral fault zone, 45° N–55° N striking, composed of subparallel breaks. The authors identify two seismic events happened respectively after the first half of the second century A.D and between the second half of the second and the seventh–ninth centuries A.D..

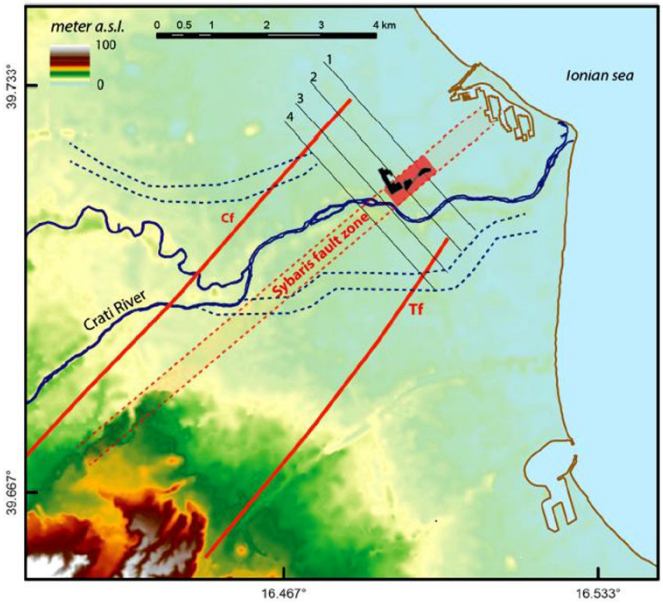

Fig. 2.18. Sibari fault zone trace by *Cinti et al*. (2015 in press) based on its evidence in the Sybaris archeological site

The Holocene activity of the Sybaris fault zone play a key role in the Sibari Plain evolution conditioning the geomorphological setting and consequently the paleoenvironments arrangement. Indeed, the northern sector, identified by stratigraphic and sedimentological data, is located on the fault hanging wall while the southern one on the foot wall.

We suggest that at the end of last-glacial transgression (around 6 kyr B.P.) (fig.2.19) a wide wetland, where flowed Coscile and Garda Rivers, and a shallow water bay environment took place in the hanging wall of the Sybaris fault zone.

Northward by the Raganello and Satanasso Streams alluvial fans bordered a wide gulf described by previous authors (*Guerricchio and Ronconi*, 1997; *Bellotti et al.*, 2003, 2009). On the foot wall, the Crati built its alluvial plain and its delta. The latter is located little far from the Favella della Corte neolithic settlement according to *Bellotti et al.* (2009).

Up to *Sybaris time* (2.7-2.5 kyr B.P.) (fig.2.19), the high subsidence on the hanging wall favoured the deposition of thick wetland deposits passing seaward to the shallow water sediment of the coastal embayment. We think that in this area only this complex depositional system combined with

the accommodation space produced by the fault activity can justify the thick fine-grained and plant materials-rich deposits observed in the northern sector. At the same time, on the foot wall the Crati Delta progradation goes on reaching the area southward from the *Sybaris* settlement.

Up to the present time, the geomorphological evolution of the Sibari Plain is strictly related to Sybaris fault zone which influences the topographic setting also currentenly producing a depressed area on the hanging wall. This area is marked by widespread presence of humid zones (fig.2.19) and it does not represent a marshy territory only thanks the reclamation work (river banks, drainage system equipped with water pumps) started at the end of the XIX century A.D..

We suggest that the fault system-controlled geomorphological setting drives the Coscile riverbed toward the Crati River after its avulsion produced by any triggering mechanism (climatic variations, earthquakes etc.). In fig.2.19, it is possible to observe the present confluence in correspondence to the traced fault zone. This hypothesis can contribute to reread the historical sources about *Sybaris* archeological site evolution. Indeed, the Sybaris destruction ascribed to the *Crathis* River flooding (*Strabo*, VI, 1, 13; *Diodorus Siculus*, XII, 9, 2; *Herodotus*, V, 45) can be related to a Coscile River southward migration so suggesting the wrong correlation between the *Crathis* River with the present Crati one which is instead represented by the *Sybaris* River how highlighted by *Taliano Grasso* (2004).

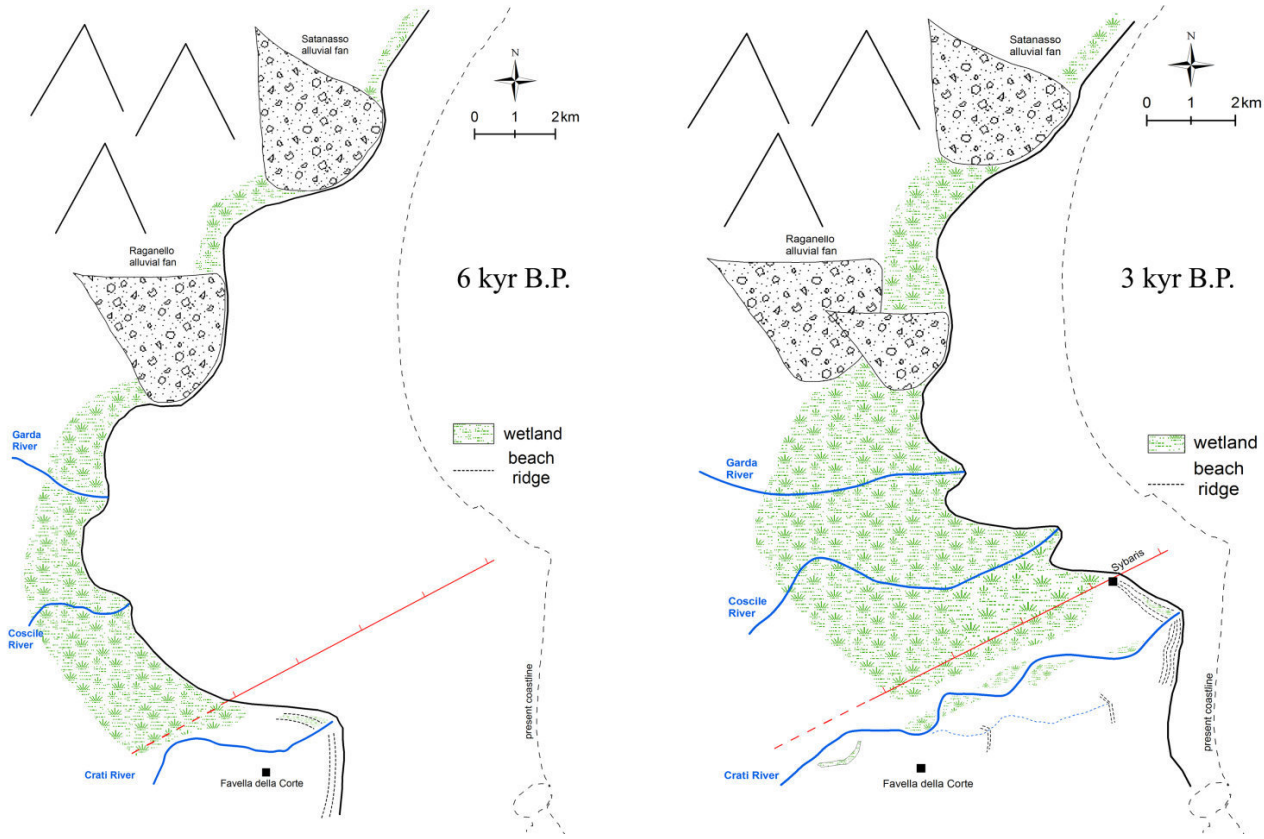

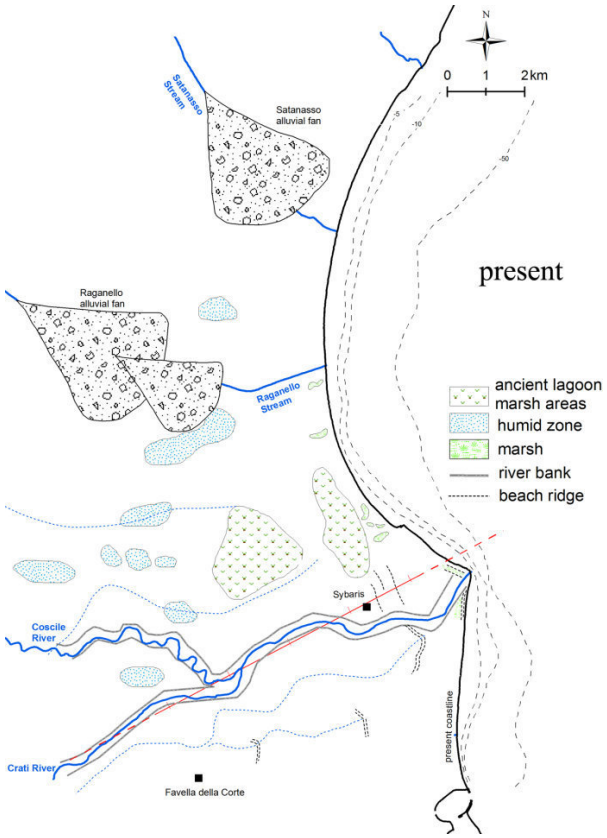

Fig. 2.19. Scenarios of the fault-controlled evolution of the Sibari Plain from about 6 kyr B.P. to present. Bathymetric contours in the present scenario are derived from 1:25000 I.G.M. topographic map.

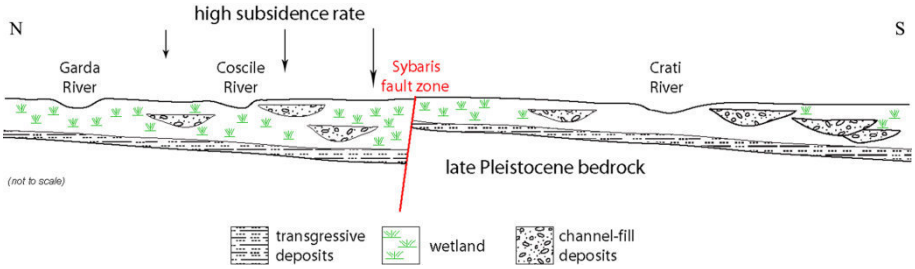

Fig. 2.20. Schematic cross section showing the fault-controlled arrangement of the sedimentary environment. The high subsidence rate on the hanging wall allow the deposition of thick fine-grained deposits.

In the described fault-controlled coastal plain, the late Holocene Crati Delta evolution happens on the southern foot wall area. The good quality stratigraphic data, available close to the archeological site, allow to observe three characteristic elements (basal late Pleistocene fluvial deposits, late Pleistocene-early Holocene shallow marine transgressive deposits and progradational deltaic deposits) of the worldwide late Pleistocene-Holocene deltaic successions described by *Stanley and Warne* (1994). Furthermore, the carbon dating available for some well-logs consent define the main evolution stages of the delta.

The post glacial succession lies on top of the late Pleistocene coarse-grained deposits which are related to the development of an coastal plain system between the Last Glacial Maximum and the

post glacial sea level rise according to *Bellotti et al.* (2003). At this time, the sea level was from -140 to -70 m lower than the present one (*Lambeck et al.*, 2004). Moreover, the climatic conditions and the high uplift rate of the Calabrian Arc (*Westaway*, 1993) favoured high rates of sediment supply and subsequently the coastal alluvial plain development.

The top of this lower stratigraphic unit, dated at about 12 kyr B.P., represents a Marine Flooding Surface overlapping by bluntly marine deposits. The development of this surface happens in correspondence of a little decrease in post-glacial sea level rise rate showed by the predicted sea-level curve for the Crati coastal plain (*Lambeck et al.,* 2011) (fig.2.21)

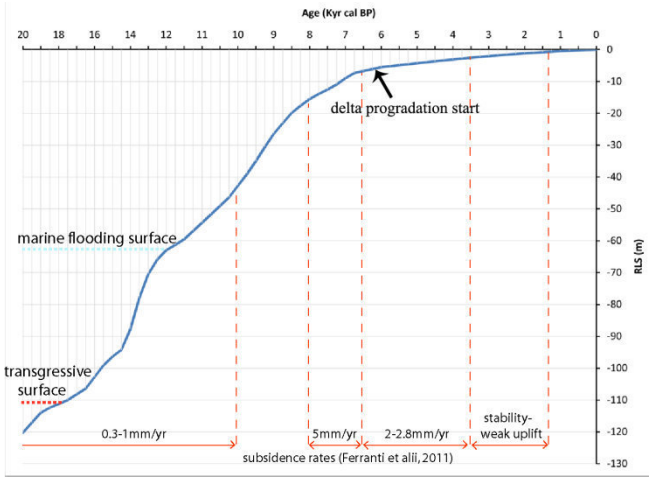

Fig.2.21. Predicted sea-level curve for the Crati coastal plain (*Lambeck et al.,* 2011) and historical subsidence rates (*Ferranti et al.* 2011) .

The previous Ravinement Surface, and associated transgressive lag, is probably recorded inside the uppermost layer of the unit where its erosive action can be inferred by the very low (1mm/yr) sedimentation rate calculated in S18 well-logs (*Cherubini et al*., 2000). The suggested Ravinement Surface can be correlated to the U-unconformity (dated at 18 kyr B.P) recognized in the Corigliano Gulf and interpreted as an erosion surface related to the last Pleistocene glacio-eustatic regression and subsequent transgression (*Romagnoli and Gabbianelli*, 1990 and references therein).

The transition between glacial to interglacial climatic condition in the Sibari Plain is shown by the increase (before about 9 kyr B.P.) of arbored/non-arbored pollen ratio and *Quercus robur* pollen grains and by the decrease of the *Artemisia* in the pollen analysis (fig.2.22) realized by *Kleine et al.* (2003) for the Forano Lake (25 km northwestward from the Crati mouth).

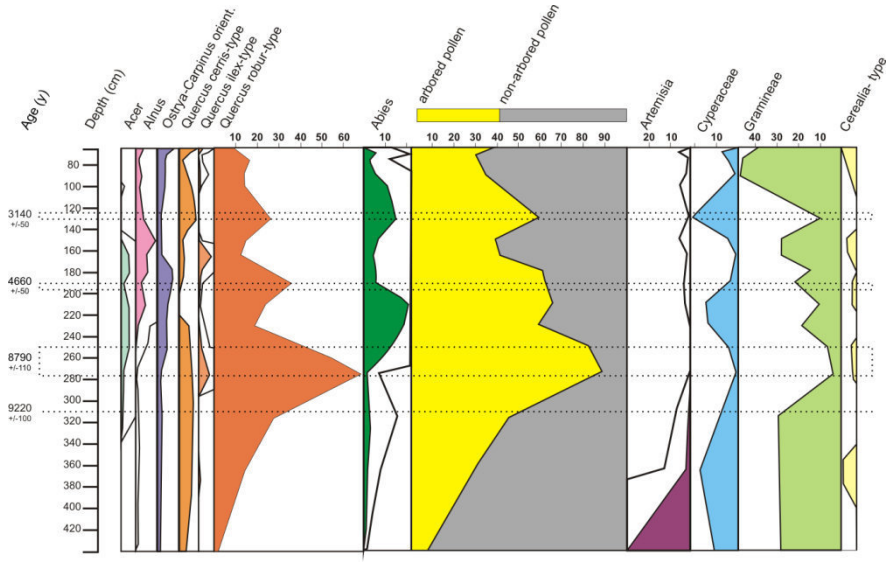

Fig.2.22. Pollen diagram of the Forano Lake (redrawn from *Kleine et al.*, 2003).

The marine deposits, on top of the Marine Flooding Surface, passing upward to a beach ridge system around 5 kyr B.P. marking the beginning of the deltaic system which is postdated in the archeological area. Indeed, the delta progradation starts about 2 km landward the *Sybaris* settlement around 6ky B.P. (according to *Bellotti et al.*, 2003, 2009). Therefore, an average progradation rate of 2 m/yr can be calculated and related to a cool (decrease of arbored pollen and *Quercus*, increase of non-arbored pollen) and wet (increase of *Abies* and *Cyperaceae*) climate (after about 5 kyr B.P.), inferred by the Forano Lake pollen diagram, which can favoured an increase of sediment supply (*Ortolani and Pagliuca*, 2014).

The deltaic complex progradation happens trough the eastward migration of a beach ridge system according to *Stanley and Bernasconi* (2009) and *Bernasconi et al.* (2010). An aggradational-progradational stacking pattern occurs between 5 and 3 kyr B.P. while later a main progradational one prevails. This can be related to the transition from ~ 2-2.8 mm/yr subsidence rates (in archeological area) to a stability-weak uplift around 3 kyr B.P.(*Ferranti et al.*, 2011) and to a cooling and drying of the climate. The latter is showed (around 3 kyr B.P.) in the Forano Lake diagram pollen by the decrease of arbored/non-arbored pollen ratio, Quercus, Abies and Cyperaceae taxa. *Joannin et al.* (2012) also observe a drying phase around 2500–1800 cal B.P. in pollen record of Trifoglietti Lake (Coastal Chain, eastern Calabria) and correlate it to the cooling phase around 2700–2500 yr cal B.P. at the Subboreal-Sublatlantic transition (*van Geel et al.*, 2000). Since 3 kyr B.P., severe land instability and degradation due to mid-Holocene climate drying and increasing human pressure are recognized in the archaeological soils of Cecita Lake (Sila Massif, middle Calabria) by *Pelle et al.* (2013). These climatic conditions can be correlated to the Little Archaic Ice Age (*Ortolani and Pagliuca*, 2007).

Furthermore, the fossil meander observed close to the present coastline suggests the existence of a greater seaward extension of the delta plain. This evolution stage can be related to Little Ice Age (1500-1850 A.D.) when very high progradation rates are observed in other Italians deltas (*Bellotti et al.*, 1995; *Ortolani and Pagliuca*, 2014).

2.8 Conclusion

The integration of well-logs, shallow geophysical and historical data allow to define the stratigraphic framework and the Holocene evolution of the Sibari Plain.

The presence of a NE-SW normal fault zone with certain activity in recent time strongly influence the plain evolution. In detail, the depressed area on the hanging wall (northward by the present Crati riverbed) favours the development of a wetland area with the deposition of thick fine-grained and peaty deposits allowed by the subsidence related both to tectonics and to sediments compaction. On the foot wall, the Crati River alluvial plain grows and the progradation of its delta starts about 6 kyr B.P.. The Crati Delta is characterized by a stratigraphic pattern very similar to the worldwide holocenic delta. Its evolution is the result of the climatic and glacio-eustatic sea level variations overlapping to the local tectonics, subsidence and human-made factors.

This study shows the fault-controlled Holocene evolution of the Sibari Plain and allows to envisage a new seismic risk scenario for this area where the widespread sandy and clayey-silty sediments can amplify the seismic shaking.

CHAPTER 3

Hydrogeological study of the Sibari Plain

3.1 Hydrostratigraphic framework of the Sibari Plain: a preliminary model.

3.1.1 Introduction

Two well-defined aquifers are recognized in the Sibari Plain by *Polemio and Luise* (2007). The shallow aquifer is extended from soil surface to -20/-30m asl and is separated from a deep one by clayey and silty-clayey layer reaching -50/-60m asl.

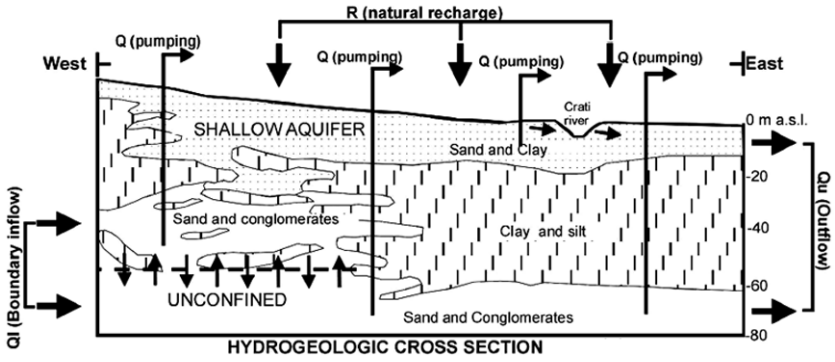

Fig.3.1.1. W-E oriented hydrogeological cross-section of the Sbari Plain proposed by *Polemio and Luise* (2007).

In the sedimentary aquifers (like that investigated here) the sedimentological and stratigraphic concepts are basic to investigate the arrangement of the hydraulic parameters (hydraulic conductivity, storage coefficient, recharge rate) (*Fraser and Davis*, 1998). Indeed, the modeling of the three-dimensional, complex, heterogeneous and anisotropic sedimentary aquifers has to based on the stratigraphic pattern reconstruction and sedimentological studies useful to define spatial variations of facies.

The previous hydrogeological and hydrogeochemical studies on the Sibari Plain (*Guerricchio and Melidoro*, 1975; *Guerricchio et al*., 1976; PTA, 2009; *Polemio et al.*, 2013) have not utilized a hydrostratigraphic framework.

A preliminary model of the Sibari Plain hydrostratigraphic framework is proposed in this work.

3.1.2 Method

The investigation of the Sibari Plain hydrostrastigraphic framework is mainly based on subsoil data analysis integrated by field survey.

Previous subsoil data, acquired for scientific and engineering aims, has been collected and critically analyzed. The following procedure has been used in the data collection:

- Research and acquisition of well-logs from public and private offices (Demanio Idrico della Provincia di Cosenza, ANAS S.p.A.), scientific papers (*Guerricchio and Melidoro*, 1975; *Casmez,* 1987*; Cherubini et alii*, 2000; *Bernasconi et alii*, 2010; *Hofman*, 2002; ISPRA, 2009), open access *database* (Archivio nazionale delle indagini nel sottosuolo L.464/84, ISPRA, 2009; ViDEPI);
- data georeference;
- Redrawing of the logs data using an omogeneous format by means of *SedLog 2.1.4* software (*Zervas et al.,* 2009);
- Creation of a GIS project to simplify data consulting.

Moreover, the well-logs database has been integrated by realization of the logs of 50 inedited boreholes.
The analyzed well-logs data are used to create cross sections in correspondence of the main hydrostratigraphic units and the aquitard top and bottom Digital Surface Model (DSM).
Furthermore, the spatial arrangement of the effective porosity is investigated by the creation of 11 maps concerning different layers between 0 and -50m (asl).

3.1.3 Characterization of the main hydrostratigraphic units

The main recognized hydrostratigraphic units are characterized by means of well-logs analysis integrated by the electrical resistivity profiles collected during the *Progetto Speciale 26* (*Casmez*, 1987). An hydrostratigraphic unit represents 'a body of rock distinguished and characterized by its porosity and permeability'(*Seaber*, 1988) and are also defined as a single entity or structure (stratum or combination of strata; fracture or fracture zone) that functions in bulk as either a water bearing (aquifer) or a water retarding (aquitard) complex relative to the adjacent strata (*Schoch*, 1989; *Maidment*, 1992).

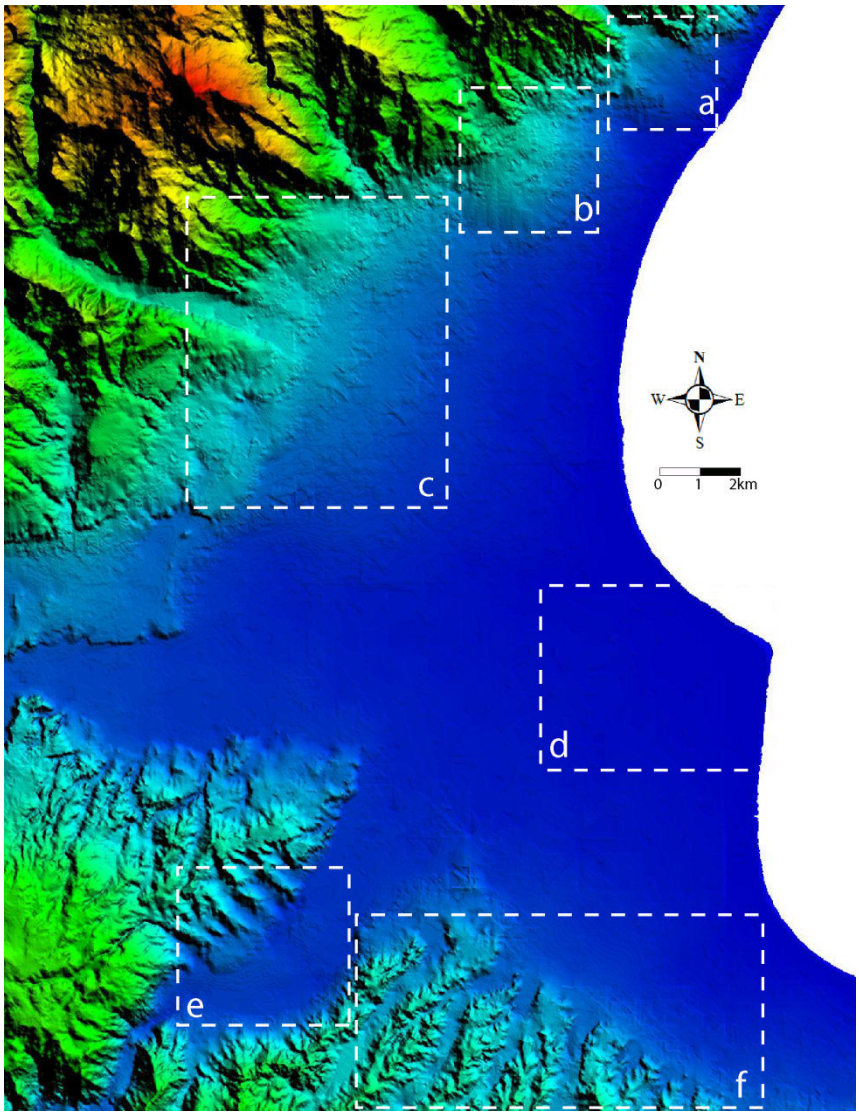

Fig.3.1.2. Location of the main hydrostratigraphic units analyzed in the Sibari Plain.

In the northernmost sector, the hydrostratigraphic framework is controlled by the Saraceno Stream alluvial fan (a), extended from the stream *knick point* to the coastline.

The beginning of the alluvial fan aggrading stage did not happen before 6.5 kyr B.P., while the still-active entrenching stage started not before 3 kyr B.P. (*Sabato and Tropeano*, 2008). The alluvial fan is mainly made by gravelly deposits, with different textures due to various sedimentological processes (debris flow, sheet flood, stream flood). Sandy bar deposits are less common and the fine-grained overbank sediments are little widespread. The maximum observed thickness of the fan is ~60 m. The coarse-grained deposits overlay, along an erosive surface, the T.te Straface Marly-Clay unit (ISPRA, 2009) which outcrops a few hundreds meters northward and southward from the alluvial fan (ISPRA, 2009; *Caruso et al.*, 2013). The clayey unit lies on top of the Saraceno Fm. (*Selli*, 1962), made by an arenaceous-pelitic alternation with controversial origin and age (*Vezzani*, 1968b; *De Blasio et al.*, 1978; *Sonnino*, 1984; *D'Alessandro et al.*, 1986; *Bonardi et al.,* 1988; *Di*

Staso and Giardino, 2002; *Torricelli and Amore*, 2003; *Caruso et al.*, 2011). In the NE sector of section 1 (fig. 3.1.3) the analysis of unpublished logs shows the presence of a cataclastic facies due to a presumed inverse fault (observe in a refraction seismic profile) which bounds the Broglio hill.

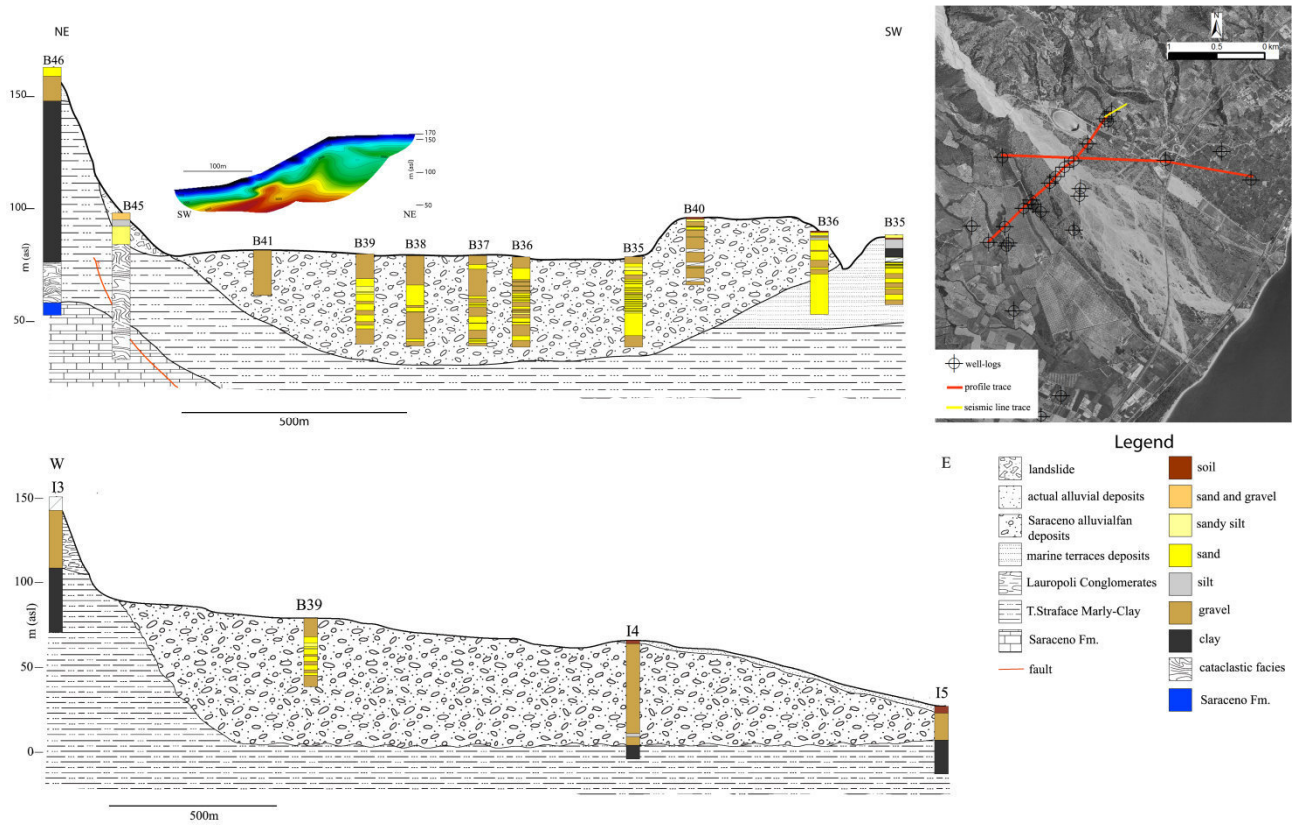

Fig.3.1.3.Cross sections of the Saraceno alluvial fan based on inedited (B) and ISPRA-L.464/84 (I) well-logs.

Southward, the Satanasso Stream alluvial fan (b) represents the main hydrostratigraphic unit. Currently it is not active and is located 2 km landward from the coastline. The fan is made by gravelly deposits with different textures. The estimated thickness reaches about 100m, but the available data do not allow to define exactly its bottom surface.

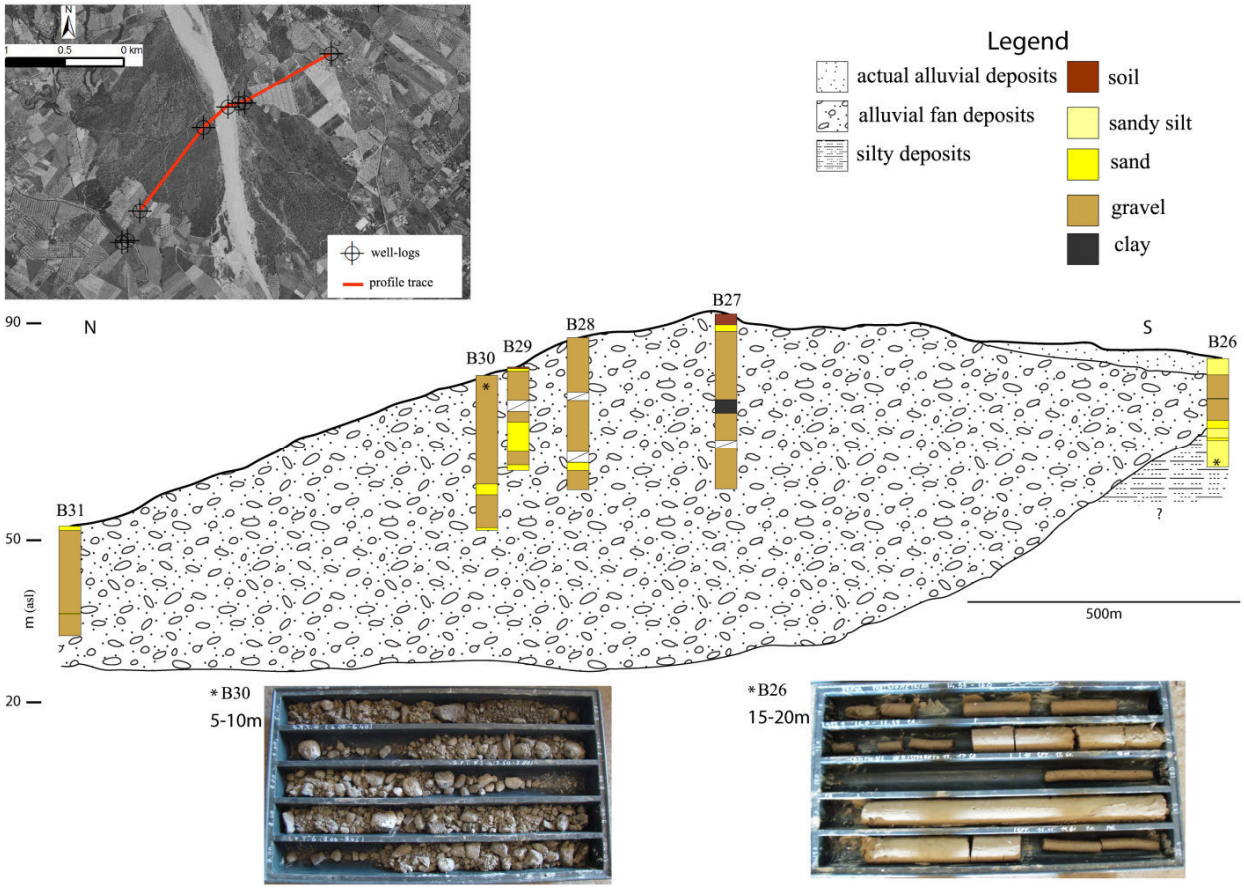

Fig. 3.1.4. Satanasso alluvial fan cross section based on inedited well-logs.

Moving southward, the Raganello Stream alluvial fan (c) is the following hydrostratigraphic unit. It consists of a telescopic alluvial fan complex and represents the bigger fan of the Sibari Plain (*Guericchio and Melidoro*, 1975). The fan thickness observed in the electrical resistivity profile (*Casmez*, 1987) exceeds 100 m. Well-logs data show 5/10m-thick silty-sandy deposits on top of the gravelly sediments which constitute the fan body.

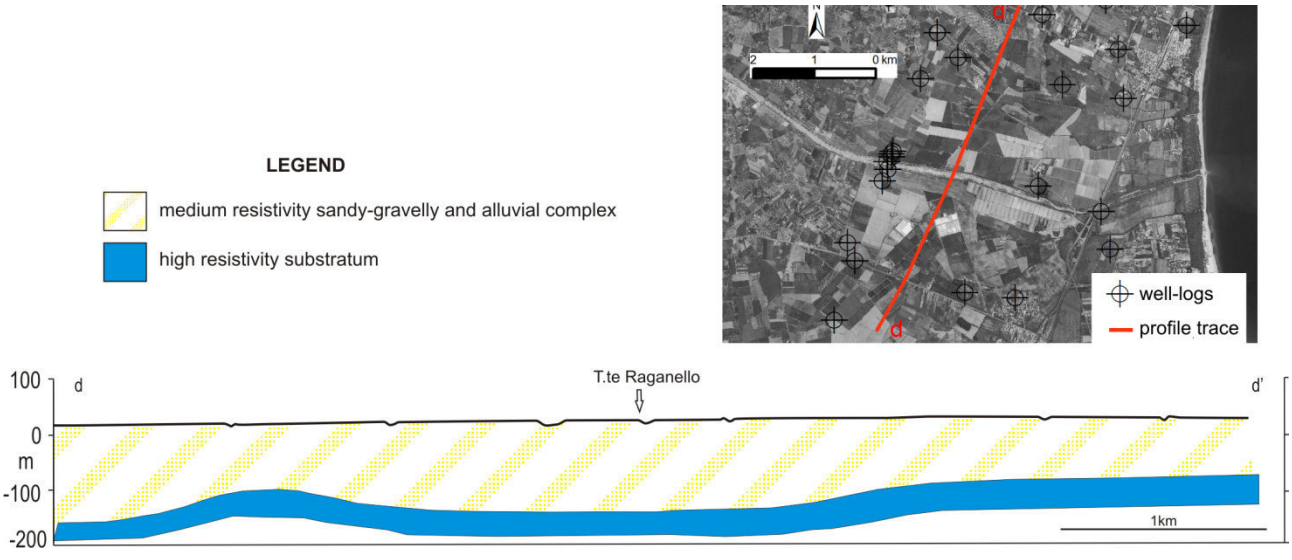

Fig. 3.1.5. Resistivity profile (*Casmez*, 1987) crossing Raganello alluvial fan.

The hydrostratigraphy of the middle sector of the investigated area is strictly related to Crati Delta (d) stratigraphic framework controlled by its Holocene evolution. In this area, the shallow aquifer consist of the sediments produced by the delta progradation started about 6 kyr B.P. (*Bellotti et al.*, 2009; Chapter 2). The underlying aquitard is made by the fine-grained deposits related to the post-glacial fast sea-level rise and lies on top of the deep aquifer which consists of late Pleistocene alluvial plain deposits (Chapter 2). The hydrostratigraphic framework is very complicated due to the heteropical transition among the sediments of the different associated depositional environments moving seaward during the delta progradation (*Stanley and Bernasconi*, 2009; *Bernasconi et al.*, 2010; Chapter 2). Another complication of the stratigraphic pattern is due to the repeated captures and separations which characterized the evolution of Crati and Coscile Rivers. Furthermore, the presence of faults with subsurface evidences (Chapter 2; *Cinti et al.*, 2013, 2015 in press) can represent a potential interchange way between shallow and deep aquifers.

In the southwestern sector of the Crati River valley, landward from its confluence with the Coscile River (e), the shallow aquifer roughly corresponds to the alluvial deposits which locally overlay the Pliocene clays (*Casmez*, 1967). The resistivity profile (*Casmez*, 1987), located near Terranova da Sibari village, shows a later extension of the alluvial deposits of ~1 km and a maximum thickness of ~75 m, while the profile 6 km toward NE reveals a thickness reaching a maximum value of ~60 m. The well-logs data allow to observe a thickness up to ~250 m for the clays which made the aquitard. The southernmost area, between S.Mauro and Cino streams, are characterized by telescopic alluvial fan complexes which started their development in the middle Pleistocene (*Guerricchio and Melidoro,* 1975).

Fig. 3.1.6. Panoramic view of a fan delta observed along Muzzolito Stream valley

3.1.4 Characterization of the aquifer thickness and geometry

We investigate the main features (thickness, geometry) of the Sibari Plain aquifers trough the creation of the aquitard top and bottom DSM. For the top layer, we select 130 well-logs retained more reliable while for the bottom one the chosen well-logs are 74. Using the created DSM and a DTM 20x20m (GN), we are able to estimate the thickness and to define the geometries of shallow aquifer and aquitard.

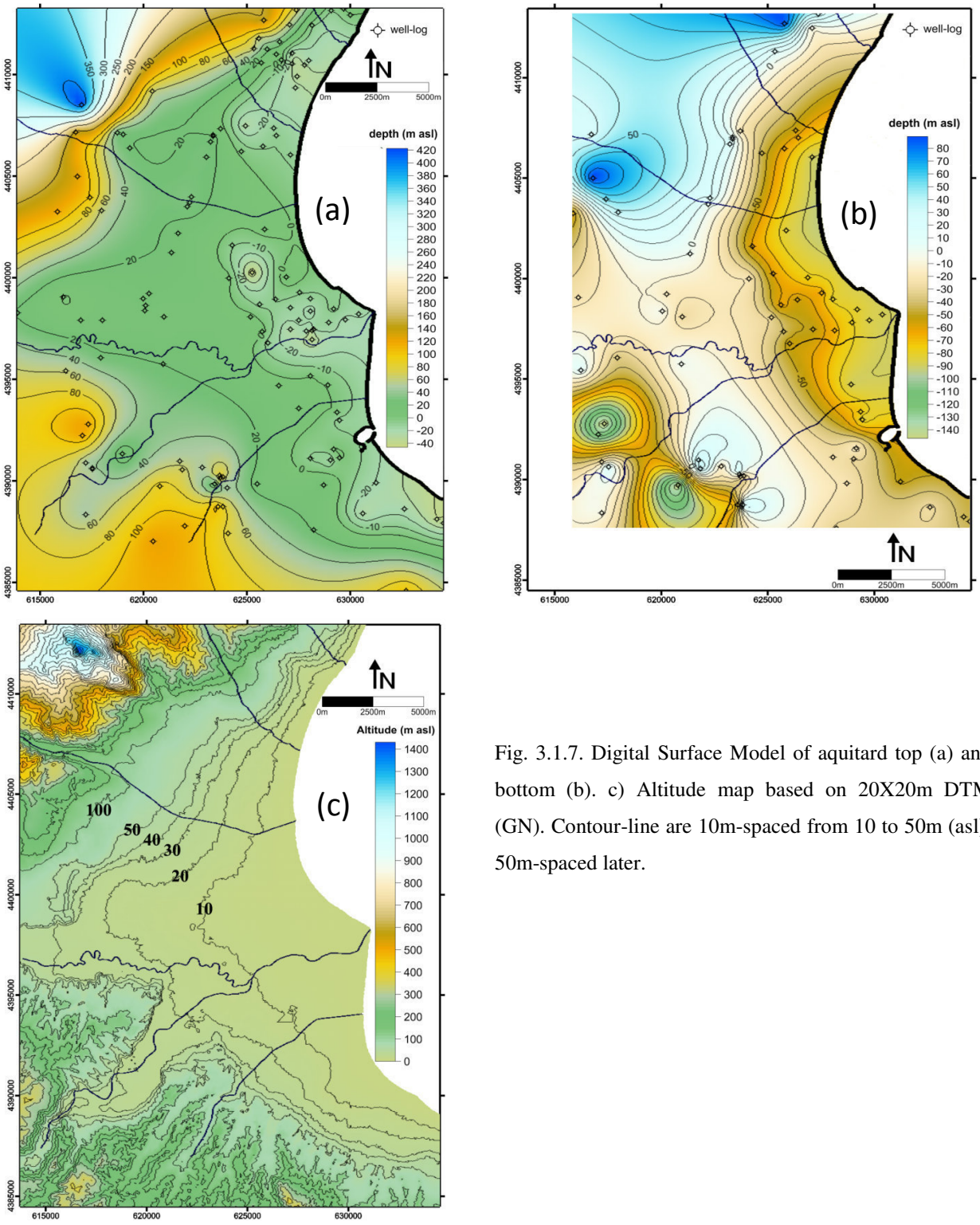

Fig. 3.1.7. Digital Surface Model of aquitard top (a) and bottom (b). c) Altitude map based on 20X20m DTM (GN). Contour-line are 10m-spaced from 10 to 50m (asl), 50m-spaced later.

Shallow aquifer is characterized by a thickness increasing from W to E and reaching its most value (~40 m) in the Crati Delta area.

In the northernmost sector, near Trebisacce village, the aquifer extension coincides with the coastal area westward bounded by the Pollino Massif. Southward, the aquifer extension increase reaching its most in correspondence of the Coscile River Valley. Toward the southern sector, the extension decreases again due to the presence of the relieves which bounded the Sila Massif. The DSM of aquitard top intersects the topography in the southwestern sector of the investigated area. In this area, field survey and the official geological maps (Casmez, 1967) confirm the aquitard (made by clayey deposits with Pliocene age) outcrop.

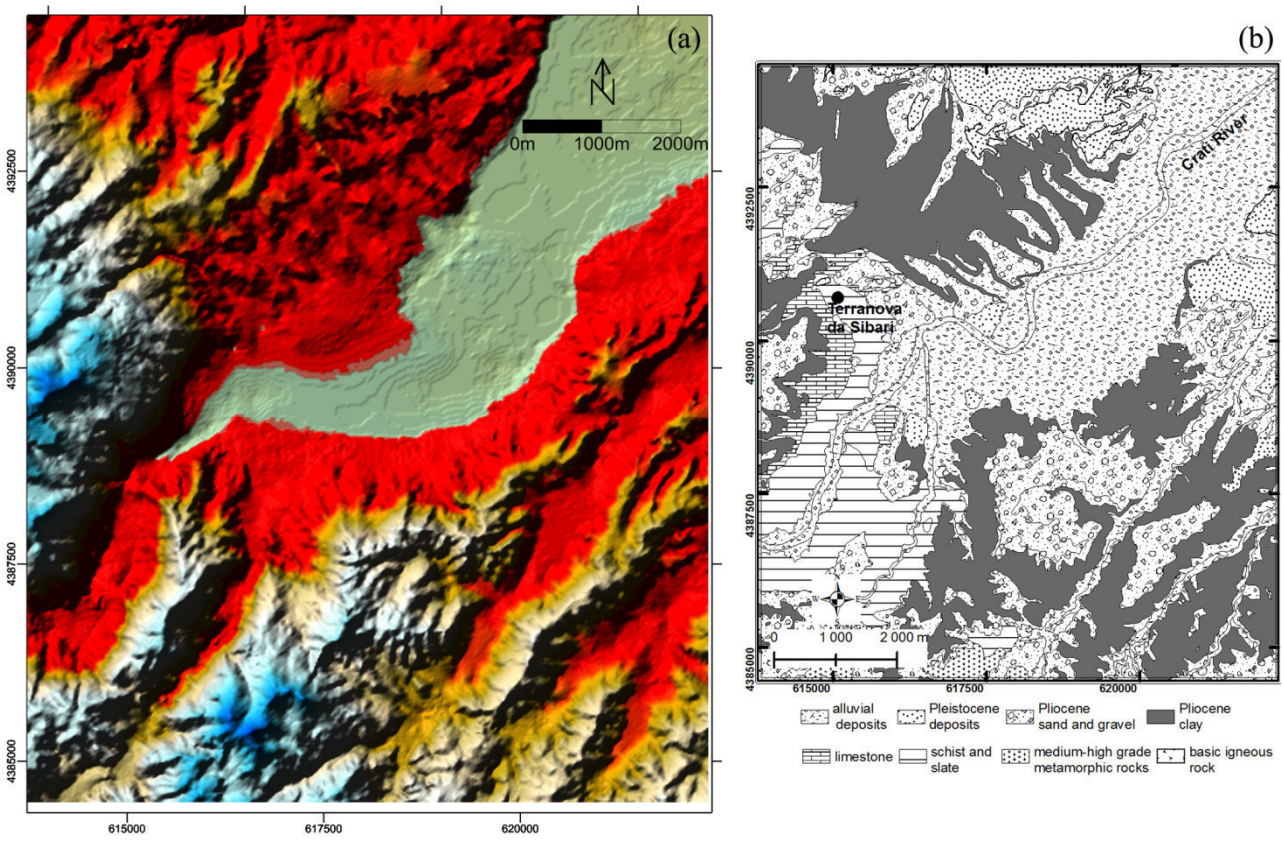

Fig.3.1.8. a) Map of the southwestern sector of the study area showing the overlap (red areas) between the topographic surface and the DSM of the aquitard top. b) Lithological map (by reprocessing of *Casmez*, 1967) of the same sector showing the outcrop of the Pliocene clays in the overlap areas.

The depth of the aquitard bottom increases gradually seaward, with the exception of the sector of the Crati Valley close to Terranova da Sibari village. Here, the acquitard bottom reaches ~ -150 m asl and the clayey deposits are 250m-thick.

The overlap of two DSM allows to observe the geometry and the thickness of the aquitard. The latter has a wedge-shape with thickness increasing seaward, except in the northwestward sector. Furthermore, the aquitard bottom intersects the top in the area of the Raganello alluvial fan revealing the contact between shallow and deep porous media. In this area, the field survey shows

the overlap of coarse-grained coastal-deltaic deposits on top of the Lauropoli Conglomerates (*Ghisetti and Vezzani*, 1983).

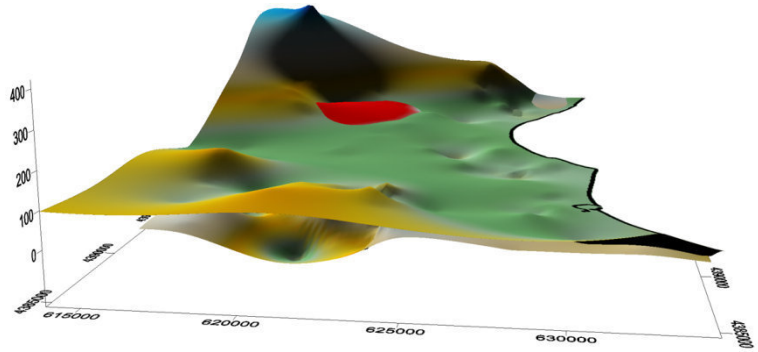

Fig. 3.1.9. Overlap of the two DSM (view from South) showing their intersection (red area) in the area close to the Raganello Stream alluvial fan (vertical scale is expressed in meters).

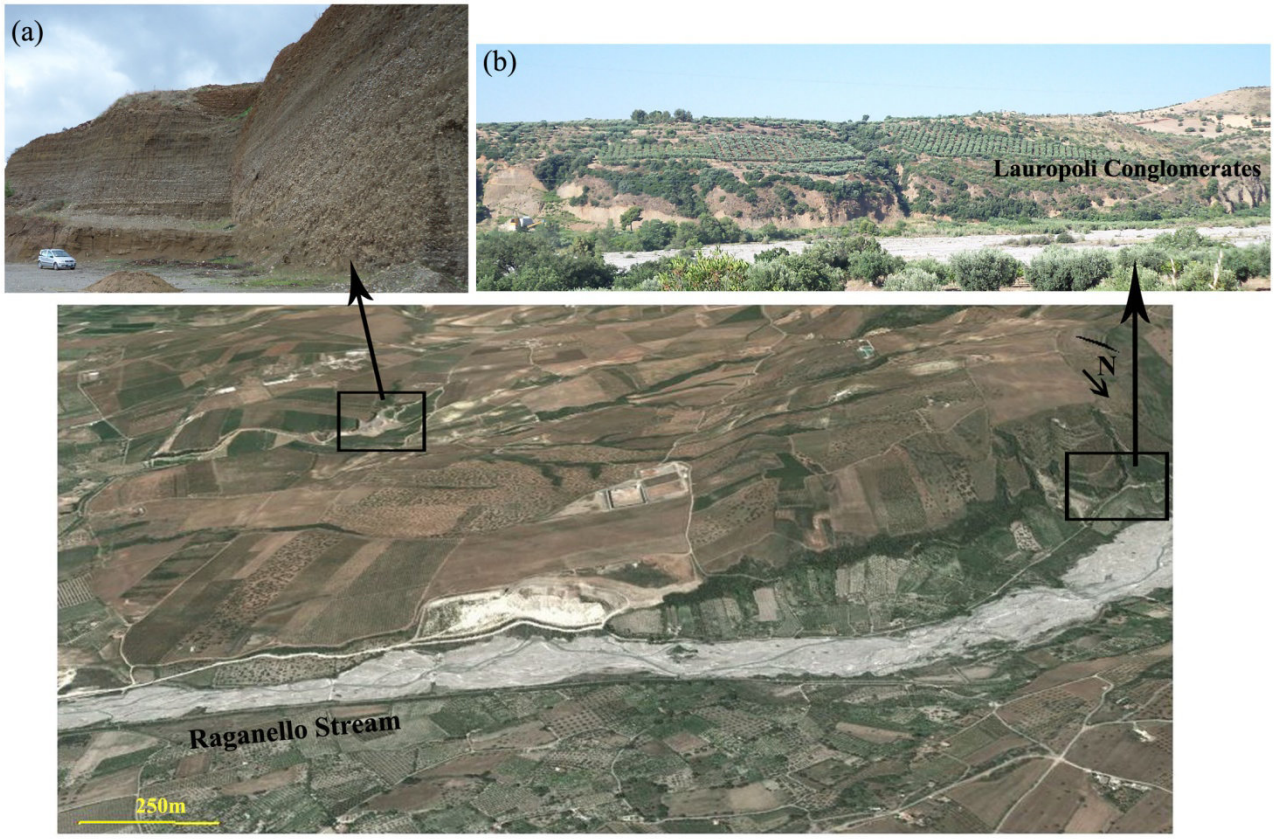

Fig. 3.1.10. View of the southern bank of the Raganello Stream (from Google Earth, vertical exaggeration 3x) showing the coarse-grained coastal-deltaic deposits (a) on top of the Lauropoli Conglomerates (b).

Along the Sibari Plain perimetral boundaries, the acquitard is made by clayey deposits with Pliocene age which can be correlated to the T.te Straface Marly-Clay unit (ISPRA, 2009). In the area close to the coastline, it is formed by silty-clayey sediments deposited during the last post-glacial transgression (*Bellotti et al.*, 2003; Chapter 2).

3.1.5 Spatial arrangement of the effective porosity and its correlation with the stratigraphic pattern

Well-log data are used to create the effective porosity (n_e) maps between 0m and -50m asl considering 11 layers (one each 5m of depth).

The effective porosity values are assigned to the different deposits referring to the values proposed by *Morris and Johnson* (1967).

lithology	**n_e**	**lithology**	**n_e**
coarse gravel	23	fine sand	23
medium gravel	24	sandy silt	8
fine gravel	25	clayey silt	5
coarse sand	27	clay	3
medium sand	28		

Table 3.1.1. n_e values (*Morris and Johnson*, 1967) assigned to different deposits

For each layer (corresponding to a different altitude) a points dataset of n_e based on the well-logs analysis is created. Later, the n_e maps are obtained by means of the interpolation method. The aim of these maps is the characterization of the aquifer heterogeneity. In detail, we investigate the relationships between porous and impermeable media. Furthermore, we try to correlate their lateral and vertical transitions to the stratigraphic pattern and the Holocene evolution of the Sibari Plain.

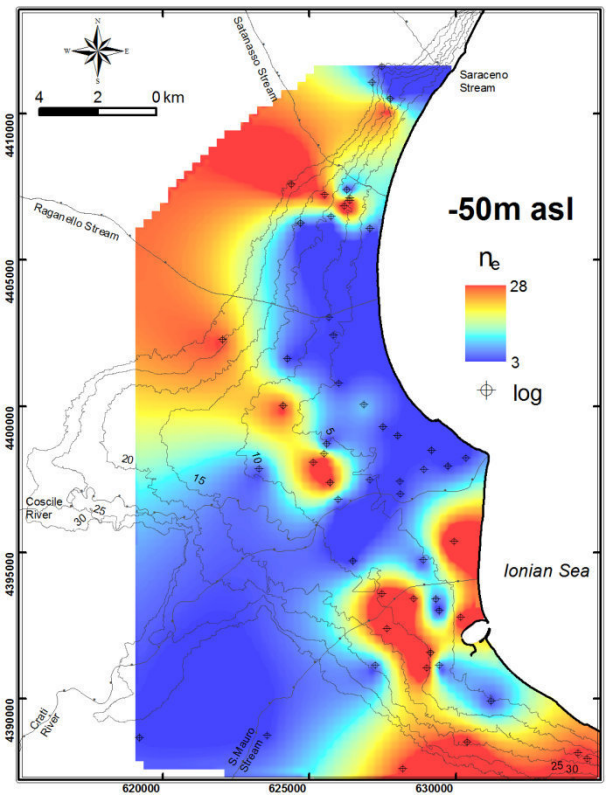
-50m asl
n_e
28
3
log
Ionian Sea
Saraceno Stream
Satanasso Stream
Raganello Stream
Coscile River
Crati River
S.Mauro Stream
4 2 0 km
620000
625000
630000
4410000
4405000
4400000
4395000
4390000

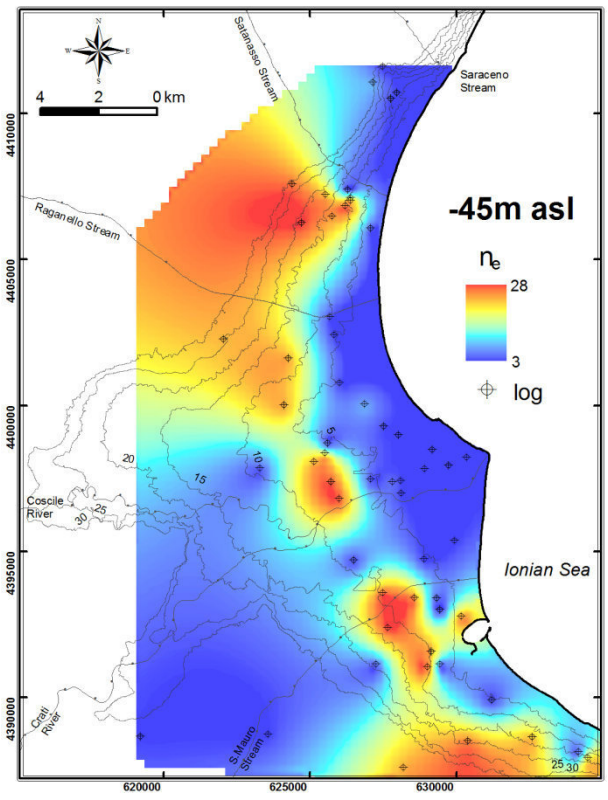
-45m asl
n_e
28
3
log
Ionian Sea
Saraceno Stream
Satanasso Stream
Raganello Stream
Coscile River
Crati River
S.Mauro Stream
4 2 0 km
620000
625000
630000
4410000
4405000
4400000
4395000
4390000

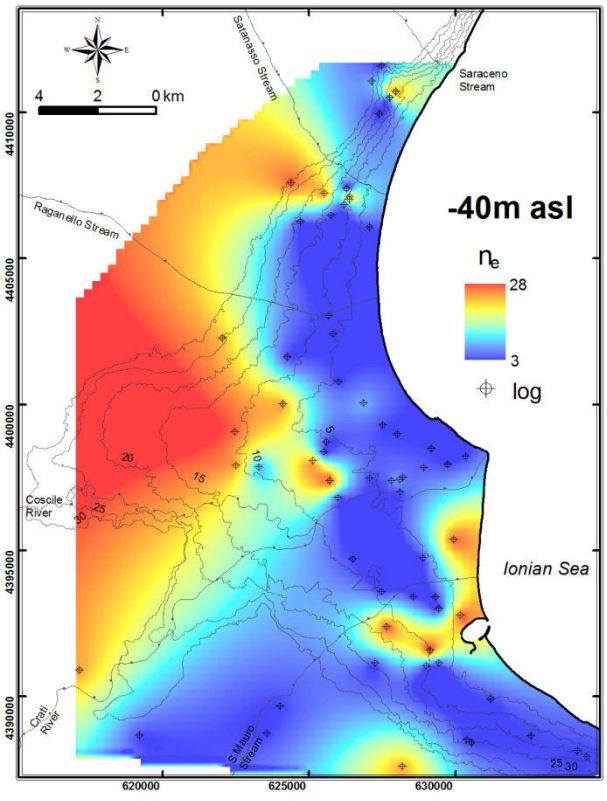
-40m asl
n_e
28
3
log
Ionian Sea
Saraceno Stream
Satanasso Stream
Raganello Stream
Coscile River
Crati River
S.Mauro Stream
4 2 0 km
620000
625000
630000
4410000
4405000
4400000
4395000
4390000

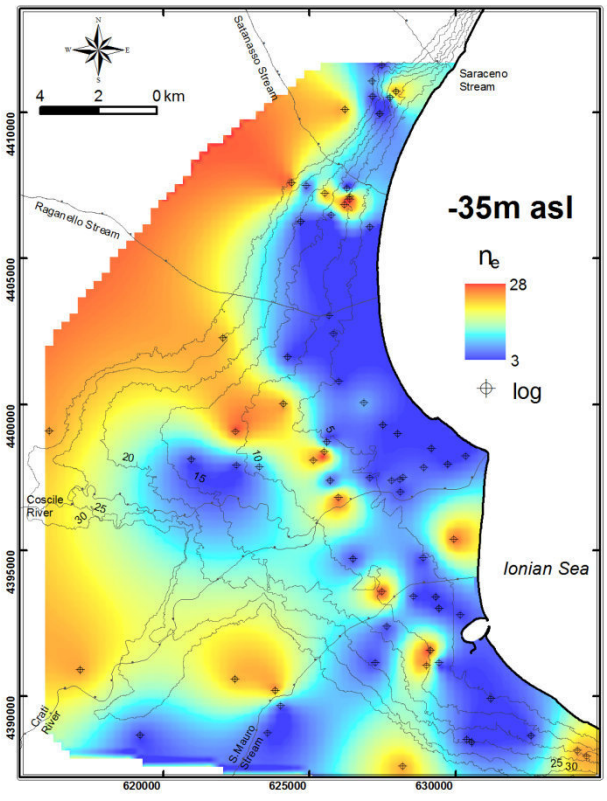
-35m asl
n_e
28
3
log
Ionian Sea
Saraceno Stream
Satanasso Stream
Raganello Stream
Coscile River
Crati River
S.Mauro Stream
4 2 0 km
620000
625000
630000
4410000
4405000
4400000
4395000
4390000

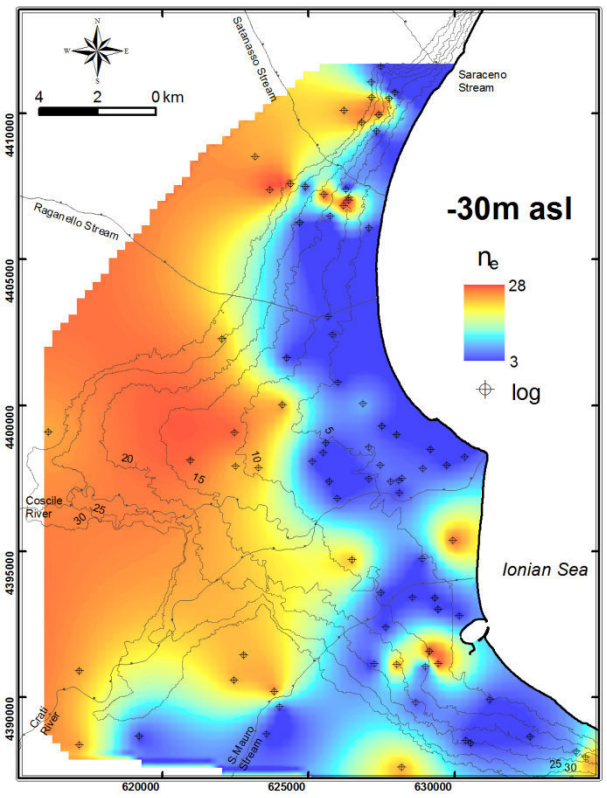
-30m asl
n_e
28
3
log
Ionian Sea
Saraceno Stream
Satanasso Stream
Raganello Stream
Coscile River
Crati River
S.Mauro Stream
4 2 0 km
620000
625000
630000
4410000
4405000
4400000
4395000
4390000

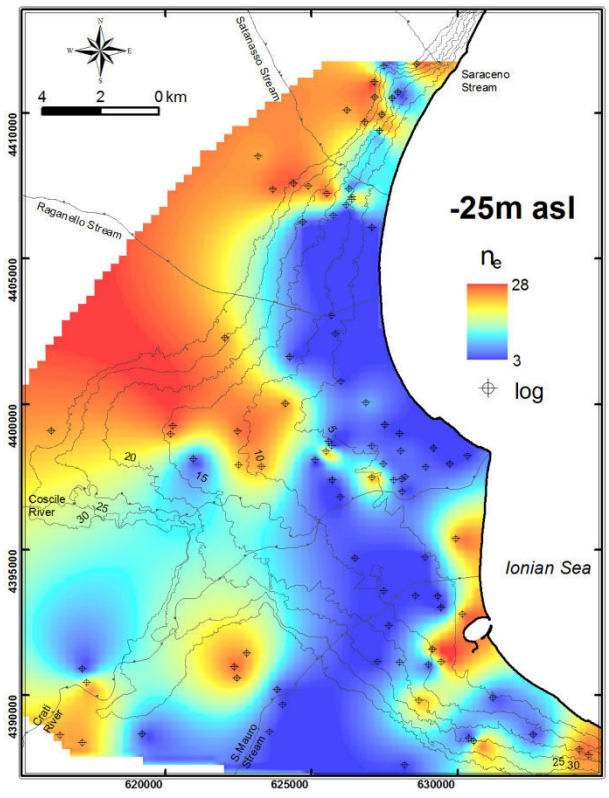
-25m asl
n_e
28
3
log
Ionian Sea
Saraceno Stream
Satanasso Stream
Raganello Stream
Coscile River
Crati River
S.Mauro Stream
4 2 0 km
620000
625000
630000
4410000
4405000
4400000
4395000
4390000

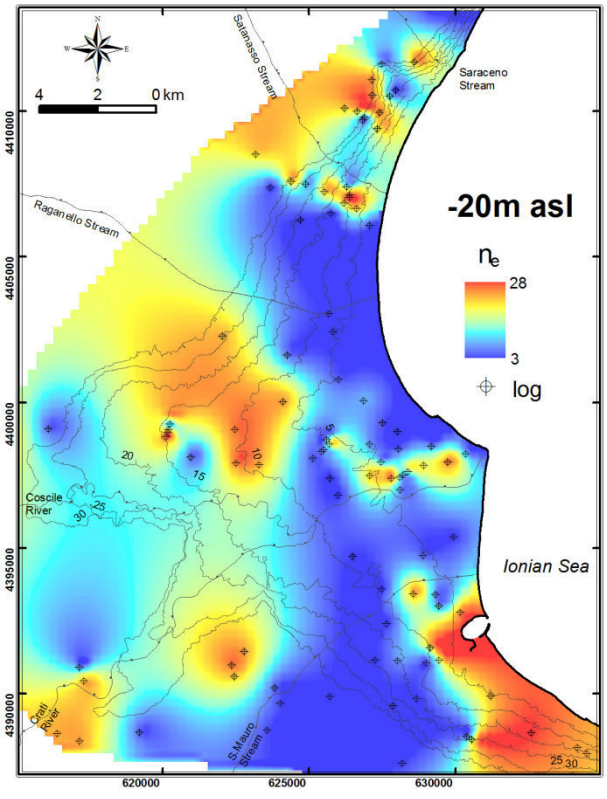
-20m asl
n_e
28
3
log
Ionian Sea
Saraceno Stream
Satanasso Stream
Raganello Stream
Coscile River
Crati River
S.Mauro Stream
4 2 0 km
620000
625000
630000
4410000
4405000
4400000
4395000
4390000

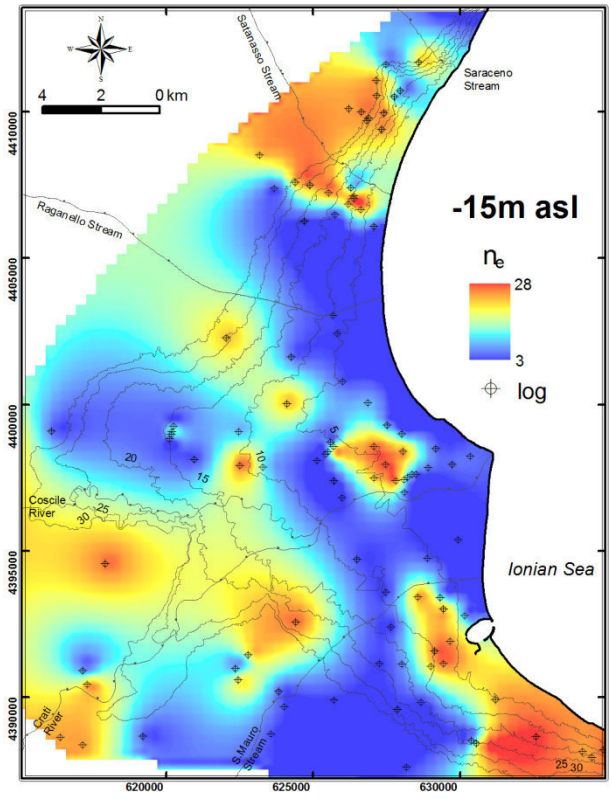
-15m asl
n_e
28
3
log
Ionian Sea
Saraceno Stream
Satanasso Stream
Raganello Stream
Coscile River
Crati River
S.Mauro Stream
4 2 0 km
620000
625000
630000
4410000
4405000
4400000
4395000
4390000

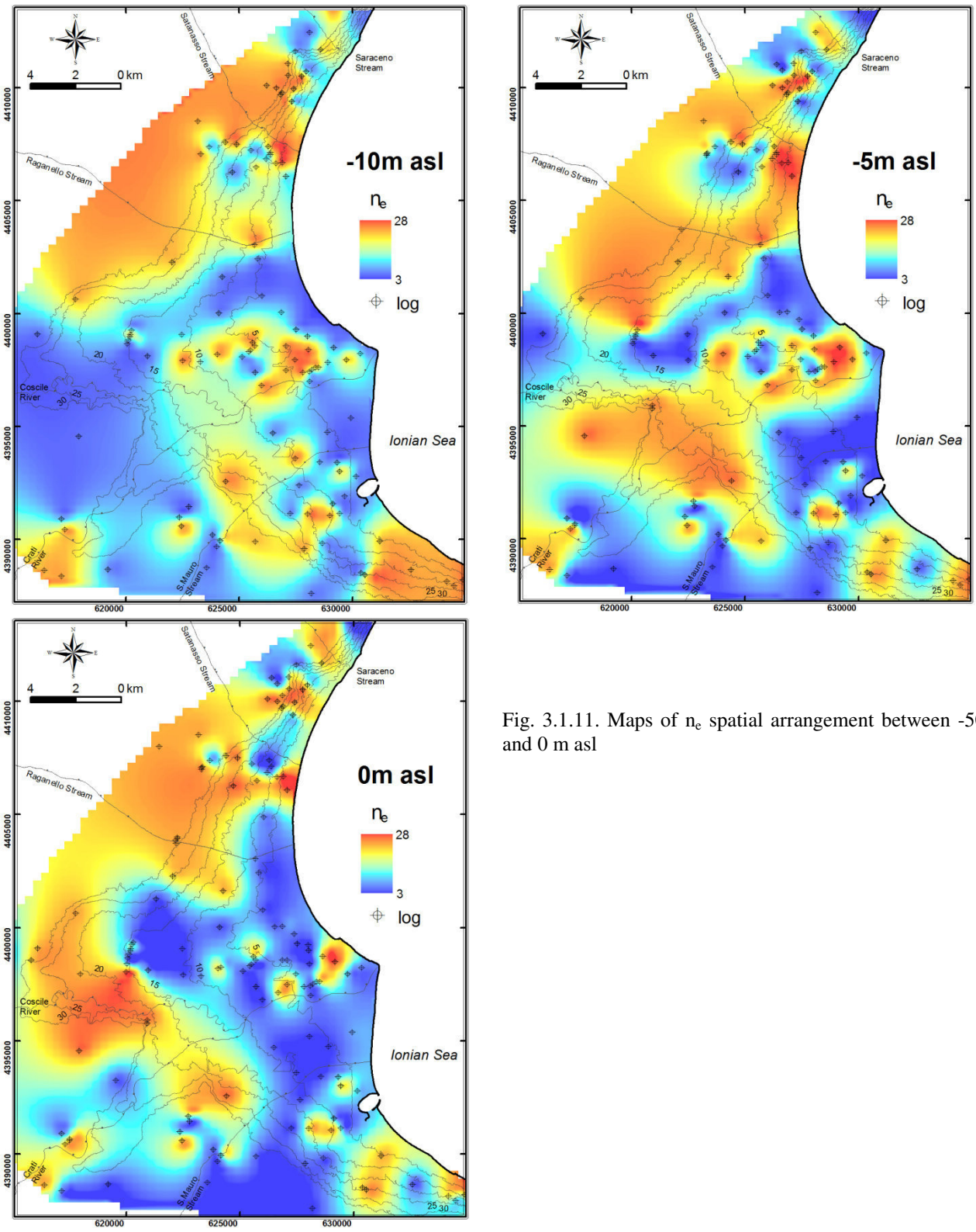

Fig. 3.1.11. Maps of n_e spatial arrangement between -50 and 0 m asl

The -50m (asl) n_e map shows a predominance of high values in NE and SW sectors. This n_e arrangement reflects the late Holocene (~6 kyr B.P.) morphological setting when the coastline ran in correspondence of the 15m-contour line (*Guerricchio and Ronconi*, 1997). A this time a wetland, passing seaward to a shallow marine bay, is present in the area northward from the actual Crati River (Chapter 2). Toward NW, the high n_e is due to the coarse-grained deposits of the Raganello

and Satanasso Streams alluvial fans, active since the middle Pleistocene (*Guerricchio and Melidoro*, 1975 and references therein), and associated coarse grained beaches. Southward, the high n_e values can be correlated to the Crati alluvial plain developed on the Sybaris Fault zone foot wall (Chapter 2).

In the -45m and -40 (asl) maps the n_e arrangement is very similar to the previous one, except for an increase of low n_e values in the coastal area probably related to the fine-grained sediments deposited during the flooding due to the post-glacial transgression (Chapter 2).

The -35m and -30m (asl) maps show a progressive increase of the high n_e values in the middle-western sector related to the shallow water embayment filling (Chapter 2). The northern sector is characterized by high n_e landward (due to the still active alluvial fans) and low n_e seaward. The SW-NE high n_e values alignment northward to the S. Mauro Stream traces the paleo-Crati riverbed (*Guerricchio and Melidoro*, 1975).

In the -25m (asl) map high n_e values appear in the coastal area close to the Corigliano harbour. It can be related with the delta plain sediments of the Crati River which debouched in the Ionian Sea close to this area (*Guerricchio and Melidoro*, 1975). Furthermore, an isolated low n_e values concentration, bounded by high n_e ones, is observed in the middle sector close to the Doria village. It represents the fine-grained and peat deposits filled an isolated morphological low (Doria Bowl) recognized by *Hofman* (2002).

The -20m (asl) shows, northward from the Crai River coastal section, an about E-W oriented alignment of high n_e bodies which record the migration toward NE of the Crati River (*Guerricchio and Melidoro*, 1975; *Belloti et al*., 2009). Moreover, low n_e values appear between Raganello and Satanasso Streams probably related to a standstill phase of the alluvial fans. The n_e arrangement in the -15m (asl) is very similar to the previous one, while the -10m (asl) map shows an increase of high n_e values in the middle sector. This increase results from the beginning (about 3kyr B.P.) of the normal regression due to the Crati Delta progradation (Chapter 2). Now, the spatial variability of n_e can be linked to the heterogeneity of sedimentological environments and processes typical of a delta plain. Furthermore, high n_e values characterize again the sector between Raganello and Satanasso Streams. The scene depicts by n_e arrangement in the -5m (asl) is the same compared to the previous map. The 0m (asl) map is instead characterized by a decrease of high n_e values (coarse-grained sediments) in the coastal areas (mainly in the middle sector). We link this decrease to the reduction of the sedimentary supply due to human-made activities as the land reclamation works (1960s-1990s) and the Tarsia dam building along the Crati River (1950s).

3.1.6 Discussion

The Sibari Plain aquifers consist of a complex association of fluvial, alluvial fan and deltaic depositional systems. In detail, in the middle plain sector the Crati Delta represents the main hydrostratigraphic unit. The delta evolution is strictly related to the Holocene post-glacial sea level rise and overlapping local factors as subsidence and tectonic (Chapter 2). The hydrostratigraphic framework in the deltaic area consists of a surface layer characterized by the heteropical transition between fluvial, deltaic and shore-zone sediments (shallow aquifer) overlay wedge-shaped fine-grained deposits (aquitard), related to the post-glacial transgression, which lie on top of a late Pleistocene coastal plain (confined aquifer).We suppose that the confined aquifer is limited to the area of the Holocene evolution and its landward boundary coincides with the maximum inland extension of the early Holocene fine-grained deposits. This theory is confirmed by the location of the artesian wells (observed in this work) (fig. 3.1.11). The thick and high conductive fluvial or shore-zone facies can facilitate the salt-wedge penetration (*Galloway and Sharp*, 1998b) which cause the saline groundwater pollution in the Crati Delta area (Casmez, 1987; PTA, 2009; this work).

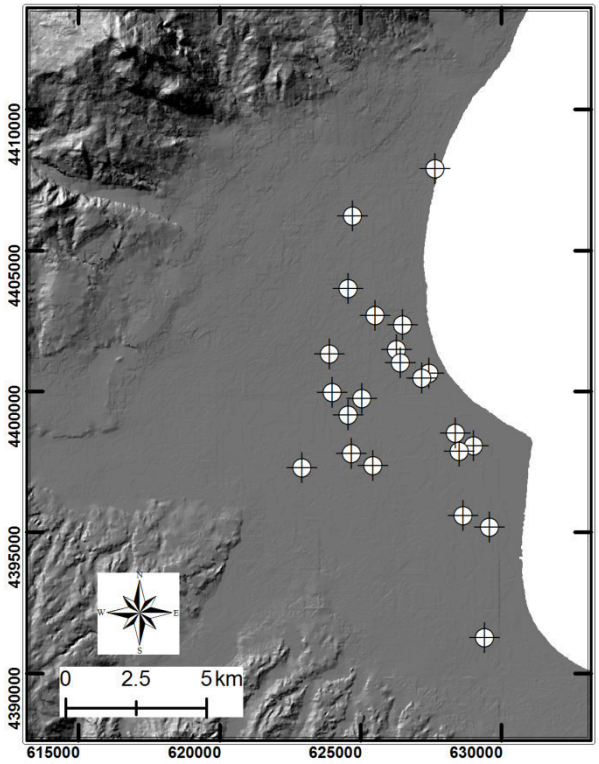

Fig. 3.1.12. Location of the observed artesian wells

The upstream sectors of Crati and Coscile Rivers represent two alluvial valleys filled by fluvial deposits. The Crati and Coscile are two mixed-load meandering fluvial systems which create a

"jigsaw puzzle" style of facies and hydrostratigraphic complexity (*Galloway and Sharp*, 1998 a, b and references therein).

The northeastern sector of the study area is instead characterized by big alluvial fans related to ephemeral streams with a prevalent coarse-grained bed load (Saraceno, Satanasso and Raganello Streams). Also these hydrostratigraphic units can be correlated to the "jigsaw-puzzle" systems (*Galloway and Sharp*, 1998a, b). In the areas between the alluvial fans, the main deposits consist of overbank or lagoon fine-grained sediments with isolated coarse-grained deposits due to processes of crevasse. These sectors are characterized by a "labyrinth" style of facies (*Galloway and Sharp*, 1998 a, b).

In the southern sector, also characterized by the presence of alluvial fans, the hydrostratigraphic pattern is very similar to the northeastern one.

Furthermore, we show that the hydrostratigraphic framework is strictly related to the middle Pleistocene-Holocene evolution of the Sibari Plain. In detail, the uplift happened along plain boundaries, testified by various orders of marine terraces (*Cucci and Cinti*, 1998; *Cucci*, 2004; *Santoro et al.*, 2009), triggered the alluvial fans development while since the early Holocene sea-level variations prevailed producing the post-glacial transgression followed by the Crati Delta progradation.

3.2 Trend of the piezometric level

The trend of the piezometric level concerning the phreatic acquifer has been analyzed using historical and field data. Historical data are chosen based on their reliability. In detail, 27 piezometric stations of 1930s reported by *LL.PP. Servizio Idrografico* and 28 field-measurement collected in 2002 by Mrs. Gatto during her degree thesis (2002).

A piezometric survey was realized in the 2013, from January to March, and 54 groundwater level measurements were collected.

Historical and field data are collected in a GIS database which allows to create the contour maps of the water-table surface of 1930s, 2002 and 2013.

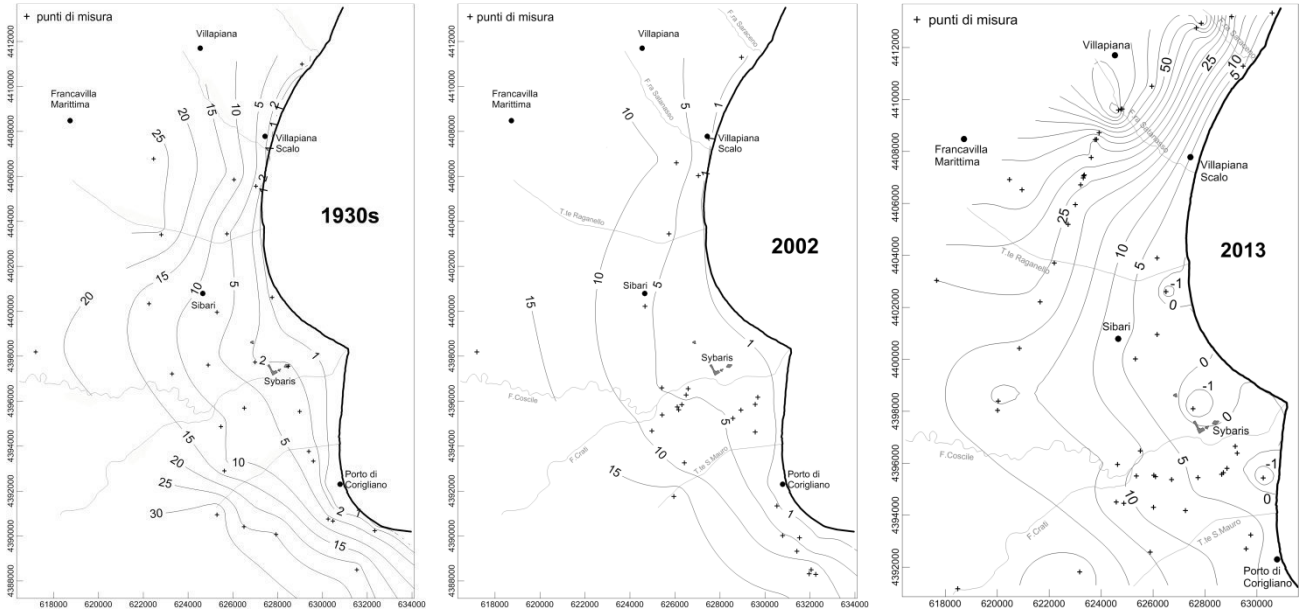

Fig.3.2.1. Contour maps of the phreatic water-table surface of 1930s, 2002 and 2013. Ground water level is expressed in m (asl).

The main ground water flow lines are created drawing the lines perpendicular to water-table contours.

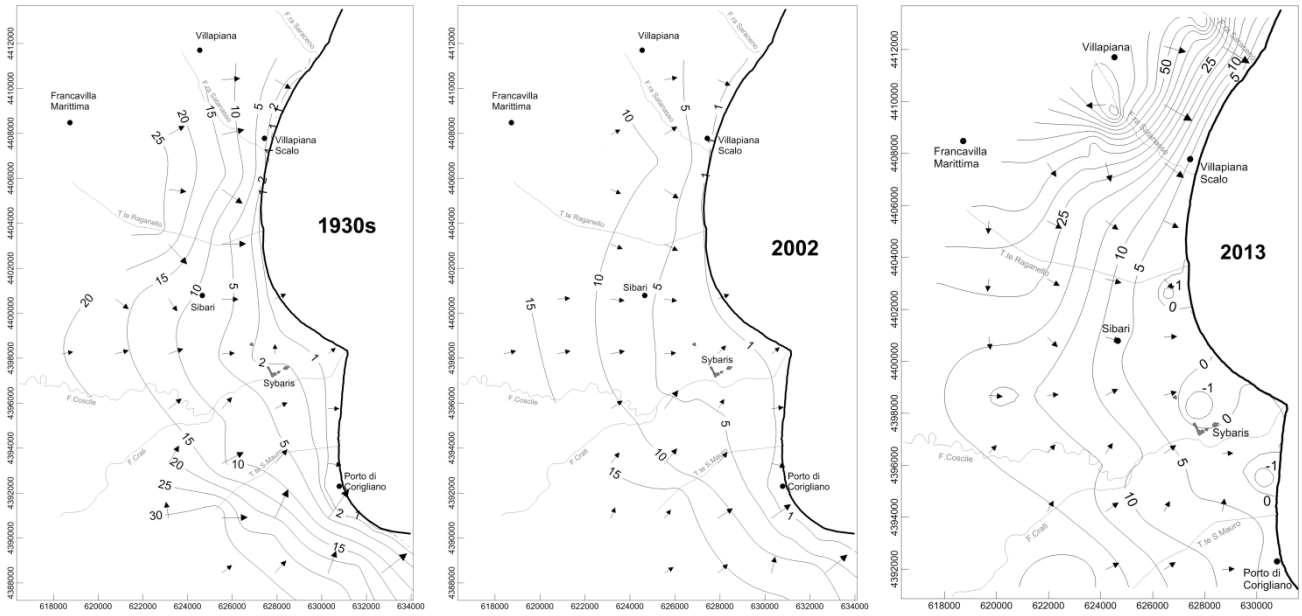

Fig.3.2.2. Groundwater flow lines of 1930s, 2002 and 2013.

The trend of the piezometric level is investigated by means of the creation of variation maps for the time periods 1930s-2002, 1930s-2013 and 2002-2013.

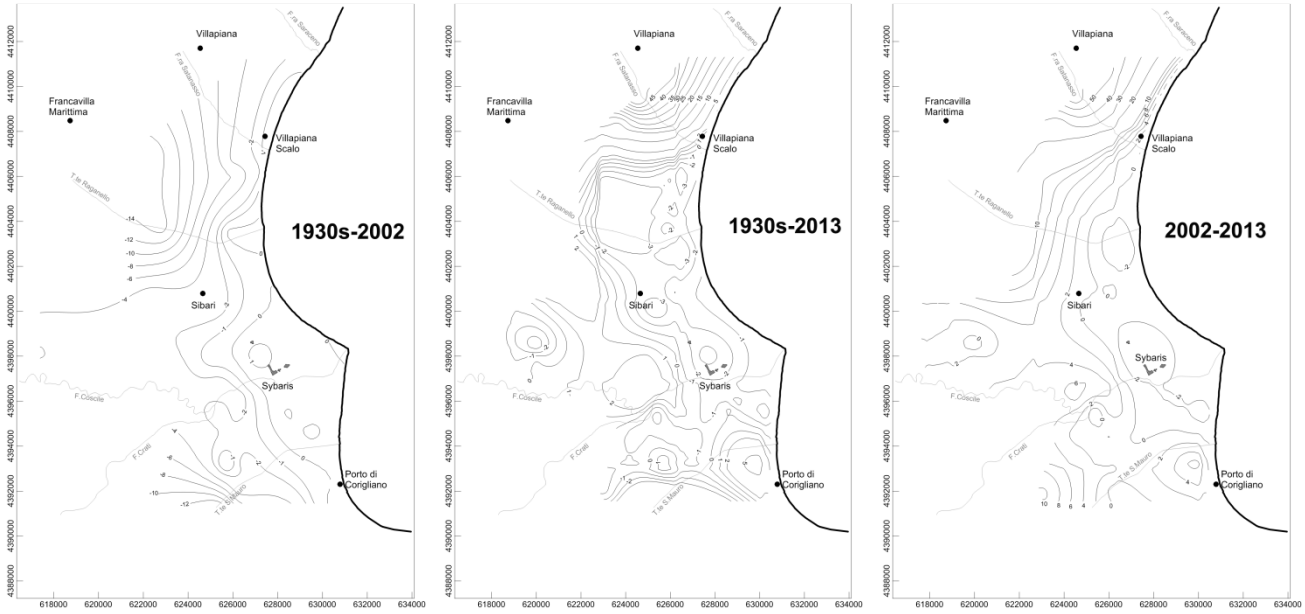

Fig.3.2.3. Water table variations maps of 1930s-2002, 1930s-2013 and 2002-2013. The variations are expressed in meters.

The 1930s-2002 variations map shows a widespread water table drop with average value of 4 m. Only in the area between *Sybaris* archaelogical site and Corigliano harbour a little water table rise is observed.

The piezometric trend between 1930s and 2013 is characterized by a water table drop (with average value of 2 m) in the coastal area between the Crati River and Villapiana Scalo, in a small area

northward from the Coscile River and in landward area between the Crati River and the S.Mauro Stream. A water table rise (with average value of 7 m) is recorded in the coastal area between Crati River and Corigliano harbour, northward from Villapiana Scalo and in a landward sector between Satanasso Fiumara and Raganello Stream.

Between 2002 and 2013 the water table fell, with an average value of 1.5m, in the coastal area between Crati River and Raganello Stream while it rose (with average value of 8 m) in other sector of study area.

The variations in the range +/- 1m cannot be considered due to the errors in the altitude definition and subsidence rates up to 2cm/yr detected by SAR data (Chapter 4).

The piezometric variations in the three time period analyzed show a widespread water table drop between 1930s and 2002 except in the area close to the Crati mouth where a small rise is observed in comparison to previous studies (*Gatto*, 2002; *Polemio et al.*, 2004, 2013).

Instead, from 2002 to 2013 a widespread water table rise occurred with a small drop only in the coastal area between the Crati River and the Raganello Stream. Furthermore, the drop peak is observed in correspondence of the *Sybaris* archaelogical site, where it can be correlated to well-points system (flow rate of 80 l/s) non-stop active to maintain the archaeological digs above the water table.

The water table drop phenomena observed during the time periods analyzed can be ascribed to the combination between ground water exploitation (agricultural uses prevails on industrial and domestic ones) and the decrease of mean rainfalls recorded both in the Sibari Plain area and in Calabria Region (*Polemio et al.*, 2004; *Buttafuoco et al.*, 2011).

In the area of the Corigliano harbour, a small water table drop in the period 1930s-2002 and a rise from 2002 to 2013 are observed despite a very high concentration of water wells (from data of the Demanio Idrico Prov. Cosenza) and the industrial groundwater exploitation.

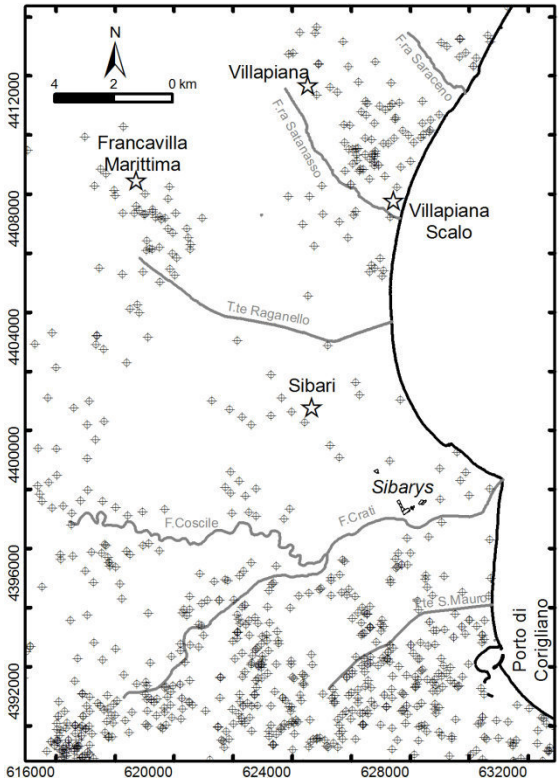

Fig.3.2.4. Location of the water wells declared at the Demanio Idrico Prov. Cosenza office (the real number is higher due to the unauthorized wells).

3.3 Potential recharge estimation of the Sibari Plain aquifers

3.3.1 Introduction

In the potential recharge area of the Sibari Plain aquifers, water balance has been calculated. In detail, all drainage basins present in recharge area (fig.3.3.1) are considered assuming the correspondence between watersheds and hydrogeological limits. The study area includes 27 drainage basins with a global area of 3466.6 km^2.

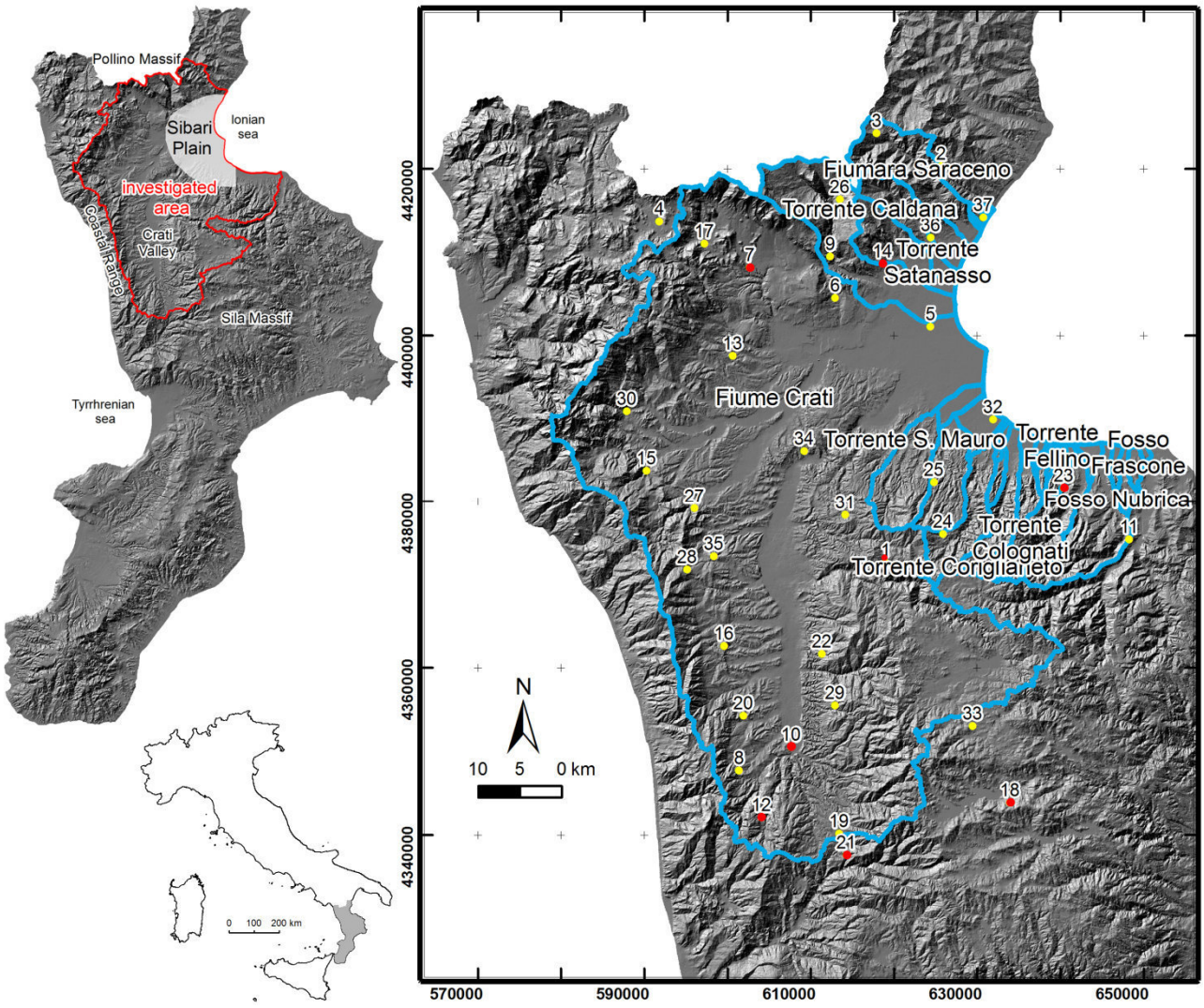

Fig. 3.3.1. Location of study area with all drainage basins considered, pluviometric (yellow circles) and thermopluviometric (red circles) stations.

The Sibari Plain is located in the northeastern sector of the Calabria Region (South Italy) in correspondence of the boundary between the Calabrian Arc and the Southern Apennine. This plain is characterized by two well-defined aquifers; the shallower one (from soil surface to -20/-30 m a.s.l.) is separated by clayey and silty-clayey layer from a deeper one (from -50/-60 m a.s.l.) (*Polemio and Luise*, 2007).

A new method, inspired to the Inverse Hydrogeological Balance (*Civita*, 2005), are used trough the integration of a correction coefficient of the potential infiltration coefficient (c.i.p.) based on the *Progetto di Bacino del fiume Arno – Stralcio Bilancio Idrico* (AdBArno, 2008). Inverse Hydrogeological Balance method is an indirect method and consists of a numerical model with parameters arranged with a GIS software. This method allows to obtain an estimation of the infiltration rate starting from climate (rain and temperature), topographic (altitude and slope) and hydrogeological (soil permeability) data. The investigated area must be divided in square cells to which are assigned all the parameters necessary for the water balance estimation. Furthermore, a new GIS procedure for the rainfall and temperature distribution has been created.

3.3.2 Method description

In this work a new method is proposed for the potential recharge estimation based on climatic, topographic, geological and hydrogeological data, elaborated with an innovative GIS procedure.

Stage 1- Meteo-climatic parameters estimation

In the first stage the meteo-climatic parameters (rainfall and temperature) of the investigated area are estimated.

The Average Pluviometric Modulus are estimated starting from the thermo-pluviometric data of Arpacal database relative to a period of thirty years (1970-2000). In detail 29 pluviometric and 8 thermopluviometric stations (fig.3.3.1, tab.3.3.1) are analyzed.

n.	station	n.	station	n.	station	n.	station
1	Acri	11	Cropalati	21	Rogliano	31	S.Sofia d'Epiro
2	Albidona	12	Domanico	22	Rose	32	Schiavonea
3	Alessandria del Carretto	13	Firmo	23	Rossano	33	Sculca
4	Campotenese	14	Francavilla Marittima	24	S.Giacomo d'Acri	34	Tarsia
5	Caselle	15	Malvito	25	S.Giorgio Alb.	35	Torano
6	Cassano all'Ionio	16	Montalto Uffugo	26	S.Lorenzo Bellizzi	36	Trebisacce
7	Castrovillari	17	Morano calabro	27	S.Marco Argent.	37	Villapiana
8	Cerisano	18	Nocelle	28	S.Marino di Finita		
9	Civita	19	Piane Crati	29	S.Pietro in Guarano		
10	Cosenza	20	Rende	30	S.Sosti		

Tab.3.3.1. List of the pluviometric and thermopluviometric stations used (for their location see fig.3.3.1).

The study area was divided in 5 sectors depending on their homogeneous morphology and climate. This subdivision is necessary because the orography of the area is complex and influences the rain distribution.

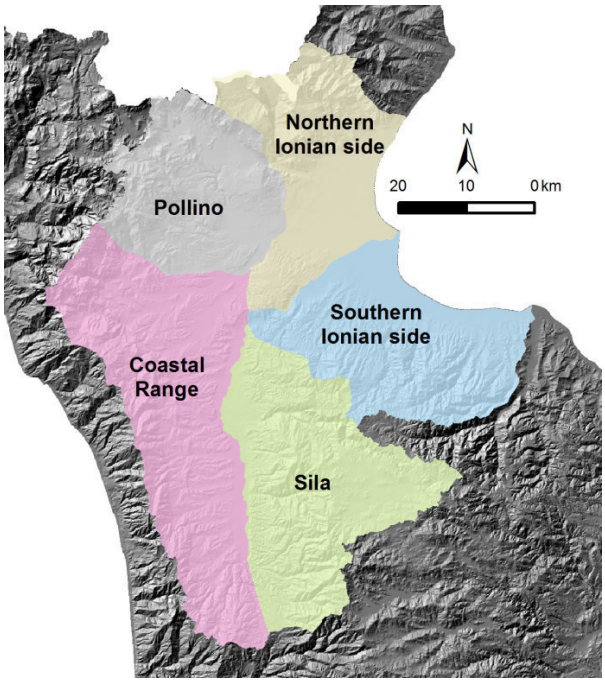

Fig. 3.3.2.Climatic sectors present in the investigated area.

In each sectors, using the data of the relative pluviometric stations, rainfalls are determined by a linear regression as function of altitude R=f(q).

- sector 1 – northern Ionian side : 0.3427808341 * q + 538.9498608 R^2=0.80
- sector 2 – southern Ionian side : 0.7342542095 * q + 563.9783327 R^2=0.80
- sector 3 – Pollino : 0.98877983079 * q + 396.9676075 R^2=0.83
- sector 4 – Sila : 0.2865014086 * q + 824.0390339 R^2=0.70
- sector 5 – Coastal Range : 1.131366381 * q + 905.7756799 R^2=0.56

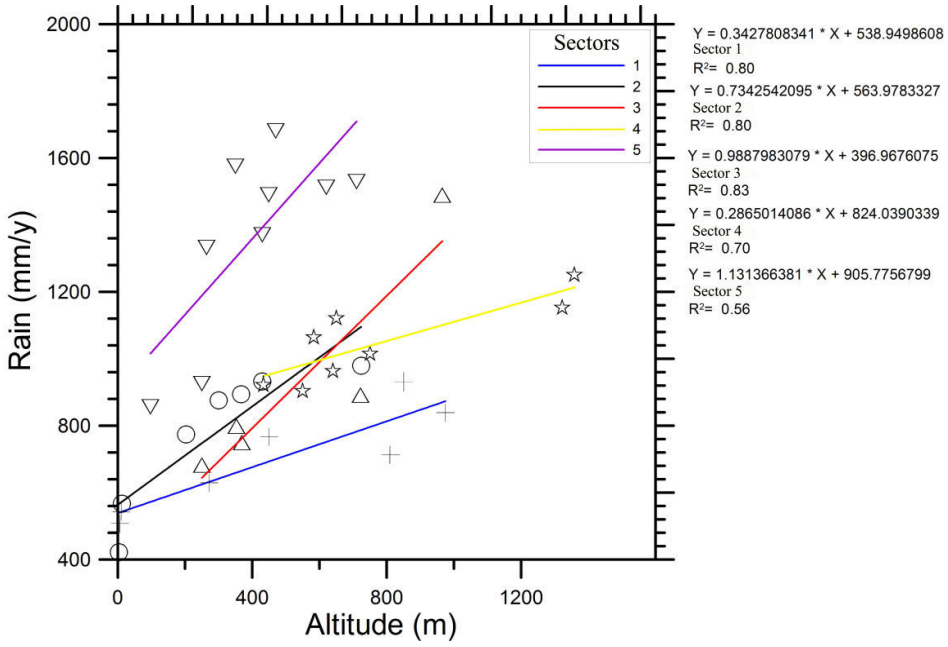

Fig.3.3.3. Functions of linear regression of the 5 sectors.

The distribution of the Average Annual Pluviometric Modulus are determined by the previous described functions and altitude data. The raster format of a DTM 20X20m (GN) was resampled with a 50X50m cell and converted from raster to a point's shapefile (one point for each cell) with associated altitude data. The altitude value of each point was used in the function R=f(q) (according to the relative sector) to obtain the average annual pluviometric modulus.

The analysis of the 8 thermopluviometric available stations allows to investigate the temperature spatial variations in the study area. In detail, we analyzed the correct temperature (Tc) depending on the rainfall. The choice of the Tc depends on the application of the simplified Turc formula (*Turc*, 1954) in the evapotranspiration calculation.

Tc was calculated for each thermopluviometric station by the formula:

$$\boldsymbol{Tc = \sum_{i=0}^{n} R_i T_i / R}$$

R_i and T_i represent respectively the average monthly rainfall (mm/yr) and temperature (°C) of the *i*-th month. *R* is the average annual rainfall (mm/yr) from 1970 to 2000.

Later, the linear regression function Tc=f(q) was defined for the whole study area and not for sectors because Tc values are corrected depending on the rainfall values.

The defined function is Tc= -0.00678224841*q +14.44436976 with R^2=0.89 which testifies the good correlation between temperature and altitude.

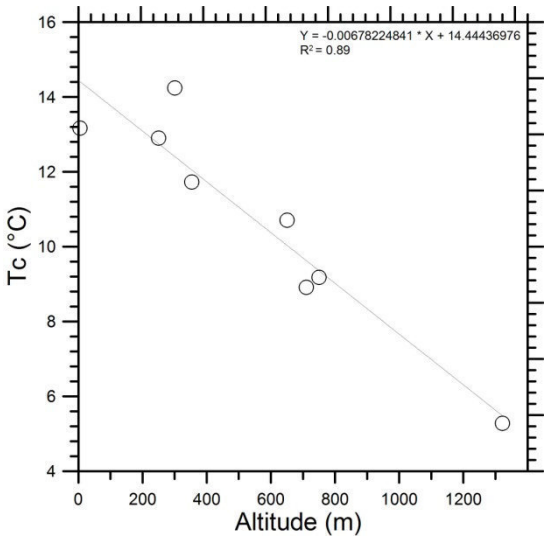

Fig. 3.3.4. Linear regression line Tc-altitude.

Using the function Tc=f(q), the Tc was calculated for all points obtained by the resampled DTM.

Known the average annual pluviometric modulus (P) and the correct temperature the Real Evotranspiration (RET) was calculated by means of the simplified Turc formula:

$$\mathbf{RET} = \frac{P}{\sqrt{0.9 + \frac{P^2}{L^2}}}$$

L represents the atmospheric power of evaporation and was calculated with the formula $L=300+25Tc+0.05Tc^3$.

The values of the average annual pluviometric modulus (P) and the Real Evotranspiration (RET), obtained for all points derived from the transformation of the resampled DTM, allow to calculate the Effective Rainfall (Reff) for each point:

$$\boldsymbol{Reff = P - RET}$$

The map of *Reff* (fig.3.3.5) was generated by the interpolation of all its punctual values.

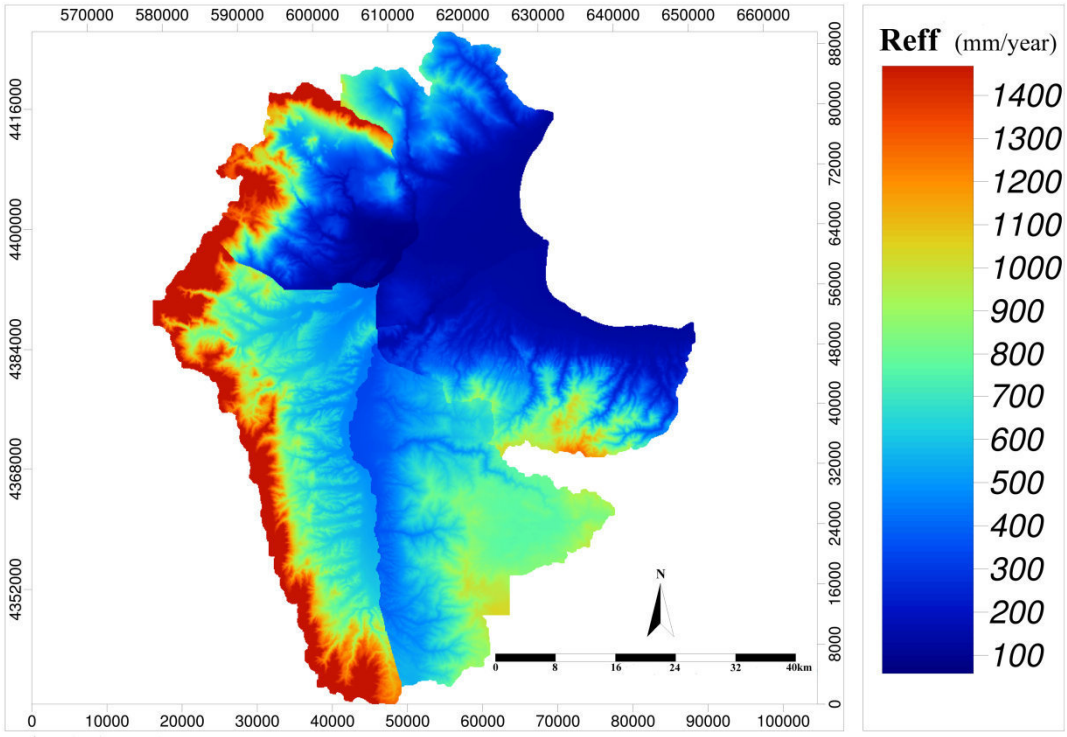

Fig.3.3.5. Map of the effective rainfall.

Stage 2 – c.i.p.$_g$ e del c.i.p.$_{ss}$ arrangement

During the second stage, the spatial variability of the potential infiltration coefficient (c.i.p.$_g$) was investigated. Furthermore, a correction factor (*c.i.p.$_{ss}$*) based on slope and soil use was calculated and mapped.

The *c.i.p.$_g$* values are strictly connected with the outcropping lithology. A simplified geolithological map (fig.3.3.6) was created to estimate *c.i.p.$_g$* values. In detail, we used the Official Geological Map of Calabria (*Casmez*, 1967-1969) and defined different lithological complexes based on genesis and compositional features of the mapped rocks.

An average *c.i.p.*$_g$ value was assigned to each complex using the range values proposed by *Celico* (1988).

Lithological complex	**c.i.p.g %**	**Lithological complex**	**c.i.p.g %**
Limestone	90-100	Lava	90-100
Dolomitic limestone	70-90	Pyroclastics deposits	50-70
Dolostone	50-70	Pyroclastite and lava	70-90
Marly limestone	30-50	Intrusive rocks	15-35
Coarse detritus	80-90	Metamorphic rocks	5-20
Alluvial deposits	80-100	Sands	80-90
Clayey-marly-sandy deposits	5-25	Clayey sands	30-50

Tab.3.3.2. c.i.p.$_g$ values proposed by *Celico* (1988).

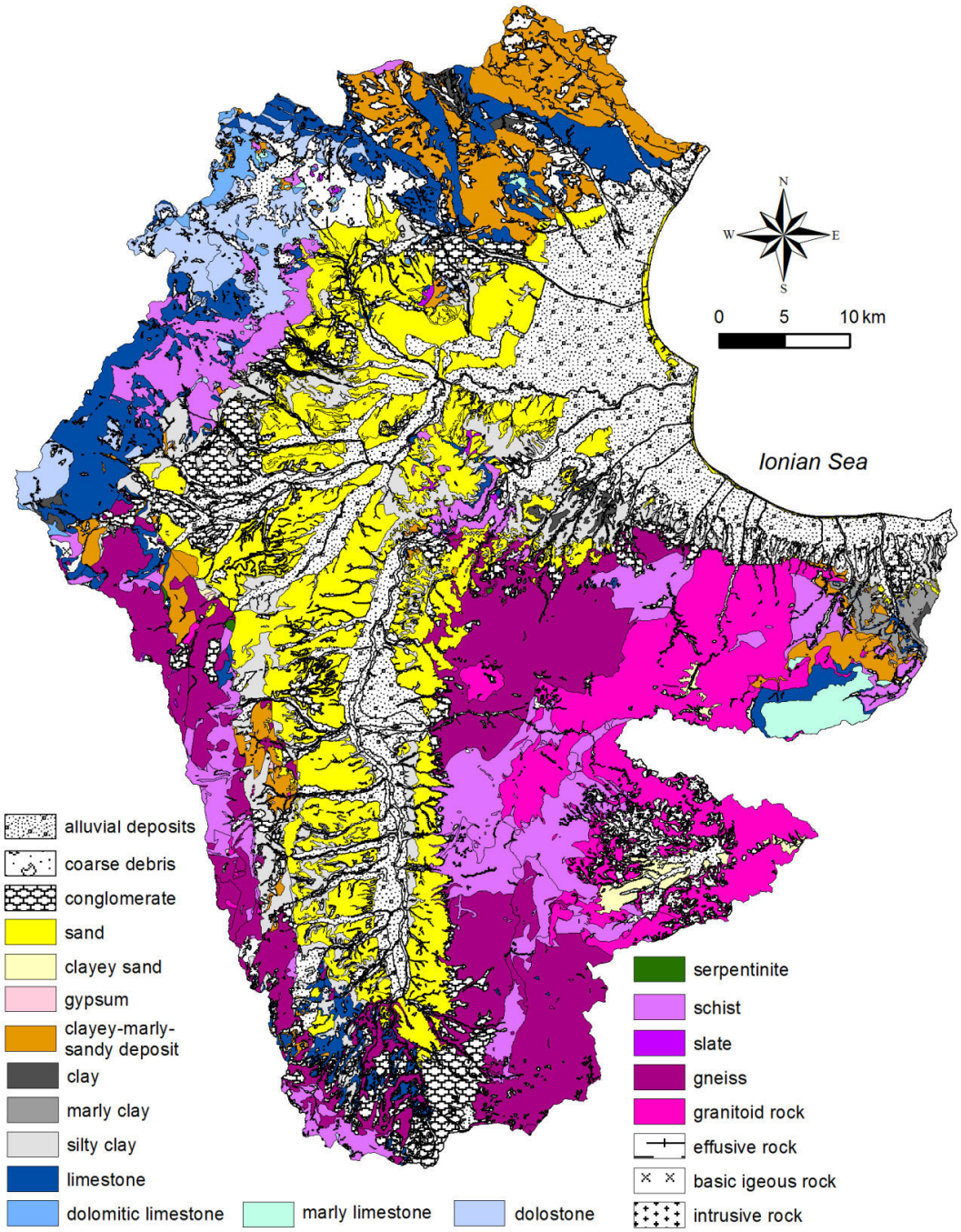

Fig.3.3.6. Simplified geolithological map obtained by the elaboration of *Casmez* (1967-1969).

The estimation of the $c.i.p._{ss}$ was based on the matrix developed in the *Bacino del fiume Arno – Stralcio Bilancio Idrico* (AdBArno, 2008).

The slope map (fig.3.3.7) was obtained starting from a 20X20m DTM (GN) and later reclassified in four classes depending on the influence of slope on the infiltration (*AdBArno*, 2008).

Soil use analysis of the investigated area was based on the maps of the CORINE Land Cover 2000 (ISPRA, 2000). In detail, we used the third level of these maps which includes 31 soil use classes; the classes were reclassified in the four categories suggested by *AdBArno* (2008): urbanized areas and uncovered rocks, grazing land, cultivated and wood land and forest.

CORINE Land Cover, level 3	**Reclassification (AdBArno, 2008)**
Sparse vegetation areas	urbanized areas and uncovered rocks
Quarries and mines	
Industrial and commercial areas	
Harbours	
Ponds	
Building sites	
Dumps	
Inland swamps	
Highways and railways	
Uncovered rocks, cliffs, outrops	
Continuous urban fabric	
Discontinuous urban fabric	
Natural grazings and high altitude pastures	grazing land
Fired areas	
Sport and recreational areas	
Stable grasslands	
Woodlands and shrublands in evolution	cultivated and wood land
Agricultural land with natural areas	
Annual cultivations associated with permanent cultivations	
Orchads	
Rice fields	
Arable lands in irrigation areas	
Arable lands in non-irrigation areas	
Permanent cultivation systems	
Beaches, dunes, sands	
Olive tree groves	
Vineyards	
Sclerophyllous vegetation areas	forest
Conifer woods	
Broad-leaved woods	
Mixedwoods	

Tab.3.3.3. Reclassification of CORINE Land Cover2000-level 3 proposed by *AdB-Arno* (2008).

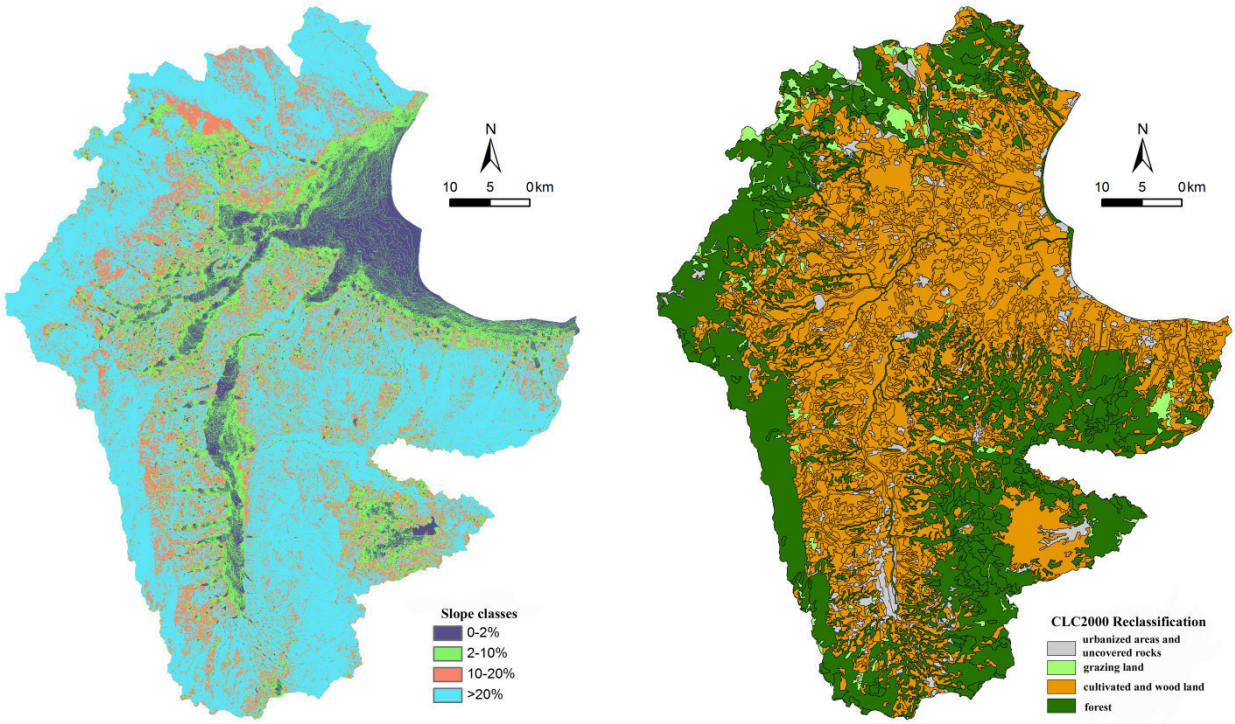

Fig. 3.3.7. Slope classes map (left) and reclassification map of CORINE Land Cover 2000-level 3 based *on AdBArno* (2008) (right).

The slope and simplified soil use maps (fig.3.3.7) was "intersected" to obtain a single shapefile containing both information. These data combination allowed to assign the *c.i.p.*$_{ss}$ values.

		Soil use			
		10	20	30	40
slope	0-2%	B	A	E	E
	2-10%	B	M	A	E
	10-20%	B	M	M	A
	>20%	B	B	M	A

class	***c.i.p.*$_{ss}$**
B	50
M	65
A	85
E	100

Tab.3.3.4. Matrix depending on slope and soil use proposed by *AdB-Arno* (2008) to assign c.i.p.$_{ss}$ values

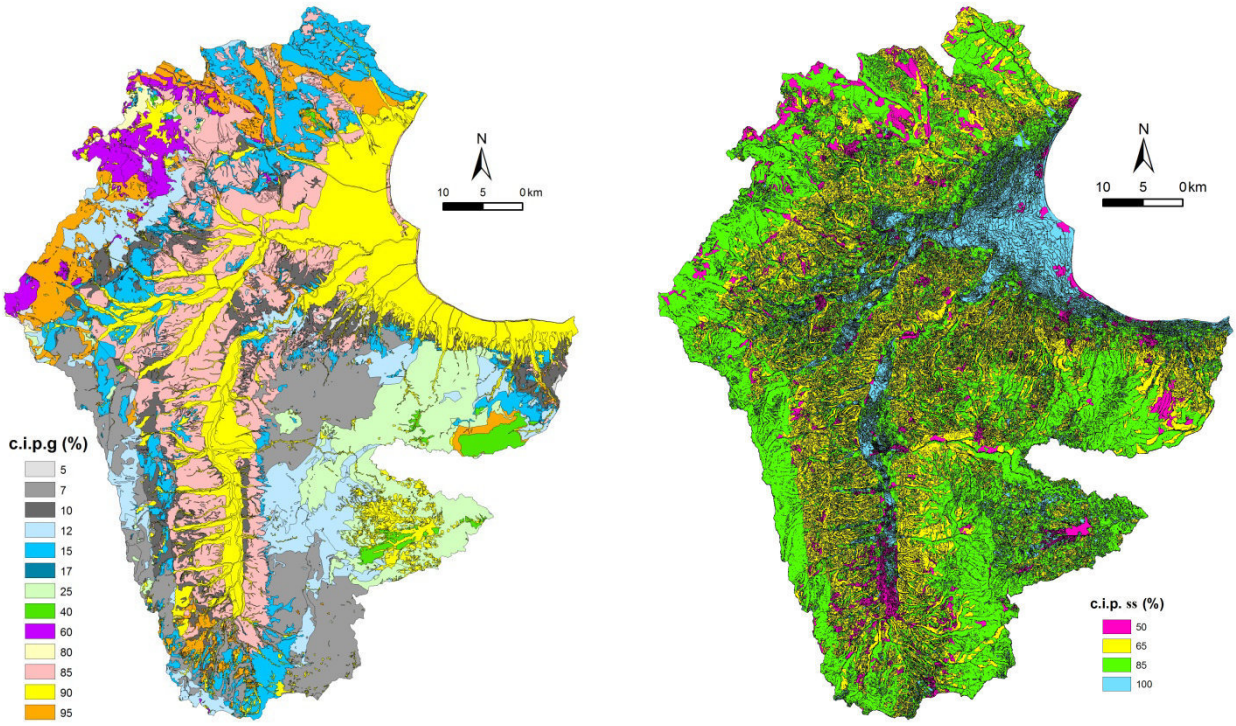

Fig.3.3.8. Map of c.i.p.$_g$ (left) based on geological simplified map. Map of c.i.p.$_{ss}$ (right) created starting from slope and soil use maps.

Stage 3 –Effective infiltration estimation

The effective infiltration (I) was calculated based on effective rainfall (Reff) values, $c.i.p._g$ and $c.i.p._{ss}$, using the formula:

$$\boldsymbol{I = Reff \times c.i.p._g \times c.i.p._{ss}}$$

The study area was divided in hexagonal cells with a diameter of 200 m and the Reff, $c.i.p._g$ and $c.i.p._{ss}$ maps were "intersected" to produce a single shapefile. The geometrical centroid of each cell was extracted obtaining a point's shapefile. Reff, $c.i.p._g$ and $c.i.p._{ss}$ values, now present in a single shapefile, are extracted for each point. Using the previous formula, the I values of all points were calculated.

The interpolation of punctual I values allowed to obtain the effective infiltration map (fig.3.3.9a). Later, the surface runoff (R) was calculated (fig.3.3.9b) and mapped using the formula:

$$\boldsymbol{R = Reff - I}$$

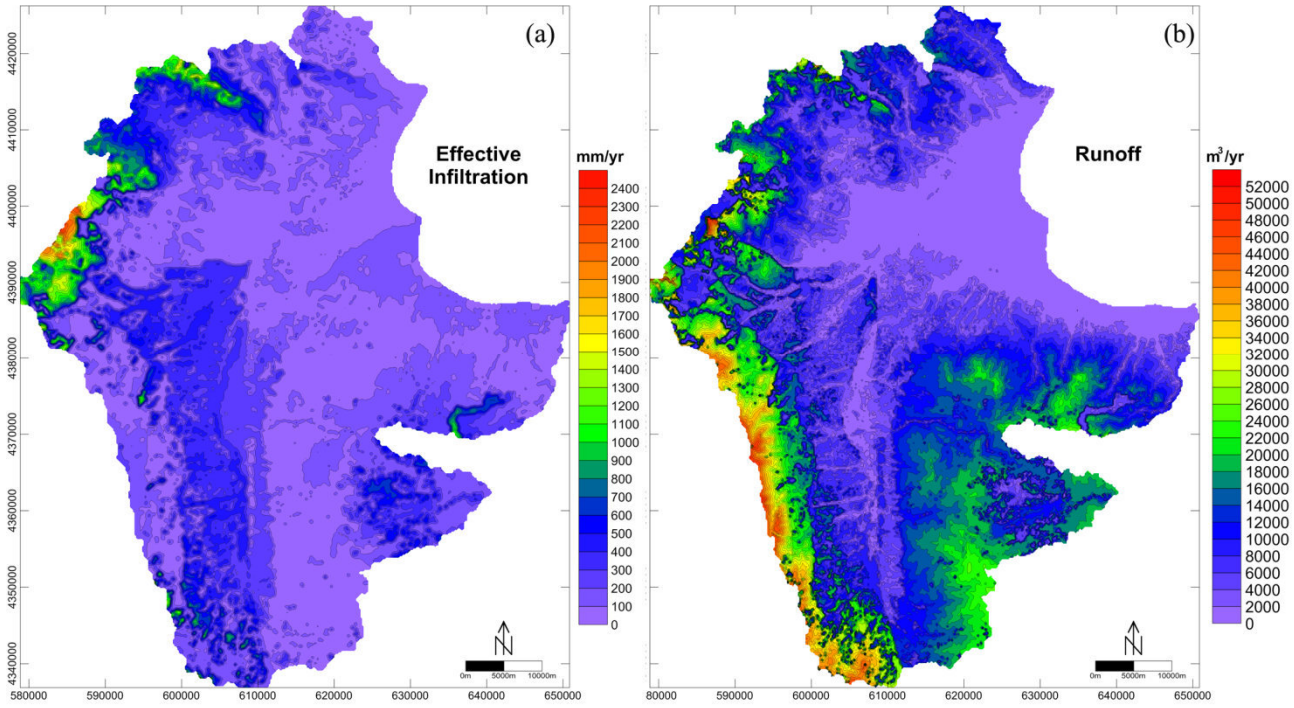

Fig.3.3.9. a) Effective infiltration map. b)Surface runoff map.

3.3.3 Discussion

The analysis of the potential recharge of the Sibari Plain aquifers allowed to identify the main recharge areas and to estimate the effective infiltration rate.

The direct recharge, due to the effective infiltration close to the Sibari Plain area, is poor (I≤ 200 mm/yr). The main aquifers recharge is due to the outflows coming from others aquifers present in the recharge area. In detail, the main recharge happens in the northwestern sector of the study area characterized by the carbonate rocks of the Pollino Massif and the "flyschioid" terranes of the Saraceno and Albidona Formations. The highest infiltration values (>2000 mm/yr) are recorded in the westernmost sector, where the high carbonates permeability is combined with the high rainfall rate due to the presence of Coastal Range. The latter represents a NNW-SSE oriented mountain chain which acts as a barrier for the winds coming from East producing high rainfall rate.

In the middle and southern sectors of the Coastal Range, lower I values (I ≤ 500 mm/yr, with isolated peak up to 1000mm/yr) are observed. In these areas, despite high rainfall rate, the effective infiltration is not helped by the low permeability of the prevailing metamorphic rocks, the high slopes and the diffuse presence of forests.

In the Sila Massif area, the low I values (I ≤ 500 mm/yr) is due to a different meteo-climatic regime and the presence of low permeable granitoid and metamorphic rocks. High I value (1000/1100 mm/yr) are observed in the eastern side of the Sila Massif, where the carbonate rocks of the Longobucco Unit crop out.

In the high and middle Crati Valley, representing a NS graben, average I value of 700 mm/yr are estimated and can be correlated with the high permeability of the alluvial deposits which fill the valley.

The spatial distribution of the effective infiltration, obtained with our innovative procedure, shows a good correlation with the meteo-climatic features of the Calabria Region and the lithological pattern of the investigated area.

The method proposed in this work is based on easily available data (geological, metereological, land use) and introduces an innovative GIS procedure to elaborate them. This procedure, relatively simple to apply, allows to create and elaborate large datasets.

Considering the reliability of the proposed method in the investigated area, we consider it very useful in the potential recharge estimation of the aquifers.

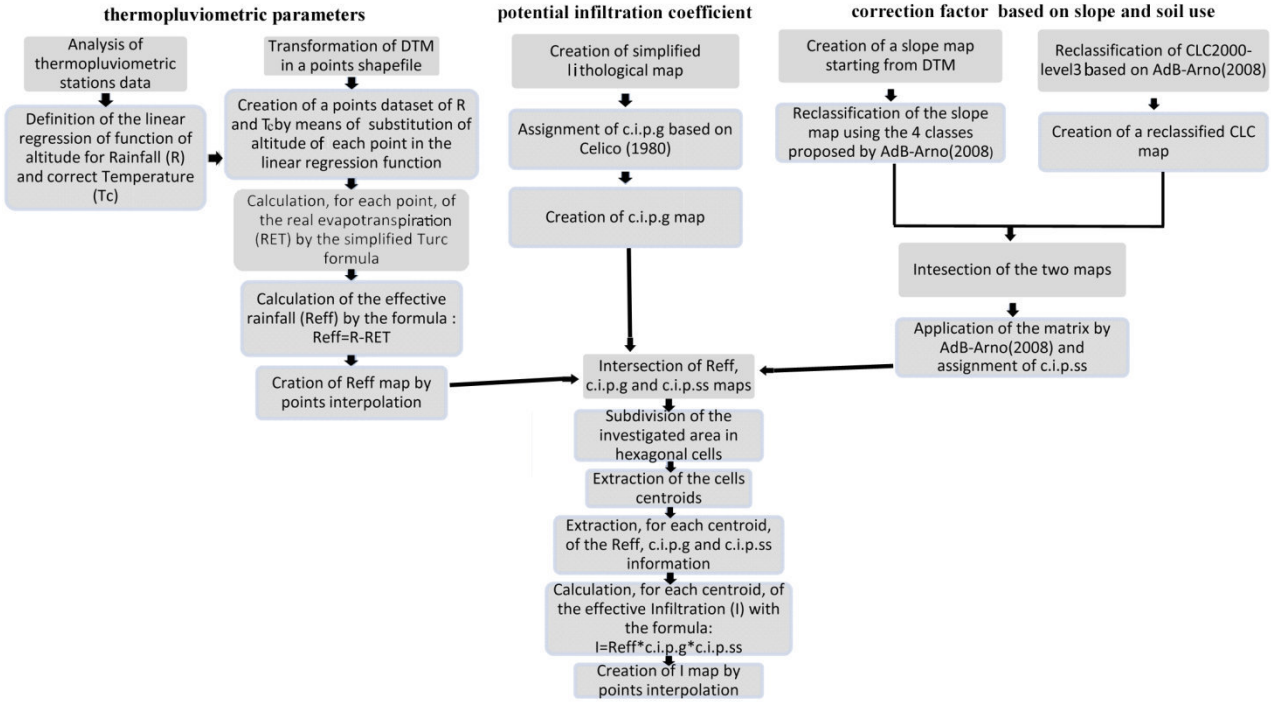

Fig.3.3.10. Flow diagram of the proposed method.

3.4 Hydrogeochemical characterization of the lower Crati valley groundwater

3.4.1 Introduction

The lower Crati valley represents a large coastal alluvial with considerable agricultural development and fast urbanization during the last 50 yr.

This area is characterized by low rainfall (average value around 500 mm/yr) and the falling of the effective rainfall (*Polemio et al.*, 2004), related to the general dropping trend recorded in South Italy (*Polemio and Casarano*, 2004), which exposes it to the risk of dryness (*Polemio et al.*, 2004).

Guerricchio et al. (1976) show a strong mineralization of the deep aquifer groundwater with a high content of sulphurs, iron manganese, carbon dioxide and methane.

In correspondence of the Crati and Coscile Rivers floodplain the groundwater has high salt content up to about 10 km landward from the coastline (*Casmez*, 1987) (fig.3.4.1). The elevated salinity is ascribed to the effects of seawater intrusion due to the groundwater overexploitation or interactions with rocks containing halite (*Guerricchio et al.*, 1976; *Guerricchio and Ronconi*, 1997) and to the groundwater long age (*Tazioli*, 1986).

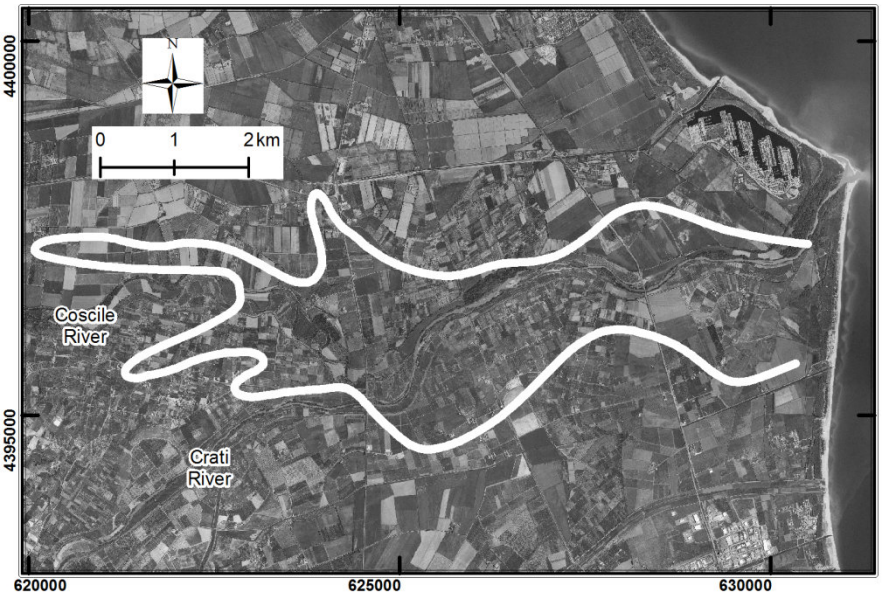

Fig.3.4.1. Boundary of water mineralization traced by *Casmez* (1987)

3.4.2 Data analysis

The main geochemical features of the lower Crati valley groundwater are investigated by means of the 103 samples (fig. 3.4.2), collected and analyzed during PON_*Amicus* project activities.

Groundwater is sampled trough wells with depth from 5m to 200m. Field determinations (electrical conductivity, temperature, pH) are carried out. The concentration of major components (Ca^{2+}, Mg^{2+}, Na^{+}, K^{+}, SiO_2, Cl^{-}, Br^{-}, HCO_3^{-}, SO_4^{2-}, F^{-}, NO_3^{-}) are estimated by Ion Chromatography.

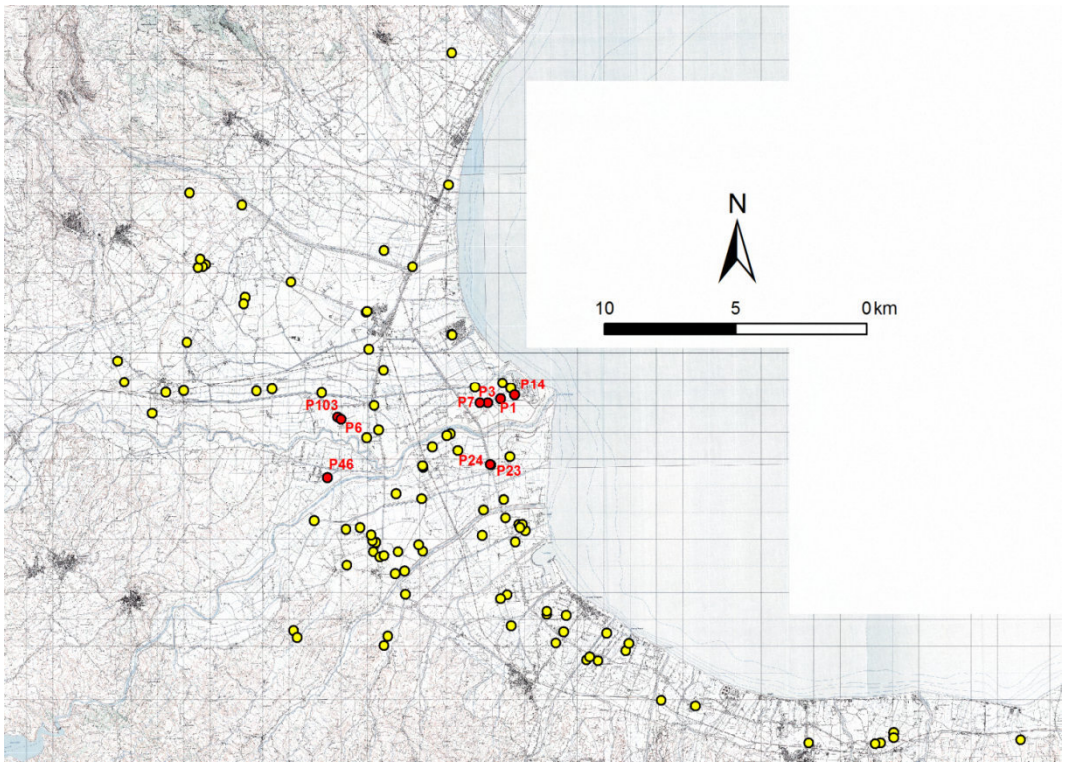

Fig.3.4.2 . Location of the 103 samples. Red circles represent the Na-Cl samples.

The different groups of water are identified using Langelier-Ludwing diagram and ternary diagrams. Ca–HCO3 and Na–Cl groups prevail; the first group is equally distribute in the investigate area while the second one is concentrated close to the Crati and Coscile riverbeds. Ca–Cl and Na–HCO3 waters are present as secondary groups.

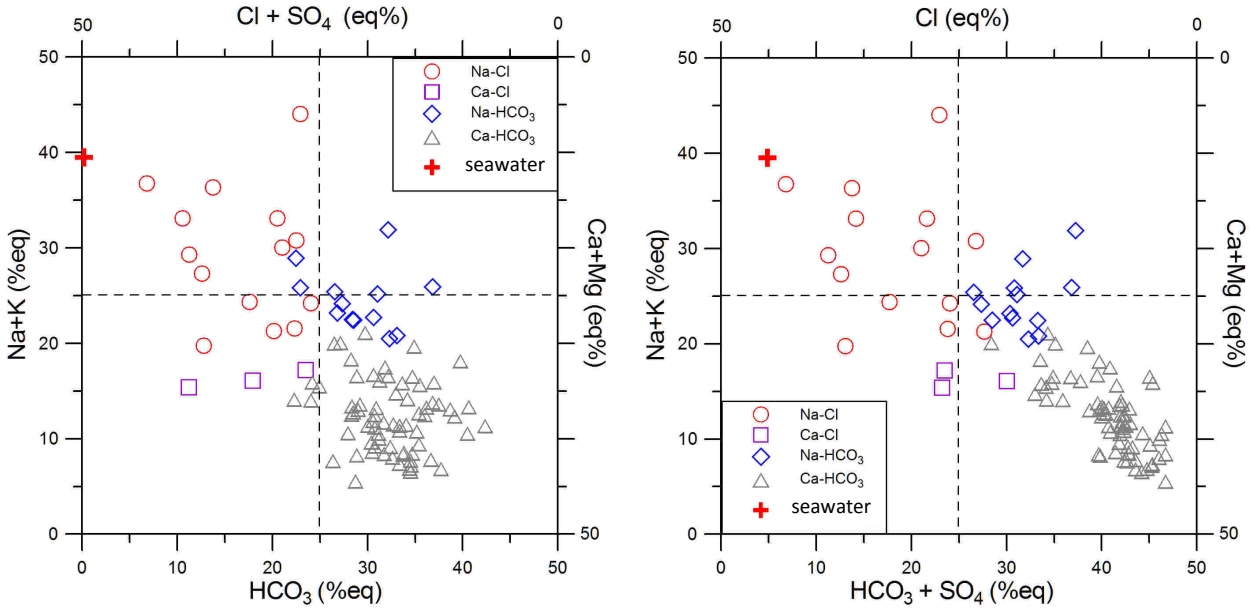

Fig. 3.4.3. Langelier-Ludwig diagram with HCO_3^- (left) and Cl^- (right) as single anion.

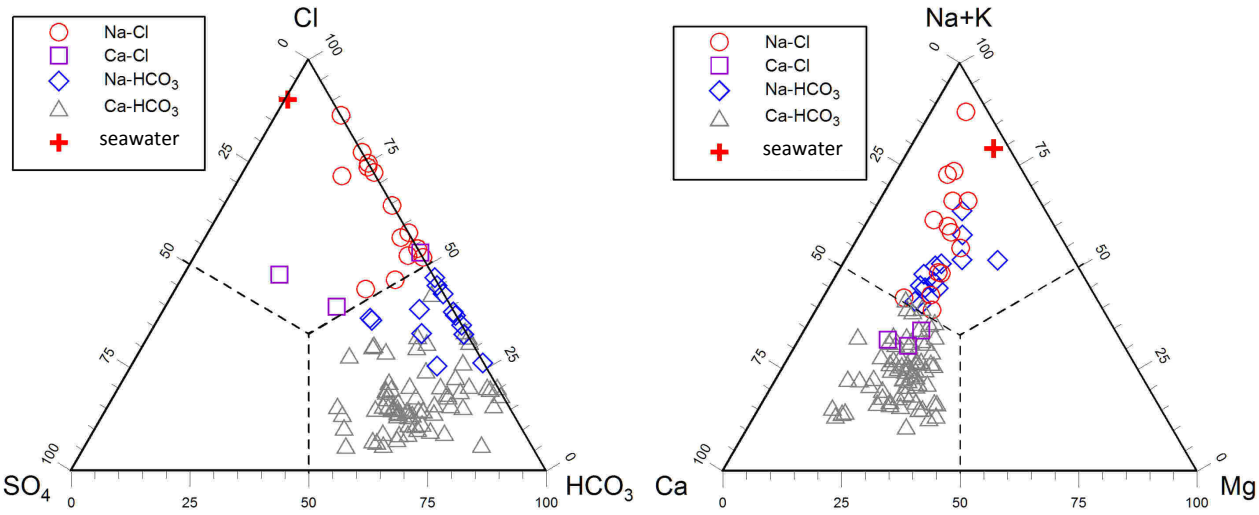

Fig.3.4.4. Ternary diagrams: Cl-HCO_3-SO_4 (left) and) (Na+K)-Mg-Ca (right).

The electrical conductivity (fig.3.4.5), Cl^- and Na^+ content distribution maps (fig.3.4.6) allow to recognize the areas affected by higher salt content in the groundwater. In detail, a ENE-WSW oriented area characterized by Na-Cl waters is identify in correspondence of the Crati riverbed.

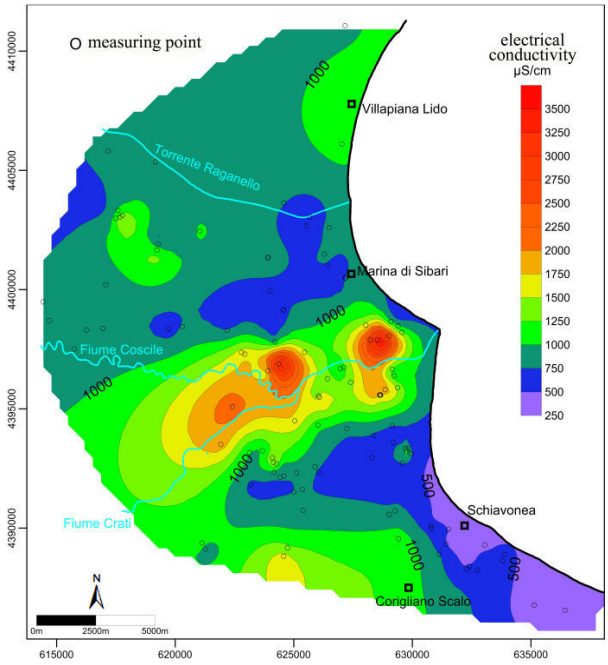

Fig.3.4.5. Electrical conductivity (µS/cm) distribution map (in the Crati mouth area supplementary measures are collected compared to the 103 samples of PON_*Amicus*).

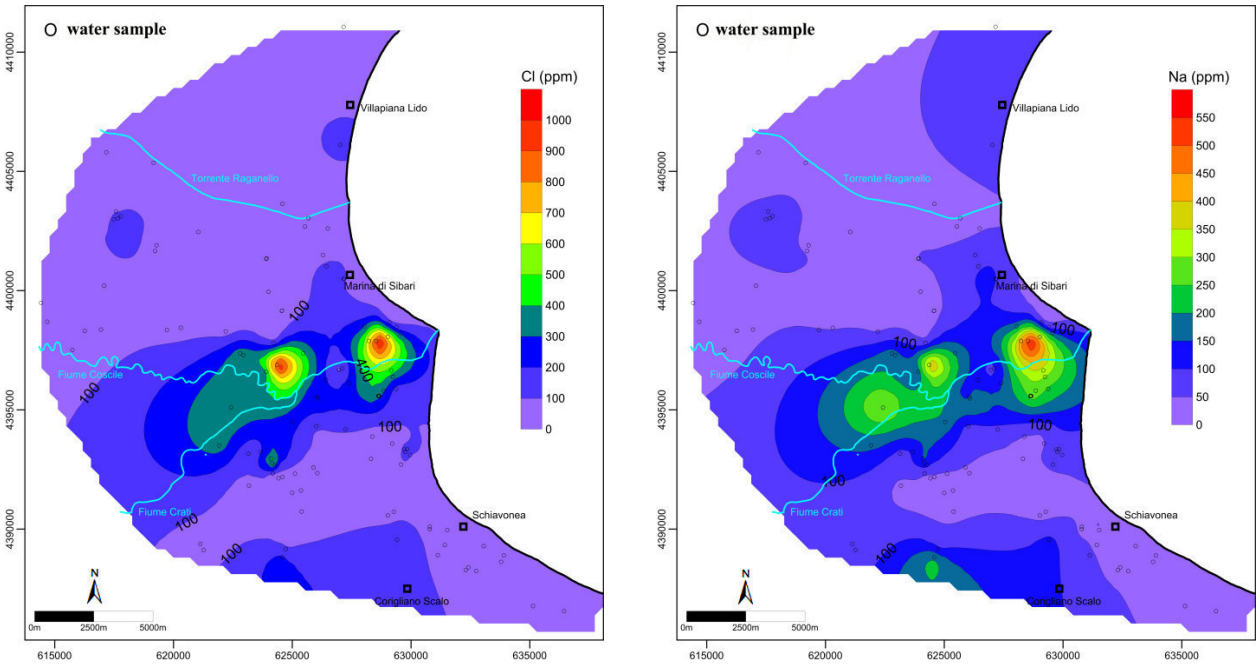

Fig.3.4.6. Cl and Na content (ppm) distribution maps.

3.4.3 Identification of salinity sources by means of ionic ratios

Major ions molar ratios are used to investigate the salinity source of the lower Crati valley groundwater and to identify a possible seawater intrusion, referring to known case studies (*Vengosh and Rosenthal*, 1994; *Vengosh et al.*, 1999; *Hsissou et al.*, 2002; *Capaccioni et al.*, 2005; *Stoessel and Prochaska*, 2005; *Cartwright et al.*, 2006; *Ghabayen et al.*, 2006; *de Montely et al.*, 2008; *Gattacea et al.*, 2009; *Kouzana et al.*, 2009; *Han et al.*, 2011; *Wang and Jiao*, 2012; *Wang et al.*, 2013).

The used ions molar ratios and their values typical in seawater intrusion case (*Ghabayen et al.,* 2006 and references therein) are shown below.

Molar ratio	Marine intrusion
Na/Cl	0.86-1
SO_4/Cl	0.05
Br/Cl	0.0015
K/Cl	0.019
Ca/(HCO3+ SO_4)	0.35 - <1
Mg/Ca	>5

Table 3.4.1. Molar ratio between the main ions typical of seawater intrusion (from *Ghabayen et al.*, 2006)

In the area with groundwater saline pollution, the Na/Cl molar ratio has an average value of 0.4836, with maximum of 1.2333 and minimum of 0.1820. In detail, the Na-Cl samples P1, P3, P6, P7, P14, P23, P24, P46, P103 have a Na/Cl molar ratio equal to 0.3683, 0.3412, 0.3163, 0.4636, 0.3671, 0.4109, 0.5996, 0.5332 e 0.2762. These values reveal a Cl enrichment compared to Na and are

lower than the values characteristic of seawater intrusion. Low values, between 0.5 and 0.8, are observed in cases of deep brines (due to buried evaporites dissolution) plumes (*Vengosh et al.*, 1999; *Ghabayen et al.*, 2006).

SO_4/Cl molar ratio is determined only for the 30% of samples (other ones have not SO_4 as major ion) and is include between 6.5893 e 0.0035. The Na-Cl samples P6, P7 and P46 have SO_4/Cl molar ratio of 0.0103, 0.1439 and 0.6699. Also this molar ratio diverges from values typical of seawater intrusion.

The Br/Cl molar ratio (calculated for the 30% of samples containing Br) has a value of about 0.008, except the 0.034 in the sample P67.

The K/Cl molar ratio has an average value of 0.0732 in the whole investigate area and 0.0679 in the Na-Cl samples, while the Ca/(HCO3+ SO_4) molar ratio assumes respectively a value of 0.130 and 0.131.

The Mg/Ca molar ratio is characterized by low values with an average value of 0.2605. In the Na-Cl samples P1, P3, P6, P7, P14, P23, P24, P46 and P103 it has values equal to 0.2465, 0.3049, 0.2557, 0.4506, 0.2700, 0.2821, 0.5571, 0.2037, 0.2079.

De Montely et al. (2008) and *Wang and Jiao* (2012) observe a good correlation between major ions (Na^+, Mg^{2+}, K^+) and Cl^- in two seawater intrusion cases.

The samples collected in the polluted area have a good Na-Cl correlation (R^2=0.84) and a poor correlations Mg-Cl (R^2=0.42) and K-Cl (R^2=0.58). In the only Na-Cl samples are observed this correlations: Na-Cl with R^2=0.84, K-Cl with R=0.68 and Mg-Cl with R^2=0.26.

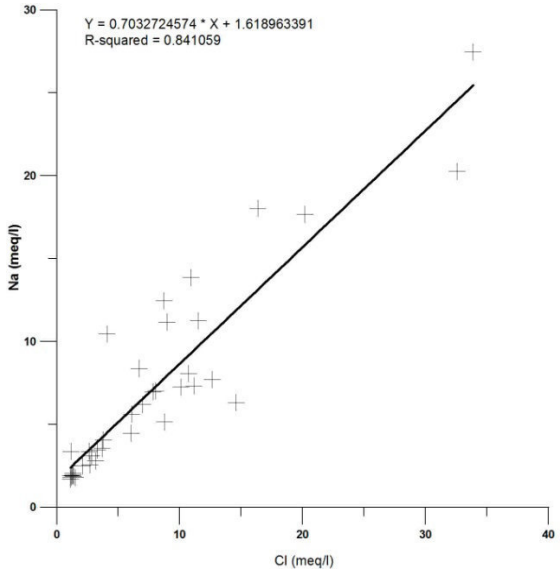

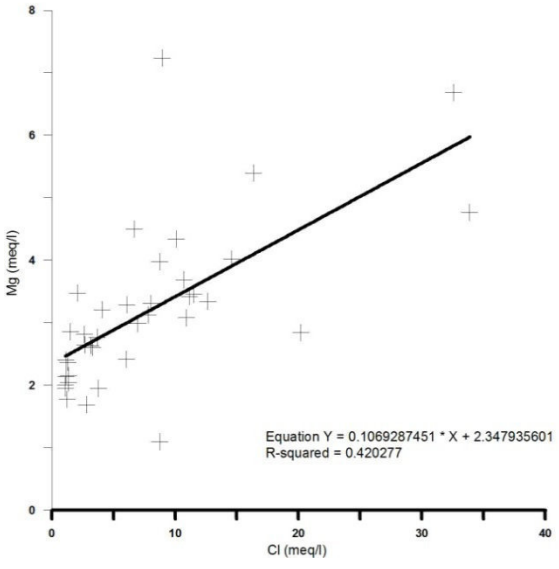

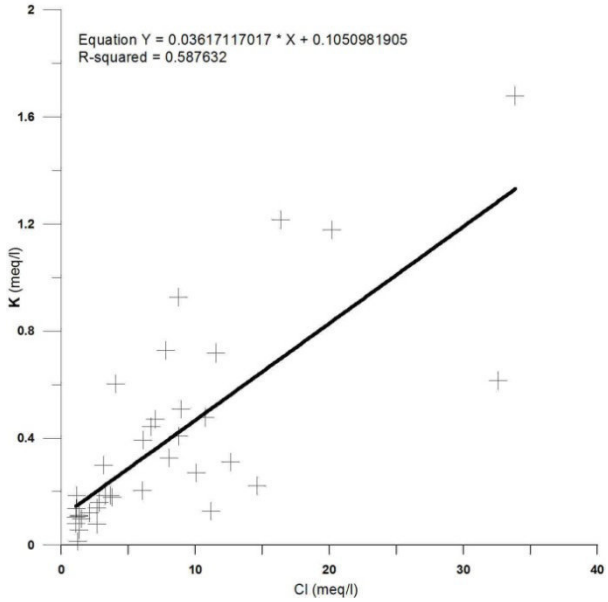

Fig.3.4.7. Correlation of the major ions (Na^+, Mg^{2+}, K^+) and Cl^- in all analyzed samples

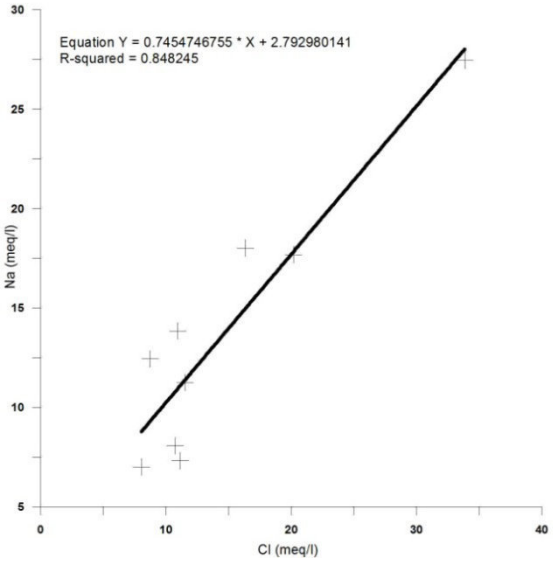

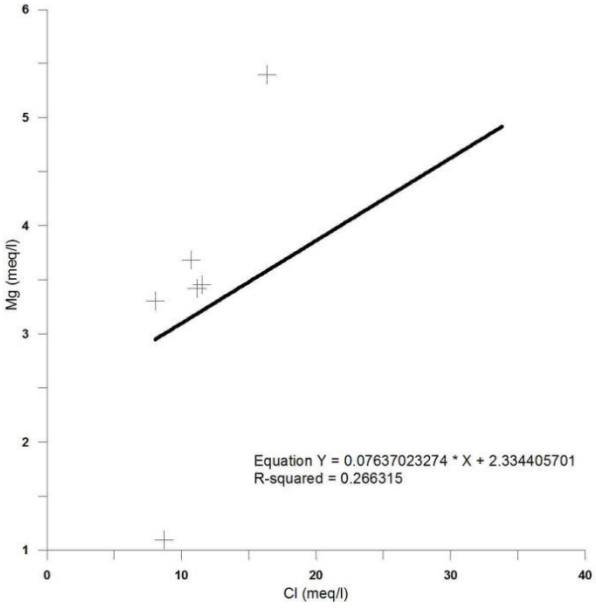

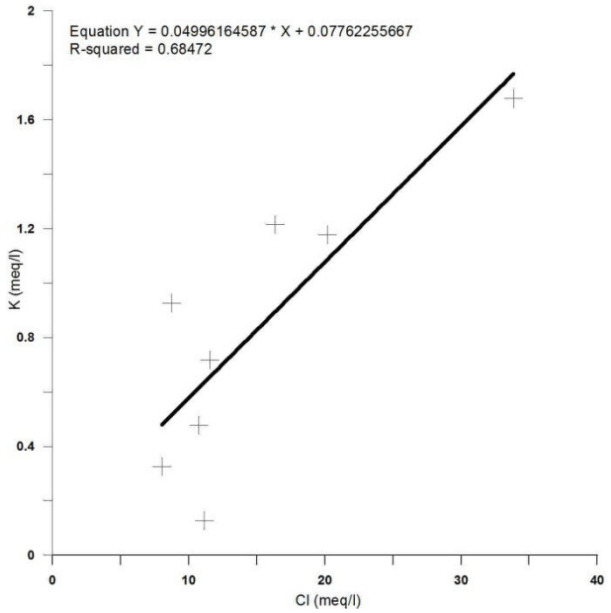

Fig.3.4.8. Correlation of the major ions (Na^+, Mg^{2+}, K^+) and Cl^- in the Na-Cl samples

3.4.4 Discussion

The analysis of the 103 water samples, performed in the PON_*Amicus* project, shows a low salt content in the lower Crati valley groundwater. Higher salt content are observed in the area close to the Crati riverbed where are recorded electrical conductivity values up to 4.25 mS/cm and Cl^- values up to 1120 ppm. These values are very low compared to the values observed in seawater intrusion cases, for example *Capaccioni et al.* (2005; Cl=9620 ppm), *de Montely et al.* (2008; cond.=44.8 mS/cm, Cl=21272 ppm), *Gattacea et al.* (2009; cond.=41.60 mS/cm, Cl=13827 ppm), *Kouzana et al.* (2009; Cl=2845 ppm) and *Wang and Jiao* (2012; Cl=14065 ppm).

In the samples collected in the polluted area, a poor correlation among Cl and Na, K and Mg is present in contrast with that observed in seawater intrusion cases (*de Montely et al.*, 2008; *Wang and Jiao*, 2012). The molar ratios Na/Cl, SO_4/Cl, Br/Cl, K/Cl and Mg/Ca have low values which diverge from the values proper to seawater intrusion (*Vengosh and Rosenthal,* 1994; *Vengosh et al.*, 1999; *Stoessel and Prochaska*, 2005; *Ghabayen et al.*, 2006; *de Montely et al.*, 2008; *Gattacea et al.*, 2009; *Kouzana et al.*, 2009; *Han et al.*, 2011; *Wang and Jiao*, 2012; *Wang et al.*, 2013). The low value of Na/Cl and Mg/Ca molar ratios are comparable with the values observed in cases of deep brine plumes (*Vengosh et al.*, 1999; *Ghabayen et al.*, 2006).

Finally, the analysis of major elements allows to exclude the seawater intrusion as the main/only cause of the saline water pollution in the lower Crati valley.

The location of the wells census at Demanio Idrico Prov.Cosenza office (the real wells number is greater due to the unauthorized wells) refutes the hypothesis, supported by various authors, of the

groundwater overexploitation as the cause of seawater intrusion and consequently of saline water pollution. In the map (fig. 3.4.9) no correlation between electrical resistivity and Cl content and the water wells location is observed.

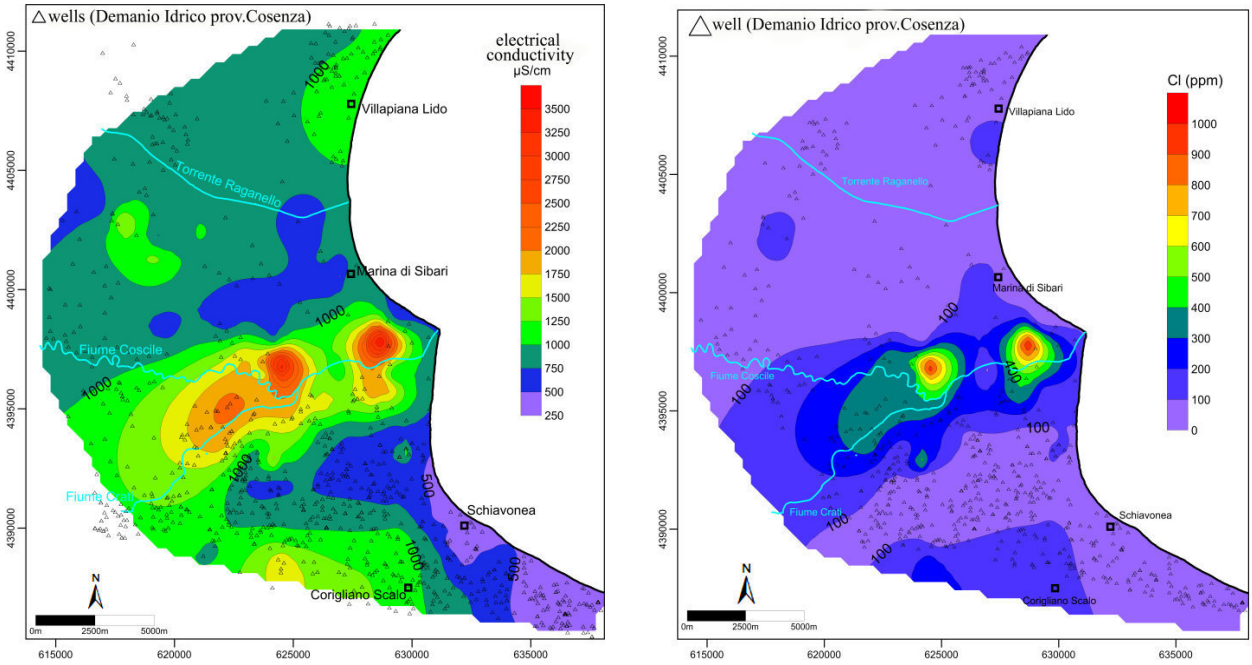

Fig.3.4.9. Water wells, census at Demanio Idrico Prov.Cosenza office, projected on the electrical conductivity and Cl content distribution maps

In the area close to the Crati and Coscile riverbeds, NW-SE tectonic structures with subsurface evidences are present (Chapter 1 and 2; *Lanzafame and Tortorici*, 1981; *Cinti et al.*, 2013, 2015). Furthermore, salt rocks and deep mineralized water bodies are recorded by ViDEPI wells.

We suggest that the deep mineralized waters can rise, using the tectonic structures as preferential ways, contributing to the saline pollution of the groundwater.

3.5 Conclusion

The analysis of the Sibari Plain hydrostratigraphic units shows a very complex framework made by the association of "jigsaw-puzzle" and "labyrinth" systems (*Galloway and Sharp*, 1998a, b). This complexity mirrors the composite late Pleistocene-Holocene plain evolution characterized by uplift and alluvial fans development along the outer limit, fault activity and delta progradation in the middle sector. Consequently, also the aquifers modeling turns out to be very complicated. Indeed, the shallow aquifer shows a variable thickness and occasionally it touches the confined one favouring water exchange.

Furthermore, the shallow aquifer is made by various aquifers layers strictly related to stratigraphic pattern. For this reason, it is not recommended the use of a "layer cake" model in the study of sedimentary aquifers like that investigated.

The analysis of the piezometric trend between 2002 and 2013 shows a water table drop (up to -2 m) in the coastal area close to the archaelogical site where it can be related to the well-points system (80 l/s) used for the excavations dewatering. On the contrary, water table rise is observed in others sectors despite the presence of many water wells. However, we suggest that a realistic monitoring of the water table variations is very complex due to the presence of various aquifer layers shown by the hydrostratigraphic reconstruction.

The direct recharge through effective infiltration of the lower Crati valley aquifers is very poor (≤ 200 mm/yr) so the main aquifers feeding are identified in the outflows coming from others aquifers spread in its large potential recharge area. This element makes even more complex the hydrogeological and hydrogeochemical modeling of this area.

An area characterized by groundwater saline pollution is identified close to the Crati and Coscile riverbeds. The electrical conductivity values and Cl^- content are low referring to worldwide cases of seawater intrusion. Moreover, also the major ions molar ratios and correlations diverge from those observed in groundwater affected by seawater contamination.

Seawater intrusion cannot be excluded for the Sibari Plain, especially for the coastal sector close to the Crati mouth where the permeable fluvial sediments and the well-points system of the archaelogical site can favoured it, but it cannot be considered the main and only trigger of groundwater salinization.

The presence of buried salt rocks, deep mineralized water bodies and fault system with subsurface evidences is shown in this work (fig. 3.5.1) in the area where saline waters are present. Therefore, the existence of plumes of deep mineralized waters which use the tectonic discontinuities to rise toward the surface can be supposed.

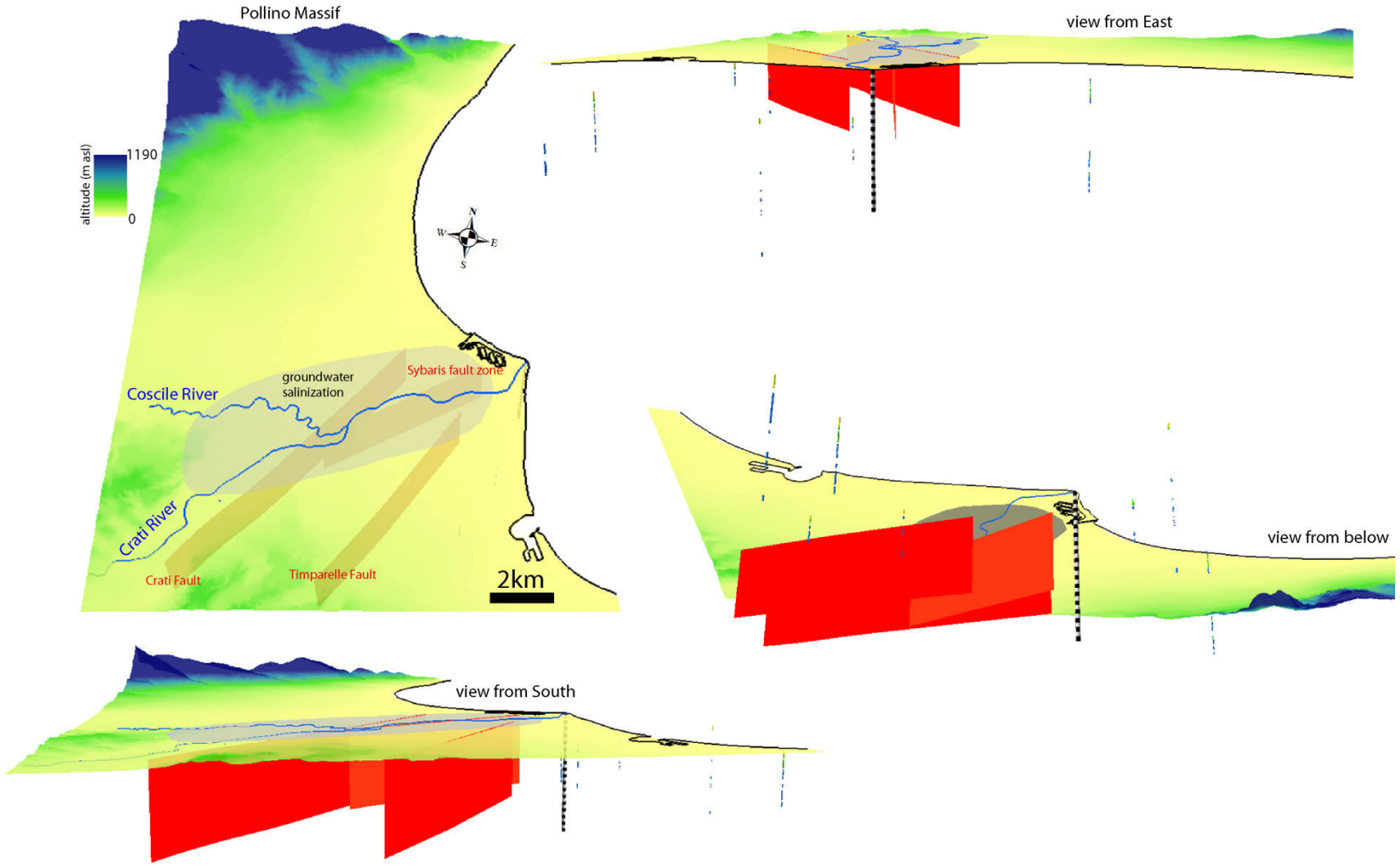

Fig. 3.5.1. 3D sketch of the main tectonic structures in the area with groundwater salinization and the mineralized water bodies recorded in the ViDEPI wells (blue=salt water; green=brackish water; yellow=freshwater). Each black and white cylinder represents 100 m of depth.

CHAPTER 4

Natural and anthropogenic ground subsidence detected by InSAR time series analysis

4.1 Introduction

A lot of worldwide coastal and delta plains are affected by land subsidence (*Jelgersma*, 1996; *Ericson et al*., 2006), which often involves anthropized areas (urban, industrial, agricultural) causing conspicuous economic cost.

Examples come from various countries and from different geodynamic, geological, climatic and social contexts. In Italy, the subsidence of Venice coastland and Po delta plain is related to the north-eastward retreat of the Adriatic subduction (*Carminati et al.*, 2003) and to tectonics, seismicity, consolidation of recent deposits and groundwater withdrawal (*Teatini et al.*, 2011; *Teatini et al.*, 2005; *Carbognin et al.,* 2004). Land subsidence affects also the coastal areas of southern Louisiana and Mississippi where it is due to the Holocene sedimentary loading in the Gulf and Mississippi River delta (*Ivins et al.,* 2007), modern-day tectonic (*Dokka*, 2006, 2011), compaction of Holocene sediments (*Meckel et al*., 2006), local groundwater pumping (*Dokka*, 2011) and hydrocarbon production (*Morton et al*., 2006). Subsidence phenomena due to a combination of natural and human-made factors are observed also in the Yellow River and Yangtze Deltas (*Liu and Huang*, 2013; *Shi et al*., 2008), along Taiwan coastland (*Liu et al.*, 2004; *Hsieh et alii*, 2011; *Tung and Hu*, 2012), in Semerang city Indonesia (*Lubis et al.*, 2011), in Thessaloniki coastal plain and Delta municipality region (Northern Greece) (*Stiros*, 2001; *Raspini et al*., 2014).

Over the last decades the land subsidence monitoring has been significantly improved thanks to the earth observation techniques based on Synthetic Aperture Radar (SAR) interferometry. Furthermore the recent advances in radar satellite capabilities and techniques based on the interferometric analysis of large datasets (*Ferretti et al*., 2001; *Berardino et al*., 2002) have been allowed more detailed spatial and temporal resolutions.

Here we apply the Differential SAR Interferometry approach (InSAR) to investigate ground deformations of the Sibari Plain (SP).

Our datasets cover the May 2003–September 2010 time interval acquired from both ascending and descending orbits by Envisat and COSMO-SkyMed satellites. The availability of ascending and descending datasets allow us to discriminate the vertical and east–west displacement component. The retrieved InSAR results were analyzed and interpreted considering the available geological and hydrogeological information collected during this work.

4.2 Historical subsidence

Subsidence is a well-known phenomenon in the Sybaris archeological area, testified by the presence of three overlapping ancient towns, the Greek Sybaris (720-510 B.C.), the Hellenistic Thurii (444-203 B.C.) and the Roman Copiae (193 B.C.), presently buried between 7 and 3.5m (*Rainey and Lerici*, 1967).

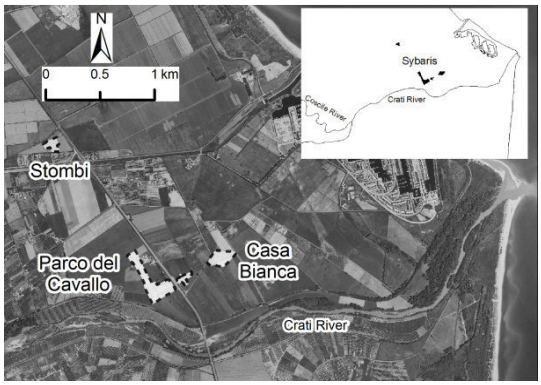

Fig. 4.1. Schematic distribution of the archeological sites.

Guerricchio and Melidoro (1975) calculate the overflooding rates by well logs, archeological excavations and carbon datings. Starting for these results the authors evaluate a subsidence rates ≥0.57 mm/yr (2330-860 kyr B.P.) and ≥4.31 mm/yr (860 kyr B.P. - present) for Casa Bianca, ≥ 0.35 mm/yr (2660-1600 kyr B.P.) and ≥2.05 mm/yr (1600 kyr B.P.-present) for Parco del Cavallo, ≥0.4 mm/yr for Stombi.

Following studies notice a subsidence in the archeological area from late Pleistocene to Holocene and identify its cause in a combination among neotectonic activity, glacio-eustatic variations and sediments compaction (*Cotecchia et al.*, 1994; *Pagliarulo et al.*, 1995; *Cotecchia and Pagliarulo*, 1996; *Cherubini et al.*, 2000). A decrease of subsidence rates is recorded, from ~5.4 mm/yr (11 kyr B.P.) to ~1.6 mm/yr (*Cotecchia et al.*, 1994; *Pagliarulo*, 2006). In the archeological area the subsidence variability is correlated to facies lateral variation (*Pagliarulo et al.*, 1995) and the most of geotechnical subsidence can be ascribed to a very compressible clayey layer, laterally discontinuous, between 35 and 40m of depth (*Pagliarulo et al.*, 1995; *Cherubini et al.*, 2000). From 1950s ~20cm of subsidence are recorded and ascribed to groundwater exploitation (*Cherubini et al.*, 2000).

Cafaro et al. (2011) propose a geotechnical model for the firsts 100 m below the archeological area and a calculation method of the subsidence imposing a water table drop; the author suggest that subsidence phenomena during the last 50 yr are caused by primary consolidation due to exploitation of depth water table.

Cucci (2005) confirms the subsidence in the Casa Bianca and Parco del Cavallo sites, superimposed to regional uplift, with rates between 0.5 and 2 mm/yr in the temporal period 0.8-0.3 kyr; for the Stombi site he calculates a mean uplift rate of ~0.6 mm/yr in the last 11.2 kyr. The same author hypothesizes that subsidence started 4 kyr and identifies its cause in the deposition of fine compressible sediments excluding the tectonic contribution.

Ferranti et al. (2011) measure the lateral and vertical variations of subsidence rates by means the analysis of well logs from previous works and news samples collected in the archeological area. In detail, in Casa Bianca and Parco del Cavallo sites the mean subsidence rates vary among ~0.7 mm/yr in the latest Pleistocene-earliest Holocene, ~5-6 mm/yr in the early Holocene, ~2-2.8 mm/yr in the Middle Holocene, stability or small uplift in historical age (~3-1.3 kyr B.P.). On the contrary in the Stombi site subsidence is not recorded during Holocene and an area 6 km toward SE from archeological area is characterized by an uplift rate of ~1.5 mm/yr. In conclusion, for the authors the subsidence is mainly controlled by local tectonic structures; in particular archeological area is located in the middle of a syncline confined between Crati and the Raganello anticlines.

4.3 Processing technique

The classical differential SAR Interferometry (InSAR) is a technique that allows to calculate the ground surface movements that occurred between two different passes of the satellite over the same area by means of Synthetic Aperture Radar (SAR) image data collected by instruments. In fact InSAR technique exploits the differences between spaceborne Synthetic Aperture Radar (SAR) images, acquired with a difference of position or with a difference of time. The phase of images is compared after proper image co-registration. The resulting difference of phases is a new kind of image, called *'interferogram'*, an interference pattern of fringes containing all the information on relative geometry (*Massonet and Feigl*, 1998). Each fringe represents a ground movement along the satellite Line of Sight equal to $\lambda/2$ (where λ is the used radar wavelength).

There are many physical phenomena contributing to phase measurements: phase variations within a pixel, the contribution of orbital variations, topography, atmosphere, and displacement. The topographic, orbital, and atmospheric contributions are removed in order to reveal ground displacements along the line of sight between the radar and the target obtaining, in the favorable cases, the accuracy of the displacement measures is better than a centimeter (*Hanssen*, 2001).

Our goal was to study the temporal evolution of the detected deformations. To this aim several different approaches have been proposed in the last decade to generate time series of ground displacement, capable of measuring the rates of ground velocities with accuracies of ~1 mm/yr (*Casu et al*., 2006). In this work we applied the Small Baseline Subset InSAR technique (SBAS;

Berardino et al., 2002). The used SAR images are coupled basing on constraints for the temporal and spatial baselines. The SBAS algorithm combines these acquisitions also included in different interferometric subsets using a minimum norm criteria combination of the velocity deformation, based on the Singular Value Decomposition (SVD) method. During the SBAS processing the estimation and removal of temporally decorrelated atmospheric artefacts is performed using double-pass filtering in the temporal and spatial domains, as explained in *Berardino et al*. (2002).Moreover, we used the SRTM DEM (30 meters posting) for the topography subtraction (http://www2.jpl. nasa.gov/srtm).Once retrieved the time-series displacements, the average ground element velocity in the time period covered by the data is calculated.

Finally, thanks to the availability of both ascending and descending LoS ground velocity maps, we calculated the Up and East component for the ASAR* and COSMO-SkyMed* data sets, respectively.

In details, we applied the SBAS technique to four image data sets, two of the European Space Agency (ESA) Envisat and two of the Italian space Agency (ASI) COSMO-SkyMed satellites. The first group contains 32 ASAR images acquired on the descending pass(track 222, frame 2803), in the period 2004–2010 and 38 ASAR images acquired on the ascending pass (track 86, frame 789), in the period 2003–2010. The second group was composed of 28 images from the ascending pass, spanning the interval 2011–2013 and 12 images from the descending orbit, acquired in the interval 2011–2012.

4.4 InSAR results

In the following, we report the large scale deformation pattern of SP retrieved by means InSAR processing and discuss in detail the chapter of results using available tectonic, stratigraphic, geomorphological and hydrogeological information. We investigate natural and/or human causes concerning the vertical and horizontal surface displacements.

The Up component (recording the vertical ground deformation) distribution shows a coastal area (from Villapiana Lido to Marina di Schiavonea) characterized by subsidence with velocity ranging ~ -20 mm/yr (Envisat and COSMO-SkyMed sensors); on the contrary boundary areas of SP show a low positive value (~1 mm/yr).

The East component (recording the horizontal ground deformation) shows, along the coastal area, common positive values (Eastward displacement) with the exception of Laghi di Sibari and the Corigliano industrial area; moving inland there are areas with negative values (Westward movements) as the Saraceno and the Satanasso fans.

In the archeological area the subsidence rate is ~2 mm/yr (Envisat) and ~3 mm/yr (COSMO-SkyMed) for the Parco del Cavallo site and ~2 mm/yr (Envisat) for the Casa Bianca site. These values are comparable to the velocities calculated by previous authors (*Guerricchio and Melidoro*, 1975; *Cucci*, 2005).

North of the Corigliano harbor, *Ferranti et al.* (2011), based on well-log data, report an uplift, whilst COSMO-SkyMed SAR velocity maps show ~ -17 mm/yr of subsidence

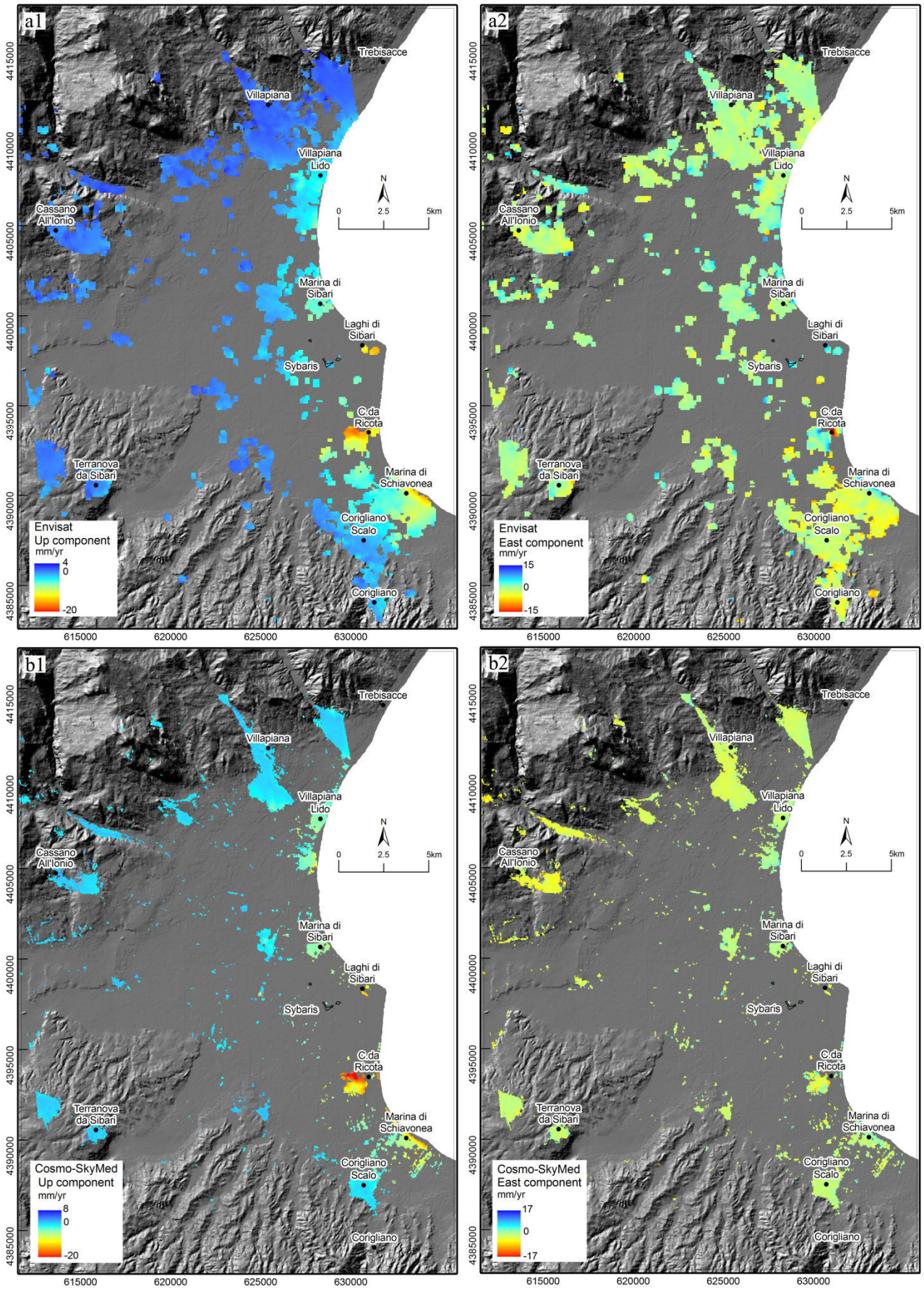
a1
Trebisacce
Villapiana
Villapiana Lido
Cassano All'Ionio
Marina di Sibari
Laghi di Sibari
Sybaris
C.da Ricota
Terranova da Sibari
Marina di Schiavonea
Corigliano Scalo
Corigliano
N
0 2.5 5km
Envisat
Up component
mm/yr
4
0
-20
4415000
4410000
4405000
4400000
4395000
4390000
4385000
615000
620000
625000
630000
a2
Envisat
East component
mm/yr
15
0
-15
b1
Cosmo-SkyMed
Up component
mm/yr
8
0
-20
b2
Cosmo-SkyMed
East component
mm/yr
17
0
-17

Fig.4.2. Mean deformation velocity components computed from Envisat (a) and COSMO-SkyMed (b) dataset (1) Up component; positive values indicate uplift and negative values subsidence. (2), East component; positive values indicate eastward displacement and negative values indicate westward displacement.

4.5 Data analysis and comparison

4.5.1 Geodynamic setting

The SP is located in correspondence of the junction of the Calabrian Arc and the Southern Apennine. Moving few kilometers toward SE from the SP, the geodynamic setting is complicated by the presence of the junction between the thin Ionian basin crust (southward) and the thick crust of the Apulian platform (northward). Moreover, an active oblique-contractional belt (the Amendolara Ridge), due to the combined effects of subduction retreat of the Ionian slab underneath Calabria and stalling of Adriatic slab retreat underneath the Apennines is present, are recognized in the Ionian Sea in front on the SP by *Ferranti et al.* (2014). This belt is made by the alignment of three anticlines (Amendolara, Rossano and Cariati) bounded by a main SW-verging back-thrust.
A flexural subsidence, that can be triggered by a back-thrusting (*Carapa and Garcia-Castellanos*, 2005), is considered one of the mechanisms to explain the ground subsidence detected by our InSAR data along coastal sector of the SP.

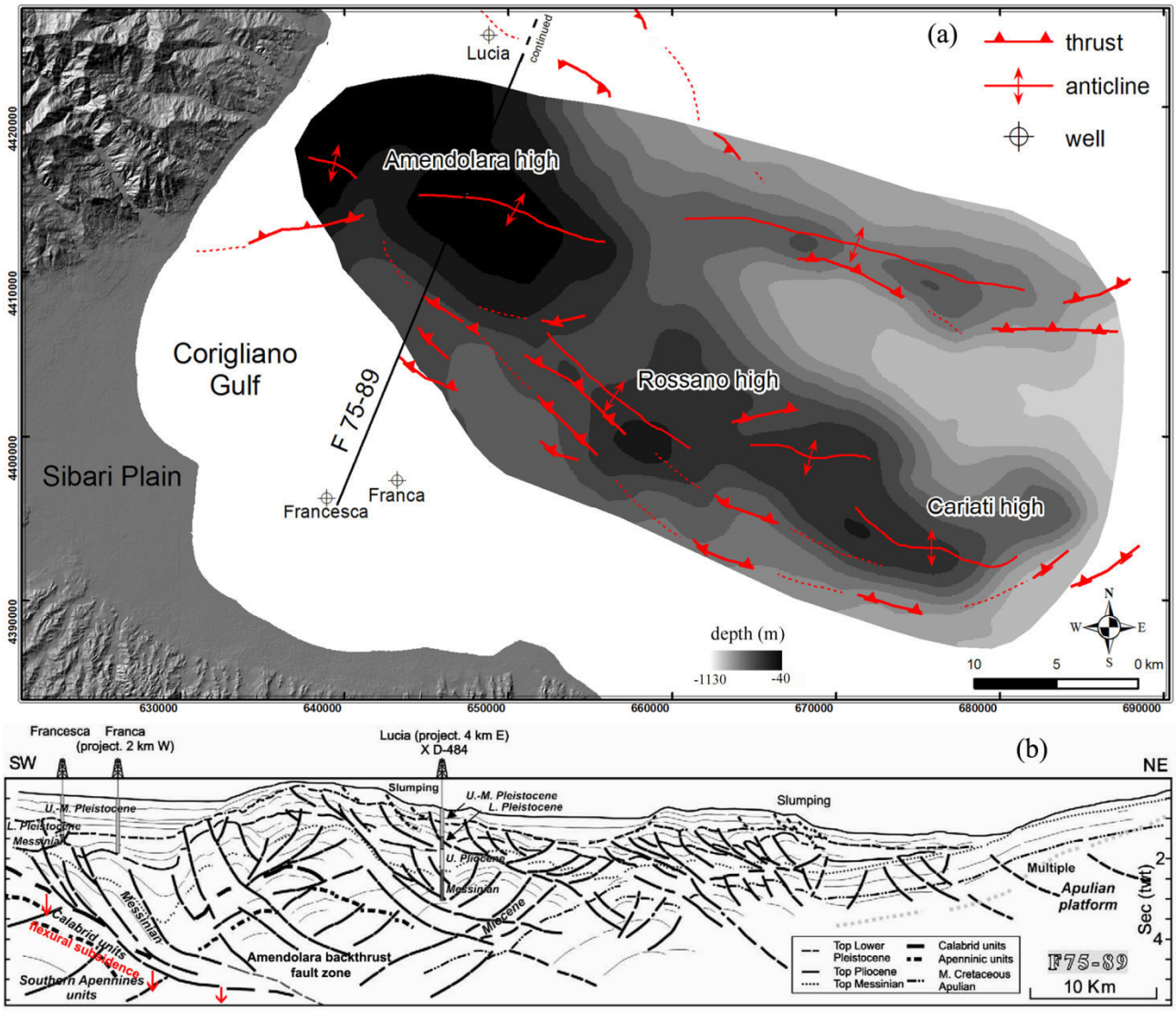

Fig.4.3. a) The Amendolara Ridge located in the Ionian Sea in front of the Sibari Plain. The bathymetric map (modified from *Civile et al*., 2012) shows the presence of three morphological highs (Amendolara, Rossano and Cariati highs). The main structural elements (thrusts and anticlines) are extracted from *Ferranti et alii* (2012). b) Seismic profile in the Corigliano Gulf interpreted by *Ferranti et alii* (2009) showing the overlap of back thrusts (Amendolara backthrust fault zone) on Calabrid and Southern Apennines units. We suggest that a flexural subsidence mechanism can be triggered by the back thrusting load.

4.5.2 Structural setting and earthquakes

We analyze the possible relationships between SP subsidence and recent tectonic activity relying on the analysis of structural lineaments reported in the Italy Hazard from Capable faults database (ITHACA, ISPRA). We divide SP in three sectors bounded by main faults (fig.6), assuming the influence of the activity of these structural elements, we expect different deformation patterns for the three sectors observing Envisat and COSMO-SkyMed both ascending and descending time series (fig.7) The analysis of the average displacement recorded by Envisat time series show very

similar trends for the three investigated sectors, although with different absolute values. Instead, COSMO-SkyMed time series show a different deformation pattern for each sector. In detail, the ascending time series reveal a general trend characterized by an increase of the negative displacements but with greater absolute values in the southern sector. The descending time series highlight an increase of negative displacements in the Corigliano sector, a trend fluctuating between 10mm and -5mm in the Villapiana-Sibari sector and a trend characterized by increasing positive values in the Crati Delta sector. The latter trend can be probably related to the location of the investigated sector in correspondence of an horst bounded by Crati and Timparelle faults (*Lanzafame and Tortorici*, 1981).

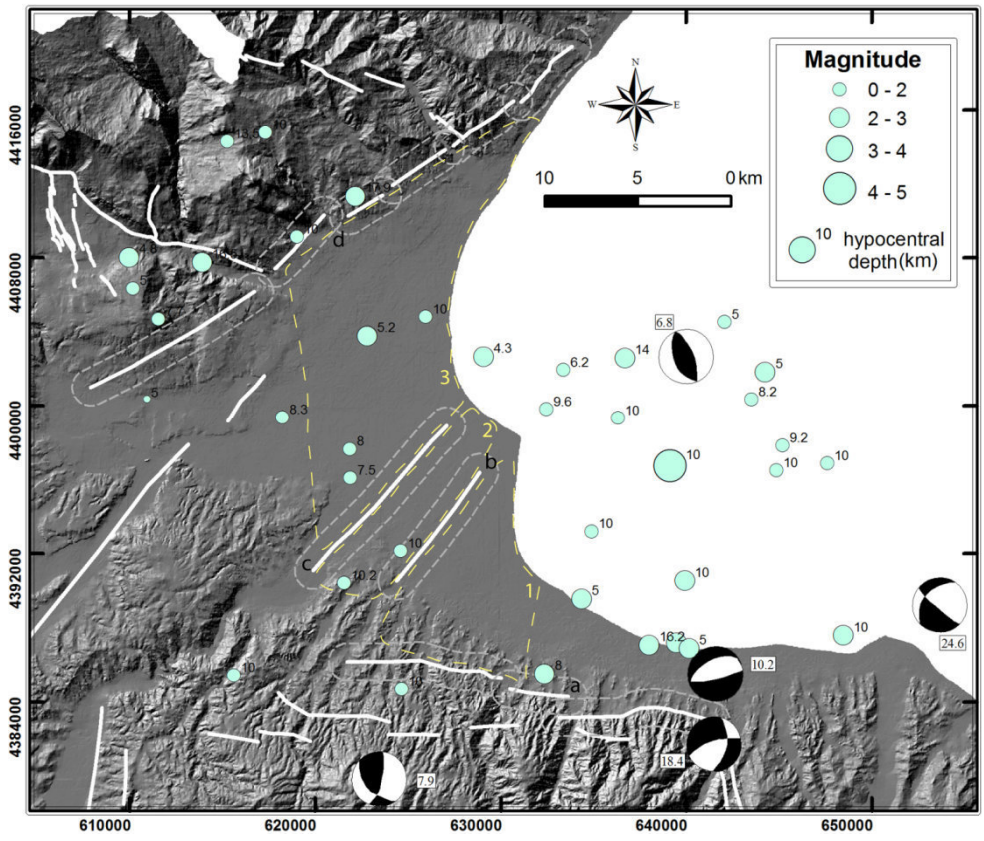

Fig. 4.4. ITHACA structural lineaments (a. Rossano-Corigliano fault system; b. Timparelle fault; c. Crati fault; d. Lauropoli-Trebisacce fault system) and hypocenters location of the earthquakes happened between 2003 and 2010 (ISIDe) with indication of relative magnitude and hypocentral depth. Focal mechanisms and depth (km) of focal solutions (boxed numbers) from *Ferranti et alii* (2009) and references therein. Yellow dashed lines are the boundaries of three sectors (1. Corigliano; 2 Crati Delta; 3. Sibari-Villapiana) selected for Envisat and COSMO-SkyMed time series analysis (fig.4.5). Grey dashed lines represent the boundaries of the buffer zones around the ITHACA faults used in the COSMO-SkyMed time series analysis (fig.4.6)

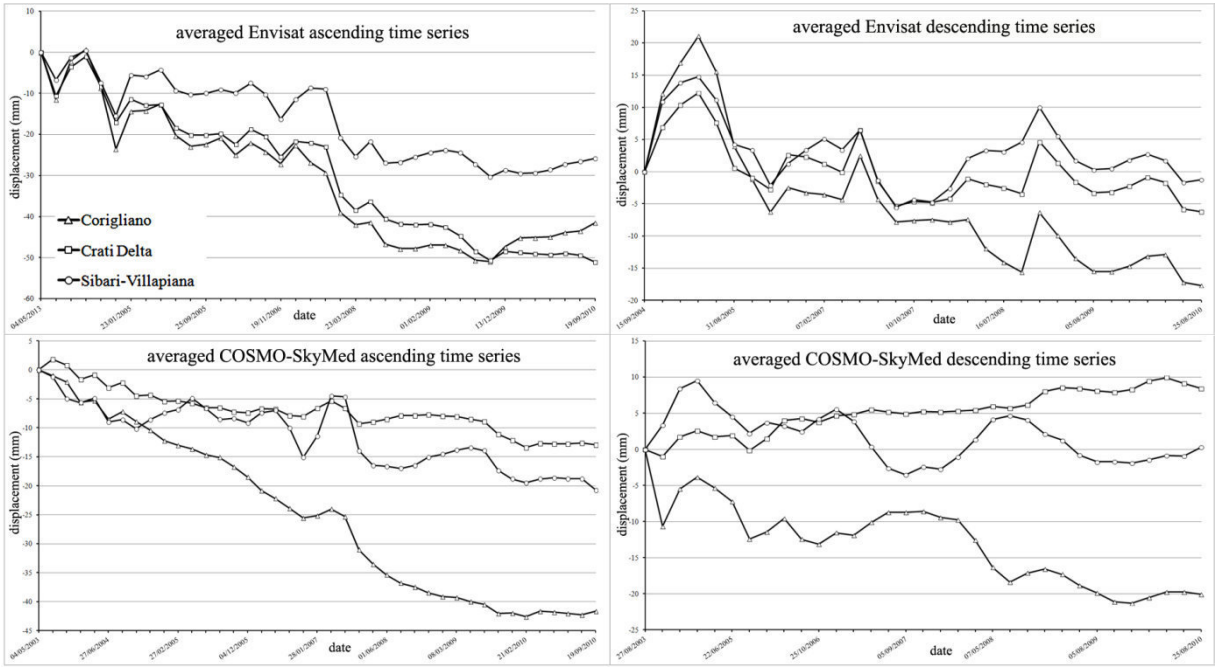

Fig. 4.5. Envisat and COSMO-SkyMed both ascending and descending time series (error = ±1mm) for the three selected sectors delimited by ITHACA faults (location in fig.4.4).

We also try to find the correlations between ground deformation pattern and earthquakes occurrence in SP area. In detail, we compare the number of earthquakes (Italian Seismological Instrumental and Parametric DataBase - ISIDe, INGV) in each time interval between two consecutive satellite passes (in the ascending and descending orbit) with the average Envisat and COSMO-SkyMed both ascending and descending time series of the areas affected by subsidence (fig.4.6). No correlation is observed.

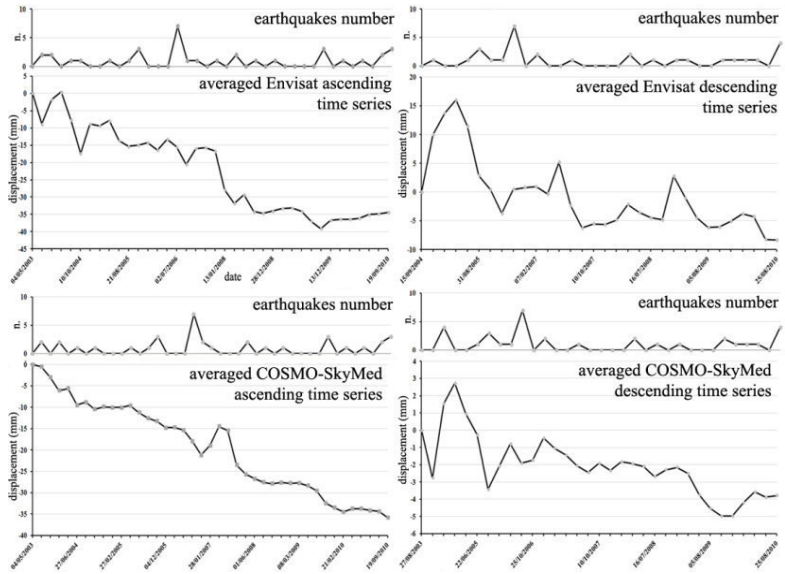

Fig.4.6. Average Envisat and COSMO-SkyMed both ascending and descending time series compared with the earthquakes number happened between each two satellite passes of the relative orbit.

Moreover, we examine the average COSMO-SkyMed both ascending and descending time series inside 1km-buffer zones around the main fault systems (Crati, Timparelle, Lauropoli-Trebisacce and Rossano-Corigliano). We do not observe correlation between the earthquakes, with hypocenter close to the faults, and ground deformation pattern (fig.4.7) so excluding seismic-induced displacements.

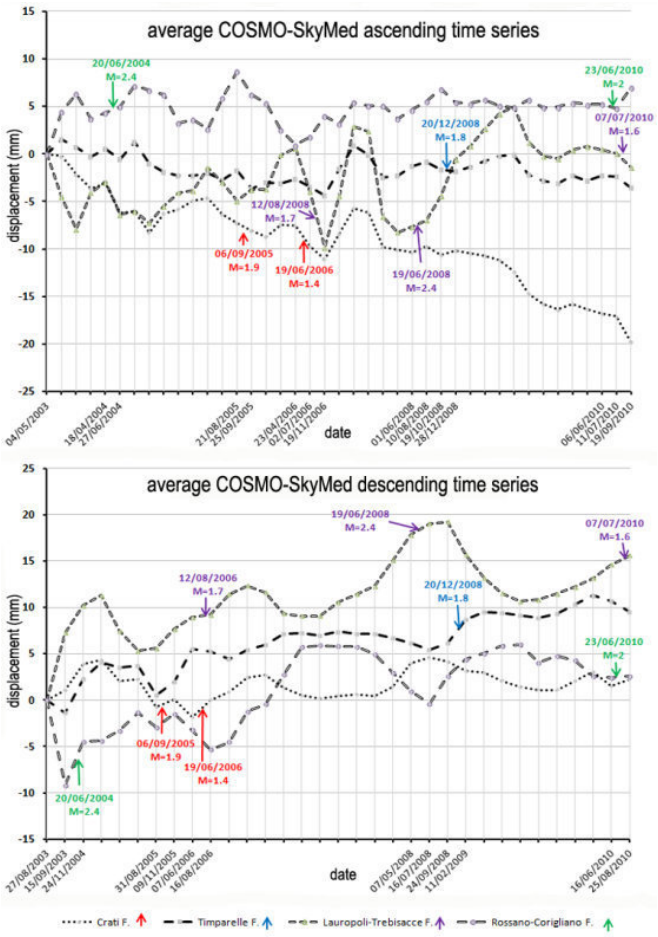

Fig. 4.7. Average COSMO-SkyMed ascending and descending time series in the 1km-buffer zones around Crati, Tiparelle, Lauropoli-Trebisacce and Rossano Corigliano faults (ITHACA) with the date of each earthquakes and relative magnitude (ISIDe).

Depending on Envisat and COSMO-SkyMed time series analysis, we suppose that the structural setting acts a control on ground deformation pattern. We also observe the absence of displacement strictly related to the earthquakes happened close to the main capable faults so excluding the contribution of recent tectonics and seismic events in the present SP subsidence phenomena, according with the conclusions by *Cucci* (2005) based on geomorphological data.

4.5.3 Role of the Plio-Quaternary succession load

We investigate the possible relationships between subsidence and spatial variation of the Plio-Quaternary succession thickness in the Crati Delta area (fig.4.8a). The thickness is reconstructed by means of available multichannel seismic profiles and well data (ViDEPI) (see Chapter 1 for more details). The thickness observed in the seismic profile is converted from twt to meter using an average velocity of 2000m/s for the Pliocene and Pleistocene deposits based on the sonic logs, available for Thurio and Ogliatrello wells, analyzed by *Spina et alii* (2011).

We compare subsidence profiles, from the Envisat Up component, and depth profiles of the top of the Miocene succession, over which the Plio-Quaternary deposits lie. To this aim, we use a Digital Surface Model (DSM) obtained combining seismic and well data (fig.4.8a).

The comparison (fig.4.8b) shows a good correlation between the general subsidence trend and the Plio-Quarernary succession thickness. We observe higher subsidence values in the E and NE sectors of Crati delta, where the Plio-Quaternary succession is thicker. In the SW sector, the reduced thickness coincides with lower subsidence values. These lower values are also detected in the S-SE sector (Corigliano harbor area), where the presence of shallow igneous-metamorphic bedrock controls the Plio-Quaternary succession thickness.

Based on the above reported analysis, we find a direct correlation between subsidence spatial trend and distribution of the thickness of Plio-Quaternary deposits. For this reason, we suppose the existence of subsidence component related to the isostatic compensation due to the Plio-Quaternary sediments load.

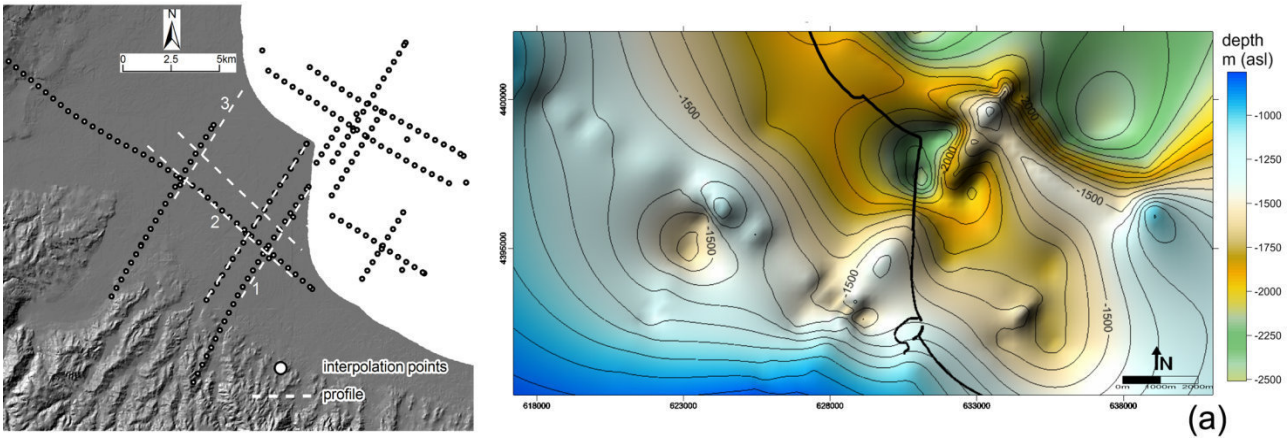

(b)

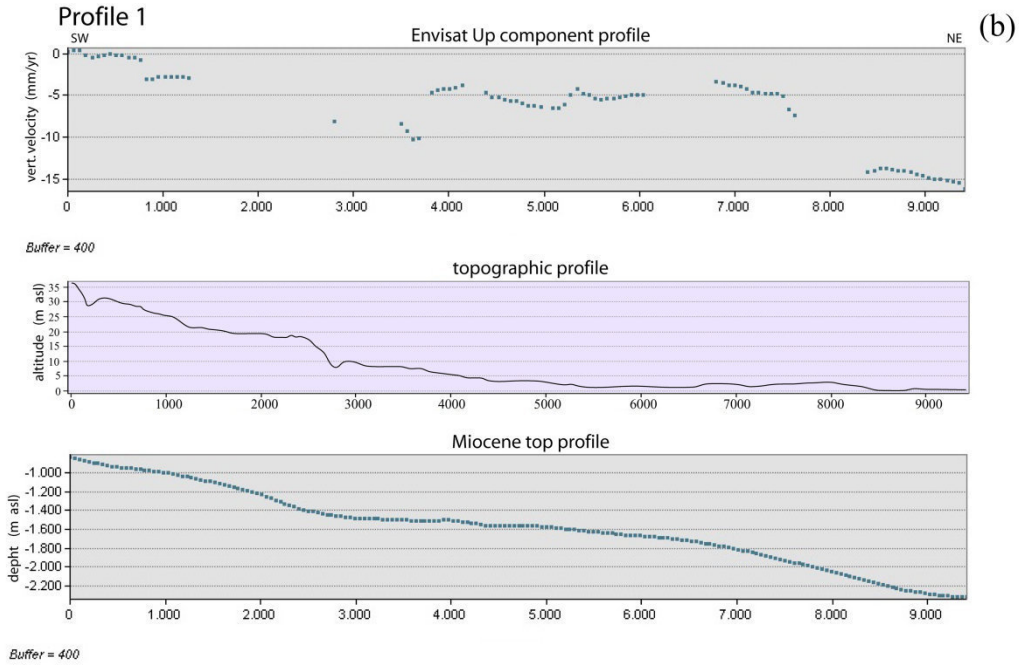
Profile 1
SW
Envisat Up component profile
NE
vert. velocity (mm/yr)
0
-5
-10
-15
0
1.000
2.000
3.000
4.000
5.000
6.000
7.000
8.000
9.000
Buffer = 400
topographic profile
altitude (m asl)
35
30
25
20
15
10
5
0
0
1000
2000
3000
4000
5000
6000
7000
8000
9000
Miocene top profile
depht (m asl)
-1.000
-1.200
-1.400
-1.600
-1.800
-2.000
-2.200
0
1.000
2.000
3.000
4.000
5.000
6.000
7.000
8.000
9.000
Buffer = 400

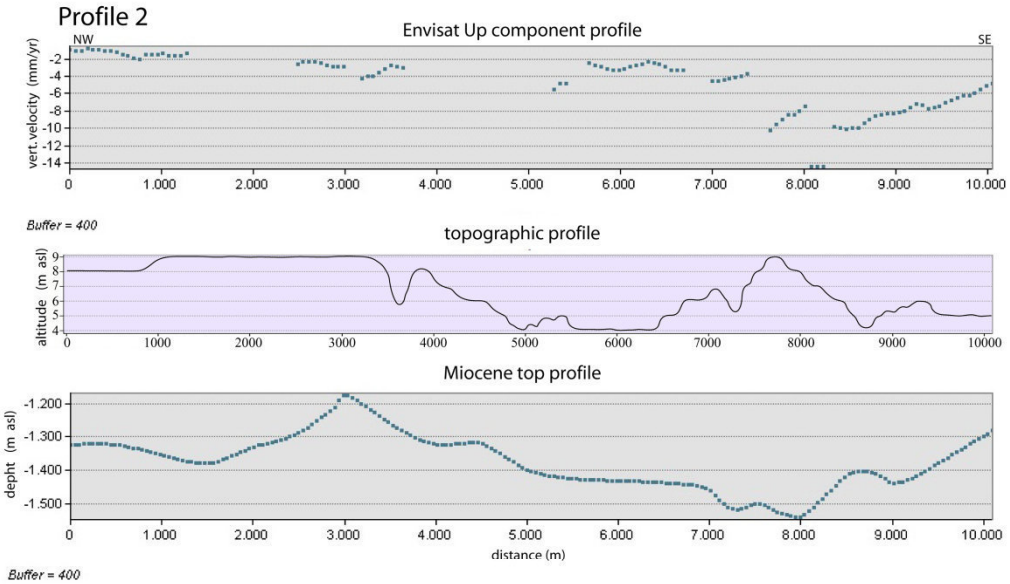
Profile 2
NW
Envisat Up component profile
SE
vert. velocity (mm/yr)
-2
-4
-6
-8
-10
-12
-14
0
1.000
2.000
3.000
4.000
5.000
6.000
7.000
8.000
9.000
10.000
Buffer = 400
topographic profile
altitude (m asl)
9
8
7
6
5
4
0
1000
2000
3000
4000
5000
6000
7000
8000
9000
10000
Miocene top profile
depht (m asl)
-1.200
-1.300
-1.400
-1.500
0
1.000
2.000
3.000
4.000
5.000
6.000
7.000
8.000
9.000
10.000
distance (m)
Buffer = 400

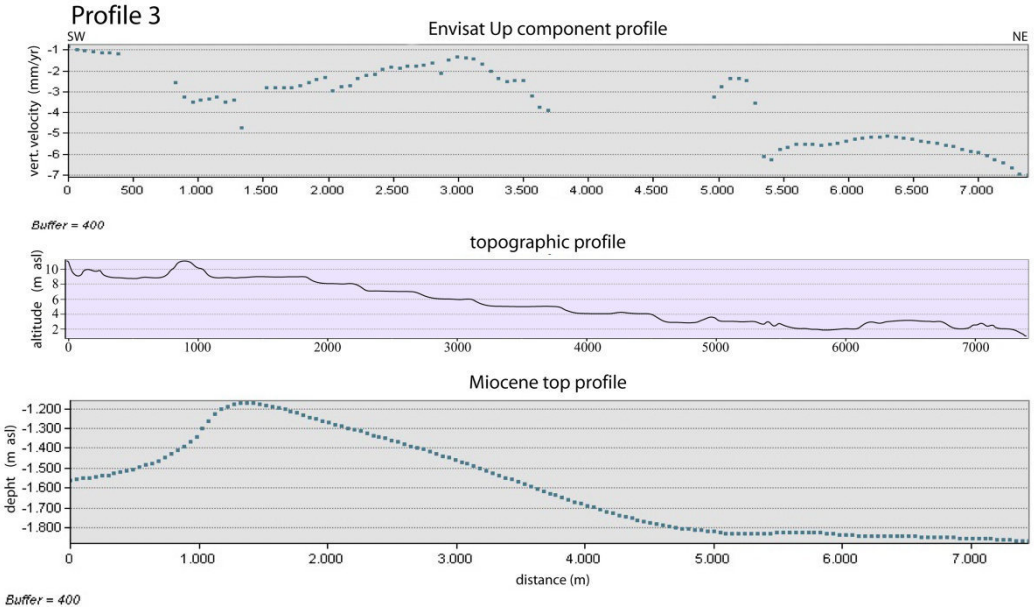
Profile 3
SW
Envisat Up component profile
NE
vert. velocity (mm/yr)
-1
-2
-3
-4
-5
-6
-7
0
500
1.000
1.500
2.000
2.500
3.000
3.500
4.000
4.500
5.000
5.500
6.000
6.500
7.000
Buffer = 400
topographic profile
altitude (m asl)
10
8
6
4
2
0
1000
2000
3000
4000
5000
6000
7000
Miocene top profile
depht (m asl)
-1.200
-1.300
-1.400
-1.500
-1.600
-1.700
-1.800
0
1.000
2.000
3.000
4.000
5.000
6.000
7.000
distance (m)
Buffer = 400

Fig.4.8 . a) DSM of the Miocene succession top (on the right) obtained by the integration of wells and seismic data (on the left). b) Comparison between the thickness of the Plio-Quaternary succession (obtained by the combination of topographic and Miocene top profiles) and displacement profiles based on the Envisat Up component. Profile traces are represented by dashed white lines in (a).

4.5.4 Holocene deposits

Previous studies on historical subsidence of the Sybaris archeological site identify the compaction of Holocene sediments and/or water pumping as causes responsible for this kind of ground deformations (*Guerricchio and Melidoro*, 1975; *Cucci*, 2005; *Cotecchia et al.*, 1994; *Pagliarulo et al.*, 1995; *Cotecchia and Pagliarulo*, 1996; *Cherubini et al.*, 2000).

We investigate the subsidence due to sediments compaction in the whole SP area and focus on the lithological features, thickness and lithofacies architecture of the late Holocene deposits which are strictly related to the Crati Delta progradation since about 6 kyr B.P..

These deposits occupy the area near the coastline and extend for about 6 km inland in the Crati Delta area (*Bellotti et al.,* 2009, Chapter 2). To map the inland boundary, we consider the T1 terrace (MIS3.1-3.3) by *Santoro et al.* (2009) which is represented by a morphological step at ~15 m a.s.l. (*Guerricchio and Melidoro*, 1975).

Using the well-logs data (Chapter 2 and 3),we also create a DSM of the Late Holocene bottom surface (fig.4.9b). Then, we compare several subsidence velocity profiles, on ascending Envisat data, with the late Holocene sediment thickness.

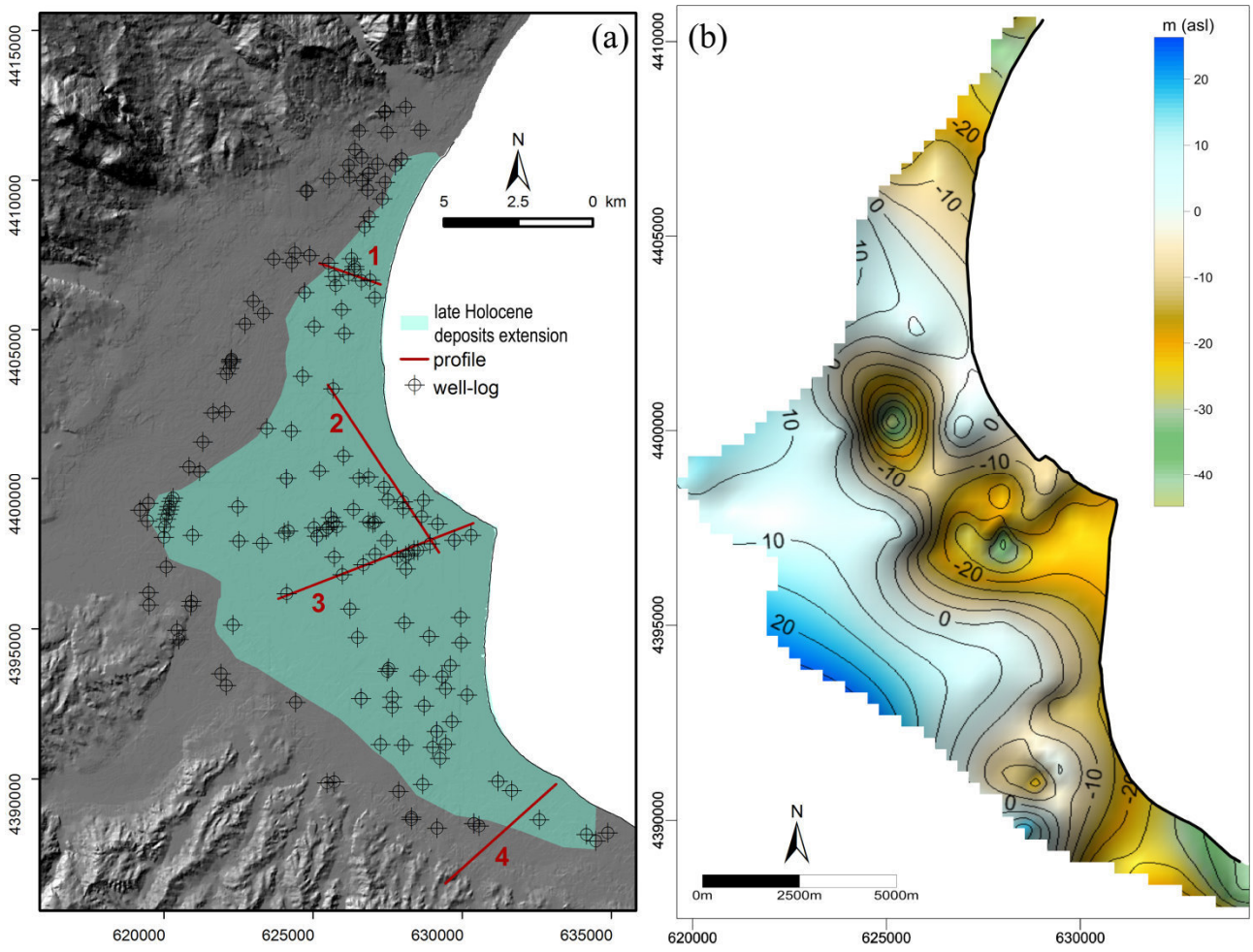

Fig.4.9. a) Holocene alluvial plain extension retrieved by the position of marine terrace correlated to MIS 3.1-3.3 (*Santoro et al.*, 2009) and location of the well-logs analyzed and used to DSM reconstruction. Red lines represents the traces of the profiles showed in fig.12 . b) DSM of the late Holocene bottom surface on which the delta plain progradation happened.

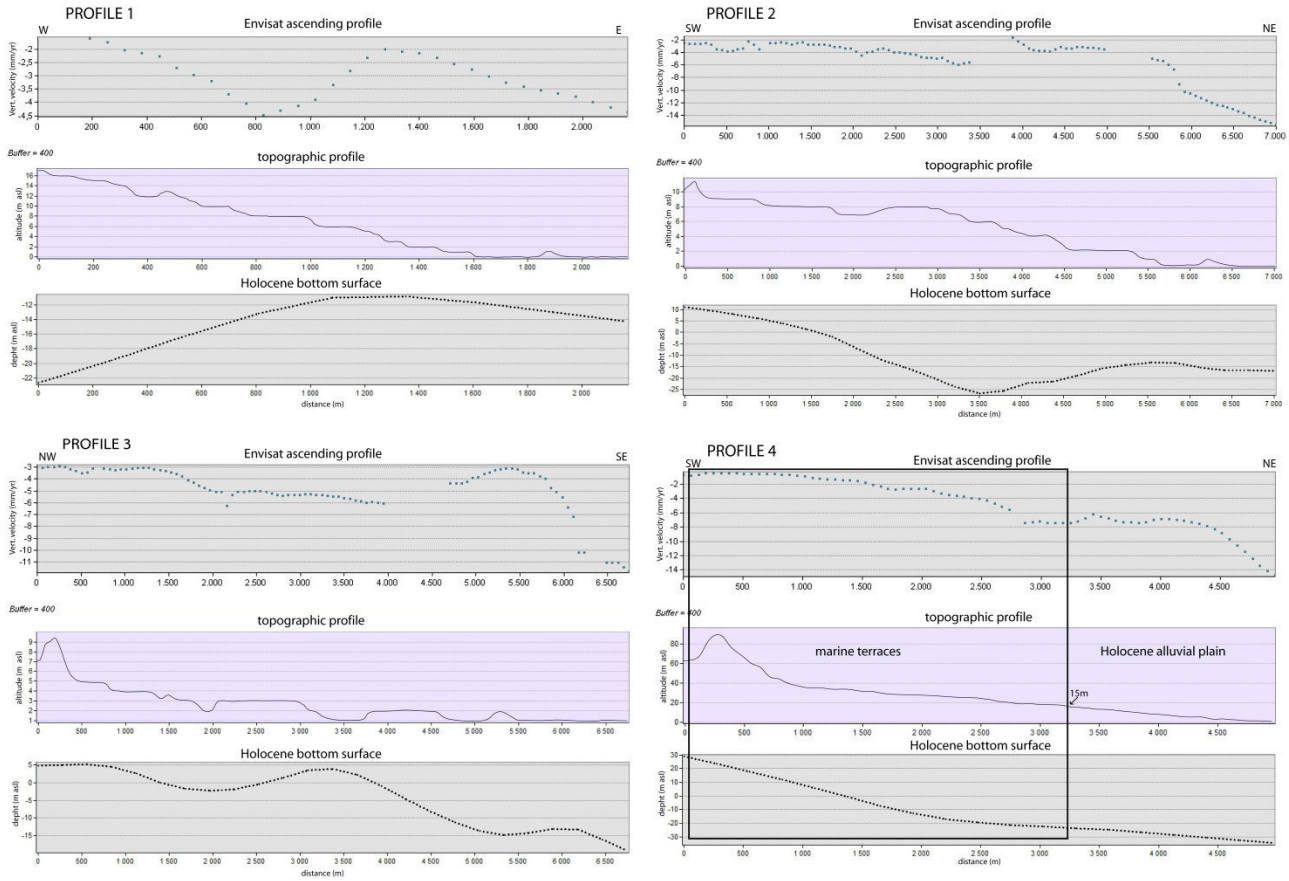

Fig.4.10. Envisat ascending velocity profiles compared with the thickness of the late Holocene succession defined by topographic and bottom surface profiles. Traces (red line) are in the Fig.4.9a.

We observe an increase of subsidence values in the area where the late Holocene succession is thicker. So that, we suppose a direct correlation between subsidence and late Holocene sediments thickness. However, referring to the Holocene stratigraphic framework proposed in the Chapter 2, the sediments compaction cannot be considered the only trigger of subsidence otherwise two different deformation patterns should exist between the area respectively on foot wall and hanging wall of the Sybaris fault zone.

Moreover, the well logs analysis allows us to a clear influence of the Holocene sediment lithology and its heteropical transitions on subsidence. In detail, we analyze the ground deformation pattern, recorded by ascending Envisat data, along two profiles cutting the Saraceno and Satanasso alluvial fans. The analysis shows negative displacement values in correspondence of the sandy-silty deposits, related to overbank river deposition, and stability on the alluvial fan bodies consists of gravelly-sandy sediments.

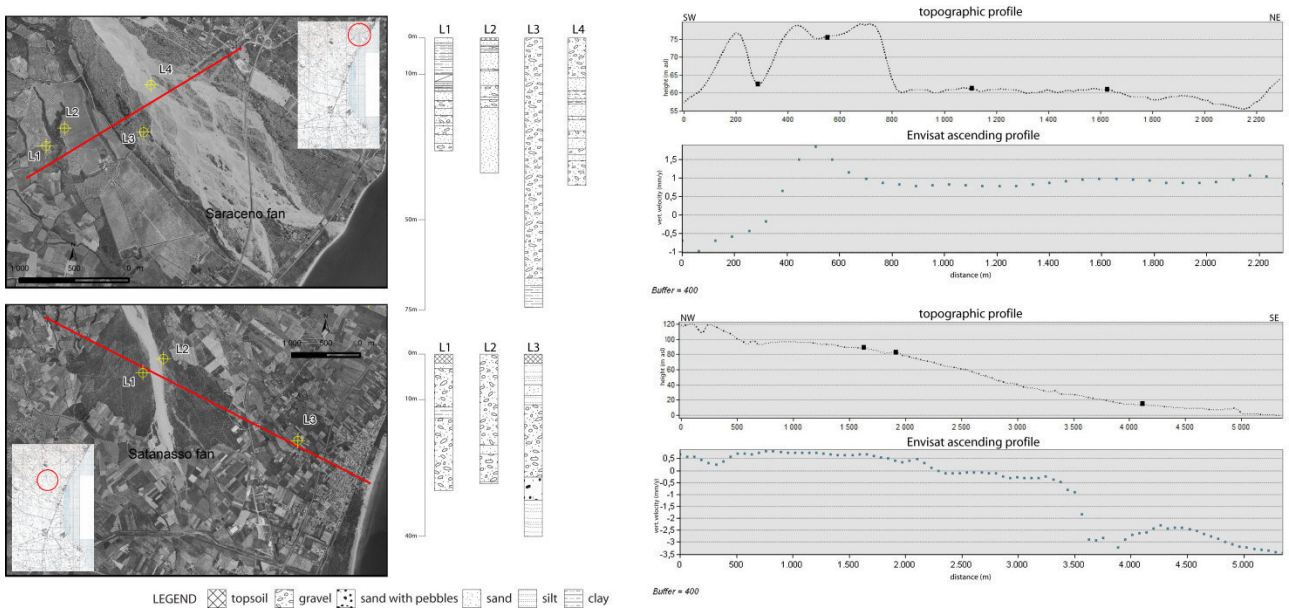

Fig.4.11. Envisat ascending velocity profiles along two sections cutting alluvial fans of Saraceno (a) and Satanasso (b) streams. The heteropical transitions between fine-grained overbank deposits and coarse-grained fan sediments is shown by well-logs located along the profiles. Traces (red line) are in the left picture.

4.5.5 Land use and historical evolution

SP represents a geomorphological system with a rapid evolution in historical and recent times controlled by geological processes (transport-sedimentation-erosion, subsidence, relative sea level variations) and human-made factors (drainage work, dam, seaports, embankments, soil use, exploitation of water resources, etc.). The present morphological setting results from the works of a 1960s-1990s land reclamation project aimed to convert a marshy area in agricultural zone.

We investigate possible connections between subsidence and land use by means of Corine Land Cover 2006 project (ISPRA, 2010). We observe the undifferentiated subsidence distribution over areas characterized by various land use (e.g. urban areas, orchards, arable soils).

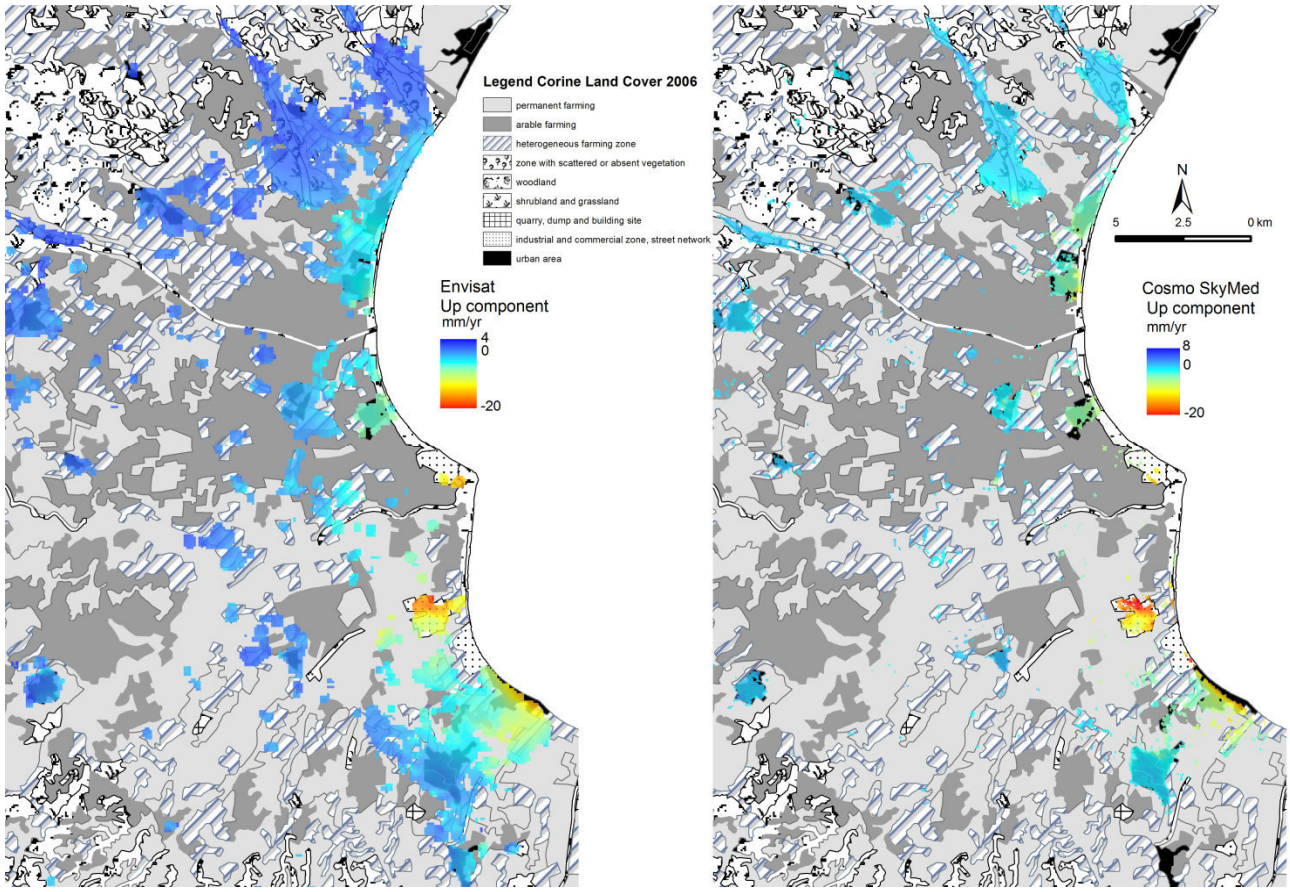

Fig.4.12. Envisat (left) and COSMO-SkyMed (right) Up component plotted on soil use map by Corine Land Cover 2006 project (ISPRA, 2010).

We analyze the 1954 and 1998 aerial photos to define land use variations; for a more detailed analysis of urban area growth effects we select three areas (Marina di Sibari; Laghi di Sibari and C.da Ricota), characterized by the same subsoil stratigraphy, and compare COSMO-SkyMed ascending and descending time series of urban and agricultural areas. For all the studied areas the subsidence in both urban and agricultural sectors shows a similar temporal trend. In Laghi di Sibari and C.da Ricota areas we observe a progressive temporal differentiation in the subsidence values which increase faster in urban areas reaching a maximum difference compared with agricultural ones of ~35 mm in August 2010 (descending time series) and of ~27 mm in September 2010 (ascending time series). Instead, subsidence values are very similar for the two considered sectors in the Marina di Sibari area, where only descending time series show a little increase (~5 mm) of ground deformation values in urban area.

We observe a diffuse subsidence irrespective of the land use, but with some increments of deformation velocity in correspondence of the urban areas (Laghi di Sibari and C.da Ricota). Therefore, we suggest that result the different land use represents a incremental factor of subsidence mainly due to the urban-induced loading.

Marina di Sibari

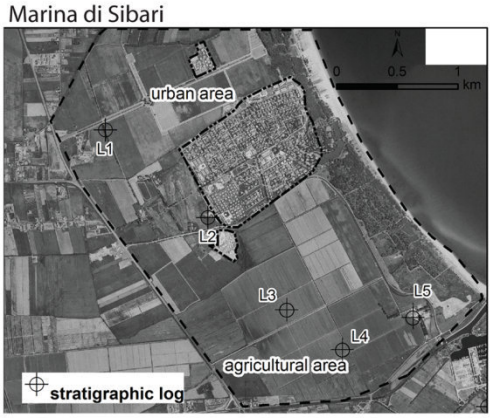

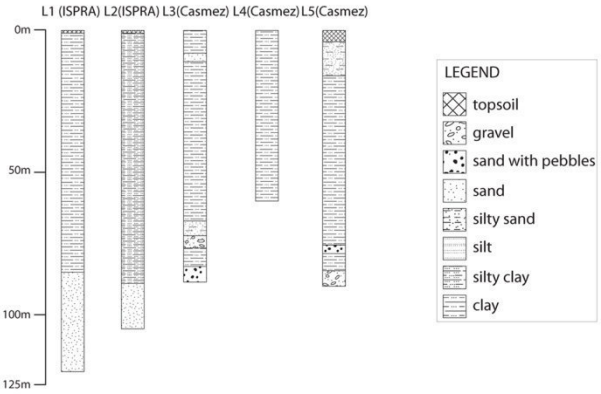

Laghi di Sibari

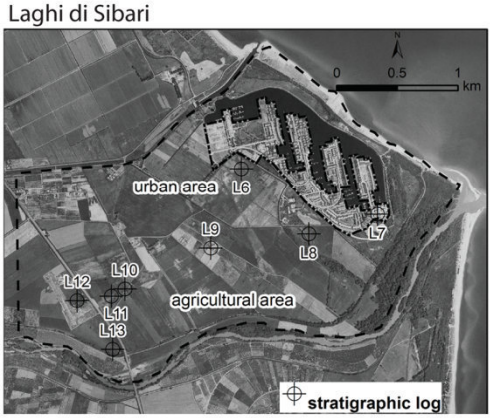

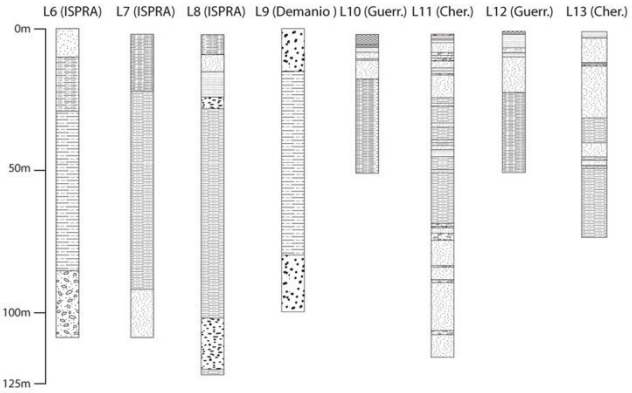

C.da Ricota

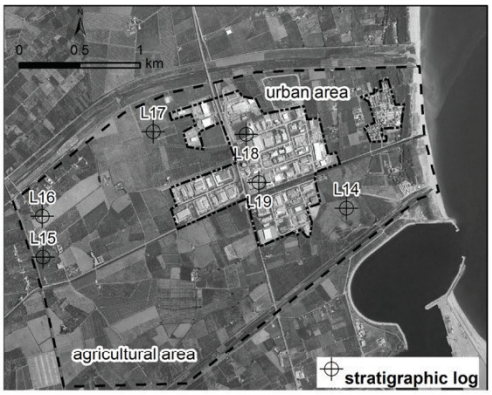

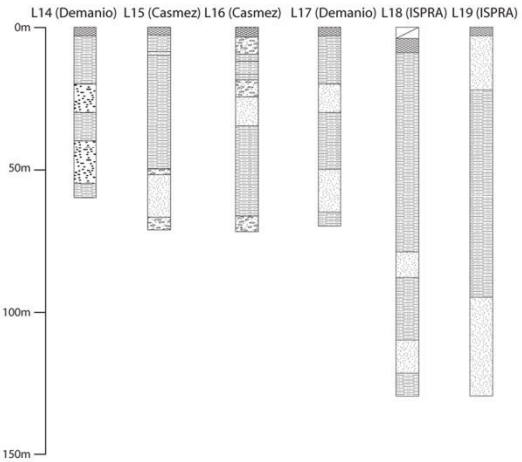

Average COSMO-SkyMed ascendig time series

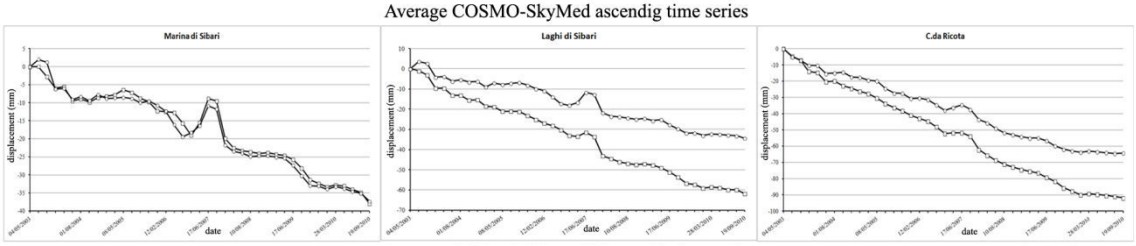

Average COSMO-SkyMed descendig time series

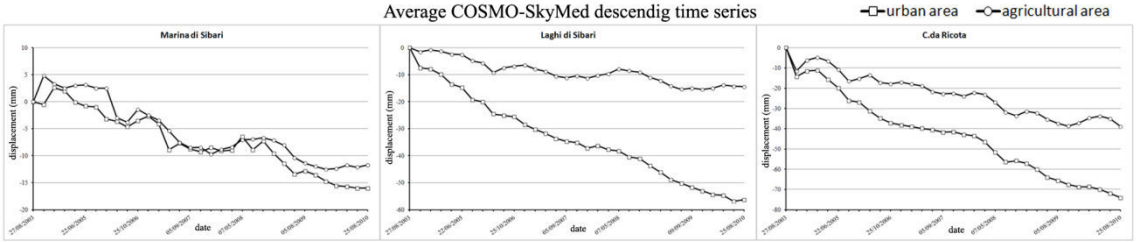

Fig.4.13. COSMO-SkyMed ascending and descending time series (error = ±1mm) comparison between urban and agricultural areas for three selected sectors characterized by same subsoil shallow stratigraphy. Stratigraphic data are collected from Demanio Idrico Provincia di Cosenza (Demanio), L.464/84 ISPRA database (ISPRA), *Casmez* (1997) , *Guerricchio and Melidoro* (1975)(Guerr.) and *Cherubini et al.* (2000) (Cher.).

4.5.6 Water table variations

SP is characterized by two well-defined aquifers; the shallower one (from soil surface to -20/-30 m a.s.l.) is separated by clayey and silty-clayey layer from a deeper one (from -50/-60 m a.s.l.) (*Polemio and Luise*, 2007). Both shallow and deep aquifers are characterized by intense water exploitation (Demanio Idrico Prov. Cosenza information). Piezometric level variations between 1930s and 2002 shows a 5 meters drop of shallow aquifer (*Polemio et al.*, 2002, 2013).

Among others *Cherubini et al.* (2000) and *Cafaro et al.* (2011) attribute the recent subsidence in the area of Sybaris archeological site to the water withdrawals.

We try to find correlations between groundwater exploitation and ground deformation comparing the spatial distribution of phreatic water table variations in the interval 1930s-2002 (*Polemio et al.*, 2004) and the Up velocity distribution from Envisat and COSMO-SkyMed data in the following 2003-2013 time interval (fig.4.14).

We observe the subsidence distribution in areas with rise, drop and stability of water table.

We consider also the effect of water table variation between 2002 (data from *Polemio et al.*, 2004) and 2013 (Chapter 3). We analyze the distribution of the Up velocity distribution (from Envisat and COSMO-SkyMed data) considering the map of 2002-2013 water table variation (fig.4.14). The subsidence location does not show a strictly correlation with the water table drop.

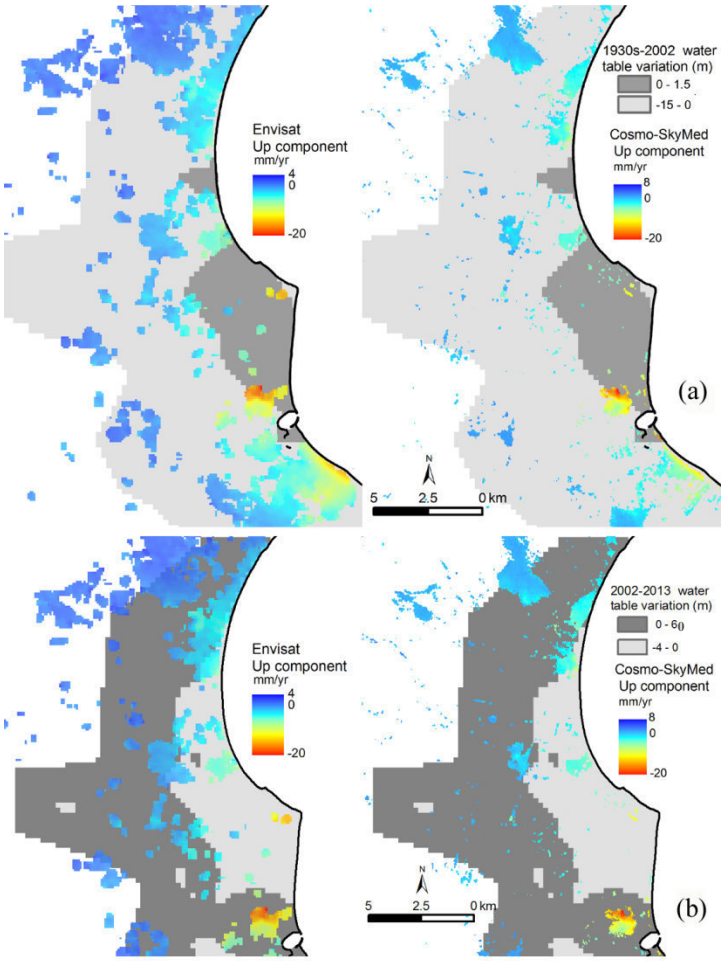

Fig.4.14. Envisat (left) and COSMO-SkyMed (right) Up component superimposed on the maps of the water table variation between 1930s and 2002 (a) (redrawn from *Polemio et al.*, 2004) and between 2002 and 2013 (b).

We propose that the water table variations in the time cannot be considered as the only responsible for recent subsidence in the SP considering the presence of negative vertical movements also in areas characterized by water table rise. So we conclude that water table variations are an incremental factor of subsidence in some area as the Sybaris archeological area, where a well-points system (80 l/s) works every time to maintain the excavations above the water table.

4.6 Conclusions

SAR data acquired from 2003 to 2013 by ESA-Envisat and ASI-COSMO-SkyMed satellites detect ground displacements in the SP area (Calabria, Southern Italy). The deformation field is characterized by a widespread ground subsidence with rate up to ~ -20 mm/yr.

The location of the SP in an area marked by geodynamic and geological complexity precludes the attribution of the ground deformation triggered factor to any unique subsidence mechanism.

We suppose that the active oblique-contractional belt in the Ionian Sea in front of SP (*Ferranti et al.*, 2014) can trigger a flexural subsidence mechanism due to the back thrusting load above the underlying Calabrid and Southern Apennines units. Furthermore, the observed correlation between Plio-Quaternary sediments thickness and ground deformation suggests that also the isostatic compensation plays an active role in the SP present subsidence.

The structural setting seems condition the ground displacement spatial pattern while faulting activity and earthquakes do not influence the current subsidence.

Other superimposed subsidence mechanism is represented by the compaction of the compressible fine-grained sediments related to the late Holocene Crati Delta progradation. Moreover, we show the effect of the heteropical transition between fine- and coarse-grained Holocene sediments on the ground deformation spatial pattern.

Human-made activities are considered an incremental factor of the SP subsidence. In fact, we observe higher subsidence velocities in the more anthropized areas, where soil compaction is amplified by urban-induced loading. Water table variations may increase the deformation velocity in some area characterized by excessive water withdrawals (e.g., Sybaris archeological site).

The results of this study show how the deformation field of complex basins like that investigated here may be due to coexisting regional and local natural processes and anthropic activities. A multiparametric monitoring of SP area must be implemented with the aim to evaluate the hazard(s) related to ground deformation.

References

AdBArno (2008). Progetto Piano Stralcio "Bilancio Idrico". Adottato nella seduta del Comitato Istituzionale del 28 febbraio 2008 e pubblicato sulla Gazzetta Ufficiale n. 78 del 2 aprile 2008.

Amodio-Morelli, L., Bonardi, G., Colonna,V., Dietrich, D., Giunta, G., Ippolito, F., Liguori, V., Lorenzoni, S., Paglionico, A., Perrone, V., Piccarreta, G., Russo, M., Scandone, P., Zanettin-Lorenzoni, E., and Zuppetta, A. (1976). L'arco Calabro-Peloritano nell'orogene appenninico Maghrebide (The Calabrian-Peloritan Arc in the Apennine-Maghrebide orogen). Mem. della Soc. Geol. It., 17, 1–60.

Amorosi, A., and Milli, S. (2001). Late Quaternary depositional architecture of Po and Tevere deltas (Italy) and worldwide comparison with coeval deltaic succession. Sedimentary Geology, 144, 357-375.

Baines, D., Smith, D.G., Froese, D.G., Bauman, P., and Nimeck, G. (2002). Electrical resistivity ground imaging (ERGI): a new tool for mapping the lithology and geometry of channel-belts and valley fills. Sedimentology, 49, 441–449.

Barone, M., Dominici, R., Muto, F., and Critelli, S. (2008). Detrital mode in late Miocene wedge-top basin northeasten Calabria, Italy: compositional record of wedge –top partitioning. Journal of Sedimentary Research, 78, 693-711.

Baruffini, L., Lottaroli, F., Torricelli, S., and Lazzari, D. (2000). Stratigraphic revison of the Eocene Albidona Formation in the type locality (Calabria, Southern Italy). Riv. It. Paleont. Strat., 106, 73-98.

Bellotti, P., Caputo C., Dell'Aglio, P.L., Davoli, L., and Ferrari, K. (2009). Insediamenti urbani in un paesaggio in evoluzione: interazione uomo-ambiente nella Piana di Sibari (Calabria ionica). Il Quaternario Italian Journal of Quaternary Sciences, 22(1), 61-72.

Bellotti, P., Caputo, C., Davoli, .L., Evangelista, S., and Pugliese, F. (2003). Sedimentological and morphological evolution of the Crati river delta (Calabria Italy). Suppl. Geogr. Fis. e Din. Quarter., 6, 25-32.

Bellotti, P., Caputo, C., Davoli, L., Evangelista, S., and Pugliese, F. (2003–04). Preliminary results of researches on sedimentology and littoral dynamics of the Crati River delta (Calabria). Geologica Romana. 37, 123–126.

Bellotti, P., Milli, S., Tortora, P., and Valeri, P. (1995). Physical stratigraphy and sedimentology of the Late Pleistocene-Holocene Tiber Delta depositional sequence. Sedimentology, 42, 617-634.

Berardino, P., Fornaro, G., Lanari, R., and Sansosti, E. (2002). A new algorithm for surface deformation monitoring based on small baseline differential SAR interferograms. IEEE Transactions on Geoscience and Remote Sensing, 40, 2375-238.

Beresnev, I. A., Hruby, C.E., and Davis C.A. (2002). The use of multi-electrode resistivity imaging in gravel prospecting. Journal of Applied Geophysics, 49, 245– 254.

Bernasconi, M.P., Stanley, J.D., and Caruso C. (2010). Sybaris–Thuri–Copia Deltaic Settings in Calabria, Italy:Molluscs, Associated Biogenic Components, and Ecobiostratigraphy Applied to Archaeology. Journal of Coastal Research, 26 (2), 377-390.

Bersezio, R., Giudici, M., and Mele, M. (2007). Combining sedimentological and geophysical data for high-resolution 3-D mapping of fluvial architectural elements in the Quaternary Po plain (Italy). Sedimentary Geology, 202, 230–248.

Bigi, G., Bonardini, G., Catalano, R., Cosentino, D., Lentini, F., Parlotto, M., Sartori, R., Scandone, P., & Turco, E. (1992). Structural Model of Italy, 1:500.000. Consiglio Nazionale delle Ricerche, Roma.

Boccaletti, M., Nicolich, R., and Tortorici L. (1984). The Calabrian Arc and the Ionian Sea in the dynamic evolution of the Central Mediterranean. Cita, M.B., Ricci Lucchi, F. (Eds.). Seismicity and Sedimentation, Mar. Geol. 55, 219–245.

Bonardi, G., Amore, F.O., Ciampo, G., De Capoa, P., Miconnet, P., and Perrone, V. (1988). Il Complesso Liguride Auct.: stato delle conoscenze e problemi aperti sulla sua evoluzione pre-appenninica ed i suoi rapporti con l'Arco Calabro. Mem. Soc. Geol. Ital., 41, 17-35.

Bonardi, G., Caggianelli, G., Critelli, S., Messina, A., and Perrone, V. (2004). P66: Geotraverse across the Calabria-Peloritani Terrane (Southern Italy). 32nd International Geological Congress, Firenze. 6, 1-60.

Bouillin, J.P., Durand-Delga, M., and Olivier, P.H. (1986). Betic-Rifian and Tyrrhenian Arcs: distinctive features, genesis and development stages. In:Wezel F.C. (Ed.), The Origin of Arcs. Elsevier Science, Amsterdam, 281–304

Bousquet, J.C. (1973). La tectonique récente de l'Apennin calabro-lucanien dans son cadre géologique et gèophysique. Geol. Romana, 12: 1-103.

Bousquet, J.C., and Gradjacquet, J.C. (1969). Structure de l'Apennin Calabro-Lucanien (Italie m´eridional). Comptes rendus des s´eances de l'Académie des Sciences 268, 13–16.

Buttafuoco, G., Caloiero, T., and Coscarelli, R. (2011). Spatial and temporal patterns of the mean annual precipitation at decadal time scale in southern Italy (Calabria region). Theor Appl Climatol., 105, 431–444.

Cafaro, F., Cotecchia, F., Lenti, V., P., and Pagliarulo, R. (2011). Criticità nella modellazione geotecnica della subsidenza dell'area di Sibari (Calabria). Incontro Annuale dei Ricercatori di Geotecnica – IARG. Torino, 4-6 Luglio 2011

Capraro, L., Consolaro, C., Fornaciari, E., Massari, F., and Rio, D. (2006). Chronology of the Middle–Upper Pliocene succession in the Strongoli area: constraints on the geological evolution of the Crotone Basin (Southern Italy). From: Moratti, G. & Chalouan, A. (eds) 2006. Tectonics of the Western Mediterranean and North Africa. Geological Society, London, Special Publications, 262, 323–336.

Caputo, R., Piscitelli, S., Oliveto, A., Rizzo, E., and Lapenna, V. (2003). The use of electrical resistivity tomographies in active tectonics: examples from the Tyrnavos Basin, Greece. Journal of Geodynamics, 36, 19–35.

Caputo, R., Salviulo, L., Piscitelli, S., and Loperte A. (2003)Late Quaternary activity along the Scorciabuoi Fault (Southern Italy)as inferred from electrical resistivity tomographies. Annals of Geophysics, 50 (2), 213-224.

Carapa, B., and Garcia-Castellanos D. (2005). Western Alpine back-thrusting as subsidence mechanism in the Tertiary Piedmont Basin (Western Po Plain, NW Italy). Tectonophysics, 406, 197– 212

Carbognin, L., P. Teatini, and L. Tosi (2004), Relative land subsidence in the lagoon of Venice, Italy, at the beginning of the new millennium. J. Mar. Syst. 51(1–4), 345–353, doi:10.1016/j.jmarsys.2004.05.021.

Carminati, E., C. Doglioni, and D. Scrocca (2003). Apennines subduction related subsidence of Venice (Italy), Geophys. Res. Lett. 30(13), 1717, doi:10.1029/2003GL017001.

Carobene L. (1996). I ripiani litostrutturali, superfici terrazzate marine e tettonica quaternaria in località Tarsia (valle del crati, Calabria). Il Quaternario Italian Journal of Quaternary Science, 9 (1), 179-186.

Carobene, L., Colalongo, M.S., Pasini, G., and Raffi, I. (1997). Sequenze de posizionali del Pleistocene medio nella valle del Fiume Crati presso Tarsia (Calabria). Boll. Soc. Geol. It., 116, 503-524.

Caruso, C., Ceravolo, R., Cianflone, G., Dominici, R., and Sonnino, M. (2013). Sedimentology and ichnology of Plio-Pleistocene marine to continental deposits in Broglio (Trebisacce, northern ionian Calabria, Italy). Journ. Med. Earth Sc., S.I., 21-24.

Caruso, C., Natoli, D., and Sonnino, M. (2011). Sedimentology and ichnology of the lower part of the Saraceno Formation (Cretaceous?, Miocene?) (northern Ionian Calabria). Rendiconti Online Soc. Geol. Ital., 17, 31.

Casmez (Cassa Speciale per il Mezzogiorno) (1987). Progetto Speciale 26. CMP.

Casmez (Cassa Speciale per il Mezzogiorno). (1967-1969). Carta Geologica della Calabria 1:25000. Foglio 221 I NO, NE, SO, SE; II NO, NE, SO, SE; III NO, NE, SO, SE; IV SE. Foglio 222 II NO, SO; IV SO. Foglio 229 I NO, NE, SO, SE; II NO, NE, SO, SE; III NE, SE; IV NO, NE, SO, SE. Foglio 230 I NO, SO; III NO, NE, SO, SE; IV NO, NE, SO, SE. Foglio 234 I NO, NE, SO, SE; IV NE, SE. Poligrafica & Cartevalori. Ercolano, Napoli.

Castellaro, S., Mulargia, F., and Bianconi, L. (2005). Passive seismic stratigraphy: a new efficient, fast and economic technique. J. Geotech. Environ. Geol., 3, 51-77.

Casu, F., Manzo, M., and Lanari, R. (2006). A quantitative assessment of the SBAS algorithm performance for surface deformation retrieval from DInSAR data. Remote Sens. Environ., 102, 195–210.

Celico, P. (1988). Prospezioni idrogeologiche. Liguori Ed., vol.II, 521 p.

Cello, G., Tortorici, L., Turco, E., and Guerra, I. (1981). Profili profondi in Calabria settentrionale. Boll. Soc. Geol. It., 109, 423-431.

Chambers, J.E., Wilkinson, P.B., Penn, S., Meldrum, P.I., Kuras O., Loke, M.H.., and Gunn D.A. (2013). River terrace sand and gravel deposit reserve estimation using three-dimensional electrical resistivity tomography for bedrock surface detection. Journal of Applied Geophysics, 93, 25–32.

Cherubini, C., Cotecchia, V., and Pagliarulo, R. (2000). Subsidence in the Sybaris Plain (Italy). In: Carbognin, L., Gambolati, G., and Johnson, A.I. (Eds.), Land Subsidencee1. Proceedings of the 6th International Symposium on Land Subsidence, Ravenna, 3-15.

Chiarabba, C., De Gori, P., Speranza, F. (2008). The southern Tyrrhenian subduction zone: Deep geometry, magmatism and Plio-Pleistocene evolution, Earth Planet . Sci . L et t . , 268, 408–423,

Ciaranfi, N., Ghisetti, F., Guida, M., Iaccarino, G., Pieri, P., Rapisardi, L., Ricchetti, G., Torre, M., Tortorici, L., and Vezzani, L. (1983). Carta neotettonica dell'Italia meridionale. C.N.R. P.F.G., 515, Bari, p. 62.

CIESM (2008). The Messinian Salinity Crisis from mega-deposits to microbiology. A consensus report. n° 33. In: Briand, F. (Ed.), CIESM Workshop Monographs. Monaco, p. 168.

Cinti, F. R., Alfonsi, L., Brunori, C.A., and Ventura G. (2013). Archaeoseismic field survey, chapter 4, in Parametrization of Active Faults in the Calabria-Lucania Region, Final Report, Deliverable Number 25/c2, Project S1 INGV-DPC 2012–2013.

Cinti, F. R., Alfonsi,L., D'alessio, A., Marino. S., and Brunori, C.A. (2014). Faulting and Ancient Earthquakes at Sybaris Archaeological Site, Ionian Calabria, Southern Italy. Seismological Research Letters, 86 (1). in press.

Cinti, F.R., Cucci, L., Pantosti, D., D'Addezio, G. and Meghraoui, M. (1997). A major seismogenic fault in a "silent area": the Castrovillari Fault (southern Apennines, Italy). Geophys. Journ. Int., 130, 595-605.

Civile, D., Ceramicola ., Caburlotto, A., Cova, A., Cotterle, D., Diviacco, P., Caffau, M., Praeg, D., Neagu, C., Critelli, S., Dominici, R., Muto, F., Romano, C., and Ramella, R. (2009). Seabed tectonic features in relation to geohazards on the Ionian Calabrian margin. Rend.Online Soc.Geol.Ital., 7, 145-146.

Civita M. (2005). Idrogeologia Applicata e Ambientale. CEA, Milano, 794 p.

Colella, A. (1984). Marine Gilbert-type deltas in lower (?) Pleistocene deposits of Crati Valley (Calabria, Southern Italy); a preliminary note. 5th IAS European Regional Mtng Abstr., 96-99.

Colella, A. (1988). Fault-controlled marine Gilbert-type fan deltas. Geology, 16, 1031-1034.

Colella, A., and Cappadona, P. (1988). Evidenze stratigrafiche del carattere trascorrente sinistro della zona di faglie del Pollino. Valutazione della velocità di trascorrenza. Atti 74 Congresso Società Geologica Italiana, 147-150.

Colella, A., and Di Geronimo, I. (1987). Surface sediments and macrofaunas of the Crati submarine fan (Ionian Sea, Italy). Sedimentary Geology, 51, 257–277.

Colella, A., De Boer, P.L., and Nio, S.D. (1987). Sedimentology of a marine intermontane Pleistocene Gilbert-type fan-delta complex in the Crati Basin, Calabria, southern Italy. Sedimentology, 34, 721-736.

Colella, A., Lapenna, V., and Rizzo, E. (2004). High-resolution imaging of the High Agri Valley Basin (Southern Italy) with electrical resistivity tomography. Tectonophysics, 386, 29– 40.

CORINE LAND COVER 2006. ISPRA. http://www.pcn.minambiente.it/viewer/

Cotecchia, V., and Pagliarulo, R. (1996). State of the art in geological, hydrogeological and geotechnical researches carried on the archaeological site of Sybaris. Geologia Applicata e Idrogeologia, 31, 43-54.

Cotecchia, V., Cherubini C., and Pagliarulo, R. (1994). Geotechical characteristics of outcropping deposits in Sibari plain. In "Procedings XIII International Conference of Soil Mechanics and Foundation Engineering". New Delhi, 860-865.

Coutellier, V., and Stanley, D.J. (1987). Late Quaternary stratigraphy and paleogeography of the eastern Nile delta, Egypt. Marine Geology, 77, 257-275.

Critelli, S. (1999). The interplay of lithospheric flexure and thrust accomodation in forming stratigraphic sequences in the southern Apennines foreland basin system, Italy. Rend. Fis. Acc. Lincei serie 9, vol. 10, 257-326.

Cucci, L. (2004). Raised marine terraces in the Northern Calabrian Arc (Southern Italy): a ~600 Ka-long geological record of regional uplift. Annals of Geophysics, 47, 1391-1406.

Cucci, L. (2005). Geology versus myth: the Holocene evolution of the Sybaris Plain. Annals of Geophysics, 48, 1017-1033.

Cucci, L., and Cinti, F.R. (1998). Regional uplift and local tectonic deformation recorded by the Quaternary marine terraces on the Ionian coast of northern Calabria (southern Italy). Tectonophysics, 292, 67-83.

D'Alessandro A., Ekdale, A.A., and Sonnino, M. (1986). Sedimentologic significance of turbidite ichnofacies in the Saraceno Formation (Eocene), Southern Italy. Jour. Sedim. Petrol., 56, 294-306.

D'Argenio, B., Pescatore, T., and Scandone, P. (1973). Schema geologico dell'Appennino Meridionale. Accademia Nazionale dei Lincei, 183, 49-72.

D'Agostino, N., and Selvaggi, G. (2004). Crustal motion along the Eurasia–Nubia plate boundary in the Calabrian Arc and Sicily and active extension in the Messina Straits from GPS measurements. J. Geophys. Res. 109, B11402. doi:10.1029/2004JB002998.

De Blasio, I., Lima, A., Perrone, V., and Russo, M. (1978). Studio petrografico e biostratigrafico di una sezione della Formazione del Saraceno nell'area tipo (Calabria nord-orientale).Riv. It. Paleont., 84, 947-972.

Di Staso, A., and Giardino, S. (2002). New integrate biostratigraphic data about the Saraceno formation (North-Calabrian Unit; Southern Apennines). Boll. Soc. Geol. Ital, vol. spec. 1, 517-526.

Dietrich, D., Lorenzoni, S., Scandone, P., Zanettin Lorenzoni, E., and DiPierro, M. (1977). Contribution to the knowledge of the tectonic units of Calabria. Relationships between composition of K-white micas and metamorphic evolution. Boll. Soc. Geol. Ital. 95, 193–217.

Doglioni, G., Merlini, S., and Cantarella, G. (1999). Foredeep geometries at the front of the Apennines in the Ionian sea (central Mediterranean). Earth and Planetary Sci. Lett., 168, 243-254.

Dokka, R. K. (2006). Modern-day tectonic subsidence in coastal Louisiana. Geology 34, 281–284.

Dokka, R. K. (2011). The role of deep processes in late 20th century subsidence of New Orleans and coastal areas of southern Louisiana and Mississippi. Journal of Geophysical Research 116, B06403, doi:10.1029/2010JB008008.

Dubois, R. (1976). La suture calabro-apenninique Cretaceé–Eocène et l'ouverture Tyrrhenienne neogene: étude petrographique et structurale de la Calabre centrale. Thèse, Paris University, 567 pp.

Dubois, R., and Glangeaud, L. (1965). Grandes structures, micro structures et sens des chevauchements de matériel cristallin a l'extramite meridionale du massif de la Sila (Calabre centrale, Italie). C.R. Somm. Soc. Geéol. France 7, 239–240.

Ericson, J.P., Vörösmarty, C.J., Dingman S.L.,Ward L.G., and Meybeck M. (2006). Effective sea-level rise and deltas: Causes of change and human dimension implications. Global and Planetary Change 50, 63–82.

Faccenna, C., Mattei, M., Funiciello, R., and Jolivet, L. (1997). Styles of back-arc extension in the central Mediterranean, Terra Nova, 9, 126 – 130.

Faccenna, C., Piromallo, C., Crespo-Blanc, A., Jolivet, L., and Rossetti, F. (2004). Lateral slab deformation and the origin of the western Mediterranean arcs. Tectonics 23, TC1012. doi:10.1029/ 2002TC001488.

Ferranti, L., Burrato, P., Santoro, E., Mazzella, M.E., Morelli, D., Passaro, S., Pepe, F., and Vannucci, G. (2014). Geometry, modeling, and seismotectonic implications of an active, segmented blind-thrust system beneath the Taranto Gulf, southern Italy. GNGTS 2012, Potenza.

Ferranti, L., Pagliarulo, R., Antonioli, F., and Randisi, A., (2011). Punishment for the sinner: Holocene episodic subsidence and steady tectonic motion at ancient Sybaris (Calabria, southern Italy). Quaternary International, 232, 56-70.

Ferranti, L., Santoro, E., Mazzella, M.E., Monaco, C., and Morelli, D. (2009). Active transpression in the northern Calabria Apennines, southern Italy. Tectonophysics, 476, 226–251.

Ferrelli, L., Michetti, A.M.,Serva, L., Vittori, E., Zambonelli, E. (1996). Tettonica recente ed evidenze di fagliazione superficiale nella Catena del Pollino (Calabria Settentrionale). Memorie Società Geologica Italiana, 51, 451-466.

Ferretti, A., Prati, C., and Rocca, F. (2001). Permanent Scatters in SAR interferometry. IEEE Transactions on Geoscience and Remote Sensing, 39, 8−20.

Finetti, I., Lentini, F., Carbone, C., Catalano, S., and Del Ben, A. (1996). Il sistema Apennino meridionale-Arco Calabro-Sicilia nel Mediterraneo centrale: sudio geologico-geofisico. Boll. Soc. Geol. It. 115, 529-559

Fraser, G.S. ,and Davis, J.M. (1998). Hydrogeologic models of sedimentary aquifers. SEPM Concepts in Hydrogeology and Environmental Geology, 1, 188 pp.

Froese, D.G., Smith, D.G., and Clement, D.T. (2005). Characterizing large river historywith shallow geophysics: Middle Yukon River, Yukon Territory and Alaska. Geomorphology, 67, 391–406.

Galloway, W.E., and Sharpe, J.M. (1998a). Characterizing aquifers heterogeneity within terrigenous clastic depositional systems. In Fraser, G.S. ,and Davis, J.M. eds.: Hydrogeologic models of sedimentary aquifers. SEPM Concepts in Hydrogeology and Environmental Geology, 1, 85-90.

Galloway, W.E., and Sharpe, J.M. (1998b). Hydrogeology and characterization of fluvial aquifers systems. In Fraser, G.S. ,and Davis, J.M. eds.: Hydrogeologic models of sedimentary aquifers. SEPM Concepts in Hydrogeology and Environmental Geology, 1, 91-106.

Gatto, L. (2002). La siccità e gli effetti sulla disponibilità di risorse idriche sotterranee in Calabria: area campione nel bacino del F.Crati. Tesi di Laurea, Università della Calabria, A.A. 2001-2002.

Geoportale Nazionale (GN), Ministero dell'Ambiente. Modello digitale del terreno - 20 metri. http://wms.pcn.minambiente.it/wcs/dtm_20m.

Ghisetti, F. (1979). Evoluzione neotettonica dei principali sistemi di faglie della Calabria centrale. Boll. Soc. Geol. It., 98, 387-430.

Ghisetti, F., Vezzani, L. (1983). Structural Map of M.t Pollino (Southern Italy).Scala 1:50000. S.EL.CA Firenze. Note illustrative sul retro.

Giacoli, A., Galli, P., Giaccio, B., Lapenna, V., Messina, P., Peronace, E., Romano, G., and Piscitelli, S. (2011). Electrical Resistivity Tomography across the Paganica-San Demetrio fault system (L'Aquila 2009 earthquake). Bollettino di Geofisica Teorica ed Applicata, 52 (3), 457-469.

Gueguen, E., Doglioni, C., and Fernandez, M. (1998). On the post 25 Ma geodynamic evolution of the western Mediterranean. Tectonophysics 298, 259–269.

Guerricchio, A., and Ronconi, M.L. (1997). Osservazioni geomorfologiche nella piana di Sibari e variazioni delle linee di costa storiche nella zona degli scavi archeologici. I Quaderni dell'IRFEA anno V, 12, 5-31.

Guerricchio, A., Melidoro, G., and Tazioli, G.S. (1976). Lineamenti idrogeologici e subsidenza dei terreni olocenici della piana di Sibari. Rivista e Sviluppo n. 9 Cassa di Risparmio di Calabria e Lucania Cosenza, 77-80.

Guerricchio, G., and Melidoro, G. (1975). Ricerche di geologia applicata all'archeologia della città di Sybaris sepolta. Geologia Applicata e Idrogeologia, 10, 107-128.

Hanssen, R. (2001). Radar Interferometry: Data Interpretation and Error Analysis. Kluwer Acad., Netherlands.

Hofman, B. (2002). The Sedimentation History of the Sybaris Plain, University of Groningen,Mediterranean Archaeology Report, 28 p.

Hollenstein, C., Kahle, H.G., Geiger, A., Jenny, S., Goes, S., and Giardini, S. (2003). New GPS constraints on the Africa–Eurasia plate boundary zone in southern Italy. Geophys. Res. Lett. 30. doi:10.1029/2003GL017554.

Hsieh, C.S., Shih, T.Y., Hu J.C., Tung H., Huang, M.H., and Angelier, J. (2011). Using differential SAR interferometry to map land subsidence: a case study in the Pingtung Plain of SW Taiwan. Natural Hazards 58, 1311–1332, doi:10.1007/s11069-011-9734-7.

Improta, L., Ferranti, L., De Martini, P.M.,. Piscitelli, S., Bruno, P.P., Burrato, P., Civico, R., Giocoli,A., Iorio, M., D'Addezio, G., and Maschio L. (2010). Detecting young, slow-slipping active faults by geologic and multidisciplinary high-resolution geophysical investigations: A case study from the Apennine seismic belt, Italy. Journal of Geoph. Research, 115, B1, 1307, doi:10.1029/2010JB000871.

Indagini nel sottosuolo (L.464/84). ISPRA. http://sgi.isprambiente.it/GMV2/index.html

ISIDe, Italian Seismological Instrumental and Parametric Data-Base. Istituto Nazionale di Geofisica e Vulcanologia. Italian Seismological Instrumental and Parametric Data-Base

ISPRA, 2009. *Carta Geologica d'Italia alla scala 1:50.000.* Foglio 535, Trebisacce.

ISPRA, 2010. *Carta Geologica d'Italia alla scala 1:50.000.* Foglio 543, Cassano allo Ionio. http://www.isprambiente.gov.it/Media/carg/543_CASSANO_ALLO_IONIO/Foglio.html

ITHACA, ITaly HAzard from CApable faults. ISPRA. http://sgi.isprambiente.it/GMV2/index.html

Ivins, E. R., R. K. Dokka, and R. Blom (2007). Post-glacial sediment load and subsidence in coastal Louisiana. Geophys. Res. Lett., 34, L16303, doi:10.1029/2007GL030003.

Jelgersma, S. (1996). Land subsidence in coastal lowlands. In: Milliman, J.D., Haq, B.U. (Eds.), Sea-Level Rise and Coastal Subsidence. Kluwer Academic Publishers, 47–62.

Joannin, S.,. Brugiapaglia, E., de Beaulieu, J.L., L. Bernardo, L.,. Magny, M., Peyron, O., Goring S., and Vannière, B. (2012). Pollen-based reconstruction of Holocene vegetation and climate in southern Italy: the case of Lago Trifoglietti. Climate of the Past, 8, 1973–1996.

Jolivet, L., and Faccenna, C. (2000). Mediterranean extension and the Africa-Eurasia collision, Tectonics 19, 6, 1095–1106.

Kastens, K. A., Mascle, J., Party, O.L.S. (1988). ODP Leg 107 in the Tyrrhenian Sea: Insights into passive margin and backarc basin evolution, Geol.Soc. Am. Bull., 100, 1140 – 1156.

Kilner, M., Westa, L.J., and Murray, T. (2005). Characterisation of glacial sediments using geophysical methods for groundwater source protection. Journal of Applied Geophysics, 57, 293–305.

Kleine, E., Woldring, H., Cappers, R.T.J., Attema ,P.A.J., and Delvigne, J.J. (2003). Il carotaggio del Lago Forano presso Alessandria del Carretto (Calabria, Italia). Nuovi dati sulla vegetazione olocenica e sulla storia dell'uso del suolo nella Sibaritide interna. Preistoria e Protostoria della Calabria, Atti delle Giornate di Studio, Pellaro (Rc) 25-26 ottobre 2003, 81-91.

Knott, S.D., and Turco E. (1991). Late cenozoic kinematics of the Calabrian Arc. Tectonics 10 (6), 1164–1172.

Lambeck, K., Antonioli, F., Anzidei, M., Ferranti, L., Leoni, G., Scicchitano, G., and Silenzi S. (2011). Sea level change along the Italian coast during the Holocene and projections for the future. Quaternary International, 232, 250-257.

Lambeck, K., Antonioli, F., Purcell, A., and Silenzi, S. (2004). Sea-level change along the Italian coast for the past 10,000 yr. Quaternary Science Reviews, 23, 1567–1598.

Lanzafame, G., and Tortorici, L. (1981). La tettonica recente della Valle del Fiume Crati (Calabria). Geogr. Fis. Dinam. Quat., 4, 11-22.

Lentini, F. (1979). Le unità Sicilidi della Val d'Agri (Appenino Lucano). Geol. Romana 18, 215-225.

Liu, C.H., Pan, Y.W., Liao, J.J., Huang, C.T., and Ouyang, S. (2004). Characterization of land subsidence in the Choshui River alluvial fan, Taiwan. Environmental Geology 45, 1154–1166, doi: 10.1007/s00254-004-0983-6.

Liu, J., and Huang, H.J. (2013). Characterization and mechanism of regional land subsidence in the Yellow River Delta, Chin. Natural Hazard 68, 687–709, doi: 10.1007/s11069-013-0648-4.

LL.PP. Servizio Idrografico, sez. Catanzaro. Annali Idrologici, parte I e II, anni 1916-1987. Istituto poligrafico e Zecca dello Stato, Roma.

Lofi, J., Déverchère, J., Gaullier, V., Gillet, H., Guennoc, P., Gorini, C., Loncke, L., Maillard, A., Sage, F., and Thinon I. (2011). Seismic atlas of the Messinian salinity crisis markers in the offshore Mediterranean domain, CCGM. Mémoires Société Géologique de France, 179, 72 pp.

Lubis, A., M., Toshinori, S.,Tomiyama, N., Isezaki, N., and Yamanokuchi, T. (2011). Ground subsidence in Semarang-Indonesia investigated by ALOS–PALSAR satellite SAR interferometry. Journal of Asian Earth Sciences 40, 1079–1088.

Lugli, S., Dominici, R., Barone, M., Costa, E., and Cavozzi, C. (2007b). *Messinian halite and residual facies in the Crotone basin (Calabria, Italy).* From: Schreiber, B.C., Lugli, S. & Babel, M. (eds) Evaporites Through Space and Time. Geological Society, London, Special Publications, 285, 169–178.

Lugli, S., Manzi, V., and Roveri, M. (2007°). New facies interpretation of the Messinian evaporites in the Mediterranean. CIESM Workshop Monographs, 67-72.

Lugli, S., Manzi, V., Roveri, M., and Schreiber, B.C. (2010). The Primary Lower Gypsum in the Mediterranean: A new facies interpretation for the first stage of the Messinian salinity crisis. Palaeogeography, Palaeoclimatology, Palaeoecology, 297, 83–99.

Maidment, D.R. (1992). Handbook of Hydrology. McGraw-Hill Inc.

Malinverno, A., and Ryan, W.B.F. (1986). Extension in Tyrrhenian sea & shortening in the Apennines as result of arc migration driven bysinking of the lithosphere. Tectonics 5, 227–254.

Manzi, V. Lugli, S., Roveri, M., and Schreiber, B.C. (2009). A new facies model for the Upper Gypsum of Sicily (Italy): chronological and palaeoenvironmental constraints for the Messinian salinity crisis in the Mediterranean. Sedimentology 56, 1937–1960.

Manzi, V., Lugli, S., Ricci Lucchi, F., and Roveri M. (2005). Deep-water castic evaporites deposition in the Messinian Adriatic foredeep (northern Apennines, Italy): did the Mediterranean ever dry down ?. Sedimentology, 52, 875-902.

Manzi, V., Roveri, M.,Gennari, R., Bertini, A., Biffi, U., Giunta, S., Iaccarino, S.M., Lanci, L., Lugli, S., Negri, A., Riva, A., Rossi, M.E., and Taviani, M. (2007). The deep-water counterpart of the Messinian Lower Evaporites in the Apennine foredeep: The Fanantello section (Northern Apennines, Italy). Palaeogeography, Palaeoclimatology, Palaeoecology 251, 470–499.

Marani, M.P., and Trua, T. (2002). Thermal constriction & slab tearing at the origin of a superinflated spreading ridge:Marsili volcano (Tyrrhenian Sea). J. Geophys. Res. Solid Earth 107 (B9), 2188. doi:10,1029 /. 2001JB000285.

Massonnet, D., and Feigl, K.L. (1998). Radar interferometry and its application to changes in the earth's surface. Rev. Geophys., 36, 441–500.

Mattei, M., Cifelli, F., and D'Agostino, N. (2007). The evolution of the Calabrian Arc: Evidence from paleomagnetic & GPS observations, Earth Planet. Sci. Let t . , 263, 259–274.

Meckel, T. A., U. S. ten Brink, and S. J. Williams (2006). Current subsidence rates due to compaction of Holocene sediments in southern Louisiana. Geophys. Res. Lett. 33, L11403, doi:10.1029/2006GL026300.

Messina, A., Russo, S., Borghi, A., Colonna, V., Compagnoni, R., Caggianelli, A., Fornelli, A., and Piccarreta, G. (1994). Il Massiccio della Sila, Settore settentrionale dell'Arco Calabro-Peloritano (The Sila Massif, northern sector of the Calabrian-Peloritan Arc). Boll. Soc. Geol. It., 113, 539–586.

Minelli, L., and Faccenna, C. (2010). Evolution of the Calabrian accretionary wedge (central Mediterranean). Tectonics, 29, TC4004, doi:10.1029/2009TC002562, 2010

Molin, P., Pazzaglia, F.J. and Dramis, F. (2004). Geomorphic expression of active tectonics in a rapidly-deforming forearc, Sila Massif, Calabria, Southern Italy. American Journal of Science, 304, 559-589.

Moretti A. (2000). Il database delle faglie capaci della Calabria: stato attuale delle conoscenze – in Galadini F., Meletti C. and Rebez A. : Le ricerche del GNDT nel campo della pericolosità sismica – CNR – Gr. Naz. Difesa dai Terremoti, Roma.

Morris, D.A., and Johnson, A.I. (1967). Summary of the hydrologic and physical properties of rock and soil materials, as analyzed by hydrologic laboratory of the U.D Geological Survey, 1948-60. Geological Survey Water-Supply Paper 1839-D.

Morton, R.A., Bernier, J.C., and Barras, J.A. (2006). Evidence of regional subsidence and associated interior wetland loss induced by hydrocarbon production, Gulf Coast region, USA. Environ. Geol. 50, 261–274, doi:10.1007/s00254-006-0207-3.

Mostardini, F., and Merlini, S. (1986). Appennino centro-meridionale. Sezioni geologiche e proposta di modello strutturale. Mem. Soc. Geol. It., 35, 177-202

Moussat, E., Angelier, J., Mascle, G., and Rehault, J.P. (1986). L'overture de la Mer Thyrhenienne et la tectonique de faille neogène quaternaire en Calabre. Giorn. Di Geol., sez.3, 48, 63-75.

Nakamura, Y. (1989). A method for dynamic characteristic estimation of subsurface using microtremor on the ground surface. Quarterly Report of Railway Technology Research Institute 30, 25-33.

Nguyen, F., Chardon, D., Garambois, S., Hermitte, D., Bellier, O., and Jongmans, D. (2007). Subsurface electrical imaging of anisotropic formations affected by a slow active reverse fault, Provence, France. Journal of Applied Geophysics, 62, 338–353.

Nguyen, F., Garambois, T.S., Jongmans, D., Pirard, E., and Loke, M.H. (2005). Image processing of 2D resistivity data for imaging faults. Journal of Applied Geophysics, 57, 260–277.

Nicolosi, I., Speranza, F., and Chiappini, M. (2006). Ultrafast oceanic spreading of the Marsili Basin, southern Tyrrhenian Sea: evidence from magnetic anomaly analysis. Geology 34, 717–720.

Nogoshi, M., and Igarashi, T. (1970). On the propagation characteristics of microtremors. J. Seism. Soc. Jpn., 23, 264-280.

Ogniben, L. (1962). Le Argille Scagliose e i sedimenti messiniani a sinistra del Trionto (Rossano, Cosenza): Geologica Romana, 1, 255–282.

Ogniben, L. (1969). Schema introduttivo alla geologia del confine calabro-lucano (Introductory scheme to the geology of the Calabrian-Lucanian boundary). Memorie della Soc. Geol. It. 8, 453–763.

Ortolani, F., and Pagliuca, S. (2007). Evidenze geologiche di variazioni climatico-ambientali storiche nell'Area Mediterranea. Quaderni della SGI, 1, 13-18.

Ortolani, F., and Pagliuca, S. (2014). Modificazioni costiere attuali nel quadro dell'evoluzione climatico-ambientale del periodo storico. Erosione Costiera in Siti di Interesse Archeologico, 3° Workshop Termoli, 3-4 ottobre 2014.

Pagliarulo, R. (2006). Coastal change and environmental evolution of the archeological site of Sybaris (Southern Italy). Geogr. Fis. E Di. Quat., 29, 51-59.

Pagliarulo, R., Cotecchia, F., Coop, M.R., and Cherubini, C. (1995). Studio litostratigrafico e geotecnico della Piana di Sibari con riferimento all'evoluzione morfologica e ambientale del sito archeologico. Geologia Applicata e Idrogeologia, 30, 375-391.

Pelle, T., Scarciglia, F., Di Pasquale, G., Allevato, E., Marino, D., Robustelli, G., La Russa, M.F., and Pulice, I. (2013). Multidisciplinary study of Holocene archaeological soils in an upland Mediterranean site: Natural versus anthropogenic environmental changes at Cecita Lake, Calabria, Italy. Quaternary International, 303, 163-179.

Pellicer, X.M., and Gibson, P. (2011). Electrical resistivity and Ground Penetrating Radar for the characterisation of the internal architecture of Quaternary sediments in the Midlands of Ireland. Journal of Applied Geophysics, 75, 638-647

Piano Tutela della Acque (PTA) (2009). Regione Calabria, Dip. Politiche dell'Ambiente. http://www.regione.calabria.it/ambiente/index.php?option=com_content&task=category&sectionid=22&id=33&Itemid=242

Polemio, M., and Luise, G. (2007). Conceptual and numerical model of groundwater flow for a coastal plain (Piana di Sibari, Southern Italy), in Riberio L., Chambel A., Condesso De Melo M.T. eds., Groundwater and Ecosystems.

Polemio, M., Dragone, V., and Romanazzi, A. (2013). La risorsa idrica. Sfruttamento, depauperamento dei serbatoi sotterranei e utilizzo razionale nel caso della Calabria, in Dramis, F., and Mottana, A., eds., L'acqua in Calabria: risorsa o problema?: Accademia Nazionale delle Scienze - Scritti e Documenti: Roma, Aracne, 2-29.

Polemio, M., Petrucci, O., and Gatto, L. (2004). Suscettività alla siccità in Calabria ed effetti sulle acque sotterranee. Atti dei Convegni lincei, 204, 245-250.

Pondrelli, S., Salimbeni, S., Ekström, G., Morelli, A., Gasperini, P., and Vannucci G. (2006). The Italian CMT dataset from 1977 to the present. Phys. Earth Planet. In., 159, 286–303.

Rainey, F.G., and Lerici C.M., (eds.), (1967). The Search for Sybaris 1960-1965, Lerici Editori, Rome, 313 p.

Raspini, F., Loupasakis, C., Rozos D., Adam, N., and Moretti, S. (2014). Ground subsidence phenomena in the Delta municipality region(Northern Greece): Geotechnical modeling and validation withPersistent Scatterer Interferometry. Int. Journal of Applied Earth Obs. And Geoinf. 28, 78-89.

Ricci Lucchi, F., Colella, A., Gabbianelli, G., Rossi, S., and Normark, W.R. (1984). The Crati submarine fan, Ionian Sea. Geo-marine Letters, 3, 71-77.

Roda, C. (1964). Distribuzione e facies dei sedimenti neogenici nel Bacino Crotonese: Geologica Romana 3, 319–366.

Roda, C. (1967). I sedimenti neogenici autoctoni ed alloctoni della zona di Ciro`-Cariati (Catanzaro e Cosenza). Mem. Soc.Geol. It., 6, 137–149.

Romagnoli, C., and Gabbianelli, G. (1990). Late Quaternary sedimentation and soft-sediment deformation features in the Corigliano Basin, North Ionian Sea (Mediterranean). Giornale di Geologia, ser. 3°, 52(1-2), 35-54.

Romeo, M., and Tortorici, L. (1980). Stratigrafia dei depositi miocenici della Catena Costiera calabra meridionale e della media valle del F.Crati (Calabria). Boll. Soc. Geol. It., 99, 303-318.

Rosenbaum, G., and Lister, G.S. (2004). Neogene & Quaternary rollback evolution of the Tyrrhenian Sea, the Apennines, & the Sicilian Maghrebides. Tectonics 23, TC1013. doi:10.1029/2003TC001518.

Roveri, M., Bernasconi, A., Rossi, M.E., and Visentin, C. (1992). Sedimentary evolution of the Luna field Area; Calabria, Southern Italy. In Spencer, A.M. (ed.) Generation, Accumulation and Production of Europe's Hydrocarbons II: European Association of Petroleum Geoscientists, S.P. 2, 217–224.

Roveri, M., and Manzi, V. (2006). The Messinian salinity crisis: Looking for a new paradigm? Paleogeography, Paleoclimatology, Palaeoecology 238, 386-398

Roveri, M., Lugli, S., Manzi, V., and Schreiber, B.C. (2007). The shallow to deep-water record of the Messinian Salinity Crisis : new insights from Sicily, Calabria and Appennine basins. CIESM Workshop Monographs, pp 73-82.

Roveri, M., Lugli, S., Manzi, V., and Schreiber, B.C. (2008). The Messinian salinity crisis: a sequence- stratigraphic approach. GeoActa, Spec. Publ., 1, 117-138.

Russo, F., and Schiattarella, M. (1992). Osservazioni preliminari sull'evoluzione morfo-strutturale del bacino di Castrovillari. Studi Geologici Camerti, 1992/1, 271-278.

Sabato L., and Tropeano M. (2008). The Holocene coastal alluvial fan of the Saraceno Fiumara (Calabria, Southern Italy) : highstand filling of an incised valley. In Amorosi A., Haq B.U. and Sabato L. (eds) Advance in Application of Sequence Stratigraphy in Italy. GeoActa S.P. 1, 15-27.

Santoro, E., Mazzella, M.E., Ferranti, L., Randisi, A., Napolitano, E., Rittner, S., and Radtke, U. (2009). Raised coastal terraces along the Ionian Sea coast of northern Calabria, Italy, suggest space and time variability of tectonic uplift rates. Quaternary International, 206, 78-101.

Sartori, R. (1990). The main results of ODP Leg 107 in the frame of Neogene to recent geology of peri-Tyrrhenian areas, Proc. Ocean Drill. Program Sci. Results, 107, 715 – 730.

Schoch, R.M. (1989). Stratigraphic Principles and Methods. Von Nostrand Reinhold, New York.

Schreiber, B.C., Babel M., and Lugli S. (2007). Introduction and overview. Geological Society, London, Special Publications 2007; v.285, pp. 1-13.

Seaber, P.R. (1988). Hydrostratigraphic Units. Geological Society of America. V. O-2, 9-14.

Selli, R. (1957). Sulla trasgressione del Miocene nell'Italia meridionale. Giorn. Geol., 26, 1-54.

Selli, R. (1962). Il Paleogene nel quadro della geologia dell'Italia centro-meridionale. Mem Soc. Geol. Ital., 3, 737-789.

Selvaggi, G., and Chiarabba, C. (1995). Seismicity & P wave velocity image of the southern Tyrrhenian subduction zone, Geophys. J. Int., 121, 818–826.

Shi, X., Xue, Y., Wu, J., Ye, S., Zhang, Y., Wei, Z., and Yu, J. (2008). Characterization of regional land subsidence in Yangtze Delta, China: the example of Su-Xi-Chang area and the city of Shanghai. Hydrogeology Journal, 16, 593–607,doi: 10.1007/s10040-007-0237-2.

Somoza. L., Barnolas, A., Arasa, A., Maestro, A., Rees, J.G., and Hernandez-Molina, F.J. (1998). Architectural stacking patterns of the Ebro delta controlled by Holocene high-frequency eustatic fluctuations, delta-lobe switching and subsidence processes. Sedimentary Geology, 117, 11-32.

Sonnino, M. (1984). Un example d'évolution de dépôts de plateforme à dépôts de bassin: la Formation du Saraceno (Eocène moyen-sup., Italie du Sud). 5ème Congr. Europ. Sédim., Marseille, Abstr., 479-480.

Spadea, P., Lanzafame, G., and Tortorici L. (1976). Serie ofioliti fere nell'area fra Tarsia e Spezzano Albanese (Calabria) : stratigrafia, petrografia, rapporti strutturali. Mem. Soc. Geol. It., 17, 135-174.

Spina, V., Tondi, E., and Mazzoli, S. (2011). Complex basin development in a wrench-dominated back-arc area:Tectonic evolution of the Crati Basin, Calabria, Italy. Journal of Geodynamics, 51, 90–109.

Stanley, J.D., and Bernasconi, M.P. (2009). Sybaris-Thuri-Copia trilogy: three delta coastal sites become land-locked. Méditerranée, 112, 75–86.

Stefani, M., and Vincenzi, S. (2005). The interplay of eustasy, climate and human activity in the late Quaternary depositional evolution and sedimentary architecture of the Po Delta system. Marine Geology, 222-223, 19-48.

Štěpančíková, P., Dohnal, J., Pánek, T., Łój, M., Smolková, V., and Šilh, K. (2011). The application of electrical resistivity tomography and gravimetric survey as useful tools in an active tectonics study of the Sudetic Marginal Fault (Bohemian Massif, central Europe). Journal of Applied Geophysics, 74, 69–80.

Stiros, S.C. (2001). Subsidence of Thessaloniki (northern Greece) coastal plain, 1960-1999. Engineering Geology 61, 243-256.

Suzuki, K., Toda, S., Kusunoki, K., Fujimitsu, Y., Mogi, T., and Jomori, A. (2000). Case studies of electrical and electromagnetic methods applied to mapping active faults beneath the thick quaternary. Engineering Geology, 56, 29–45.

Taliano Grasso, A. (2004). Tra il Sibari e il Crati. Daidalos (Studi e Ricerche Del Dipartimento di Scienze del Mondo Antico), 6°estratto, 189-198.

Tansi, C., Muto F., Critelli S., and Iovine G. (2006). Neogene-Quaternary strike-slipe tectonics in the central Calabrian Arc (southern Italy). Journal of Geodynamics 43, 393-414.

Tazioli, G.S. (1986). Indagini idrogeologiche volte allo sfruttamento delle risorse idriche sotterranee. Tecniche per la difesa dall'inquinamento, VII Corso di aggiornamento, Cosenza, Italy.

Teatini, P., L. Tosi, T. Strozzi, L. Carbognin, U. Wegmüller, and F. Rizzetto (2005). Mapping regional land displacements in the Venice coastland by an integrated monitoring system. Remote Sens. Environ. 98(4), 403–413, doi:10.1016/j.rse.2005.08.002.

Teatini, P., Tosi, L., and Strozzi, T. (2011). Quantitative evidence that compaction of Holocene sediments drives the present land subsidence of the Po Delta, Italy. Journal of Geophysical Research 116, B08407, doi:10.1029/2010JB008122.

Torricelli, S., and Amore, M.R. (2003). Dinoflagellate cyst and calcareous nannofossils from the Upper Cretaceous Saraceno Formation (Calabria, Italy): implications about the history of the Liguride Complex. Riv. It. Paleont. Strat. 109, 499-516.

Tung, H., and Hu, J. C. (2012). Assessments of serious anthropogenic land subsidence in Yunlin County of central Taiwan from 1996 to 1999 by Persistent Scatterers InSAR. Tectonophysics 578, 126–135.

Turc, L. (1954). Calcul du bilan de l'eau: evaluation en function des precipitation et des temperatures. IAHS Publ., 37, 88-200.

Turco, E., Maresca, R., and Cappadona, P. (1990). La tettonica plio-pleistocenica del confine calabro-lucano: modello. Memorie della Società Geologica Italiana 45, 519–529

Valensise, G., and Pantosti, D. (Ed.) (2001). Database of potential sources for earthquakes larger than 5.5 in Italy. Annals of Geophysics,, 44 (suppl. to no. 4), pp. 175.

Van Dijk, J.P. (1990). Basin dynamics and sequence stratigraphy in the Calabrian Arc (Central Mediterranean); records and pathways of the Crotone Basin: Geologie en Mijnbouw, 70, 187–201.

Van Dijk, J.P., Bello, M., Brancaleoni, G.P., Cantarella, G., Costa, V., Frixa, A., Golfetto, F., Merlini, F., Riva, M., Torricelli, S., Toscano, C., and Zerilli, A. (2000). *A regional structural model for the northern sector of the Calabrian Arc (southern Italy)*. Tectonophysics 324 , 23–60.

van Geel, B., Heusser, C. J., Renssen, H., and Schuurmans, C. J. E. (2000). Climatic change in Chile at around 2700 BP and global evidence for solar forcing: a hypothesis. Holocene, 10, 659–664.

Vezzani, L. (1968a). Studio stratigrafico della Formazione delle Crete Nere (Aptiano - Albiano) al confine calabro-lucano. Atti Acc. Gioenia Sc. Nat. Catania, s. 6, 20, 189-222.

Vezzani, L. (1968b). Distribuzione, facies e stratigrafia della Formazione del Saraceno (Albiano-Daniano) nell'area compresa tra il Mare Jonio e il Torrente Frido. Geol. Romana, 7, 229-275.

ViDEPI, Visibilità Dati Esplorazione Petrolifera in Italia. http://unmig.sviluppoeconomico.gov.it/videpi/kml/webgis.asp

Vignaroli, G., Minelli, L., Rossetti, F., Balestrieri, M.L., and Faccenna, C. (2012). Miocene thrusting in the eastern Sila Massif: Implication for the evolution of the Calabria-Peloritani orogenic wedge (southern Italy). Tectonophysics 538–540, 105–119

Vittori, E., Ferrelli, L., Michetti, A.M., and Serva, L. (1995). Holocene paleo-earthquakes along the Pollino fault zone (Northern Calabria-Italy): implications for seismic hazard assessment, in Proceedings of the Fifth International Conference on Seismic Zonation (EETI, AFPS), Nice, 1400-1407.

Westaway, R. (1993). Quaternary Uplift of Southern Italy. Journal of Geoph. Research, 98B12, 21741-21772.

Wortel, M. J. R., and Spakman, W. (2000). Subduction & slab detachment in the Mediterranean-Carpathian Region, Science, 290, 1910 – 1917.

Zecchin, M., Caffau, M., Di Stefano, A., Maniscalco, R., Lenaz, D., Civile, D., Muto, F., and Critelli, S. (2013b). The Messinian succession of the Crotone Basin (southern Italy) II: facies architecture and stratal surfaces across the MioceneePliocene boundary. Mar. Pet. Geol. 48, 474-492.

Zecchin, M., Civile, D., Caffau, M., Muto, F., Di Stefano, A., Maniscalco, R., and Critelli, S. (2013°). The Messinian succession of the Crotone Basin (southern Italy) I: stratigraphic architecture reconstructed by seismic and well data. Mar. Pet. Geol. 48, 455-473.

Zervas, D., Hall, R., Murtagh, F., and Nichols, G. (2009). SedLog Version 2.1.4. http://www.sedlog.com

Zuppetta, A., Russo, M., Turco, E., and Gallo, L. (1984). Età e significato della Formazione di Albidona in Appennino Meridionale. Boll. Soc. Geol. It., 103, 159-170.

Historical maps

"Austrian Army" (1822). Carta delle Provincie continentali dell'ex Regno di Napoli, Sezione 10 - Colonna VIII

Beneventanus, M. (1508). Tabula nova Italie. In Claudius Ptolemaeus (ed.) Geographia, Roma.

Blaeu, W.J. (1680). Calabre Citra. In Mortier, P. (ed.) Nouveau Theatre de l'Italie.

Bulifon, A. (1650-1700). Calabria citra. Carte de' Regni di Napoli e di Sicilia, loro provincie ed isole adiacenti.

Hondius J. (1627). Calabria Citra et Ultra. Nova et accurata Italiae Hodiernae description. Italia

Magini, G.A. (1620). Calabria citra, olim Magna Graecia

Marzolla B. (1851). Provincia di Calabria Citeriore. La Descrizione del Regno delle Due Sicilie (1854).

Parisio, P. (1589). Calabriae descrip. Per Prosperum Parisium consent. Theatro del mondo di Abrahamo Ortelio, da lui poco inanzi la sua morte riueduto, & di tauole nuoue, et commenti adorno. Vrients, J.B ed..

Reilly (von), F.J.J. (1791). Der Neapolitanischen Landschaft Calabria Citra Noerdlichen Theil n.446.

Rizzi Zannoni, G.A. (1783). Calabria Citeriore. Zatta, A. ed..

Rizzi Zannoni, G.A. (1908). Atlante geografico del Regno di Napoli delineato per ordine di Ferdinando IV RE delle Due Sicilie & C., Tav. 26.

Zuccagni Orlandini, A. (1840). Provincia di Calabria Citeriore. Corografia fisica, storica e statistica dell' Italia e delle sue isole corredata di un atlante di mappe geografiche e topografiche. Firenze (1835-1845).

Historical Sources

Diodorus Siculus (1st century A.D.). Bibliothecae historicae XII, 9, 2.

Herodotus (484-425 B.C.). Ἱστορίαι (Histories) V, 45.

Plinio il Vecchio (1st century A.D.). Naturalis Historia III, 97.

Strabo (64 B.C.- 21 A.D.). Γεωγραφικά (Geography) VI, 1, 13.

Thucydides (460-404B.C.). Περὶ τοῦ Πελοποννησίου πολέμου (Peloponnesian War) VII, 35, 1.